Access to Electronic Thesis

Author:	Vanessa Hearnden
Thesis title:	Developing tissue engineered models of oral mucosa and oral cancer to study novel therapeutic and diagnostic techniques.
Qualification:	PhD
Date awarded:	21 January 2011

If this electronic thesis has been edited by the author it will be indicated as such on the title page and in the text.

Developing tissue engineered models of oral mucosa and oral cancer to study novel therapeutic and diagnostic techniques

Vanessa Hearnden

Thesis submitted to the University of Sheffield for the degree of Doctor of Philosophy

Department of Materials Science and Engineering

University of Sheffield

October 2010

Abstract

In the UK in 2008 over 1,800 people died from oral cancer. Despite advances in surgery and therapy the survival rates for those diagnosed with oral cancer have not significantly improved over the past 20 years. There is a need for both better detection and treatment. Early detection could reduce these mortality rates but unfortunately diagnosing oral cancer, which is often symptomless, in the early stages of the disease is incredibly challenging. More targeted treatments for oral cancer are also needed which can be administered to the site of disease with higher efficiency and accuracy to reduce side effects and allow higher concentrations of therapeutic agents to be delivered to tumour cells.

This project used a tissue engineered oral mucosa model to develop models of oral cancer progression. These oral cancer models incorporated many pathological features of oral cancer progression including features seen in dysplastic epithelia, carcinoma *in situ* and early invasive squamous cell carcinomas. Multi-cellular tumour spheroids were created from an oral cancer cell line to model solid expanding tumour masses.

The tissue engineered models of oral mucosa and the multi-cellular tumour spheroids were used to test the behaviour of polymersomes, a novel drug delivery system, in three dimensional tissues. Polymersome distribution and penetration in the tissue engineered models was examined over time, to investigate the potential of polymersomes to deliver therapeutic agents into and/or across the oral mucosa and into solid expanding tumours. Drug delivery agents that are able to reach the central hypoxic region of solid expanding tumours are particularly important as these cells are often resistant to both radio- and chemotherapy and correlate with poor patient prognosis. In addition, we explored the potential of polymersomes to cross the oral epithelial permeability barrier and act as delivery vehicles for topical delivery of therapies for oral mucosal diseases and as an alternative to parenteral administration for the systemic delivery of drugs. Results showed good penetration of polymersomes into the oral mucosa and the multi-cellular tumour spheroids demonstrating the potential to develop these drug delivery vehicles to deliver anti-cancer drugs and other therapeutic agents in the future.

The tissue engineered models of cancer were next utilised to test four non-invasive diagnostic technologies. These included a cell metabolism marker, impedance spectroscopy, Fourier transform infra-red and optical coherence tomography. The results obtained from these different techniques showed varying degrees of promise with the images from OCT demonstrating that this technology has real diagnostic potential. The 3D models proved useful test-beds for some but not all of these diagnostic imaging techniques. They provide convenient models to tackle some of the key issues in the preclinical development of novel diagnostic technologies for oral cancer and oral dysplastic lesions.

Publications

Hearnden, V., Lomas H., MacNeil, S., Thornhill, M. T., Murdoch, C., Lewis, A.L., Madsen, J., Blanazs, A., Armes, S.P., and Battaglia, G. (2009). "Diffusion studies of nanometer polymersomes across tissue engineered human oral mucosa." <u>Pharmaceutical Research</u> **26**(7): 1718-1728.

Hearnden, V., MacNeil, S and Battaglia, G. (2011). Tracking Nanoparticles in Three-Dimensional Tissue-Engineered Models Using Confocal Laser Scanning Microscopy. <u>3D Cell Culture: Methods and Protocols</u>. J. W. Haycock, Humana Press. **695**.

Massignani, M.,Canton, I., Sun, T., **Hearnden, V**., MacNeil, S., Blanazs, A., Armes, S. P., Lewis, A., Battaglia, G. (2010). "Enhanced fluorescence imaging of live cells by effective cytosolic delivery of probes." <u>PLoS One</u> **5**(5): e10459.

Murdoch, C., **Hearnden, V**., Colley, H., Massignani, M., Reeves, K. J., Canton, I., Madsen, J., Blanazs, A., Armes, S. P., Lewis, A. L., Mac Neil, S., Brown, N., Thornhill, M. and Battaglia, G. (2010). "Internalization and biodistribution of polymersomes into oral squamous cell carcinoma cells in vitro and in vivo." <u>Nanomedicine</u> **5**(10): 1025–1036

Picard, C., **Hearnden, V**., Massignani, M., Achouri, S.,Battaglia, G., MacNeil, S. and Donald, A. (2010). "A micro-incubator for cell and tissue imaging." <u>Biotechniques</u> **48**(2): 135-8.

Publications in preparation

*Sankar V., **Hearnden, V**., et al. (in preparation) "Local Drug Delivery for Oral Mucosal Diseases:
      Challenges and Opportunities" <u>Oral Diseases</u>

***Hearnden, V**., Sankar, V., et al. (in preparation) "New Developments in Topical and Systemic Oral
      Mucosal Drug Delivery"

Colley, H., **Hearnden, V**., et al. (in preparation) "Development of tissue engineered models of oral
      dysplasia and early invasive oral squamous cell carcinoma"

Colley, H., **Hearnden, V**., et al. (in preparation) "Multi-cellular tumour spheroids- A useful model for

head and neck cancer studies"

Smith, L. E., **Hearnden, V**., et al. (in preparation) "Evaluating the use of optical coherence tomography for the detection of epithelial cancers *in vitro*."

*Reviews written as part of the World Workshop on Oral Medicine 2010.

Oral Presentations

"Penetration of polymersome drug delivery nanoparticles into *in vitro* models of head and neck cancer and tissue engineered oral mucosa" International Academy of Oral Oncology (2009), Toronto, Canada

"Tissue engineered models of head and neck cancer and healthy oral mucosa; an *in vitro* method to study polymersome penetration for potential drug delivery." The Biomaterials and Tissue Engineering Group (BiTEG) 11th Annual Work in Progress Meeting (2010), University of York, UK

"Using tissue-engineered oral cancer models to evaluate non-invasive diagnostic technologies". The European Association of Oral Medicine (EAOM), 10th Biennial Congress (2010), UCL, London, UK

"Penetration of polymersomes into *in vitro* tissue engineered models of oral mucosa and head and neck cancer" Tissue and Cell Engineering Society (TCES) Conference (2008), University of Nottingham, UK

Poster Presentations

"Diffusion of polymersomes into 3D models of head and neck cancer" Frontiers of Research Meeting and Macro Group Young Researchers Meeting (2008), University of Warwick, UK

"Penetration of polymersomes into *in vitro* tissue engineered models of oral mucosa and head and neck cancer" IRC Polymer Showcase (2008), University of York, UK

"Penetration of polymersomes into *in vitro* tissue engineered models of oral mucosa and head and neck cancer" European Association of Oral Medicine (EAOM) 9th Biennial Congress (2008), Salzburg, Austria

"Diffusion of Nanometer Polymersomes through Full Thickness Tissue Engineered Oral Mucosa" Controlled Release Society (CRS) Meeting (2009), Copenhagen, Denmark

"Diffusion of Nanometer Polymersomes Through Head & Neck Tumours *in vitro* and *in vivo*" Controlled Release Society (CRS) Meeting (2009), Copenhagen, Denmark

Acknowledgements

Initial thanks go to my fantastic supervisory "team", yes on occasions four supervisors was a bit of a juggling act but for the most part it helped me enormously and I have learnt a huge amount from all members of the "team". Thanks to Professor Sheila MacNeil for securing the EPSRC studentship, without which this research could not have taken place. Thanks also to Professor Sheila MacNeil for her continuous stream of enthusiasm, ideas and wisdom. Thanks to Professor Martin Thornhill for giving me some fantastic opportunities over the past 3 years and for providing me with invaluable support and advice throughout. Thanks to Dr. Craig Murdoch for all the practical help and knowledge in and out of the lab; Craig's knowledge of laboratory techniques at times seemed to be endless. Thanks to Dr Beppe Battaglia for his inspiration, passion and for all the opportunities he has made available to me during my time as a PhD student.

Thank you to Dr. Anthony Bullock for getting me off to a great start and teaching me (almost) everything I know about cell and tissue culture. Thanks also to Anthony for tolerating my constant question asking in the early days. Thanks to Dr. Helen Colley for teaching me all about spheroids, passing on her knowledge and techniques and for being a great companion and guide throughout my PhD. Thanks to Keith Blackwood for many hours spent helping me out in the lab and for teaching me histology. Thank you to Dr. Irene Canton for helping with the polymersome problem solving and for much guidance over the years. Thanks to Munirah Mansor for all her hard work on the FTIR part of the project and for processing all the data in MATLAB for me.

Thanks also go to Sue Newton (FACS), Marzia Massignani (polymersomes), Hannah Lomas (polymersomes, DLS and TEM), Peter Highfield and Jamie Healey (impedance spectroscopy), Dr. Lousie Smith, Dr. Steven Matcher, Dr. Nikola Krstajic and Dr. Zenghei Liu (OCT), Christopher Mody and Richard Mills (Optovue OCT). Thanks to Dr Keith Hunter for his help with determining the pathology of my models and for the staff in Oral Pathology for allowing me to use their histology equipment. Thanks to Dr. Paul Topham, Mr. Nick Warren, Dr. Jeppe Madsen and Dr. Adam Blanazs from Prof. Steve Armes's research group for producing the polymer required for this project. Thanks to Biocompatibles UK Ltd. and the University of Sheffield Learned Society for their financial support towards conferences. I would also like to thank the members of the three research groups I have been a part of and all the lab technicians who have all helped me out a great deal along the way.

Finally, huge thanks go to my friends and family for supporting me over the last 3 years, for making my time in Sheffield so enjoyable and for making sure my work-life balance was a healthy one.

Abbreviations

λ	wavelength
°C	degrees celcius
2D	Two Dimensional
3D	Three Dimensional
AIDS	Acquired Immunodeficiency Syndrome
ALI	Air-liquid interface
ASG	Ammonium Sulphate Gradient
ATCC	American Type Culture Collection
ATR	Attenuated total reflectance
ATRP	Atomic transfer radical polymerisation
a.u.	arbitrary units
BSA	Bovine Serum Albumin
CIN	Cervical Intraepithelial Neoplasia
CLSM	Confocal laser scanning microscopy
COX-2	Cyclo-oxygenase -2
CPAS	Cervical Probe Applications Software
Da	Daltons
DAB	3,3'-Diaminobenzidine
DAPI	4',6-diamidino-2-phenylindole
DED	De-epidermised Dermis
DMEM	Dulbecco's modified Eagle's Medium
DMSO	Dimethyl sulfoxide
DNA	Deoxyribonucleic acid
DOK	Dysplastic Oral Keratinocyte
DOX	Doxorubicin
DPX	Dibutylphthalate Polystyrene Xylene
ECACC	European Collection of Animal Cell Cultures
ECM	Extra-cellular Matrix
EDTA	Ethylene Diamine Tetra-acetic acid
EGF	Epidermal Growth Factor
EGFR	Epidermal Growth Factor Receptor
EMT	Epithelial Mesenchymal Transition
EPR	Enhanced Permeation and Retention
FACS	Fluorescence Activated Cell Sorting
FCS	Foetal Calf Serum
FDA	Food and Drug Administration
FD-OCT	Fourier Domain Optical Coherence Tomography
FSC	Forward scatter
FTIR	Fourier Transform Infra-Red
GFP	Green Fluorescent Protein
GI	Gastro-Intestinal
GPC	Gel Permeation Chromatography
g	gram
h	hours
HCl	Hydrochloric acid
HGF	Hepatocyte Growth Factor
HIV	Human Immunodeficiency Virus
HNSCC	Head and Neck Squamous Cell Carcinoma
HOE	Human Oral Epithelium
Hz	Hertz
i3T3	irradiated Swiss mouse fibroblasts
IDMEM	Iscove's Modified Dulbecco Minimum Essential Medium
IU	International Units

IR	Infra-red
KGF	Keratinocyte Growth Factor
L	litre
LSM	Laser Scanning Microscopy
μ	micro
m	milli-
m	metre
M	Molar
MCGs	Membrane Coating Granules
MCTS	Multi-cellular tumour spheroids
MD	Michelson Diagnostics
MMP	Matrix metalloprotinase
MRI	Magnetic Resonance Imaging
MTT	(3-(4,5-dimethylthiazol-2-yl)-2,5 diphenyl tetrazolium bromide)
n	nano
NA	Numerical Aperture
NaOH	Sodium Hydroxide
NCI-DTP	National Cancer Institute Developmental Therapeutics Programme
NIR	Near Infra-Red
NOF	Normal human Oral Fibroblasts
NOK	Normal human Oral Keratinocytes
OCT	Optical Coherence Tomography
OSCC	Oral Squamous Cell Carcinoma
PAA	Poly (acrylic acid)
PBS	Phosphate Buffered Saline
PCL	Polycaprolactone
PDPA	poly(2-(diisopropylamino)ethyl methacrylate)
PEG	Poly (ethylene glycol)*
PEO	Poly(ethylene oxide)*
pH	potentiometric hydrogen ion concentration
pKa	Acid dissociation constant
PLA	Poly (lactic acid)
PML	Potentially Malignant Lesions
PMPC	2-((methacryloyloxy)ethyl phosphorylcholine)
PS	Poly (styrene)
R	Reflectance
rBM	Reconstituted Basement Membrane
RFP	Red Fluorescent Protein
rho	Rhodamine
RNA	Ribonucleic acid
RPMI	Roswell Park Memorial Institute (cell culture medium)
rpm	revolutions per minute
SCC	Squamous Cell Carcinoma
SCC	Side scatter
s.d.	Standard deviation
SHG	Second Harmonic Generation
SLED	Superluminescent light emitting diode
SS-OCT	Swept source Optical Coherence Tomography
T_3	3,3,5-Tri-iodothyronine
T	apo-transferrin
TAX- Paclitaxel	
TD-OCT	Time Domain Optical Coherence Tomography
TEM	Transmission electron microscopy
TEOM	Tissue engineered oral mucosa.
THF	Tetrahydrofuran
Ti:Sa	Titanium Sapphire

TM	Trade Mark
UV	Ultra-violet
V	Volt
v	volume
w	weight

* NB PEG and PEO are different names for the same chemical entity

Table of contents

Table of Figures

Chapter 1: Introduction

1.1 Oral mucosa

The Normal Oral Mucosa

Human oral mucosa is comprised of a stratified squamous epithelium and a connective tissue component, separated by a basement membrane (Figure 1.1) (Nanci 2003). Adjacent to the basement membrane lays the basal keratinocytes; these cells are "stem-like" proliferative cells which repair and replenish the epithelium. Superficially to these are the partially differentiated supra-basal cells which are also highly proliferative. Above the supra-basal cells lies the prickle cell layer or stratum spinosum. In the prickle cell layer cells are joined by desmosomes, these desmosomes remain attached between cells during histological processing however, the cells shrink, making cells appear prickly. In keratinized regions of the oral cavity (gingivae and hard palette) the most superficial layer of the epithelium is made up of terminally differentiated keratinocytes (Nanci 2003; Salamat-Miller *et al.,* 2005). In non-keratinised areas like the buccal mucosa there is less keratinisation of superficial layers which are then termed para-keratinised. The keratinised layer contains a large amount of keratin and the cells are flattened with little or no nuclei. In the connective tissue the predominant cell type is fibroblasts. These are responsible for producing extracellular matrix proteins and releasing factors important in epithelial development (Mackenzie and Fusenig 1983). The connective tissue also contains cells involved in the immune system and a vasculature component.

The oral mucosa has potential as a site for local drug delivery for mucosal diseases and for the trans-mucosal systemic delivery of drugs without the need for injections (reviewed in (Hearnden *et al.,* in preparation; Sankar *et al.,* in preparation)).

Permeability of the Oral Mucosa

The permeability barrier of the oral mucosa is responsible for preventing exogenous and endogenous materials entering the body *via* the oral mucosa and prevents loss of fluid from the underlying tissues to the environment. The permeability barrier is predominantly due to the lipid content of the upper layers of the epithelium. As supra-basal cells differentiate they form strong intercellular desmosomal junctions and membrane coating granules (MCGs) on their apical surfaces (Shimono and Clementi 1976; Shojaei 1998). These MCGs release lipophilic material into the intercellular spaces to ensure epithelial cohesion. This lipophilic material slows the passage of hydrophilic materials across the epithelium (Salamat-Miller *et al.,* 2005). It has also been hypothesised that tight junctions play a role in permeability barrier function however, these are not commonly found in the oral epithelium (Shimono and Clementi 1976).

Kulkarni *et al.* looked at the permeability of the epithelium and the connective tissues using varying thicknesses of porcine buccal mucosa and mathematical derivation (Kulkarni *et al.,* 2009). It was shown that the epithelium is the major barrier to permeability with the connective tissue providing some resistance to lipophilic materials due to the connective tissue's high level of hydration.
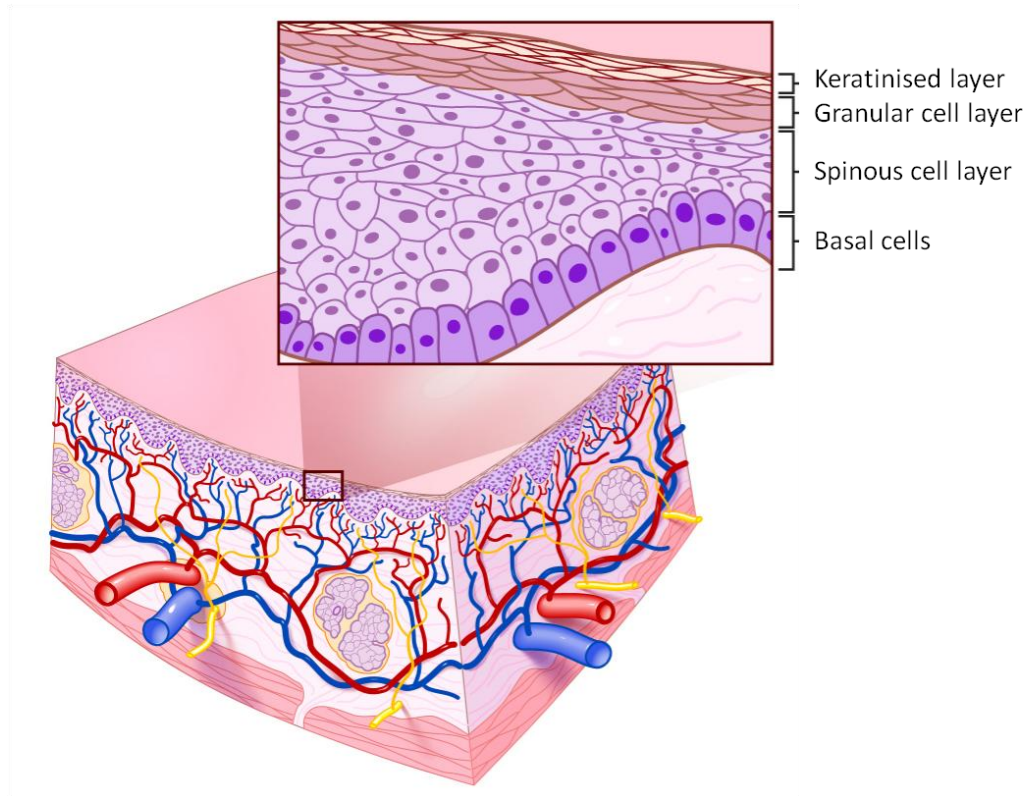
Figure 1.1 Structure of the oral mucosa and the oral epithelium (insert)
Image reproduced from (Hearnden *et al.,* in preparation).

There is variation in permeability across different regions of the oral mucosa due to the differing thickness of the epithelium and degree of keratinisation at different sites. Keratinised tissues display a lower permeability than non-keratinised tissue, this is however, due to the lipid composition of the membrane coating granules in the keratinised vs. non-keratinised tissues rather than the content of keratin itself (Ganem-Quintanar *et al.,* 1997). The degree of permeability is least in keratinized gingiva followed by the buccal mucosa with the most easily permeated area of the oral cavity the sublingual mucosa (Squier and Hall 1985).

There are three methods of diffusion across the oral mucosa's permeability barrier (i) passive diffusion including trans-cellular (through cells) and para-cellular (where material passes through lipid rich domains around the cells), (ii) carrier mediated transport and (iii) endocytosis/exocytosis where material is actively taken up and excreted by cells via the endocytic pathway (Li *et al.,* 2005; Salamat-Miller *et al.,* 2005; Sudhakar *et al.,* 2006). The

most easily diffusible materials are lipid soluble and non-ionized species and those with low molecular weights. Dextran with a molecular weight below 20,000 Da is diffusible however, dextrans with larger molecular weights are not (Hoogstraate *et al.,* 1994). The route of passive diffusion taken by a particular material depends on the material's lipophilicity, partition coefficient between lipophilic and hydrophilic regions and the diffusion coefficient of the substance in the intercellular space (Sood *et al.,* 2005). Drugs which have a high pKa (acid dissociation constant) diffuse across the mucosa better (Madhav *et al.,* 2009). For drugs that act on intracellular targets the trans-cellular route is desired.

Advantages of the Oral Mucosa For Drug Delivery Applications

The oral cavity has been proposed as a potential topical delivery site for the delivery of local and systemic delivery of therapeutic agents. When compared to parenteral delivery the oral mucosa is appealing to patients as the administration is painless, it can be self-administered and is easily withdrawn (Sudhakar *et al.,* 2006). The oral cavity has advantages over other mucosal membranes as it is well tolerated by patients, it is easily accessible and is rapidly repaired after damage or trauma. This short recovery time limits potential damage caused by long term topical drug delivery and the rich blood supply to the oral cavity makes systemic delivery viable and very rapid (Sudhakar *et al.,* 2006). There are also fewer Langerhans cells found in the oral mucosa compared to the skin reducing the risk of an allergic response, a drawback commonly experienced in transdermal delivery. The oral cavity is also versatile with different areas of the oral cavity exhibiting different permeability characteristics. The oral mucosa is between 4 and 4000 times more permeable than the skin (Galey *et al.,* 1976). The high permeability and excellent blood supply and rapid onset of action make the oral mucosa an ideal drug delivery site for acute conditions such as angina and pain. Delivery *via* the oral mucosa can enable rapid delivery to the circulation, smaller dosing and better bioavailability for some drugs.

Limitations and Drawbacks of the Oral Mucosa For Drug Delivery Applications

There are problems associated with transmucosal delivery which include: (i) finding drugs that can overcome the permeability barrier, (ii) protecting biological drugs such as peptides and proteins from enzymatic degradation, (iii) finding drugs that are able to penetrate the mucus coating of the epithelium, (iv) finding drugs that have an acceptable taste to patients and (v) designing delivery devices that are not easily swallowed by accident (Sudhakar *et al.,* 2006). The oral mucosa has a small surface area compared to skin and limited exposure times make this delivery route most appropriate for drugs exhibiting high therapeutic potency as relatively small quantities of drug can be delivered (Madhav *et al.,* 2009).

The oral cavity is constantly bathed in saliva, produced by the salivary glands to provide protection and lubrication in the mouth. The volume of saliva varies but it is usually between 0.5 and 2 L per day with a pH between 5.5 and 7 (Shojaei 1998). The constant washing of the oral cavity by saliva can limit the length of exposure to a drug or delivery system, dilution of the drug in the oral cavity and washing of a drug into the gastrointestinal tract. Saliva can also be beneficial in providing a highly hydrated environment in which to dissolve the drugs and wash drugs around the entire oral cavity. Mucoadhesive systems enable longer exposure of a delivery system to the mucosa (Madhav et al., 2009).

Mastication, the action of chewing, can both hinder drug delivery in the oral cavity and enhance it. Mastication can cause damage to or loss of mucoadhesive drug delivery systems however, it can also be utilised by loading drugs into chewing gum which are released when the gum is chewed (Maggi et al., 2005).

Efforts to overcome some of these problems include research into permeability enhancers and enzyme inhibitors (Shojaei 1998). However, as of yet no oral mucosal products are available commercially that use permeability enhancers (Madhav et al., 2009).

1.2 Head and Neck Cancer: The Clinical Challenge

Introduction to Head and Neck Cancer

Head and neck cancer is the 15th most common cancer in the UK with around 5,000 new cases being diagnosed every year (CancerResearchUK 2009). In all regions of the UK male incidence rates are higher compared to female incidence, a trend seen across the world (IARC 2004). Worldwide there were an estimated 405,000 new cases of oral cancer in 2002 (IARC 2004; CancerResearchUK 2009). The incidence of oral cancers worldwide varies widely between countries. Figure 1.2 gives a pictorial idea of the variation seen worldwide in men and women (IARC 2004).

Oral cancer includes cancers of the mouth cavity (30%), tongue (30%), oropharynx, hypopharynx and piriform sinus (combined 30%) and lip (6%) (CancerResearchUK 2009). The majority of oral cancers (over 90%) are oral squamous cell carcinomas (OSCC) (CancerResearchUK 2009), predominantly caused by epithelial exposure to alcohol and tobacco (Argiris et al., 2008). Figure 1.3 shows how combined alcohol consumption and tobacco increases the relative risk of developing OSCC (CancerResearchUK 2009). Those who smoke and drink heavily are over 35 times more likely to develop oral and pharyngeal cancer compared to those who abstain from both (Blot et al., 1988). In South Asia the incidence of oral cancer is high due to the habit of chewing betel quid (also known as paan) and related areca nut use (CancerResearchUK 2009). Human papillomavirus (HPV), poor

oral hygiene, immunocompromised individuals including those suffering from HIV/AIDS, deprivation, infections such as syphilis and candidiasis, diseases including diabetes and low fruit and vegetable intake have all also been identified as factors which contribute to OSCC (Scully and Bagan 2009).
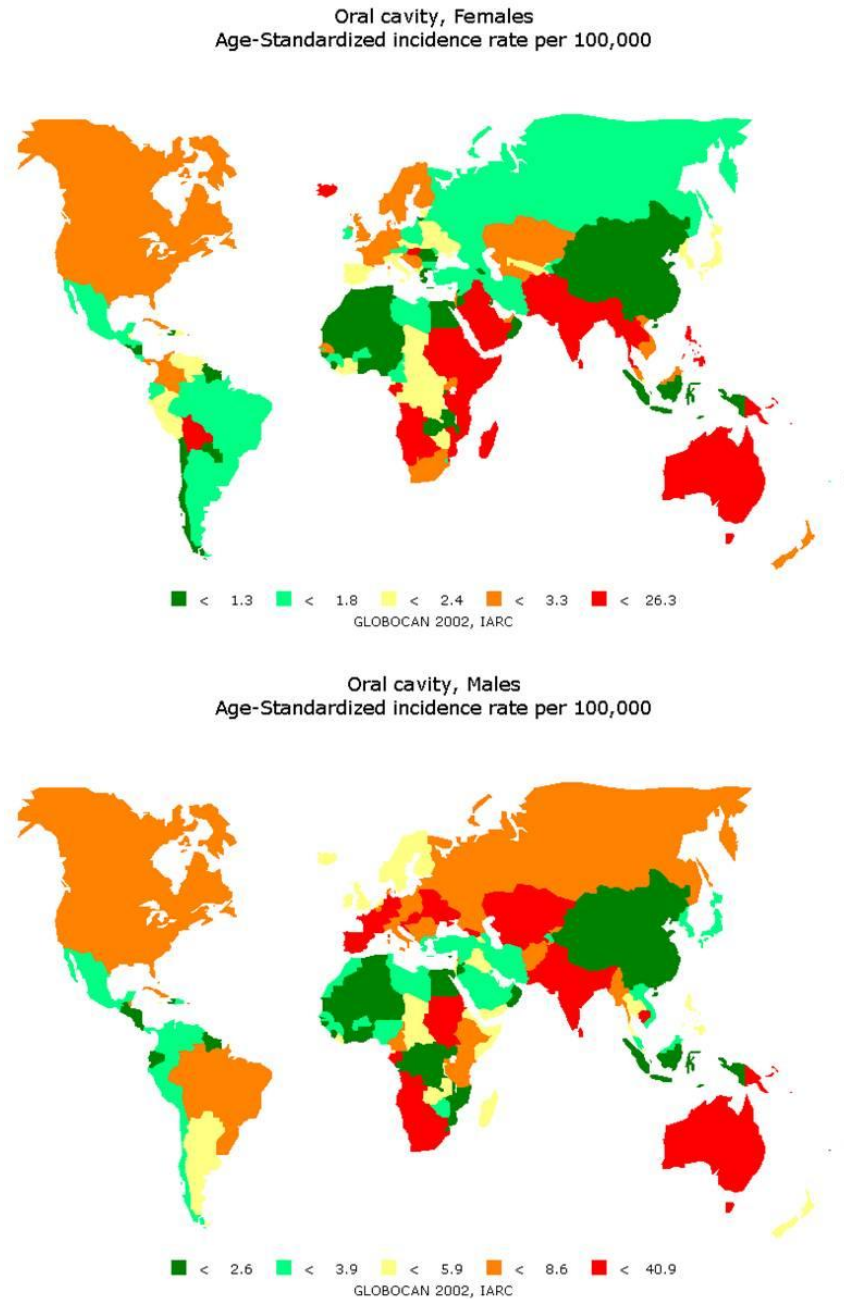
Figure 1.2 Incidence of oral cancer globally for females (top) and males (bottom). Reproduced from (IARC 2004).

Figure removed for copright purposes

Figure 1.3 Relative risk of developing oral and pharyngeal cancer based on tobacco and alcohol consumption (US measures).
Graph reproduced from (CancerResearchUK 2009)

The outlook for patients diagnosed with cancer of the head and neck is poor, especially if diagnosed with late stage cancer. For the one third of patients who present with stage I or II of the disease there is an 80% or 65% chance of being cured, respectively (Yao *et al.,* 2007). Unfortunately, for the two thirds of patients who present in the late stages of the disease the prospects are worse as treatment becomes harder and the disease progresses to other parts of the body. Stage III is defined as when the tumour can be seen in the lymph nodes and stage IV when the tumour is metastatic (CancerResearchUK 2005). 5 year survival rates for patients who present with stage III or IV are between 10 and 40%.

One reason for this poor survival rate is because detection of OSCC is difficult and always requires histological verification, often leading to late detection. A recent study by Rogers *et al*., looked at the reasons patients delayed in presenting symptoms of oral cancer to a medical specialist (Rogers *et al.,* 2010). The majority of patients felt the initial symptoms (non-healing ulcers, sore mouth or a persistent lump) were trivial and believed they would heal of their own accord. This study highlights the need for greater awareness of the symptoms of oral cancer to encourage patients to present their symptoms earlier, and improve disease outcomes (Rogers *et al.,* 2010).

Despite advances in surgical techniques and post-operative therapy, there has been no significant improvement in patient survival rates over the last 20 years (Scully and Bagan 2008). Hence, there is a major focus for developments in novel diagnostic and drug delivery systems for OSCC (Harrington *et al.,* 2005).

From healthy oral mucosa to OSCC

Figure 1.4 shows the various stages of squamous cell carcinoma development from healthy epithelium to carcinoma *in situ*. The terminology used to describe different stages of OSCC varies; however, here we will use the oral scheme of terminology which has been recommended by the World Health Organisation (WHO) (Speight 2007). There are five distinct categories of diagnosis which relate to a variety of different architectural and cytological features. Hyperplasia is used to describe potentially malignant lesions such as leukoplakia and erythroplakia which do not show signs of dysplasia. The features of the different grades of dysplasia are described in Table 1.1.
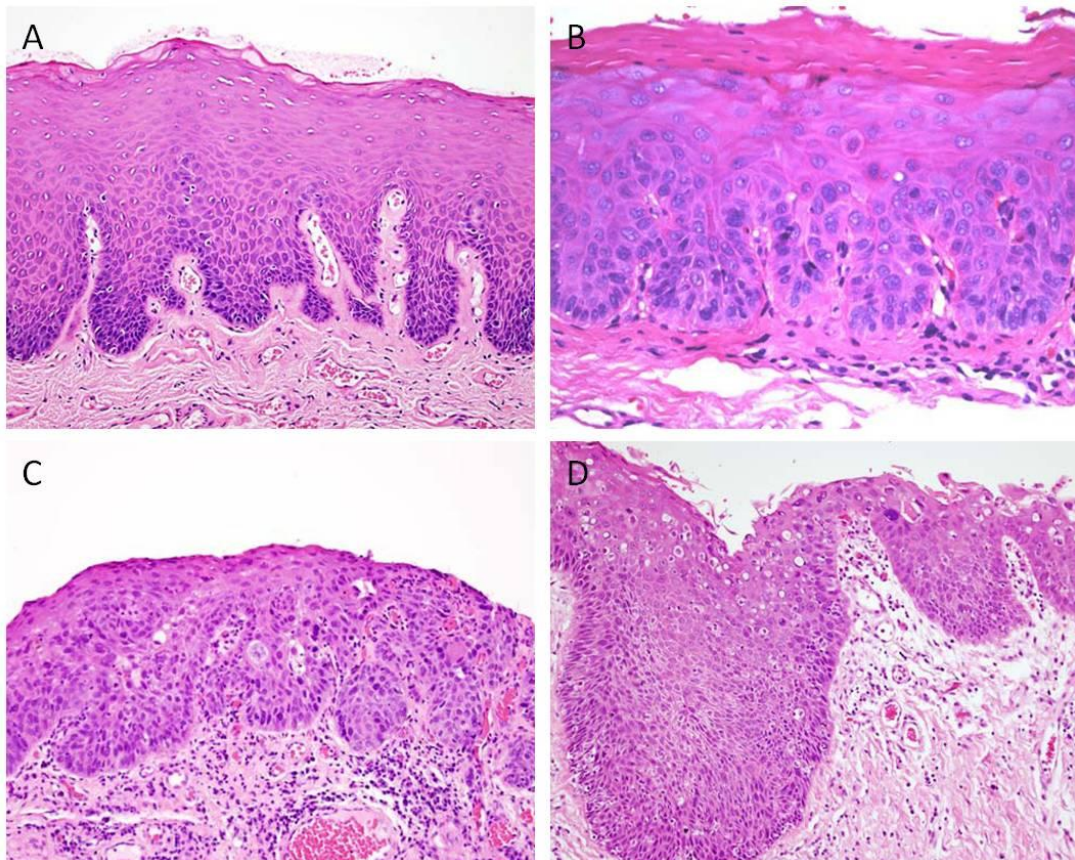
Figure 1.4 Examples of the appearance of haematoxylin and eosin stained histology sections showing the progression from mild dysplasia (A), to moderate dysplasia (B), severe dysplasia (C) and carcinoma *in situ* (D) in patients.
Image from (Speight 2007)

	Hyperplasia (leukoplakia & erythroplakia)	Mild dysplasia (grade I)	Moderate dysplasia (grade II)	Severe dysplasia (grade III)	Carcinoma *in situ*
Proliferative changes	N/A	Proliferation or hyperplasia of cells in basal 1/3 of epithelium	Proliferation of atypical cells in basal 2/3 of epithelium	Abnormal proliferation throughout epithelium	Throughout the epithelium
Cytological changes	None	Slight cytological atypia (mild cell and/or nuclear pleomorphism) Hyperchromatism	Hyperchromatism Prominent cell and nuclear pleomorphism Abnormal mitotic figures in basal layers	Prominent pleomorphism Abnormally large nuclei Multiple nucleoli Abnormal suprabasal mitotic figures Apoptotic bodies	Full thickness cytological changes as seen in earlier stages
Architectural changes	Thickened epithelium Hyperkeratosis	Minimal Basal cell hyperplasia	Loss of basal polarity Atypical hyperplasia Bulbous rete pegs Hyperkeratosis Increased cellular density	Loss of stratification Abnormal keratinisation Keratin pearls Bulbous rete pegs (sometimes with lateral extensions and branches) Thickened epithelium, or epithelial atrophy Increased cellular density Basal cell hyperplasia	Full thickness architectural changes as seen in earlier stages
Malignant transformation	0.1-2% per year progress to cancer	< 5% progress to cancer	30% progress to cancer	50% progress to cancer	

Table 1.1
Features of the different stages of dysplasia. (Information from (Speight 2007))

Some pathologists describe carcinoma *in situ* as a pre-malignancy however, others see carcinoma *in situ* as a malignant lesion, without visible signs of invasion (Speight 2007). Diagnosis of invasive carcinoma can be difficult and is often subjective. In some cases breaches in the basement membrane make it clear that the lesion is invasive although inflammatory infiltrates and the position of the pathological section make it unclear (Speight 2007). Islands of epithelial cells with keratinisation in the connective tissue are a clear indication of invasion.

Current treatments for OSCC

The majority of OSCC cases are treated by surgical resection followed by radiation therapy (Argiris *et al.,* 2008). Recently, focus has moved towards using chemotherapy alongside surgery and radiotherapy (Yao *et al.,* 2007).

Surgical intervention

The anatomy of the oral cavity along with its role in essential functions means removing tumours by surgery whilst maintaining speech and swallowing, is very challenging. Surgical advances, such as transoral laser microsurgery, have improved the prognosis with improved maintenance of function (Argiris *et al.,* 2008). However, there are still limitations, the most significant being the difficulty of identifying all the cancerous regions of the oral mucosa leading to incomplete excision of tumours and disease recurrence (Argiris *et al.,* 2008).

Radiotherapy

Radiotherapy is used instead of surgery to treat early tumours or if the tumour location means there will be serious functional loss from surgical excision (Argiris *et al.,* 2008). Radiotherapy works by exposing cancerous tissues and associated lymph nodes to ionizing radiation. This radiation damages the DNA within cells either directly or through the production of free radicals from ionized water. This DNA damage can lead to cell death *via* apoptosis or reduced cell division. Cancer cells have a reduced ability to repair damaged DNA compared to healthy cells however, healthy cells surrounding the tumour are also damaged leading to severe toxic side effects (Argiris *et al.,* 2008). Research into radiotherapy aims to improve the effectiveness of treatment whilst limiting toxic side effects including mucositis and xerostomia (dry mouth).

Fractionated radiotherapy is a method which increases the dose intensity of radiotherapy while reducing the overall exposure time compared to conventional radiotherapy. An analysis of 15 randomised trials on fractionated dose radiotherapy found an 8% improvement in 5 year survival rates with hyperfractionated radio therapy (delivering 2-3 fractions daily with a reduced dose per fraction) compared to conventional fractionated radiotherapy (1 fraction per day) (Mazeron *et al.,* 2009).

Chemotherapy

Chemotherapy was previously used to alleviate symptoms of OSCC. However, it now plays a central role in curative programmes particularly for more advanced or inoperable tumours (Argiris *et al.,* 2008). The chemotherapeutic agents most commonly used in the treatment of OSCC include Doxorubicin, Paclitaxel, Cisplatin and 5-Fluorouracil (5-FU), although many more anti-cancer drugs exist.

Unfortunately, chemotherapy is associated with high toxicity and severe side effects which often limit their effectiveness. Attempts to reduce systemic toxicity and improve the anti-tumour effects have led to the development of complex chemotherapy regimes which use multiple drugs delivered in pulsed or phased delivery schedules. Chemotherapy requires good vasculature to deliver chemotherapeutic agents into cancerous regions. The centres of solid tumours have a poor blood supply making it difficult to deliver chemotherapeutics into these areas. This poor blood supply also makes the central regions hypoxic and resistant to radiotherapy (Ljungkvist *et al.,* 2000). Fortunately, OSCC cancers have relatively good vasculature compared to other cancers making chemotherapy more effective.

Chemoradiotherapy

Chemoradiation therapy, i.e. combined chemo and radiotherapy, gives survival rates similar to surgical excision for early lesions but function preservation is improved with chemoradiation (Yao *et al.,* 2007). For more advanced tumour progression chemoradiation therapy is often combined with surgical excision. When compared to radiotherapy alone, four out of five randomised trials showed a significant improvement in overall survival using chemoradiation (Yao *et al.,* 2007). Platinum based chemotherapeutic agents, such as Cisplatin, demonstrated greatest improvement and the majority of benefit from concomitant chemoradiotherapy is seen in locoregional disease control with only marginal effects seen at metastatic sites (Mazeron *et al.,* 2009).

It is believed chemoradiation gives improved survival rates by preventing regrowth of tumours between doses of radiation and inhibiting the repair of radiation damaged DNA (Yao *et al.,* 2007). Unfortunately, local morbidity, mucositis and toxicity are high following chemoradiation (Yao *et al.,* 2007). There are a number of studies investigating the best combination of chemotherapeutics and dosages with the aim of reducing morbid effects (Fuwa *et al.,* 2007).

1.3   Current problems with OSCC drug delivery

Methods of delivery

Systemic administration of chemotherapeutics by intravenous injection is the most common method of delivery. The drug is delivered directly into the circulation and ensures a known concentration of drug is delivered. Systemic circulation avoids problems experienced with oral delivery of drugs including drug degradation in the acidic and enzymatic environment of the gastrointestinal tract and drug loss caused by the first pass effect. The main drawback with intravenous drug delivery is that it is non-specific which results in drugs reaching all areas of the body. This causes side effects in many healthy areas of the body but also enables chemotherapy to reach and treat unknown metastasises. Problems associated with systemic delivery include the permeability of drugs into poorly vascularised regions of tumours, systemic side effects and solubility of hydrophobic drugs into injectable liquids at therapeutic concentrations.

For the treatment of accessible solid tumours, drugs can be directly injected into the tumour. Intra-tumoural delivery does not rely on vasculature or penetration of drug across tissues to get the drugs to the disease site. The drug must still be able to diffuse throughout the tumour tissue once it has been injected to ensure complete distribution of drug within the tumour. Intra-tumoural injection is not common and can be painful; however, there is research into its use in particular circumstances including this Phase II study for locally recurrent tumours (Duvillard *et al.,* 2004).

Local drug delivery is the delivery of drugs topically directly to the site of disease. The main advantages of local drug delivery include (i) reduced off target side effects, (ii) more efficient delivery: less drug is wasted or lost elsewhere in the body, (iii) targeted delivery: drugs can be targeted to the site of action more easily when delivered locally. Topical drug delivery may be a possibility for dysplastic lesions and early invasive SCC. It is probably not viable for larger more established OSCC and stage IV metastatic disease. There are several challenges which need to be overcome for topical delivery to be successful, most importantly the permeability barrier of the oral mucosa (described on page 16).

Targeting cancer

The ability to target drugs directly to tumours would greatly improve chemotherapies enabling higher doses to be used and better efficacy and cure rates to be achieved. Unlike antibiotics which act on foreign organisms within the body and target bacterial proteins; cancer treatments act on cancerous human cells which are inherently similar to healthy human cells making treatment more challenging. Many chemotherapeutics target highly proliferative cells by

preventing cell division or damaging DNA, this however, leads to damage elsewhere in the body with healthy rapidly dividing cells. The normal oral mucosa is particularly susceptible to such damage, which presents as oral mucositis, due to the high proliferation rate of basal oral keratinocytes.

Molecular targeted therapy

There is currently great interest in developing drugs which target specific molecules which are found in higher concentrations in cancer cells compared to in healthy cells. Molecular targets such as growth factors, growth factor receptors, signal transduction genes, oncogenes and hormones are all being investigated as potential sites for targeting chemotherapy (Hamakawa *et al.,* 2008). Attempts to inhibit cell motility, inhibit tumour angiogenesis and to increase apoptosis have also been investigated using molecular targets involved in these processes. Targeting epidermal growth factor receptors (EGFRs) to inhibit OSCC proliferation is attractive as EGFRs are over expressed in many solid tumours including head and neck tumours and this is often an indication of poor prognosis (Nicholson *et al.,* 2001). EGFRs are targeted by tyrosine kinase inhibitors such as Gentifinib which cause cell cycle arrest and thus prevent proliferation of malignant cells (Hamakawa *et al.,* 2008). An *in vitro* study into the effect of Cetuximab (Erbitux®) (a monoclonal antibody which acts as an antagonist to the EGFR), resulted in reduced cell proliferation, enhanced radio-sensitivity and increased apoptosis of OSCC (Huang *et al.,* 1999). Cetuximab was later shown to improve survival rates of patients with stage III/IV recurrent and/or metastatic OSCC in a Phase III clinical trial (Vermorken *et al.,* 2007). Another target is the enzyme cyclooxygenase 2 (COX-2). Levels of COX-2 are increased in several cancers including head and neck relative to healthy surrounding tissue (Hamakawa *et al.,* 2008). Elevated COX-2 levels decrease radio sensitivity so it is hoped that by targeting COX-2 the effects of radiation therapy can be improved (Hamakawa *et al.,* 2008).

Research into predictive markers which are able to indicate the effectiveness of a specific molecular therapy based on the molecular finger-print of an individual patient's disease could increase the effectiveness of these therapies in the future. Predictive markers could also prevent treatments being dismissed during development when they may only be effective in a subset of OSCC cases. Molecular targeted therapies and their future use is reviewed in (Lorch *et al.,* 2009).

Passive targeting

The next method of tumour targeting described here utilises the unique pathophysiology of tumours compared to healthy tissues. Rapidly growing tumours require a good supply of nutrients and oxygen which is achieved with extensive angiogenesis in and around the tumours. This disorganised and leaky tumour hypervasculature along with poor lymphatic

drainage and an increase in permeability enhancing factors can be exploited to encourage passive targeting of macromolecules to tumours; a process known as the enhanced permeability and retention (EPR) effect (Maeda *et al.,* 2000).

First discovered in 1986 (Matsumura and Maeda 1986) the EPR effect passively targets and retains macromolecules in all but a few solid tumours. As the tumour endothelium is poorly formed it is no longer a continuous barrier to materials in the blood stream enabling materials not usually able to leave the vasculature to pass into the tumour. Macromolecules above 40 kDa (the renal excretion threshold) accumulate in solid tumours and can be seen at concentrations 10-30 times higher in tumours than in systemic blood. If the macromolecule is delivered *via* the tumour feeding artery this difference in concentration can be up to 2000 times (Maeda *et al.,* 2009). Not only are these macromolecules found at higher concentrations in tumours, poor lymphatic drainage means they are also retained within the solid tumour for days to weeks (Maeda *et al.,* 2000; Maeda *et al.,* 2009).

This passive targeting by the EPR effect can be seen in all hypervascular tumours (Maeda *et al.,* 2009), and has led to significant interest in the development of macromolecular cancer therapies. Currently, the majority of chemotherapy agents are low molecular weight compounds and therefore there is great interest in encapsulating traditional low molecular weight drugs into macromolecular carriers including: micelles, liposomes and most recently polymersomes (Discher *et al.,* 2007). The EPR effect is already utilized in imaging of solid tumours, for example the accumulation of radioactive gallium (Maeda *et al.,* 2000). The EPR effect also has potential to be exploited in the field of polymer therapeutics which includes macromolecular polymer drugs and polymer drug conjugates (Duncan 2003). The enhanced retention of materials by the EPR effect does not necessarily lead to increased uptake of the material intracellularly (Wang and Thanou 2010).

Gene Therapy

Gene therapy is the delivery of DNA or RNA into cells to treat diseases which have a genetic basis, or to deliver a gene into the body to perform a specific function, for example converting pro-drugs into cytotoxic agents within target cells for cancer therapy. Gene therapy has been the subject of much research for many years yet no gene therapy treatments have so far gained FDA approval for clinical use (FDA 2009). One of the biggest challenges associated with gene therapy is the efficient and safe delivery of genetic material intracellularly at high enough concentrations to exert a therapeutic effect. In some cases gene therapy must also be targeted to specific cells so the effect is only delivered where it is therapeutically required (Harrington *et al.,* 2005). Many of the problems with gene therapy are associated with the use of viral vectors to deliver therapeutic genes into cells. There has therefore been a growth of interest in developing non-viral delivery vectors such as liposomes and polymersomes.

There has been a lot of research into gene therapeutics for oral cancer (Xi and Grandis 2003). However, despite promising results *in vitro* and in animals there is still no strong evidence to suggest that gene therapy for oral cancer is effective in humans (Shillitoe 2009). Gene therapy for head and neck cancer has been recently reviewed in (Scully and Bagan 2008; Thomas and Grandis 2009).

1.4   Novel delivery vectors

Drug Delivery Vectors

In order for the issues highlighted in the previous section regarding the challenges associated with drug delivery to OSCC and other cancers to be overcome there needs to be novel methods and techniques to deliver drugs. One area of research which has been extensively studied is that of novel delivery vectors.

Drug delivery vectors work on the principle that encapsulated drug molecules within a delivery device can be protected from damaging biological environments, have improved transport characteristics and can provide a method to target drugs to a specific site. These improvements can be achieved without altering the structure or activity of the drug and provides an opportunity to design a delivery vector which is able to optimally deliver the drug to its site of action and thus improve bioavailability. Delivery vectors can also be designed to give controlled release profiles, improved circulation times and better penetration across the epithelium. Materials such as some peptides and nucleic acids which are highly hydrophilic and highly susceptible to enzymatic degradation show limited diffusion across epithelia and could benefit greatly from an appropriate delivery carrier (de la Fuente *et al.,* 2008).

Drug delivery vectors are currently being studied for both local and systemic delivery purposes. For local drug delivery, vectors should be designed to deliver their payload into the epithelium, at the site of disease. For diseases such as OSCC and potentially malignant lesions, this means delivery across the permeability barrier and into the basal cells. For systemic drug delivery, delivery vectors have been designed to protect the drug from excretion and immune or reticulo-endothelial destruction once in the circulation. "Stealth" nanoparticles, coated in a material not detected by the immune and reticulo-endothelial systems are also being developed as a means to increase circulation times.

Most drug delivery carriers can be categorised as hydrophobic or hydrophilic. Hydrophobic drug carriers have the advantage of exhibiting slow sustained release but can be unstable in biological fluids, show poor interaction with biological surfaces and poorly encapsulate hydrophilic macromolecules (de la Fuente *et al.,* 2008). Hydrophilic drug carriers on the contrary adhere well to biological surfaces, show a strong affinity to hydrophilic macromolecules but have a fast release profile (de la Fuente *et al.,* 2008). Combination

therapies such as hydrophilic coatings on hydrophobic nanoparticles have been designed to improve transport across mucosal surfaces whilst retaining the slow release profile of hydrophobic carriers. These hydrophilic coatings include materials such as poly(ethylene glycol) (PEG) and chitosan.

Copying nature: phospholipid membranes

Many drug delivery vectors which have been studied in recent years, and the delivery vectors used in this project, utilise the self-assembling properties of amphiphiles in aqueous solutions. Self-assembling amphiphiles, which produce stable and versatile delivery vectors, are based on the properties of the plasma membranes of cells. Phosopholipid cell membranes are comprised of many amphiphilic phospholipids containing a hydrophilic (polar) head group and two hydrophobic (non-polar) fatty acid chains (Alberts *et al.,* 2002). Amphiphilic molecules such as these self-assemble into vesicular or cellular structures when in aqueous solution to achieve the most entropically favourable configuration.

Lipid bilayer membranes are essential for the cell to maintain well defined, intra- and extra-cellular environments (Alberts *et al.,* 2002). This compartmentalisation allows the cell to have discrete compartments within the cell for specialised functions. All organelles within the cell are enclosed by membranes, enabling biochemical gradients to exist between parts of the cell and allowing distinct biochemical reactions to take place in the right place and at the right time within the cell. The permeability of materials across the cell membrane is determined by Fick's law of diffusion. If a material is highly hydrophilic it will not be soluble in the hydrophobic membrane and therefore will not diffuse across the membrane, this is the case for salts. If however, a material is partially soluble in the membrane and soluble in water then the material is able to passively diffuse across the membrane, this is the case for glucose. If a material is highly hydrophobic and not soluble in water then this material will remain trapped within the membrane. Therefore, the transport of materials which are not able to diffuse across these membranes is regulated and controlled by transmembrane proteins. Without this segregation the level of complexity within the cell would not be possible on such a small scale.

Liposomes

The first membrane-enclosed structures designed in a laboratory in the 1960s were liposomes made from naturally derived phospholipids (Figure 1.5) (Bangham 1961). Bangham used these liposomes to look at the effects of various stimuli and substances on cell membranes as well as to study membrane permeability. Liposomes have now been developed for use as drug carriers for hydrophobic drugs as well as carriers of DNA for transfection (Lasic and Papahadjopoulos 1998). Liposomal preparations of anti-cancer therapies are clinically available for a number of agents including Daunorubicin and Doxorubicin (Park 2002). Liposomes are used to increase the solubility of lipophilic therapeutic agents and show passive targeting to tumours *via* the

EPR effect, described on page 27. However, there are several limitations with liposomal preparations. Liposomes exhibit low circulation times in the bloodstream due to removal by macrophages and the reticulo-endothelial system. The release profile of materials encapsulated into these liposomes is also hard to control; some material leaks out quickly while other material is never released (Lasic 1997; Duncan 2003; Discher *et al.,* 2007).

To increase circulation times, stealth liposomes coated with poly(ethylene glycol) (PEG) to reduce detection and removal by the reticulo-endothelial system, have been developed (Lasic 1994).

Polymer amphiphiles

The difficulties experienced with liposomes led to the generation of drug delivery vectors comprised of synthetic, polymer amphiphiles. The configuration created by the self-assembly of polymer amphiphiles depends on the concentration of the molecules and the ratio of hydrophobic to hydrophilic portions within an amphiphilic block co-polymer (Discher *et al.,* 1999; Discher and Eisenberg 2002; Du *et al.,* 2005; Smart *et al.,* 2008). Configurations include spherical micelles, worm-like micelles, lamellar gels and polymersomes (Figure 1.6) (Battaglia 2005). The morphology is dictated by the time-average molecular shape the diblock co-polymer has in an aqueous solution. This could be a cylinder (membrane or vesicle), a wedge (worm like micelle) or cone shaped (spherical micelle) (Discher and Eisenberg 2002). This is described by the packing parameter, p.

$p = v/al_c$

The packing parameter (p) is defined by the volume of the hydrophobic block (v), the length of the hydrophobic block (l_c) and the surface area between the two blocks at the interface between them (a) (Figure 1.7) (Battaglia 2005).

Building blocks: Phospholipid eg. Phosphatidylcholine

Hydrophilic head group

Hydrophobic tails (fatty acids)

Building block: Amphiphilic block co-polymers

Hydrophilic polymer chain eg. polyethylene glycol

Hydrophobic polymer chain eg. polybutylene oxide
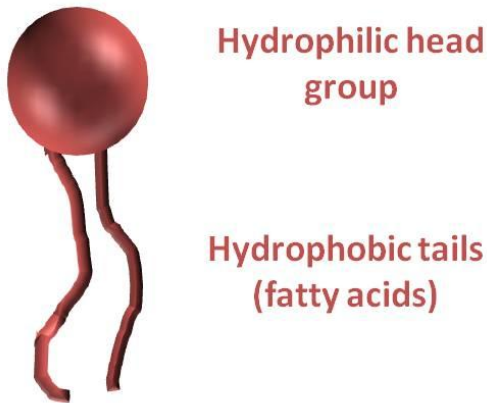
Cross section through liposome

Cross section through polymersome
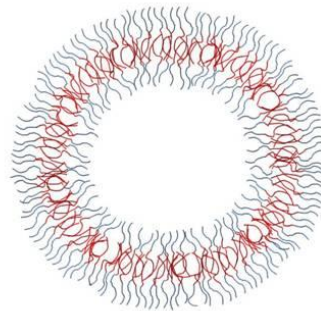
Liposome
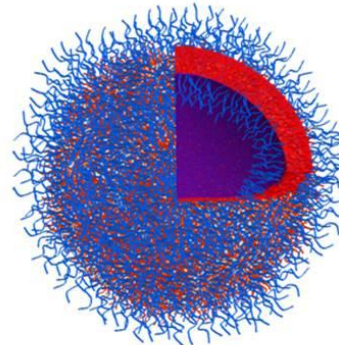
Polymersome

Figure 1.5 Illustration of liposomes and polymersomes and their building blocks. Diameters are generally between 50 – 500nm.

1/2 < p ≤ 1

Polymer vesicle (polymersome)

1/3 < p ≤ 1/2

Polymer cylindrical micelle

p ≤ 1/3

Polymer spherical micelle
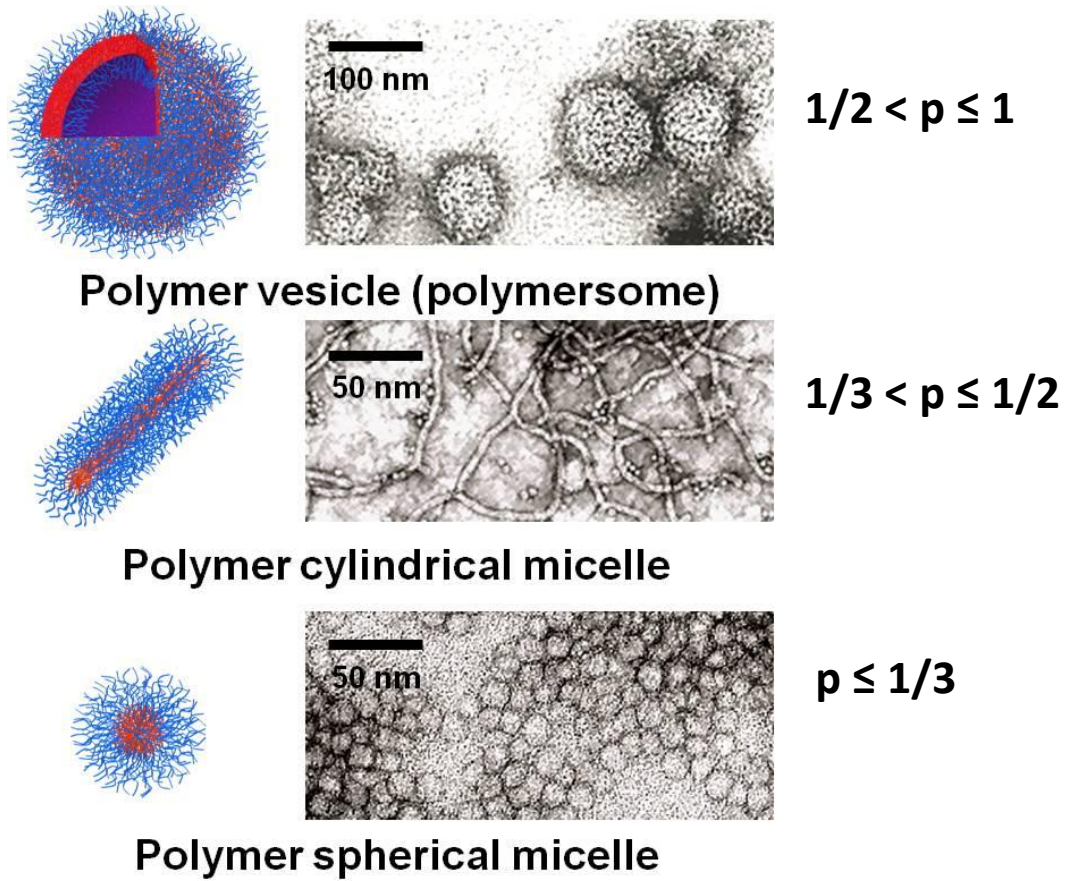
Figure 1.6 Macromolecular structures depend on the packing parameter, p.
Reproduced from (Battaglia 2005) (Smart *et al.,* 2008)
.
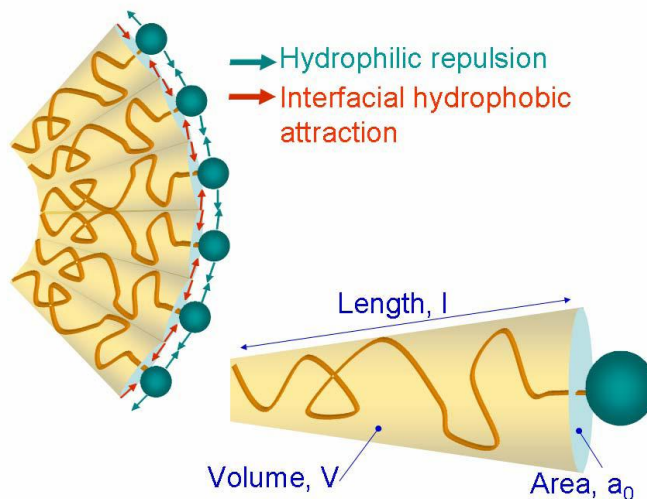
Figure 1.7 Geometric parameters of a block co-polymer amphiphile.
Reproduced from (Battaglia 2005)

Major advances in polymer chemistry, such as reversible addition–fragmentation chain transfer (RAFT) and atomic transfer radical polymerisation (ATRP) have opened up limitless possibilities for block co-polymer formulations and therefore numerous structures (Matyjaszewski and Spanswick 2005). The versatility of block co-polymers mean structures created from them can be designed for a desired application with different stabilities, fluidities and dynamic behaviours depending on the molecular weights and chemistries of the blocks used (Discher and Eisenberg 2002).

Micelles

Polymeric micelles are self-assembling polymer structures which contain a hydrophobic core surrounded by a hydrophilic corona. Anti-cancer drugs can be chemically conjugated to polymers within the micelle or physically trapped within the micelle by taking advantage of the hydrophilic effect. For this reason there has been great interest in developing micelles as anti-cancer delivery vehicles. There are clinical trials underway including: Phase I trials for micelles encapsulating cisplatin (NC-6004) and SN-38 (NK102) and a Phase II trial of the paclitaxel-incorporated micelle, NK105, against stomach cancer (Matsumura 2008).

Polymersomes

This project investigates the use of the membrane-enclosed vesicle structures known as polymersomes (Figure 1.5). Polymersomes, also known as polymer vesicles, are created *via* the self-assembly of synthetic amphiphilic block co-polymers (Discher *et al.,* 1999).

One of the most extensively studied applications for polymersomes is as a delivery vector for therapeutic agents. The membrane-enclosed core is hydrophilic and can encapsulate hydrophilic materials in aqueous solution; whereas the core of the membrane, defined by the bilayer interdigitation of the co-polymer chains, is hydrophobic. This means that polymersomes can also be used to encapsulate hydrophobic materials such as anti-cancer drugs (Battaglia *et al.,* 2007) (Lomas *et al.,* 2007), hydrophilic materials such as nuclei acids (Lomas *et al.,* 2007) or can be used to deliver hydrophilic and hydrophobic materials simultaneously for synergistic treatment of cancer (Discher and Ahmed 2006).

Polymer amphiphiles can have higher molecular weight polymer chains compared to phospholipids creating highly entangled bilayer membranes with improved stability compared to liposome membranes (Battaglia and Ryan 2005). Both liposomal bilayer membranes and polymersome membranes have the ability to remodel and heal if damaged due to the hydrophobic effect (Aranda-Espinoza *et al.,* 2001).

The permeability of polymersome membranes can be adjusted using different chemistries. It is possible to make polymersome membranes 10 times less permeable to water than phospholipid bilayers (Discher *et al.,* 1999) or more permeable to select materials (Battaglia *et al.,* 2006)

depending on the application. This adjustment of polymersome properties means they can be designed to be less leaky and more retentive than liposomes, ideal properties for drug delivery vectors. Li *et al*., have developed polymersomes which are stable for 4 months at 4 °C (Li *et al., 2007*). Comparing this to liposomal formulations, some of which only have a shelf life of 1 month, highlights one advantage of polymersomes for clinical applications (Epstein *et al., 2008*).

Many anti-cancer compounds are only effective once delivered inside the cell or the nucleus. It is therefore desirable to deliver anti-cancer drugs intracellularly reducing off-target toxicity and clearance by the lymphatic system. Duncan *et al*., have shown that the safe dosing of Doxorubicin (DOX) can be four or five times higher when it is conjugated to the co-polymer N-(2-hydroxypropyl) methacrylamide and delivered intracellularly, suggesting toxicity is due to extracellular DOX (Duncan 2003). The versatility of polymersomes allows them to be designed to be internalised by cells (Discher and Eisenberg 2002; Ahmed *et al., 2006*). The degradation and subsequent release of cargo from polymersomes can also be adjusted. pH sensitive polymersomes (Du *et al., 2005*), oxidative species (Cerritelli *et al., 2007*) and biodegradable polymers all degrade within the body in response to different stimuli (Meng *et al., 2005*; Ben-Haim *et al., 2008*; Rameez *et al., 2008*) allowing them to be tailored to the specific application and drug/destination of interest. For example, the pH sensitive polymersomes studied in our laboratory release their cargo into the cytosol when the polymersomes experience a drop in pH in the cell's endosomal compartments (Lomas *et al., 2008*; Massignani *et al., 2010*). These polymersomes are able to deliver encapsulated material into the cytosol of cells when internalised *via* endocytosis (Massignani *et al., 2008*).

Materials thus far encapsulated into polymersomes include DNA for transfection (Lomas *et al., 2007*; Lomas *et al., 2008*), anti-cancer drugs for intercellular delivery (Discher *et al., 2007*) and contrast agents for *in vivo* imaging (Ghoroghchian *et al., 2005*). The chemotherapeutic agents which have been successfully encapsulated include Doxorubicin (Choucair *et al., 2005*; Upadhyay *et al., 2009*), Paclitaxel (Li *et al., 2007*), Docetaxel (Upadhyay *et al., 2010*) and a combination therapy of Paclitaxel and Doxorubicin (Ahmed *et al., 2006*). Other groups have developed polymersomes which can act as haemoglobin substitutes (Arifin and Palmer 2005; Rameez *et al., 2008*).

Ahmed *et al*. have shown that using polymersomes affects not only the distribution of the chemotherapeutic agent but also the efficacy of the cancer therapy (Ahmed *et al., 2006*). In an *in vivo* murine breast carcinoma xenograph model they showed increased tumour shrinkage with systemically delivered doxorubicin and paclitaxel encapsulated in PEG-PLA (poly(ethylene glycol) poly(lactic acid)) polymersomes compared to free drug administration (Figure 1.8) (Discher and Ahmed 2006). Saline and empty polymersome controls showed no

effect on the rapidly growing tumours whereas the free drugs slowed the growth but did not reduce the size of the tumour compared to the size at the time of treatment. Further analysis showed the level of apoptosis (programmed cell death) was twice as high with the encapsulated drug when compared to free drugs alone (Discher *et al.,* 2007). This has yet to be shown for oral cancer or for topical delivery. Polymersome delivery into a xenograft murine model of oral carcinoma has been investigated in (Murdoch *et al.,* 2010).
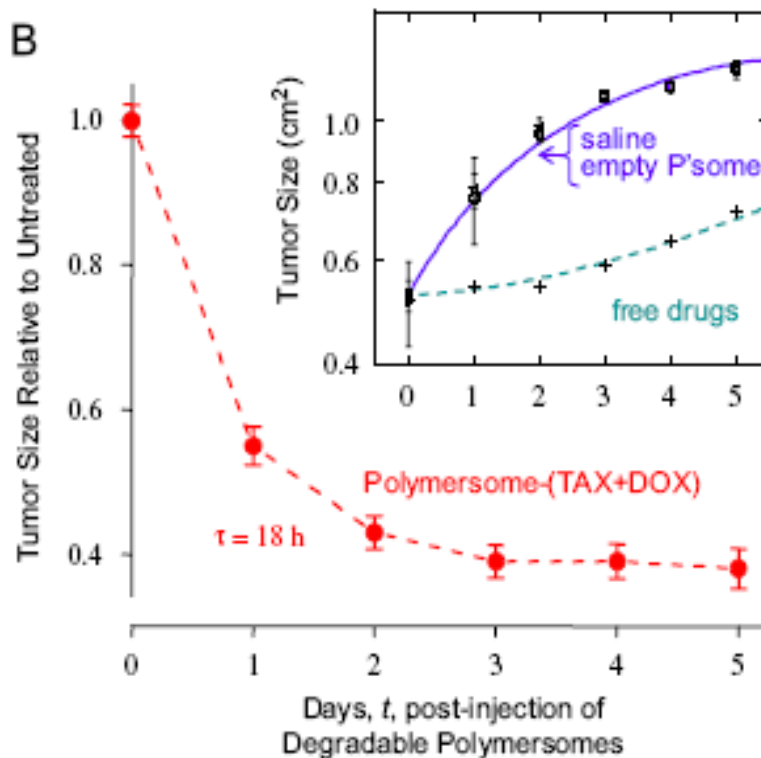
Figure 1.8 Polymersomes loaded with anti-cancer drugs shrank tumours compared to free drug and polymer alone in this *in vivo* study (Discher *et al.,* 2007).

Targeting nanoparticles

There are different ways to target drugs to cancer cells and thus reduce side effects. These include the molecularly targeted therapies described previously on page 27. Targeting *via* cancer specific biomarkers is growing in popularity. These biomarkers which include: mutant genes, RNAs, proteins, lipids, carbohydrates and small metabolite markers are specific to the cancerous tissue and can provide a specific target for drug delivery systems (Wang and Thanou 2010). Combining knowledge of biomarkers and development of nanoparticle delivery systems has made attaching ligands or bio-recognition molecules onto the surface of a drug delivery system possible. This enables targeting of the delivery system to sites of disease and means the drug can be favourably delivered there, reducing side effects. Many biomarkers investigated are cell membrane receptors, as ligands to these can not only target the delivery

systems but also promote receptor mediated endocytosis, delivering the drug intracellularly, where the drug will be active (Wang and Thanou 2010).

Important considerations when functionalising a nanocarrier with bioactive molecules include: (i) the stability and half-life of the targeting moiety (e.g. peptides are quickly degraded in the circulation), (ii) the orientation/accessibility of the target when assembled with the nanocarrier, (iii) the affect attaching a targeting moiety will have on the hydrophilic:hydrophobic ratio of the nanocarrier and the affect this may have on the configuration (e.g. micelle or polymersome) and (iv) if the ligand is also expressed by healthy cells (potential side effects).

Hammer *et al.,* have engineered polymersomes which model the binding of leukocytes to a surface which is coated with the inflammatory adhesion molecules (P-selectin and ICAM-1) to mimic the endothelium (Hammer *et al.,* 2008; Robbins *et al.,* 2010). Their leuko-polymersomes are functionalised on the outer surface with biotin and utilise the avidin-binding mechanism to attach a biotin conjugated antibody against ICAM-1 and a biotinylated selectin ligand sialyl-Lewis[x] to the corona of the polymersomes. Hammer *et al.*, demonstrated these leuko-polymersomes were capable of specific adhesion to inflammation adhesion molecules at physiological flow rates usually experienced by leukocytes (Hammer *et al.,* 2008). It is possible these leuko-polymersomes, if combined with therapy or an imaging modality, could be useful in the diagnosis and/or treatment of inflammatory diseases and cancer.

Nanoparticles for imaging

Nanoparticles also have the ability to help in imaging cancer and diagnosing tumours. Ferumoxtran-10® is used as a contrast agent for the magnetic resonance imaging (MRI) of lymph nodes (Wang and Thanou 2010). Iron oxide particles covered in dextran are taken up by macrophages which populate healthy lymph nodes (as well as liver and spleen). In patients with malignant cancers the lymph nodes get colonised by malignant cells reducing the number of macrophages, and therefore changing the appearance of the lymph nodes when examined using MRI (Leung 2004). Zhou *et al.*, also produced polymersomes capable of enhancing ultrasound imaging by developing air-encapsulated biodegradable polymersomes which were acoustically active (Zhou *et al.,* 2006). Ghoroghchian *et al.*, made polymersomes which could be imaged through 1cm of solid tumour tissue in an animal model (Ghoroghchian *et al.,* 2005). Their polymersomes encapsulated multi(porphyrin), near infra-red (IR) fluorophores, into the hydrophobic membrane of the polymersomes with controlled inter-spatial separation of the fluorophores (Ghoroghchian *et al.,* 2005). The ability to image polymersomes *in vivo* not only has applications for cancer imaging and diagnosis but also for studying the bio-distribution of polymersomes without needing to sacrifice the animal in *in vivo* experiments (Levine *et al.,* 2008).

Degradation and clearance of polymersomes

The degradation and safe clearance of nanoparticle delivery vectors such as polymersomes is as important as the initial delivery. In order for nanoparticles to be well tolerated by the body they must either degrade into non-toxic by products, which can be easily excreted (as is the case with PEO-b-PCL poly (ethylene oxide)-(poly(caprolactone) polymersomes) or the delivery vector itself must be able to be excreted (Levine *et al.,* 2008). Toxicity from bioinert polymers or by-products which cannot be excreted will hinder the usefulness clinically of nanoparticles.

Commercially available nanoparticle drug delivery systems

There are two nanoparticle delivery systems which are currently FDA approved and commercially available (Wang and Thanou 2010). The first of these is Doxil®, a liposome formulation designed to improve the delivery of doxorubicin for recurrent ovarian carcinoma and AIDS-related Kaposi's sarcoma (Gabizon *et al.,* 2003). This PEGylated liposome formulation shows good circulation times and reduced cardio-toxicity, an adverse effect which often limited the maximum dosage of free doxorubicin that could be delivered (Gabizon *et al.,* 2003). The circulation times and bioavailability of doxorubicin were improved with Doxil® compared to free drug (Safra *et al.,* 2001; Gabizon *et al.,* 2003). Abraxane®, the second FDA approved nanomedicine, is an albumin taxol conjugate approved for the treatment of metastatic breast cancer (Wang and Thanou 2010). Abraxane® provides a safer and more efficient method of delivering Paclitaxel compared to the previous delivery carrier Chremophor EL (which is used to increase solubility of hydrophobic drugs) (Harries *et al.,* 2005). Albumin is a natural carrier of endogenous hydrophobic materials in the circulation. It aids endothelial transcytosis, encourages caveolae formation and binds to osteonectin, found in breast, lung and prostate cancers. Albumin therefore provides a safe material for the delivery of hydrophobic agentss and has a natural capacity to target and bind to some cancers making it a popular choice in the field of nanomedicine research (Wang and Thanou 2010).

The future of nano drug delivery vectors

Personalised therapies are now looking possible as more biomarkers are discovered and methods to characterise the biomarker profile of a particular patient's cancer can be achieved. In the future this could lead to delivery vectors being designed with targeting moieties attached that are designed for individual's biomarker profile, enabling the delivery of higher doses of drug to the target area.

1.5 Tissue engineering: Progress and Limitations

Tissue Engineering

Tissue engineering is a multidisciplinary field which incorporates materials scientists, cell biologists, and clinicians with the aim of producing organotypic tissues for use in tissue repair, replacement and research. Tissue engineered replacements for skin (Chakrabarty *et al.,* 1999), bladder (Atala *et al.,* 2006) and urethra (Bhargava *et al.,* 2004; Bhargava *et al.,* 2008) have all been successfully used in patients. Some tissue engineered products are available commercially including Carcitel®, autologous cultured chondrocytes for repair of focal articular cartilage defects and Infuse®, a device designed to release bone morphogenic protein 2 (BMP-2) for spinal fusion. Other engineered tissues including cornea (Deshpande *et al.,* 2009), nerve (Madigan *et al.,* 2009), and blood vessels are all showing promise in *in vitro* experiments (Hunziker *et al.,* 2006).

Historically, most *in vitro* biological research has relied on two dimensional monolayer cell culture studies. Whilst these can provide valuable information regarding cell behaviour and responses, they are poor at replicating the three dimensional (3D) behaviour of tissues and are not always clinically relevant or representative of the *in vivo* situation. Furthermore, because of differences in the cell microenvironment, cells grown in three dimensions behave differently than those cultured as monolayers (reviewed in (MacNeil 2007), (Gottfried *et al.,* 2006; Moharamzadeh *et al.,* 2007)).

Tissue engineering allows scientists to study tissues in a more physiologically relevant way compared to traditional two dimensional cell cultures and reduces the need for animal studies.

Tissue engineered oral mucosa

There are several tissue engineered oral mucosa models being developed for *in vitro* and clinical applications, reviewed extensively in (Moharamzadeh *et al.,* 2007). Uses of tissue engineered oral mucosa include (i) the replacement of tissues damaged or removed as a result of disease or surgery (Lauer and Schimming 2001; Bhargava *et al.,* 2004; Ohki *et al.,* 2006; Rameez *et al.,* 2008) (ii) a model to study biological and pathological aspects of oral epithelium (Costea *et al.,* 2003; Duong *et al.,* 2005) and (iii) as a substitute for animals when testing the safety and efficacy of pharmaceuticals and other consumer products (Schmalz 2002; Schmalz *et al.,* 2002; Klausner *et al.,* 2007). Tissue engineered oral mucosa and oral epithelial sheets have not only been developed for the replacement of oral tissue (Lauer and Schimming 2001; Rameez *et al.,* 2008), but for other tissues including urethral (Bhargava *et al.,* 2004; Bhargava *et al.,* 2008; Selim *et al.,* 2010), oesophageal (Ohki *et al.,* 2006) and ocular (Inatomi *et al.,* 2008) epithelium replacement. This is partly due to the ease with which oral

mucosal tissue can be harvested for tissue engineering but also because of the excellent healing properties and lack of scarring associated with oral mucosa wound healing.

Epithelial models

Keratinocytes cultured according to the method described by Rheinwald and Green (Rheinwald and Green 1975) to form confluent sheets of epithelial cells are the simplest form of epithelial substitute. Cultured epithelial cell sheets have been used to repair oesophageal mucosa post surgery (Ohki *et al.,* 2006). After submucosal dissection of oesophageal carcinomas severe inflammation, scarring and stenosis can occur. Ohki *et al*., used autologous epithelial sheets attached to a polyvinylidene difluoride support membrane to repair damaged oesophageal tissues in patients. Complete wound healing could be seen 4 weeks after transplantation with no sign of stenosis. Cultured oral epithelial sheets were able to reduce the amount of contraction and promote wound healing through the release of various growth factors and cytokines in the oesophagus (Ohki *et al.,* 2006).

Lauer *et al.,* used large (75cm^2) epithelial sheets cultured from autologous biopsies to repair intraoral defects resulting from the removal of squamous cell carcinomas (Lauer and Schimming 2001). These large grafts provided a good epithelial covering with normal patterns of differentiation in 5 out of 6 patients. Although all grafts contracted post application, speech and tongue mobility was improved in all patients (Lauer and Schimming 2001).

Oral epithelial sheets proved effective in the above examples however, in other applications the simplicity of the epithelial sheet, difficulty in handling and potential for blistering post grafting made them unsuitable (Cooper *et al.,* 1993; Feinberg *et al.,* 2005). Epidermal sheets were tested for use as skin grafts in athymic mice but they did not form a good attachment with the dermal component. They lacked basement membrane proteins collagen IV and laminin, did not result in a mature epithelium after 42 days and did not show features such as rete ridges (Cooper *et al.,* 1993).

Commercially available multi-layer epithelium models

Cells behave differently in three dimensions and cells grown in 3D better model the conditions seen *in vivo*. Multilayer epithelial only models have been developed commercially for use in *in vitro* testing. These models provide researchers with a, quick and reproducible alternative to animal testing (Corporation 2008; SkinEthic 2008), but they are extremely expensive and are not commonly used in research laboratories. Since March 2009 there has been a ban by the European Commission on testing any cosmetic products, ingredients or combination of ingredients in animals (EuropeanCommission 2010) creating a need to develop alternative testing methods.   One multilayer epithelium only model is the commercially available

SkinEthic (Nice, France) buccal mucosa model. The SkinEthic model is cultured from the cell line TR146, a cell line derived from OSCC (SkinEthic 2008). The model is not keratinised and the cell behaviour is different to that of a healthy oral epithelium because of the immortalised nature of the cell line used (Moharamzadeh *et al.,* 2007). Multilayer models such as EpiOral™ and EpiGingival™ developed by MatTek Corporation (Ashland, MA, USA) differ from the SkinEthic models in utilising normal epithelial cells derived from humans grown on a collagen gel matrix compared to the polycarbonate membrane of the SkinEthic model (Klausner *et al.,* 2007; Moharamzadeh *et al.,* 2007; Corporation 2008). Klausner *et al.* have evaluated the effect of various mouthwashes and toothpastes on cell viability in the EpiOral™ and EpiGingival™ models (MatTek, USA) (Klausner *et al.,* 2007; Corporation 2008). These models were highly reproducible within and between different batches. However, no comparison was made with results from currently accepted established toxicity test methods such as animal models (Klausner *et al.,* 2007). It is likely these types of models will be very important for high throughput experiments to test the effects of substances on oral epithelia during product development.

Full thickness tissue engineered oral mucosa

The above mentioned models only contain epithelial components however, MacKenzie *et al.* and many others have demonstrated that fibroblasts and subepithelial connective tissue influence the formation of epithelia (Mackenzie and Fusenig 1983). Factors released by fibroblasts in the connective tissue affect keratinocyte differentiation and proliferation (Mackenzie and Fusenig 1983; Costea *et al.,* 2003; MacNeil 2007). Culturing the model at an air-liquid interface (ALI) increases expression of differentiation markers and encourages the epithelial cells to stratify and organise themselves to imitate natural oral mucosa (Bhargava *et al.,* 2004; Feinberg *et al.,* 2005). Therefore models comprised of keratinocytes, fibroblasts and connective tissue grown in three dimensions at ALI are the most clinically relevant when looking at the response of tissue to substances and stimuli.

Alaminos *et al.,* used a tissue engineered oral mucosa to study the gene expression over time in the maturation of the epithelium (Alaminos *et al.,* 2007). Their model comprised of oral keratinocytes and fibroblasts grown on a fibrin-agarose scaffold. This model formed a mature epithelium with intracellular junctions and a basement membrane. Looking at gene expression alongside morphological analysis enabled them to understand more regarding the genes involved in epithelial differentiation and maturation (Alaminos *et al.,* 2007). Other applications include the work of Chai *et al.*, which used a tissue engineered model of oral mucosa to test the interaction between dental implants and soft tissue (Chai *et al.,* 2010) and Moharamzadeh *et al.*, who used 3D tissue engineered oral mucosa to assess the safety of

antiseptic mouthwashes (Moharamzadeh *et al.,* 2009) and dental composite resins (Moharamzadeh *et al.,* 2008).

Scaffolds

Several materials are being developed for connective tissue substitutes to mimic as closely as possible naturally occurring oral mucosa when cells are grown on them. Scaffold materials include natural substances such as acellular skin (Bhargava *et al.,* 2004) and amniotic membranes as well as synthetic polymer scaffolds (Moharamzadeh *et al.,* 2007; Blackwood *et al.,* 2008; Selim *et al.,* 2010). Some models include gels into which fibroblasts are seeded to form a substitute connective tissue component (Duong *et al.,* 2005; Klausner *et al.,* 2007). Materials used for these gels include collagen (Klausner *et al.,* 2007), gelatine and fibrin (Hsieh *et al.,* 2010), reviewed extensively in (Moharamzadeh *et al.,* 2007).

Klausener *et al.* describe a full thickness oral mucosa model in which keratinocytes were cultured on top of a collagen matrix mixed with gingival fibroblasts (Klausner *et al.,* 2007). The histology showed detachment between the epithelial and connective tissue components with limited fibroblasts in the collagen gel (Klausner *et al.,* 2007).

Kinikoglu *et al.*, have developed a model of oral mucosa which is para-keratinised and resembles human native tissue histologically (Kinikoglu *et al.,* 2009). The connective tissue component of their models used a porous cavity collagen glycosaminoglycan-chitosan scaffold into which fibroblasts could be seeded. Transmission electron microscopy analysis of the model demonstrated there was a continuous, well-organised basement membrane onto which the epithelium was strongly attached and the presence of desmosomes (Kinikoglu *et al.,* 2009). The immunohistochemistry profile, of this tissue engineered non-keratinised oral mucosa, closely matches that of naturally occurring para-keratinised oral mucosa. There was strong expression of keratin 3 and 13, with no expression of keratin 10. Laminin V could be seen continuously along the basement membrane of the tissue engineered oral mucosa model demonstrating that the cells in the model were capable of producing basement membrane proteins in a well organised manner which resembled naturally occurring oral mucosa (Kinikoglu *et al.,* 2009).

Acellular skin can be processed in a way that retains the naturally occurring basement membrane proteins aiding cell attachment in the model (Chakrabarty *et al.,* 1999). Acellular skin is durable with good structural properties and shows reduced antigenic reactions compared to other materials when implanted (Moharamzadeh *et al.,* 2007). Histologically, models grown on acellular skin closely resemble natural oral mucosa. Immunohistochemical analysis showed similar cytokeratin 16 profiles in the cultured models and the natural oral mucosa, while maintaining differences such as a lack of cytokeratin 10 expression (Ophof *et*

al., 2002). Heparin sulphate was present in the basement membrane of normal oral mucosa and in the models after 14 days culture (Ophof *et al.,* 2002).

Tissue Engineered Models of Oral Squamous Cell Carcinoma

Monolayer cell culture studies are often the primary tool used for the evaluation of cancer therapies before their investigation in animal models. Although simple, well established and versatile the 2D monolayer method has several limitations. In order for a cancer treatment to be effective the bio-distribution within a tumour as well as its action on different stages of cancer progression and in different microenvironments within solid tumours are all important considerations. These factors cannot be tested in monolayer studies, therefore 3D models, which model stages of cancer progression and which posses a genetic expression profile which is similar to naturally occurring tumours, are an important tool (Hirschhaeuser *et al.,* 2010). Often drugs tested in 2D and 3D produce different results (Knuchel *et al.,* 1989) possibly explaining why many compounds which appear promising in 2D fail to show the same results in animal studies. Testing more novel drug compounds in 3D models could increase our ability to predict a drug's efficacy in *in vivo* studies, reducing the number of failed animal studies and preventing potentially useful drugs being eliminated at the *in vitro* testing stage.

OSCCs are epithelial in origin, progressing from a dysplastic, disordered epithelium to a carcinoma *in situ* where the whole epithelium is abnormal and displays the properties described previously (page 22). The next stage of disease progression is invasive OSCC, where cancer cells invade into the connective tissue underlying the oral epithelium. Once these cells have invaded they form tumour islands, solid expanding masses of cancer cells.

Here we describe two types of OSCC models: (i) a 3D model of epithelial OSCC comprised of cancer cell lines and a connective tissue component and (ii) a 3D model of a solid expanding OSCC tumour.

3D epithelial models of OSCC

Being able to model the different degrees of OSCC progression from dysplasia to carcinoma *in situ* would provide a useful tool for *in vitro* studies investigating the mechanisms of lesion progression and OSCC invasion as well as being a tool for testing treatment and diagnostic technologies for pre-cancerous and cancerous lesions. The stromal portion underlying the oral epithelium is known to play an important role in cancer progression (Mueller and Fusenig 2004; Gaballah *et al.,* 2008) and invasion (Figure 1.9) (Costea *et al.,* 2006). Therefore a model which incorporates epithelial and connective tissue portions is important in order to study tumour progression and potential treatments.
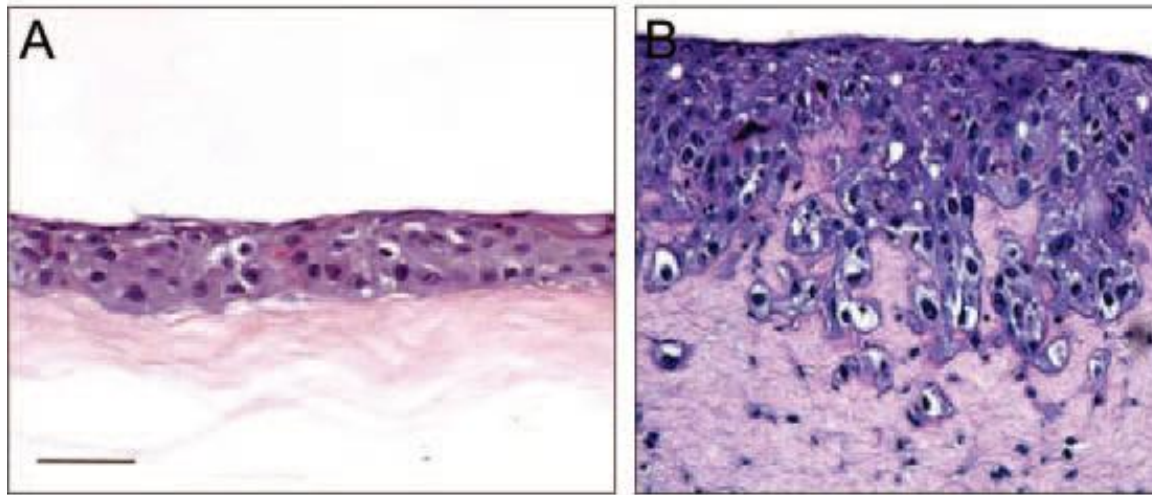
Figure 1.9 Effect of human fibroblasts on invasion of dysplastic oral keratinocytes (DOK) cells. A = DOK cells grown on collagen matrix, B = DOK cells grown on collagen matrix with human fibroblasts incorporated. (Costea *et al.,* 2006)

Currently just a few models of this type have been developed for oral cancer. Gaballah *et al*., have developed models of mild, moderate and severe dysplasia using keratinocytes and fibroblasts isolated from clinical lesions on collagen scaffolds (Gaballah *et al.,* 2008). Using various different strains of keratinocytes and fibroblasts derived from different lesions with different characteristics they used a scoring system, which included changes in stratification, polarity, intraepithelial keratinisation, nuclear size, nuclear pleomorphism and proliferation index (measured by Ki67) to determine the severity of dysplasia resulting from different culture conditions and different cell types.

As well as cancer progression these organotypic models can be used to study the mechanisms of invasion, determine the invasiveness of certain cells and to assess the effect of different conditions on the invasiveness of OSCC *in vitro*. For example, the model created by Duong *et al*. used OSCC cell lines cultured on a collagen gel with fibroblasts incorporated into it to model cancer cell invasion into the connective tissue (Duong *et al.,* 2005). A gel containing basement membrane proteins including laminin and collagen IV was added to the top of the collagen gel prior to seeding the squamous cell carcinoma cell lines onto the top of this. The effects of hypoxia and cell migration factors on the invasion of the cancer cells were able to be imaged over time using an Opticell™ chamber (Duong *et al.,* 2005). Nyström *et al.,* devised a method to quantify the invasion of cancer cell lines into a collagen gel embedded with fibroblasts using a computer-assisted digital analysis system (Nyström *et al.,* 2005).

Fibroblasts and stromal component

The relationship between the stromal compartment, including fibroblasts, and their effect on carcinomas has long been investigated in animal models. Reviewed in (Elenbaas and

Weinberg 2001) it is clear that elements within the stroma of tumours are important in tumourigenesis. However, this relationship is complicated and is most likely a combination of effects from fibroblasts, immune cells and endothelial cells involving growth factors, extracellular matrix proteins, proteases and protease inhibitors (Elenbaas and Weinberg 2001).

The effect of fibroblasts on the invasiveness of DOK cells, a dysplastic non-tumourigenic cell line, was determined in (Costea *et al.,* 2006). DOK cells were cultured on collagen gels containing no cells, human fibroblasts or mouse fibroblasts (Costea *et al.,* 2006). Local invasion of DOK cells into the connective tissue was seen with the presence of human fibroblasts but little or no invasion was seen in models cultured without fibroblasts or with fibroblasts from mice. Local invasion was also seen when the models were cultured in the presence of conditioned medium from a DOK and human fibroblast model, but not with the conditioned medium from human fibroblast monolayer culture (Costea *et al.,* 2006). This result suggests that for fibroblasts to initiate invasion they require co-culture with the epithelial cell type, and the co-culture encourages different factors to be released compared to monoculture. Collagen IV production was seen in those models which invaded but was not seen in the models which were non- invasive (or minimally invasive) suggesting fibroblast and keratinocyte co-culture encourages collagen IV production.

Fibroblasts found in the stroma of carcinomas are sometimes called myofibroblasts. These cells are similar to the fibroblasts found in wound healing and behave differently to fibroblasts found in healthy tissues. Myofibroblasts are more proliferative, express different extra-cellular matrix proteins and produce more growth factors compared to normal fibroblasts.

Culturing normal keratinocytes with fibroblasts extracted from dysplastic clinical lesions, resulted in dysplastic epithelium, demonstrating the effect fibroblasts can have in the development of dysplastic epithelia (Gaballah *et al.,* 2008). In xenograph models of carcinomas the addition of myofibroblasts, as opposed to normal fibroblasts, enhanced the tumour promoting activity (Elenbaas and Weinberg 2001). It is thought that by returning the stroma and its constituents to a normal state, tumour progression could be slowed or even reversed (Mueller and Fusenig 2004), a theory which could be tested simply in tissue engineered models that incorporate dysplasia associated myofibroblasts.

Growth factors

Gaballah *et al*., tested the effect of culturing models with media supplemented with keratinocyte growth factor (KGF) or epidermal growth factor (EGF) and found KGF encouraged polarisation of the epithelium, reduced the thickness of the epithelium and increased the Ki67 score (Ki67 is an immunohistochemistry stain which detects proliferating cells) in basal cells. In contrast EGF, a growth factor important in wound healing, increased the Ki67 score of suprabasal cells (a characteristic of dysplasia) and increased the architectural

and cytological changes in the resulting epithelia, leading to higher dysplasia scores compared to models cultured with KGF (Gaballah *et al.,* 2008).

Model of solid expanding cancer: Multi-Cellular Tumour Spheroids

In the 1970s, Sutherland *et al*., developed a method to study cancer cell lines in a way which more accurately models the *in vivo* tumour microenvironment (Sutherland *et al.,* 1971). These multi-cellular tumour spheroids (MCTS) are solid cell aggregates comprised of cancer cell lines which behave in a way that mimic avascular areas of solid tumours.

The tumour islands modelled by the MCTS model are those which have grown to a size where cells at the centre of the tumour are sufficiently distant from nutrient blood vessels to be at the limits of nutrient, oxygen and waste product diffusion. These tumour islands have central areas of necrosis and hypoxia further away from the blood supply and are often resistant to anti-cancer treatments. MCTS models are able to expand beyond the natural diffusion range for nutrients, oxygen and waste products and this leads to pathophysiological diffusion gradients being established that replicate many of the classical features seen within tumours *in vivo.* There are many different versions of the MCTS model which have been employed for a variety of different applications, some of which are reviewed here along with a rationale for the development of these models.

Properties of MCTS

Multi-cellular tumour spheroids closely resemble tumour nodules, tumour islands and avascular areas of solid tumours. The extent of these characteristics depends on the size of the MCTS, the cell line used to culture them and the speed at which they form and grow. Figure 1.10 shows the characteristics typically seen in MCTS including nutrient distribution and apoptosis.

The outermost cells behave in a similar way to those cells seen near the vascular supply *in vivo*, receiving plenty of nutrients and discarding waste products into the cell culture medium. These cells, seen in all MCTS, are highly proliferative and have high metabolic activity. The oxygen, nutrient and catabolite gradients only become apparent in MCTS larger than 150μm, while the necrotic and apoptotic core only become apparent in MCTS above 500μm in diameter (Hirschhaeuser *et al.,* 2010). The necrosis in the core of MCTS is caused by several factors including accumulation of waste products, low pH, deficiency of nutrients and deficiency of oxygen, a phenomenon also seen in tumour cells *in vivo* over 100μm away from a blood supply (Kunz-Schughart and Knuechel 1998; Cottin *et al.,* 2010).

Poor oxygen perfusion into the central region of the MCTS causes the core to become hypoxic, similar to the hypoxia found in naturally occurring tumours. This is of particular interest as

intra-tumoural hypoxic regions are often resistant to anti-cancer treatments and are an indicator of poor patient prognosis (Subarsky and Hill 2003; Duong *et al.,* 2005). Prolonged hypoxia can lead to genomic instability and this may contribute to the progression of metastases (Subarsky and Hill 2003). Hypoxic tissues *in vivo* are known to release pro-angiogenic factors which enable the tumour to continue its growth as new blood vessels grow and supply the tissue with nutrients needed for proliferation and tumour growth (Timmins *et al.,* 2004).

The cells which surround the necrotic and hypoxic core adapt their behaviour to maintain homeostasis despite changes in the microenvironment. These cells alter their proliferative behaviour, protein expression and react in different ways to drugs and drug candidates. Penetration barriers, cell-cell and cell-matrix interactions, signalling pathways, cellular targets and changes in the cell cycle distribution all contribute to the altered response of these cells to drugs and therapeutic compounds (Hirschhaeuser *et al.,* 2010). These changes, as well as changes to metabolic activity, collagen production and genetic expression are accounted for in this 3D model demonstrating a clear advantage of the MCTS model over monolayer studies (Horning *et al.,* 2008).
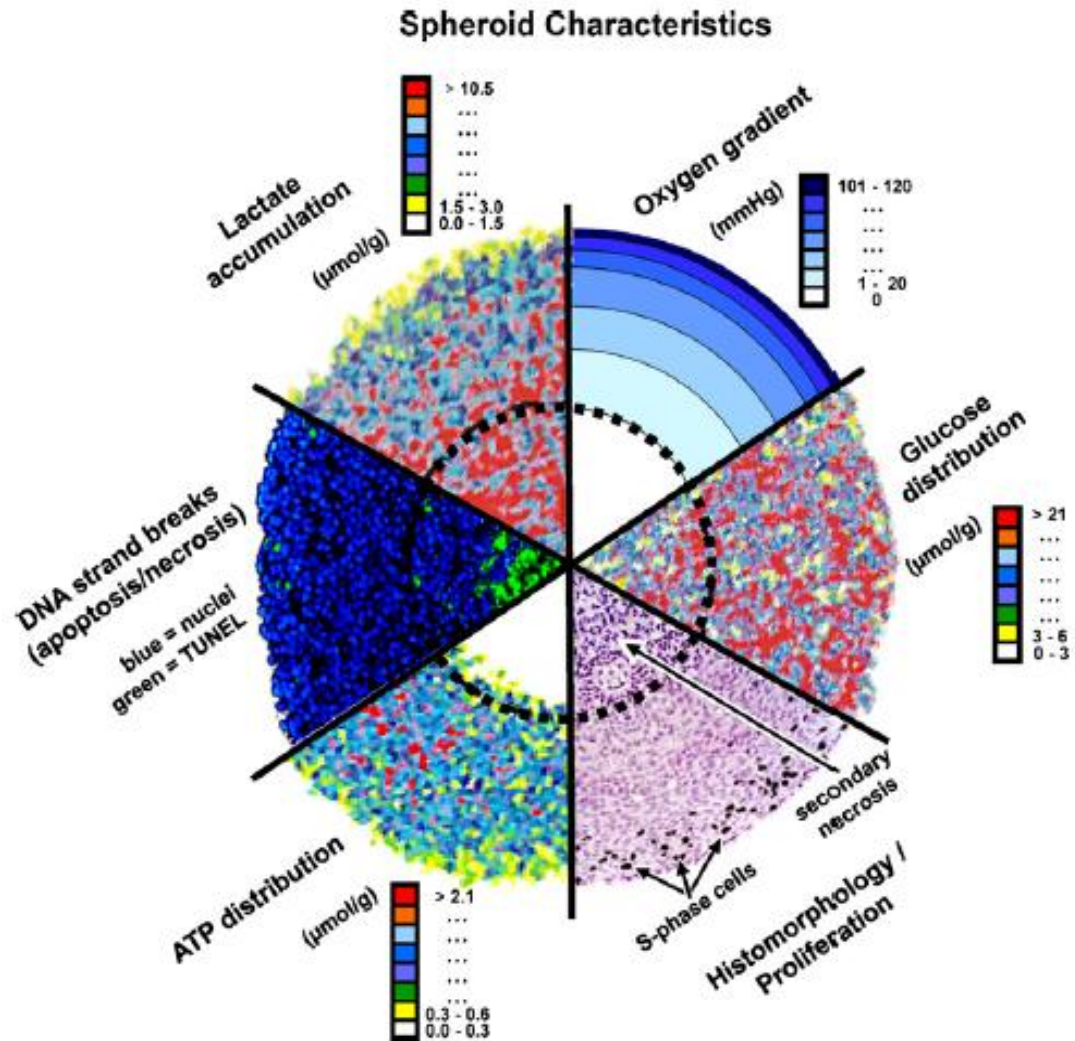
Figure 1.10 Characteristics of spheroids determined by autoradiography, TUNEL assay, bioluminescence imaging, probing with oxygen microelectrodes and immunohistochemistry.
Image from (Hirschhaeuser *et al.,* 2010)

Methods to produce MCTS

There are several ways to culture MCTS including the liquid overlay method developed by Carlsson and Yuhas (Carlsson and Yuhas 1984), hanging drop method (Kelm *et al.,* 2003), spinner flasks, roller tubes and gyratory flasks (Figure 1.11) (Friedrich *et al.,* 2007). All these methods work by inhibiting cell attachment and therefore encouraging the cells to adhere to one another.

For the liquid overlay method (Carlsson and Yuhas 1984) cancer cell lines are cultured in 96 well plates coated with agarose or agar or in non-adherent round bottomed plates, all of which encourage cells to collect in the centre of the well and inhibit attachment to the plate

encouraging cells to adhere to one another. This method enables reproducible MCTS to be produced (dependant on the cell line), relatively simply, in large numbers and enables single MCTS monitoring over time. For drug candidate testing this method does not require large quantities of drugs to be used, a benefit in commercial applications. A robust method for the production of MCTS for high-throughput drug screening applications utilising the liquid overlay method has been developed by Friedrich *et al*., (Friedrich *et al., 2009)*. The main problem with stationary culture methods, such as the liquid overlay method, is the nutrient gradients experienced in the cell culture medium within the 96 well plates. This method can also produce irregular shaped, fragile MCTS (Kelm *et al., 2003)* therefore selection of appropriate cell lines in important.

More recently the hanging drop technique, commonly used for culturing embryoid bodies, has been employed to produce MCTS (Friedrich *et al., 2007)* and has proved useful for MCTS initiation in cell lines that fail to form MCTS by the more conventional methods (Kelm *et al., 2003)*. However, producing MCTS using this technique is technically harder and changing the medium is difficult. Despite these challenges it is possible to produce reproducible spheroids using the hanging drop method and its use has been demonstrated for the screening of numerous chemotherapeutic compounds (Herrmann *et al., 2008)*.

Spinner flasks, roller tubes and gyratory flasks all work by inhibiting cell attachment to the culture flask; in this case through continuous movement. The spinner flask method produces large numbers of MCTS with reproducible size up to 1-2mm in diameter (Kunz-Schughart and Knuechel 1998). The disadvantages of these rotating cultures include the effects caused by the sheer stress seen in the culture flask and the large volumes of cell culture medium required. The NASA bioreactor overcomes the problem of sheer stress as the wall rotates while the MCTS are in suspension in cell culture medium. The bioreactor incorporates continuous media and oxygen perfusion and waste removal. This system however, is very expensive, uses large volumes of cell culture medium and is cumbersome limiting its use.

When choosing a method for MCTS production reproducibility in size and volume of MCTS, the numbers of MCTS required, volume of culture medium (and therefore test drug) needed and ease of production must all be considered.
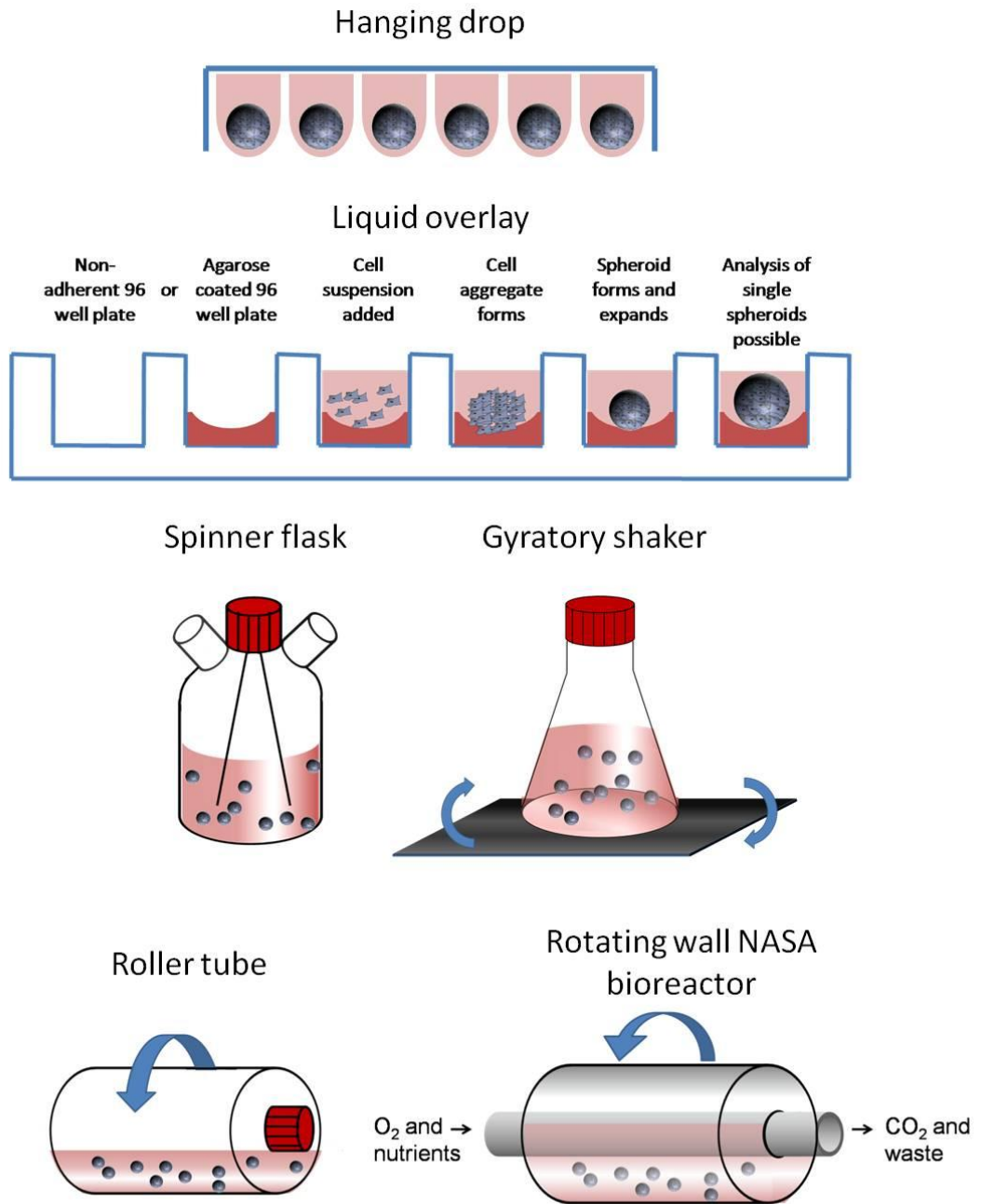
Figure 1.11 Methods of producing MCTS *in vitro*

Promoting MCTS formation

The tumour models described above all rely on the inherent ability of cancer cells to adhere to one another and create MCTS. Ivascu *et al*., tested the addition of reconstituted basement membrane (rBM), collagen type I and IV, fibronectin, laminin, heparin sulphate proteoglycane and chondronitin on a breast cancer cell line to initiate MCTS formation (Ivascu and Kubbies 2006). Only rBM (a mixture of laminin, collagen type IV and entactin) was able to successfully induce MCTS formation.

Other groups have used scaffolds into and onto which cancer cells can grow; enabling the formation of solid tumour models from cell lines which are usually unable to form MCTS. Horning *et al*., used poly(lactic acid) (PLA) microparticles (diameter 160-180µm diameter) with internal interconnecting pores to culture a 3D model of breast cancer using the cell line MCF-7 (Horning *et al., 2008*).

Fragment spheroids (also called F-spheroids) are *in vitro* models in which a piece of excised cancerous tissue is cultured for diagnostic and research purposes. This method requires tissue from patients to be donated and is less reproducible, or amenable to large scale testing compared to the models described previously. However, F-spheroids do have the advantage that they include a mixed population of cells which is comparable to naturally occurring tumours. The cell population includes fibroblasts, macrophages, endothelial cells and epithelial cells which are in both differentiated and progenitor forms (Hirschhaeuser *et al., 2010*).

Applications of MCTS

MCTS can be used to study (i) responses to drugs and cancer treatments such as radiotherapy, (ii) basic cell biology in tumours e.g. angiogenesis and cell invasion and (iii) epigenetic mechanisms involved in regulation of differentiation, proliferation and cell death (Kunz-Schughart and Knuechel 1998).

One of the most studied applications for MCTS is drug screening. Many in the field hope screening in 3D models such as these will be commonplace in the future to improve drug candidate screening before testing *in vivo*. Herrmann *et al*., screened a number of different drugs in MCTS produced from different cell lines using the hanging drop method (Herrmann *et al., 2008*). The level of apoptosis induced by the drugs and cell viability was measured in MCTS and compared to cells grown as monolayers. The viability and apoptosis levels between the two was markedly different for almost all drugs tested highlighting the value of this technique for the screening of large numbers of drugs in a more physiologically relevant way compared to monolayers (Herrmann *et al., 2008*).

The penetration of chemotherapeutics into avascular regions of tumours dictates the efficiency of the drug and its ability to treat solid tumours effectively. Cottin *et al*., used MCTS models of glioblastoma and osteocarcinoma to test the hypothesis that gemcitabine, a chemotherapeutic drug commonly used in the treatment of pancreatic, ovarian and lung cancers, exerts its anti-cancer effects *via* a gap junction mediated "by-stander" effect (Cottin *et al., 2010*). They found gemcitabine was able to inhibit growth and reduce the viability of cells within MCTS models within 2 hours of treatment. This effect was not seen when a gap junction inhibitor was added, implying the anti-cancer effects of gemcitabine are achieved *via* the diffusion of gemcitabine and its metabolites *via* gap junctions into the central region of the MCTS. This highlights the potential of gemcitabine for the treatment of solid tumours with regions of poor vasculature *in vivo* (Cottin *et al.,* 2010).

Other groups have also utilised MCTS models to evaluate the penetration and delivery of nanoparticle drug delivery systems. For example, Waite *et al*., demonstrated the delivery of active siRNA into MCTS, comprised of malignant glioma cells (Waite and Roth 2009). The delivery of dendrimers associated with siRNA was enhanced by the attachment of RGD ligands which enhanced the interaction between integrin ECM contacts in the MCTS and the dendrimer SiRNA complex (Waite and Roth 2009). Novel therapies including radioimmunotherapy (Essand *et al.,* 1995), cell- and antibody based immunotherapy (Ballangrud *et al.,* 2001), hyperthermia and photodynamic treatment (Dubessy *et al.,* 2000) have all been studied using 3D models of MCTS.

The genetic expression of cells within MCTS can be evaluated. When combined with data on the efficacy of chemo- and radio-therapy, these MCTS can help us to understand the genetic factors involved in chemo and radio-resistance (Hirschhaeuser *et al.,* 2010) potentially improving the treatment of resistant tumours.

Co-culture MCTS

Monoculture MCTS, comprised of one cell type, do not take into account other cells which affect tumour behaviour *in vivo.* MCTS incorporating other cell types such as fibroblasts, endothelial cells and immunocompetant cells have been developed (Kunz-Schughart and Knuechel 1998; Hirschhaeuser *et al.,* 2010).

Incorporation of immune cells into the MCTS has been achieved by adding a suspension of immune cells to preformed spheroids in culture. These models are of great benefit to understand the role of immune cells in the development of tumours, as their role is currently unclear. Some cells of the immune system are capable of recognising and destroying malignant cells, whereas other immune cells may be responsible for releasing growth factors and other signals that encourage tumour growth (Kunz-Schughart and Knuechel 1998).

Hauptmann *et al*,. used a MCTS model of colon cancer to test the effect of three different types of macrophage on tumour proliferation and migration (Hauptmann *et al.,* 1993). Konur *et al*., used MCTS comprised from different cancer cell lines to investigate the maturation of monocytes into tumour associated macrophages and found the maturation was different for different tumour tissues (Konur *et al.,* 1998).

Angiogenesis, the formation of new blood vessels from existing vascular beds, is essential for the continual growth of solid tumours as the blood supply delivers nutrients and oxygen, essential for growth and proliferation, as well as being important in the removal of waste products. The blood supply to tumours is also responsible for transporting malignant cells to metastatic sites. For this reason anti-angiogenic treatments are gaining popularity as an alternative method to halt, or slow, the growth of tumours.

In order to test novel anti-angiogenic therapies *in vitro,* solid tumour models, which incorporate an endothelial component are essential. Models incorporating endothelial components are also a valuable tool to study the mechanisms involved in angiogenesis and tumour growth. Studies in monolayers, involving the co-culture of endothelial cells and cancer cells, have limited value as blood vessel formation is a complex 3D process.

Timmins *et al*., created micro-vascularised MCTS by introducing isolated endothelial cells to pre-formed solid tumour spheroids using the hanging drop technique. They demonstrated it was possible to incorporate an endothelial component without the addition of angiogenic factors or a need for endogenous supplements (Timmins *et al.,* 2004). Vascular endothelial growth factor (VEGF) was up-regulated in MCTS, compared to the same cell lines cultured as monolayers (Timmins *et al.,* 2004).

1.6   Imaging and Diagnostic Techniques

Visual Diagnosis of OSCC and potentially malignant lesions

Diagnosis of OSCC and potentially malignant lesions currently relies on histological analysis of surgically removed biopsies. This is an accurate and well established method for the diagnosis of oral cancers and other mucosal diseases however, there are drawbacks. The procedure of surgical biopsies is invasive, causing pain and discomfort for the patient. There is a delay before the patient can be presented with a diagnosis causing anxiety and delaying treatment where needed. A non-invasive and instant method for diagnosing potentially malignant lesions would overcome these problems and could enable more widespread and regular screening of at risk patients. This would be particularly beneficial in the treatment of oral cancer where low survival rates are often due to late diagnosis when the cancer is already at an advanced stage.

Real time imaging could also help the surgeon define the margins of the lesions, helping them to completely remove diseased areas while maintaining as much healthy tissue as possible. Being able to take an "optical biopsy" non-invasively and without the need for ionising radiation would mean larger areas of tissue could be investigated compared to the areas of tissue examined in a surgical biopsy. One technology which is proving to be promising for this application is optical coherence tomography (OCT).

General dentists do not often see oral cancer cases and are therefore not as experienced at diagnosing and referring these patients when the cancer is still in the early stages (Keller 2010). Technology which is simple to use, affordable and gives reliable results could provide general dentists with a great aid to spot oral cancer earlier and therefore improve survival rates.

Two thirds of oral cancers are not diagnosed until they have spread from their original location. Pre-malignant lesions are often invisible to the naked eye and can have an appearance which is indistinguishable from other mucosal conditions including non-specific ulcers, frictional keratosis and lichen planus (Keller 2010).

Commercially available detection systems

Photosensitisers

Photosensitisers are topically applied materials which create a strong fluorescent signal in the oral cavity. This fluorescent signal is higher and appears more quickly in areas of pathology and can therefore be used to locate potential areas of oral cancer. Photosensitisers have the advantage of being non-invasive, quick to perform and the only special equipment required is an inexpensive red diode type laser to detect the fluorescence. A drawback to this technology is the fact that the dye is non-specific and often stains not only areas of oral cancer but also other oral pathologies such as non-specific ulcers, frictional keratosis and oral lichen plaus. The exposure of tissue to the red-diode type laser can also be damaging so this exposure needs to be minimized.

Toludene blue

Toludene blue is a metachromatic vital dye (Zila Tolonium Chloride) which has been used for many years in dental practices. The stain is rinsed around the oral cavity and is taken up by live cells. Those cells which have higher metabolic activity will accumulate more dye than those with a lower metabolic activity. The accuracy of this technique depends on the experience of the clinician. Those who use the stain regularly can achieve 90% sensitivity however, specificity is low (Wilder-Smith *et al.,* 2009) and less experienced clinicians are not able to obtain such high sensitivity. This poor specificity often results in false positive results.

ViziLite

ViziLite is a system which is often used in conjunction with Toludene blue. The patient is required to wash their mouth with acetic acid, to dehydrate the cytoplasm of cells. This enhances the difference in retractile properties caused by the higher nuclear: cytoplasmic ratio of cancerous cells compared to healthy cells. The ViziLite stick then uses chemo-luminescence to show areas of potentially malignant and malignant lesions as white patches. This method is not very sensitive and many in the field believe a trained eye is more reliable.

The advantages of Toludene blue and ViziLite are that they are fast, cheap and relatively simple to use. The limitations of Toludene blue and ViziLite are that they cannot distinguish between the different degrees of dysplasia and carcinoma and also provide a high proportion of false positive results.

VELscope

VELscope is a spectroscopy device which does not require any prior tissue staining or treatment to image lesions in the oral cavity. It works using the inherent optical properties of dysplastic or malignant tissue compared to healthy tissue. A blue light (wavelength 400-460nm) is shone onto the tissue being examined and the appearance of autofluorescence is different in areas of pathology. It is believed this system uses auto-fluorescence from nicotinamide adenine dinucleotides (NADH) and flavin adenine dinucleotides (FAD) to distinguish between healthy tissues and potentially malignant lesions which lose this autofluorescence as a result of increased metabolism (Poh *et al.,* 2007; Schwarz *et al.,* 2008). Healthy tissue appears apple green while suspicious lesions appear dark with a loss of fluorescence (VELscope 2009). In a pilot study VELscope showed 98% sensitivity and 100% specificity identifying severe dysplasia/ carcinoma *in situ* or invasive carcinoma from healthy tissue (Poh *et al.,* 2007). However, other types of lesion such as non-specific ulcers, frictional keratosis and oral lichen planus were not included in the study which may artificially raise the specificity of the methodology. Anecdotally its specificity is thought to be similar to that of Toludene Blue and ViziLite. Its ability to diagnose dysplasia and earlier stages of pre-malignancy has yet to be shown in a randomised control trial of at risk patient groups. It has however, been demonstrated in a case study of a patient with a case of recurring moderate dysplasia (Poh *et al.,* 2007) that was not visible to the naked eye. VELscope is not an alternative to biopsies but is used as a adjunctive device to help clinicians know where to take biopsies (VELscope 2009).

Trimira Identafi 3000

The Trimira Identafi® 3000 is a multi-spectral oral cancer screening system. Approved by the FDA for clinical use in 2008, this device uses three different light sources to distinguish abnormalities in tissues more clearly. The first is a regular white light which can highlight some suspicious lesions, but not all. The second light is a violet light which enhances the

tissue's natural fluorescence. This is the same method by which the VELscope works. In addition to the violet light there is a green-amber wavelength light which enables easier visualisation of vasculature. In normal tissues the vasculature is well defined and organised but in dysplastic and malignant tissues the vasculature is more diffuse and distinguishable from normal tissue. By combining these three different imaging modalities it is hoped that the number of false positives can be reduced.

Impedance Spectroscopy

Impedance spectroscopy is a non-invasive, real time type of spectroscopy which measures the bioimpedance of a tissue. A sinusoidal current is applied to the tissue at a variety of frequencies. The voltage drop caused by impedance in the tissue is referred to as bioimpedance and varies between different types of tissues and physiological changes within tissues. The electrical properties of the tissue give rise to different impedance signals at different frequencies. Low frequencies (10Hz-10kHz) relate to differences in the ionic environment surrounding cells whereas higher frequencies (10kHz-10MHz) measure changes in structure relaxation (Sun *et al.,* 2010). Changes in the levels of water and salts within cells as well as orientation of cells and membrane permeability can all result in changes to the electrical impedance. These factors change during the transformation of tissue from healthy to malignant tissue and therefore make impedance spectroscopy a feasible method for screening cancer.

Impedance spectroscopy has been shown to be able to detect the degree of cervical intraepithelial neoplasia (CIN) with sensitivities of 74% and specificities of 53% (Abdul *et al.,* 2006). The use of impedance spectroscopy for detecting breast cancer has been reviewed in (Zou and Guo 2003). Differentiation between malignant breast tissue and surrounding tissue has been shown to be possible and positive trials of one device for impedance spectroscopy, the TS2000, led to its approval by the FDA for it to be used in association with mammography for the diagnosis of breast cancer (Zou and Guo 2003). There has been some evidence *in vitro* and *in vivo* that impedance spectroscopy is able to distinguish between benign and malignant breast tissue (Sun *et al.,* 2010) although, this has yet to be proved in patients (Zou and Guo 2003). Although commercially available the TS2000 is not without problems, the depth of penetration (3-3.5cm) is only able to detect breast cancers near the surface of the body, false positive results are common due to interference from other tissue types and skin lesions (Zou and Guo 2003). The accuracy of detection must be improved before this technique can have a real impact on the detection of cancerous breast tissue.

Impedance spectroscopy has the advantage that it is relatively low cost, quick to do and requires little training compared to traditional histology and pathological analysis of suspicious

lesions. The immediate results and ease of use also makes it suitable for use in resource poor settings and primary care.

The first study of impedance spectroscopy for the investigation of oral lesions was published by Sun *et al,*. (Sun *et al., 2010*). In their study, bioimpedance of cancerous tissue on the tongue of twelve patients with tongue cancer was measured and compared to healthy tissue on the patient's tongue, at least 10mm away from the cancerous region of the tongue, and measurements from the tongues of healthy volunteers. The bioimpedance for the healthy tissue was compared to cancerous regions at six different frequencies (20Hz, 50 kHz, 1.3 MHz, 2.5 MHz, 3.7 MHz and 5 MHz).

Measurements of impedance, phase angle, real part of impedance and imaginary part of impedance were taken. At 20Hz and 50 kHz the difference in all four of the parameters measured was statistically significant between the cancerous region of the tongue, the healthy region of the patients' tongues and the measurements taken from healthy volunteers. At frequencies below 1MHz the current is unable to pass through the cells, therefore the current flows around the cells and impedance is affected by the intracellular space. In healthy tissues the cells are tightly packed with strong intracellular connections making the resistance high as the current must take an arduous route around the cells. In cancerous tissues the extracellular space widens and intracellular connections are lost, resulting in lower resistance and therefore lower bioimpedance values.

Higher frequencies detect changes to the electrical properties inside cells as well as intracellular spaces as the higher frequency current is able to pass through cells. Impedance measurements at higher frequencies were not significantly different between healthy and malignant tissues.

This paper demonstrates the potential of this technology in diagnosing changes to the oral epithelium in a quick and non-invasive way. Further studies looking into various degrees of dysplasia and metastatic progression in different regions of the oral cavity will be interesting.

Fourier Transform Infra-Red spectroscopy

Spectroscopy enables the detection of specific chemical compounds within a sample by measuring the absorption, emission or scattering of electromagnetic radiation. In the case of Fourier Transform Infrared (FTIR) the radiation used is broad spectrum infrared (IR) light which includes many wavelengths. IR radiation is aimed at the sample and different wavelengths are absorbed depending on the bonds present. The absorption results in less radiation returning to the detector. The Fourier Transform algorithm is used to convert raw data into information regarding the absorption at each specific wavelength.

Each wavelength corresponds to different bond types, enabling a molecular "finger-print" of the bonds present in a sample to be identified (including information on the functional groups, bonding types and molecular configurations present).

Mid-FTIR measures between 400 and 4000 cm^{-1} wavenumbers. This method is highly sensitive to strong polar bonds such as C=O, C-O, O-H, and C-H. These bonds are commonly found in lipids, carbohydrates and proteins. FTIR has therefore been able to detect changes in cell proliferation and distinguish cells in different stages of their life cycle and between malignant and healthy cells (Kendall *et al.,* 2009).

Unfortunately, the strong absorption of IR light by O-H bonds means that the presence of water can limit the use of mid IR FTIR for *in vivo* applications.

Raman Spectroscopy

Raman spectroscopy (RS) is commonly used in conjunction with FTIR as the spectroscopic method detects differences in C=C bonds and carbon triple bonds found in aromatic amino acids (Kendall *et al.,* 2009). RS detects subtle changes in wavelengths (called a Raman shift) which results from inelastic collisions of photons from incident light with molecules in the sample. Raman is not affected by water so is currently being developed for *in vivo* probes as well as histopathology diagnosis aids.

Optical Coherence Tomography

Introduction

Optical coherence tomography (OCT) is a non-invasive method of imaging which utilizes the high penetration capacity of long wavelength light to image tissues beneath the surface. OCT, often referred to as "optical ultrasound", measures light back scattered and reflected from different tissue structures beneath the surface of a sample. Differences in the optical properties and reflectivity of tissue components create distinguishable signals from different depths of the sample. These signals can be processed to produce a 2D cross section of a region of tissue (and in some systems a complete 3D reconstruction). OCT imaging systems comprise of two interferometer arms. Light from the low coherence light source is split using a beam splitter (usually a Michelson interferometer). The first of these arms focuses the light onto the sample, scans the area being visualised and collects the backscattered light. The second interferometer arm provides the reference light beam. The speed of light means the method for calculating the depth corresponding to a particular signal is more complicated than in ultrasound.   In ultrasound the time taken for a sound wave to be reflected back to the detector is measured. In OCT there are two different methods for working out the depth of a signal, time domain OCT and Fourier domain OCT (Illustrated in Figure 1.12 and Figure 1.13).

TD OCT

In time domain OCT (TD-OCT), also called temporal domain OCT, there is a moving reference mirror in the reference arm (Figure 1.12). The reference mirror scans in the z direction as the sample is exposed to the light from the sample arm. When light from the two arms have travelled the same distance the two light paths optically interfere with one another. The interference between the two light paths creates interference fringes which are detected and analysed. This analysis provides information on the magnitude and echo time delay of the sample beam and a grey-scale cross-sectional image of the tissue can be created.

FD-OCT

In Fourier domain OCT (FD- OCT), also known as spectral domain OCT, there is a stationary mirror in the reference arm (Figure 1.13). In order to calculate the depth of a signal's source the phase shift of the backscattered or reflected light is compared with the phase of the signal from the stationary mirror. The spectra of back scattered light from the sample can be measured over the entire optical bandwidth simultaneously enabling fast imaging without the need for a moving mirror. Signal depth information can be extracted from this spectral measurement using digital signal processing (Fourier transform). The advantage of FD-OCT over TD-OCT is the speed at which an image can be obtained. Eliminating the need for the moving mirror means that images can be obtained much faster, an obvious benefit when imaging live moving patients.
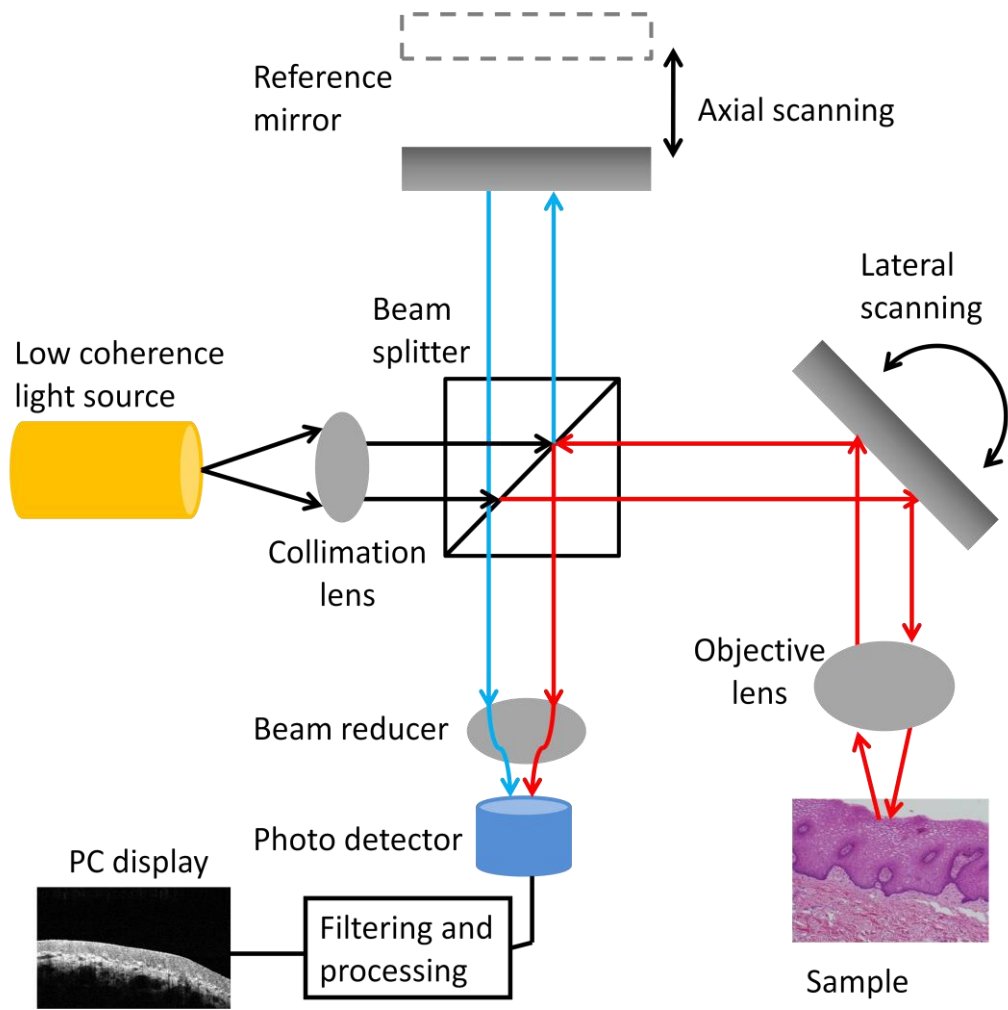
Figure 1.12 Simplified schematic diagram of Time domain OCT configuration
Blue = reference beam, Red = sample beam
Collimation lens = to align light beams into a parallel configuration
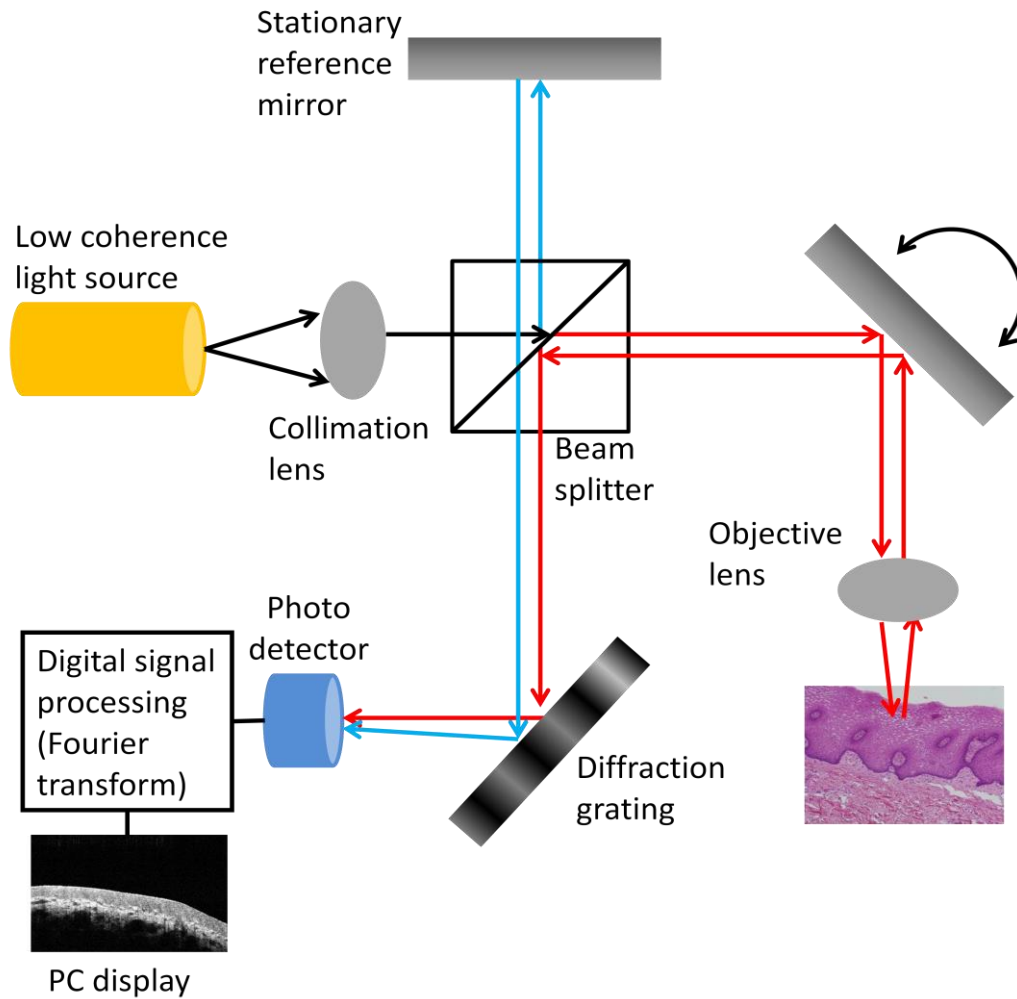
Figure 1.13 Simplified schematic diagram of Fourier domain OCT configuration. Blue = reference beam, Red = sample beam. Collimation lens = to align light rays into a parallel configuration.

Light source

The light source is the most expensive and important component of the OCT device. The light source must be broadband, low coherence light. This can be femto-second mode lock pulsed lasers, super-luminescent diodes or fibre amplifiers. The light source is important in determining the depth of imaging and the resolution. Near IR light is used because these long wavelengths penetrate well into tissues, are not absorbed by haemoglobin and are scattered less than light of shorter wavelengths.

Resolution

The coherence length of the light source determines the axial resolution of the resulting image. The coherence length of a light source is determined by how long the phase of a beam of light remains correlated (Figure 1.14). Light has a finite length of coherence as light travels in wave trains (Olsen 1996). Each wave train has a finite length which determines the length of the light phase which is correlated. Coherence is inversely proportional to the bandwidth of a light source, meaning light sources which simultaneously produce a wide range of wavelengths (or frequencies as one is inversely proportional to the other) have lower coherence than a single wavelength light source (with a narrow bandwidth) (Chen *et al.,* 2007). Signals from the reference arm and the sample arm only interfere when the path length difference is smaller than the coherence length. This means, by using a low coherence length light source, signals from different depths of a sample can be distinguished when they occur a few microns apart. Standard OCT systems give axial resolution of approximately 10μm however, novel OCT systems with laser light sources have achieved resolutions down to 1μm (Morgner *et al.,* 2000). This axial resolution is up to 100 times better than ultrasound making it more suitable for imaging morphological changes to smaller biological structures such as epithelia. The transverse resolution is dependant of the optical properties on the sample arm, for example the numerical aperture of the lens and the size of the focus spot on the sample.

Depth of penetration

The maximum imaging depths of OCT depend on the light scattering and attenuation properties of the tissue being imaged as well as the wavelength of light used. Light of longer wavelengths (750- 1400nm) is used as it is able to penetrate further into tissues as it experiences less scattering effects compared to shorter wavelength light. Transparent tissues such as those in the eye give the greatest depth of imaging. Depths of 2-3mm have been achieved in tissue engineered structures (Georgakoudi *et al.,* 2008) which is the limit in many tissues (Fujimoto 2003). This depth of imaging is low compared to other imaging techniques such as x-ray, ultrasound, magnetic resonance imaging (MRI) and computed tomography (CT) but OCT has the advantage of not requiring ionizing radiation (used in x-rays) and has a greater resolution compared to these methods.

The thickness of healthy oral mucosa epithelia vary between 75µm - 550µm in different regions (Ridgeway *et al.,* 2006). Many mucosal diseases are associated with considerable epithelial thickening however, a depth of 2mm is adequate to gain information in the majority of mucosal diseases, which often manifest in the boundary region between the epithelium and connective tissue. This depth of penetration is considerably better compared to other imaging modalities such as contact endoscopy, methylene blue, acetic acid and indigo carmine. These technologies provide transverse resolution of between 10 – 71 µm and enable signals from 100µm deep to be seen (Ridgeway *et al.,* 2006). This information is however, visible as a plane view rather than the more informative (and histologically comparative) cross section which is achievable with OCT.
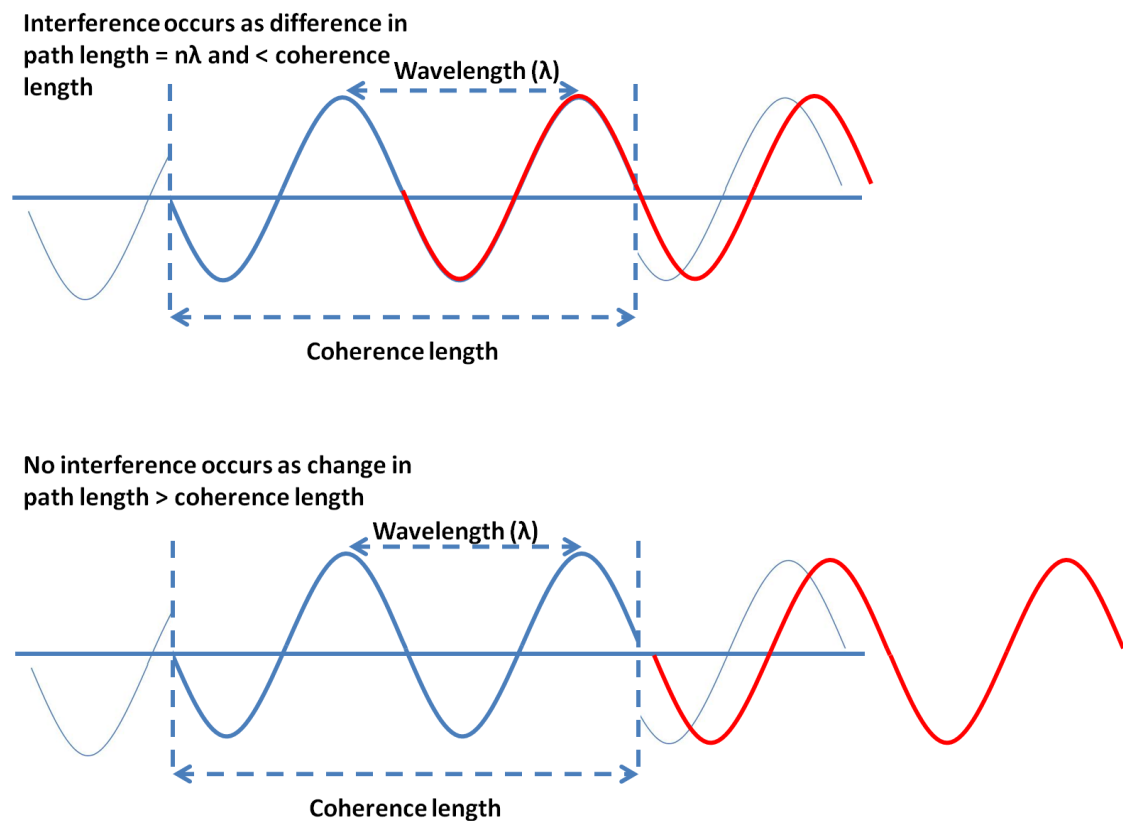
Figure 1.14 An illustration of coherent light source interference

Applications

OCT is currently widely used in ophthalmology as the optical properties of the eye make it relatively easy to image compared to other tissues which have higher light scattering properties. OCT for retinal applications was first demonstrated *in vivo* in 1993 (Fujimoto 2003). Its ability to produce real time images of defects and morphological differences on the

retina non-invasively has changed the way ophthalmologists image and treat retinal conditions. OCT has now been applied to many areas of ophthalmology and is used for imaging and diagnosing macular holes, macular oedema, choroidal neovascularization, vitreomacular traction, epiretinal membranes, glaucoma, age-related macular degeneration, uveitis and cataract (Sakata *et al.,* 2009; Bechtel 2010). Dr Walsh, of the Doheny Eye Institute, sees the potential for OCT to be used as a diagnostic tool in the developing world for the diagnosis of global blindness. The simplicity of the system and the falling costs of light sources make it plausible that in the future diseases leading to global blindness could be diagnosed in a simpler way that is accessible to patients without the need for on-site ophthalmologists (Bechtel 2010).

It is hoped that the technical advances which have been born from OCT's use in ophthalmology may enable it to be used in a number of other areas of diagnostics and imaging. The technology has progressed rapidly since 1991 and continues to improve with a large amount of research into OCT taking place. Other applications under investigation include cancer diagnosis in several areas of the body (Jeres *et al.,* 2010), intracoronary imaging to evaluate stent dissolution and lumen architecture (Bezerra *et al.,* 2009) and Doppler OCT for functional imaging of blood flow in vascular disease and post photodynamic therapy in carcinoma (Standish *et al.,* 2008).

OCT and OSCC

Rdigeway *et al*., examined various locations of the oral cavity and oropharynx in 41 patients using time domain OCT (Ridgeway *et al.,* 2006). Patients were under general anaesthetic to reduce movement artefacts experienced when using time domain OCT systems. The speed of scanning used here was 500 A-scans (axial direction scans) per second however, more recently scan speeds of 40,000 scans/second have been achieved with Fourier domain OCT (Sakata *et al.,* 2009), removing the need to anaesthetise patients prior to imaging. Many different anatomical features of the oral mucosa in various locations could be seen using OCT in healthy patients (Figure 1.15). These included the epithelial connective tissue junction, stratified squamous epithelium and lamina propria (connective tissue) in all areas of healthy tissue. More location specific features could also be determined including the filiform papillae on the dorsum of the tongue, seromucous glands on the mucosal side of the lower lip, glandular duct architecture in the floor of the mouth and blood vessels in the floor of the mouth (Ridgeway *et al.,* 2006). Blood vessels containing blood and ducts containing clear fluid both appeared as black regions on the cross-sectional images however, the blood vessels produced an "optical shadow"; as light was absorbed by haemoglobin (and other components of the blood), images could not be obtained underneath the blood vessels. This optical shadow was not seen with the ducts containing clear fluids.

The appearance of healthy buccal mucosa, dysplastic oral mucosa and OSCC of the alveolar ridge when imaged using OCT could be detected (Figure 1.16). The dysplastic buccal mucosa has a different appearance around the epithelial connective tissue border and there is less difference between the brightness of the epithelium and the connective tissue in this image compared to the healthy buccal mucosa. The squamous cell carcinoma shows a complete disruption to the image. There in banding throughout the image (vertical white bands) and the definition between the epithelium and the connective tissue is lost.
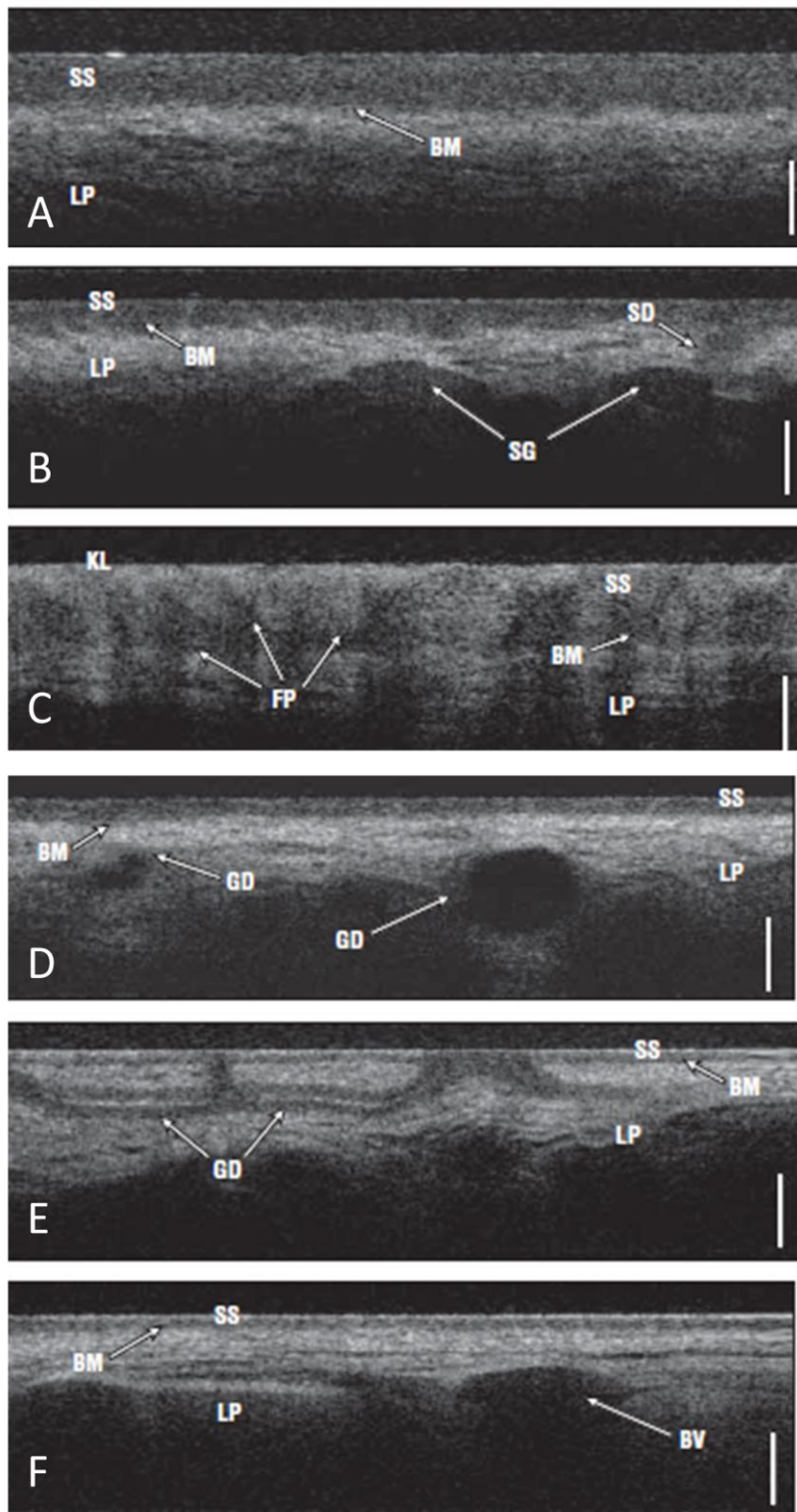
Figure 1.15 OCT of different regions of healthy oral mucosa.
(A) Healthy buccal mucosa, (B) Mucosal side of lower lip, (C) Dorsum of the tongue, (D)
Surface of healthy tongue, E) Floor of the mouth, (F) Floor of the mouth.
Scale bar 500µm
SS = stratified squamous epithelium, BM= basement membrane, LP = lamina propria
SD = seromucocinous duct, SG = seromucinous glands, FP = Filiform papillae, KL = keratin
layer, GD= Gland duct, BV= blood vessel
 Images reproduced from (Ridgeway *et al.,* 2006)

Healthy buccal mucosa
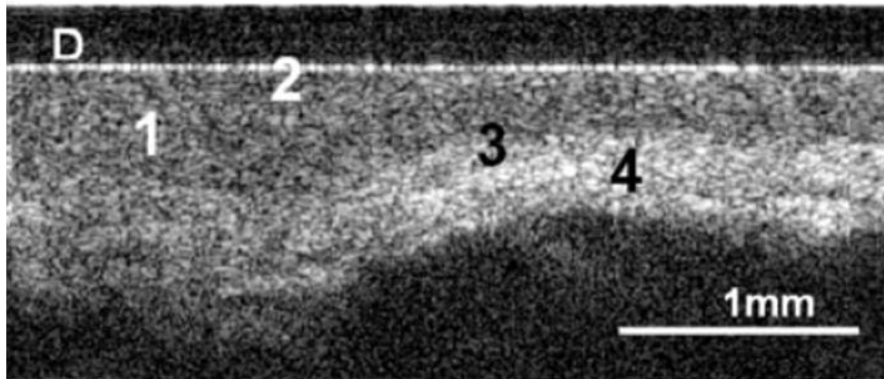
Dysplastic buccal mucosa
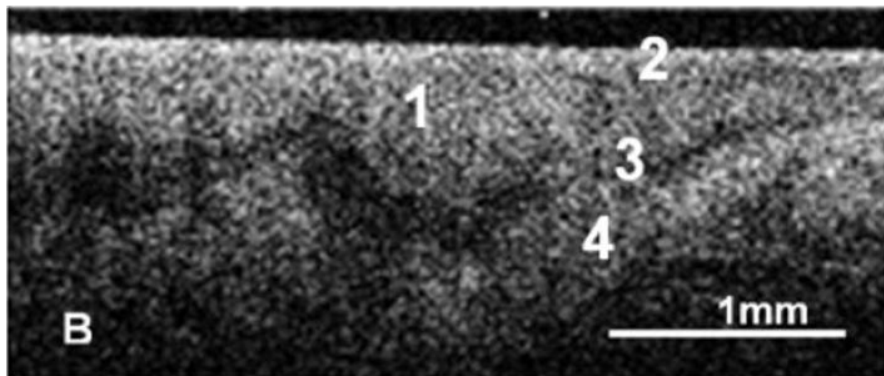
Squamous cell carcinoma of alveolar ridge
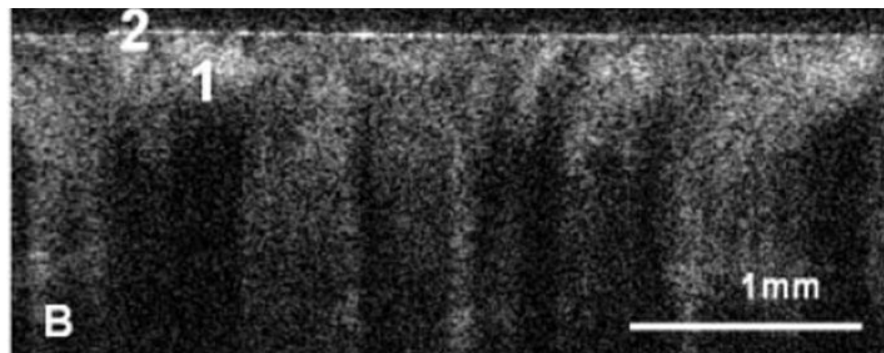
Figure 1.16 OCT image of pathological lesions in the oral cavity.
Images adapted from (Wilder-Smith *et al.,* 2009). (1) Stratified squamous epithelium,
(2) keratinized epithelial surface layer, (3) basement membrane, (4) submucosal.

Wilder-Smith *et al*., tested the ability of clinicians to diagnose different stages of oral cancer progression in three different regions of the oral cavity (tongue, buccal and floor of mouth) from OCT images (Wilder-Smith *et al.,* 2009). Observers were trained to score OCT images for severity of cancer progression in two hours. They were displayed 50 OCT images and the corresponding histology of those OCT images.   OCT from 50 patients was then scored by the trained observers and these scores were compared to scores (on the same scale) given by separate histo-pathological diagnosis. The intra- and inter- observer diagnosis was established as well as the level of agreement with histo-pathological diagnosis of the same samples. Agreement between scores and histlpathology was calculated using Cohen's λ statistics. Inter- and intra-observer agreement was very good with λ values of 0.872 (intra) and 0.870 (inter) for OCT diagnosis (inter- observer agreement for histo-pathological diagnosis was 0.923). The diagnosis from the OCT images was in good agreement with the diagnosis from histopathology, with a Cohen's λ of 0.896. The specificity for detecting SCC versus all other modalities (healthy, dysplasia and carcinoma *in situ*) was 0.931 and the specificity was 0.973. This specificity and sensitivity was good and shows the value of OCT in diagnosing OSCC. The sensitivities and specificities for diagnosing stages of dysplasia were not stated so may not have been as high. Despite this the agreement of OCT diagnosis with histopathology diagnosis was strong (0.896) and the time taken to train (2 hours) is far less compared to the experience required to gain high specificities using other techniques such as Toludene Blue (Wilder-Smith *et al.,* 2009).

Tsai *et al*., imaged patients with various stages of dysplasia and OSCC, using swept source OCT, in an attempt to produce a quantitative method to diagnosis between mild dysplasia, moderate dysplasia, early stage OSCC and well developed OSCC (Tsai *et al.,* 2009). Three markers, observable in OCT images, were used to determine the stage of dysplasia or OSCC. The first of these markers was the epithelial thickness as epithelial hyperplasia is often seen as a precursor to mild dysplasia and is observed in dysplasia. An increase in epithelial thickness was observed from normal buccal mucosa < mild dysplasia < moderate dysplasia. Once the lesion had progressed to OSCC the basement membrane could no longer be clearly seen in the OCT images, this same observation was also noted in (Ridgeway *et al.,* 2006).

The second marker for staging the level of cancer progression was to look at the variation in the intensity of the signal from different depths of the epithelial portion of OCT images. To calculate this, depth dependant lateral scan standard deviation was plotted. Lines with a length of 2mm were drawn laterally across the epithelium at specific depths between 0 and 1.5mm. The standard deviation of intensity for each lateral line, calculated from the intensity profile, was plotted as a function of depth. This was done for all 5 conditions (from normal epithelium to well developed OSCC) and the profiles of each condition were markedly different. The graphs for OSCC were clearly distinguishable from the dysplastic and healthy profiles

(standard deviation decayed with time for OSCC). For healthy mucosa, mild dysplasia and moderate dysplasia the highest standard deviation corresponded to the location of the basement membrane. The profile of these three graphs had distinct differences. To quantify this difference Tsai *et al.,* calculated the axial distance for which the standard deviation was above 70% of the maximum. For the four mildly dysplastic and four moderately dysplastic samples they analysed there was a difference, the moderate dysplasia showed higher standard deviation over a greater depth compared to the mild dysplasia.

The early stage and well developed OSCC, although easily distinguished from healthy and dysplastic tissue using the previous analysis could not be distinguished from one another. Therefore, a third method was employed to determine the difference between early stage OSCC and well developed OSCC. In the early stage OSCC white and black vertical bands could be observed through the lamina propria. Tsai *et al*., propose this image pattern was due to the connective tissue papillae observed in the histology from the early stage OSCC, which is not visible in the well developed OSCC. Therefore, the lateral intensity of an area of banding was plotted and the standard deviation of this early stage OSCC was compared to the standard deviation of the lateral intensity profile of the same depth in well developed OSCC. The standard deviation was higher for all 4 early stage OSCC compared to the 4 well developed OSCC samples examined. A difference between early stage and well developed OSCC could also be observed in the decay profile of the intensity of the signal in the axial direction. The intensity of the signal decayed as samples were imaged deeper. More light was absorbed in the well developed OSCC compared to the early stage OSCC, therefore the exponential decay constant was greater in well developed OSCC. This provides another quantifiable method to distinguish between the two stages of OSCC. It is believed this increased absorption of light is due to the high density of cancer cells in well developed OSCC and the amount of capillaries, and therefore blood, which will absorb the light in greater quantities compared to the lamina propria (connective tissue) (Tsai *et al.,* 2009).

The sample size (four samples for each stage) is small so further work is needed in a larger sample size randomised control trial to test these parameters for their specificity and accuracy in staging oral cancer using OCT. These results are encouraging and show that OCT may not just provide qualitative information of disease progression but may also provide a quantifiable standardised method for diagnosis (Tsai *et al.,* 2009).

Aims and Objectives

The aim of this project was to develop and utilise *in vitro* 3D tissue engineered models of oral mucosa and oral cancers to test novel therapeutic and diagnostic technologies.

The three main objectives of this thesis were:

1) To develop and characterise tissue engineered models which model all stages of oral cancer progression from normal oral mucosa through dysplastic oral lesions and carcinoma *in situ* to early invasive oral squamous cell carcinoma and ultimately to solid expanding tumour islands of squamous cell carcinoma.

2) To investigate the behaviour of polymersomes as future vehicles for delivering agents into oral tissue. This involved looking at the distribution and penetration capacity of this novel drug delivery system in 3D models of healthy oral mucosa and solid expanding tumours.

3) To use the tissue engineered models of oral cancer to test the ability of novel diagnostic technologies to distinguish dysplastic and malignant lesions from healthy tissue. These technologies included: a metabolic cell marker (Vybrant™ cell metabolic activity kit with C_{12}-resazurin), impedance spectroscopy, Fourier tansform infra-red and optical coherence tomography.

Chapter 2: Developing Tissue Engineering Models of Oral Cancer

2.1 Aim

To develop and characterise tissue engineered models which have characteristics of all stages of oral cancer development from a healthy oral mucosa to a dysplastic epithelium right through to a solid expanding tumour mass.

2.2 Introduction

Tissue engineered models of healthy human tissue have been developed for the replacement and repair of tissues in the body. These models along with models of diseases, such as cancer, provide important *in vitro* tools for the study of disease development, therapeutics and diagnostic technologies.

In this chapter three types of models are presented. The first is a 3D model of healthy human oral mucosa which comprises of an epithelium with underlying connective tissue component. This tissue model has been developed in the MacNeil laboratory and has been developed for clinical applications (Bhargava *et al.,* 2004). This tissue engineered oral mucosa (TEOM) has been successfully used in the clinic to replace scarred tissue in the urethra (Bhargava *et al.,* 2008) with three year follow up.

The second group of models developed here are models of dysplasia and carcinoma *in situ*. Oral cancer most often originates in the epithelium as epithelial cells transform from healthy cells to dysplastic and finally become malignant cells. This method of transformation is widely accepted however, it is not proven that all malignant cells go through the transition of being dysplastic before become malignant. Here we produce models using a variety of different oral cancer and dysplastic oral cell lines to look at the morphology of epithelia produced when these cell lines are cultured on a connective tissue scaffold along with healthy fibroblasts. It is our aim to produce models for all stages of oral cancer progression from mild dysplasia to carcinoma *in situ*, and subsequently invasive OSCC.

The third model is the multi-cellular tumour spheroid (MCTS) model. MCTS model solid expanding tumour masses, found deep in tissues once OSCC has invaded. MCTS have previously been developed to model several different types of cancer from cell lines originating from cancers in different regions of the body. MCTS have shown real potential as

71

a more accurate method for high through-put screening of novel drug compounds (Hirschhaeuser *et al.,* 2010). Here we characterise the MCTS currently used in our laboratory and look at the oral cell types which are able to spontaneously form MCTS under the right *in vitro* conditions.

2.3   Materials and Methods

Cell culture basics

All cell culture work was carried out in Class II laminar flow hoods (Walker Safety Cabinets, Glossop, Derbyshire, UK). Laminar flow hoods and equipment used within them were sterilised prior to use using 70% (v/v) industrial methylated spirits (IMS) (Fisher Scientific UK Ltd, Loughborough, UK) or by autoclave sterilisation. Laboratory plastic wear for cell culture was purchased from Costar, High Wycombe, Buckinghamshire, UK and Greiner Bio-one, Gloucestershire, UK. Liquid materials were either purchased sterile from the supplier or were filter sterilised prior to use. All cells were incubated at 37°C in humidified incubators containing 5% CO_2.

Cell culture medium

Materials

Dulbecco's modified Eagle's Medium (DMEM)
DMEM was purchased from Gibco, Paisley, UK and came supplemented with 4500mg/l glucose GlutaMAX™ I and sodium pyruvate.

Nutrient Mixture F12 (Ham's F12)
From Biosera, East Sussex, UK, supplemented with L-glutamine and sodium bicarbonate.

Fetal Calf Serum (FCS)
FCS (heat inactivated) from Biosera, East Sussex, UK was stored frozen. New batches were tested prior to use to ensure comparable cell growth and behaviour from the previous batch.

Penicillin/Streptomycin
From Sigma Aldrich, Dorset, UK.

Amphotericin B
Amphotericin B from Sigma Aldrich, Dorset, UK. Store protected from light.

Adenine
0.5g Adenine powder (Sigma Aldrich, Dorset, UK) was mixed with 70ml distilled water. 1M Hydrochloric acid (HCl) was added to the mixture until the powder dissolved completely. The solution was filter sterilised and made up to 80ml with distilled water to give a final concentration of 6.25µg/ml.

Insulin

10mg Bovine Insulin powder (Sigma Aldrich, Dorset, UK) was added to 1ml of 0.01M HCl. Once dissolved 9ml of distilled water was added to give a final concentration of 1mg/ml.

3, 3, 5- Tri-iodothyronine/Apo-Transferrin

13.6mg T_3 (Sigma Aldrich, Dorset, UK) was dissolved in the minimum volume of 0.02M sodium hydroxide (NaOH). Once dissolved the solution was made up to 100ml with distilled water. 250mg apo-transferrin (Sigma Aldrich, Dorset, UK) was dissolved in 30ml of PBS. 0.5ml of the T_3 solution was added to 30ml of the apo-transferrin solution and the volume was made up to 50ml with PBS.

Hydrocortisone

25mg of hydrocortisone powder (Sigma Aldrich, Dorset, UK) was added to 1ml distilled water. The volume was then made up to 10ml with PBS.

Epidermal Growth Factor (Human Recombinant from E. Coli)

Epidermal growth factor (EGF) was purchased from Sigma Aldrich, Dorset, UK. 100μg was dissolved into 1ml of distilled water.

Cholera Toxin

Cholera toxin (extracted from *Vibrio cholera)*, was purchased from Sigma Aldrich, Dorset, UK. A 1mg aliquot was dissolved into 1.18ml distilled water, this was stored as stock at 4°C. 100μl of stock was diluted into 10ml of media with serum.

RPMI 1640 AQ media

From Sigma Aldrich, Dorset, UK, RPMI contained sodium bicarbonate and L-glutamine.

IMEM

Iscove's Modification of DMEM from Gibco, Paisley, UK was supplemented with L-glutamine.

Preparation of Cell culture medium

Normal Oral Keratinocytes

Normal Oral Keratinocytes were cultured in Green's Medium. Media was made 500ml at a time, stored at 4°C and used for up to one month. Sterility of cell culture medium was checked by incubating 10ml of cell culture medium at 37°C for 24 hours prior to use. The composition of Green's medium is outlined below:

Component	Volume and stock solution	Final concentration	Storage
Dulbecco's modified Eagle's Medium	330ml	66%	4°C
Nutrient Mixture F12	108ml	21.6%	4°C

(Ham's F12)			
Fetal Calf Serum	50ml	10%	-20°C
Penicillin/Streptomycin	5ml of 10,000i.u./ml penicillin and 10,000µg/ml streptomycin	100i.u./ml penicillin and 100µg/ml streptomycin	-20°C
Amphotericin B	1.25ml of 250µg/ml	0.625µg/ml	-20°C
Adenine	2ml of 6.25µg/ml	0.025µg/ml	-20°C
Insulin	2.5ml of 1mg/ml	5µg/ml	4°C
3, 3, 5- Tri-iodothyronine/ Apo-Transferrin	0.5ml of 1.36µg/ml T_3 and 5mg/ml apo-transferrin	1.36ng/ml T_3 and 5µg/ml apo-transferrin	-20°C
Hydrocortisone	80µl of 2.5mg/ml	4µg/ml	4°C
Epidermal Growth Factor	25µl of 100µg/ml	5ng/ml	-20°C
Cholera Toxin	500µl of 8.47µg/ml	8.47ng/ml	4°C

Table 2.1 Green's medium

Normal Oral Fibroblasts

Normal Oral Fibroblasts (NOF) were cultured in supplemented DMEM (see Table 2.2). Media was made 500ml at a time, stored at 4°C and used for up to one month. Sterility of cell culture medium was checked by incubating 10ml of cell culture medium at 37°C for 24 hours prior to use. The composition of 10% DMEM is described below:

Component	Volume and stock solution	Final concentration	Storage
Dulbecco's modified Eagle's Medium	443.75ml	89%	4°C
Fetal Calf Serum	50ml	10%	-20°C
Penicillin/Streptomycin	5ml of 10,000i.u./ml penicillin and 10,000µg/ml streptomycin	100i.u./ml penicillin and 100µg/ml streptomycin	-20°C

Amphotericin B	1.25ml of 250µg/ml	0.625µg/ml	-20°C

Table 2.2 10% DMEM medium

FaDu (ATCC HTB-43)

FaDu cells were obtained from ATCC (HTB-43), Manassas, VA, USA. FaDu are a squamous cell carcinoma human cell line from a male patient's pharynx. FaDu cells were cultured in 10% RPMI (Table 2.3).

Component	Volume and stock solution	Final concentration	Storage
RPMI 1640	443.75ml	89%	4°C
Fetal Calf Serum	50ml	10%	-20°C
Penicillin/Streptomycin	5ml of 10,000i.u./ml penicillin and 10,000µg/ml streptomycin	100i.u./ml penicillin and 100µg/ml streptomycin	-20°C
Amphotericin B	1.25ml of 250µg/ml	0.625µg/ml	-20°C

Table 2.3 FaDu cell culture medium

SCC4 (ATCC CRL-1624), SCC9 (ATCC CRL-1629), SCC25 (ATCC CRL-1628)

SCC4, SCC9 and SCC25 are squamous cell carcinoma human cell lines originally isolated from the tongues of different patients. All these cell lines were obtained from ATCC (Manassas, VA, USA). Cells were cultured in the following cell culture medium (Table 2.4).

Component	Volume and stock solution	Final concentration	Storage
Dulbecco's Modified Eagle's Medium	225ml	45%	4°C
Nutrient Mix F12 (Ham's F12)	225ml	45%	4°C
Fetal Calf Serum	50ml	10%	-20°C
Penicillin/Streptomycin	5ml of 10,000i.u./ml penicillin and 10,000µg/ml	100i.u./ml penicillin and 100µg/ml streptomycin	-20°C

	streptomycin		
Amphotericin B	1.25ml of 250µg/ml	0.625µg/ml	-20°C
Hydrocortisone	80µl of 2.5mg/ml	0.4µg/ml	4°C

Table 2.4 SCC cell culture medium

Cal27 (ATCC CRL-2095)

A squamous cell carcinoma human cell line isolated from the tongue was purchased from ATCC (Manassas, VA, USA). This cell line established as a squamous cell carcinoma has recently been found to show behaviour and morphology more like an adenosquamous cell carcinoma (Jiang *et al.,* 2009). Cal27 cells are culture in 10% DMEM (Table 2.2)

DOK (ECACC 94122104)

A dysplastic oral keratinocyte cell line isolated from the tongue of a 57 year old man. The patient had a squamous cell carcinoma and the remaining dysplasia was removed and used to establish this cell line. The dysplasia was described as mild to moderate. DOK cells were obtained from the European Collection of Cell Culture (ECACC) *via* Sigma Aldrich (Dorset, UK). Cells were cultured in 10% DMEM supplemented with hydrocortisone to promote cell growth (Table 2.5).

Component	Volume and stock solution	Final concentration	Storage
Dulbecco's modified Eagle's Medium	443.75ml	89%	4°C
Fetal Calf Serum	50ml	10%	-20°C
Penicillin/Streptomycin	5ml of 10,000i.u./ml penicillin and 10,000µg/ml streptomycin	100i.u./ml penicillin and 100µg/ml streptomycin	-20°C
Amphotericin B	1.25ml of 250µg/ml	0.625µg/ml	-20°C
Hydrocortisone	1ml of 2.5mg/ml	5µg/ml	4°C

Table 2.5 DOK cell culture medium

PE/CA-PJ34 (Clone C12), (ECACC 97062513)

A human basaloid squamous cell carcinoma cell line established from cells removed from a 60 year old male patient. PE/CA-PJ34 cells were obtained from the European Collection of Cell

Culture (ECACC) *via* Sigma Aldrich, Dorset, UK and cultured in IMEM medium supplemented with 10% FCS (Table 2.6).

Component	Volume and stock solution	Final concentration	Storage
Iscove's Modification of DMEM (IMEM)	443.75ml	89%	4°C
Fetal Calf Serum	50ml	10%	-20°C
Penicillin/Streptomycin	5ml of 10,000i.u./ml penicillin and 10,000µg/ml streptomycin	100i.u./ml penicillin and 100µg/ml streptomycin	-20°C
Amphotericin B	1.25ml of 250µg/ml	0.625µg/ml	-20°C

Table 2.6 PE/CA-PJ34 cell culture medium

D19 and D20

The D19 and D20 cells are dysplastic cell lines which were kindly donated by Dr Keith Hunter at School of Clinical Dentistry, University of Sheffield (McGregor *et al.,* 1997; McGregor *et al.,* 2002). D19 and D20 cells were cultured in Green's medium (see Table 2.1).

Passaging, counting and storage of cells

Materials

Phosphate buffered saline (PBS)

PBS tablets (Dulbecco A) were purchased from Oxoid Ltd, Basingstoke, Hampshire, UK. One PBS tablet was added to every 100ml of distilled water in a bottle able to withstand autoclaving to give a PBS concentration of 100mM. PBS was autoclaved for 10 mins at 115°C and stored at room temperature.

Trypsin EDTA

Trypsin/EDTA (0.05% trypsin/ 0.02% EDTA w/v) was purchased from Sigma Aldrich (Dorset, UK) and stored at -20 °C.

Cryopreservation Medium

Cryopreservation medium was made using 90% fetal calf serum (Biosera, East Sussex, UK) and 10% dimethyl sulphoxide (DMSO) (Sigma Aldrich, Dorset, UK) (v/v).

Passaging of cells

When cells reached 80% confluency they were transferred into a new cell culture flask with lower cell numbers to enable cell proliferation to continue. To passage cells the cell culture medium was removed and cells were washed with 10ml of PBS to remove any serum proteins in the residual cell culture medium. Cells were incubated with 5ml 0.05% trypsin/0.02% EDTA (w/v) for 5 minutes or until all cells had detached. The trypsin EDTA was neutralised using cell culture medium containing FCS at a 1:1 (v/v) ratio. Cells were next centrifuged at 1200 revolutions per minute (rpm) for 5 minutes using a bench top centrifuge. The supernatant was discarded in bleach and the cellular pellet re-suspended in the desired volume of cell culture medium.

Counting cells

Cell counts were performed using a modified Neubauer haemocytometer (Weber Scientific International, Middlesex, UK). At least two $1mm^2$ squares (volume 1×10^{-4} ml) were counted and their average taken. Cell number was calculated as follows:

$$\frac{\text{average number of cells counted per } 1mm^2 \text{ square x dilution factor}}{\text{volume counted } (1 \times 10^{-4} \text{ml})} = \text{Cells/ml}$$

e.g. average cell count of 100 with no dilution = 1 million cells per ml

Freezing cells for cryo-preservation

For cryopreservation cells were treated as for passaging (described above). However, rather than re-suspending the cellular pellet in media, cells were re-suspended into cryopreservation media (90% FCS, 10% DMSO). The pellet was re-suspended to give a concentration of between 0.5 million and 3 million cells per ml of cryopreservation medium, depending on the cell type. 1ml of this cell suspension was pipetted into each cryovial (Cellstar cryovials from Greiner bio-one, Gloustershire, UK) and cryovials were placed in a Nalgene™ Cryo 1°C freezing container (Nalgene Co., New York, USA). This freezing container, which contained 250ml of iso-propanol, controlled the rate of cooling to be 1°C per minute in a -80 °C freezer. After a minimum of 4 hours the vials were then transferred into a liquid nitrogen dewar (temperature of -196 °C).

Thawing cells

Cryovials were removed from liquid nitrogen using appropriate safety precautions and the cells in the DMSO mixture were quickly thawed in a 37 °C water bath. Once thawed, the cell solution was diluted in cell culture medium and centrifuged for 5 mins at 1200 rpm. The supernatant was discarded and the cellular pellet re-suspended in cell culture medium.

Cancer cell line culture

Cells were cultured in T75 tissue culture flasks until 80% confluent. Cell culture medium was replenished ever 2-3 days. Cells were used up to 15 passages after the passage they were purchased, or until their behaviour (eg. speed of growth) changed. Stocks of low passage number were kept in liquid nitrogen. Cells were periodically tested for mycoplasma infection and any infected cells were discarded.

Primary Cell Extraction from Oral Biopsies

Materials and preparation

"Difco trypsin"

Difco trypsin was prepared at a concentration of 0.1% (w/v). 0.5g of Difco Trypsin powder from Difco, West Molesey, Surrey, UK was dissolved in 500ml of PBS with 0.5g of D-glucose. The pH of the solution was adjusted to pH 7.4 with 2M NaOH. The solution was filtered sterilised using a filter with 0.22µm pores, divided into 10ml aliquots and stored at -20°C. Difco trypsin solution was supplemented with 100 IU ml^{-1} penicillin, 100 mg ml^{-1} streptomycin and 0.625 µg ml^{-1} amphotericin B prior to use.

Syringes and filters

Sterile syringes and filters for sterilisation were purchased from BD Biosciences, Oxford, UK. The pore size of these filters was 0.22µm enabling them to remove contaminating bacteria or fungi.

Collagenase A

Collagenase A extracted from *Chlostridium histolyticum* (Sigma Aldrich, Dorset, UK) was dissolved in Dulbecco's Modified Eagle's Medium (DMEM) supplemented with 10% Fetal Calf Serum (FCS) and stored at -20°C. The final concentration of collagenase was 0.05% (w/v).

Scalpel blades

Scalpel handles and blades, size 22, were purchased from Swann-Morton, Sheffield, UK.

Surgical removal of biopsy

Buccal or gingival tissue was obtained from consenting patients during routine dental surgeries (Sheffield Research Ethics Committee approval (Ref: 07/H1309/105)) or from willing volunteers by a dentist. Once removed the biopsy, typically around 5-10mm^2, was collected in a sterile tube containing PBS supplemented with 100 IU ml^{-1} penicillin, 100 mg ml^{-1} streptomycin and 0.625 µg ml^{-1} amphotericin B and stored at 4°C before processing.

Preparation of Irradiated Feeder Layer

XCELLentis 3T3 murine fibroblast cells (XCELLentis, Gent, Belgium) were used as a feeder layer for proliferating keratinocytes. These mouse cells were expanded first in regular cell culture flasks and subsequently using a CellSTACK® (Corning Life Sciences Inc, New York,

USA). The CellSTACK® was used to obtain large numbers of cells as this had a surface area of 6,360cm^2. Once the cell stack was 80% confluent cells were passaged as described in the previous section and put into a sterile sealed 25ml universal tube (in fresh cell culture medium). The cells were exposed to 60 Grays using a cobalt-60 source irradiator to arrest the 3T3 cell growth. Once irradiated the cells, referred to as irradiated 3T3s (i3T3) were cryopreserved as described on page 78. Cells were resurrected immediately prior to use.

Isolation of primary normal oral keratinocytes

Oral biopsies were incubated overnight at 4°C in 0.1% w/v Difco trypsin. The epithelium was then peeled from the connective tissue component. Keratinocytes were gently scraped from the underside of the epithelium and the top side of the connective tissue layer using a scalpel in a Petri dish containing the Difco trypsin solution. The large lumps of tissue remaining were removed and stored in PBS supplemented with 100 i.u./ml penicillin, 100 mg/ml streptomycin and 0.625 µg/ml amphotericin B for subsequent fibroblast extraction. The scraped cells and trypsin solution was centrifuged at 1200 rpm for 5 minutes. The cellular pellet was resuspended in Green's medium (Table 2.1 Green's medium on page 74) and seeded onto an irradiated mouse fibroblast (i3T3) feeder layer in a T75 cell culture flask.

Normal Oral Keratinocyte Culture

NOKs were cultured according to the method of Rheinwald and Green (Rheinwald and Green 1975). Briefly, cells were cultured on an irradiated mouse fibroblast (i3T3) feeder layer in Green's media. Cells were cultured until 80% confluent and cell culture medium was replenished every 2-3 days. NOK cells could be used up to and including passage 3 however, after this the cells lost their ability to adhere to cell culture surfaces and could no longer be cultured.

For NOK cell culture the i3T3 feeder layer of cells was detached using 0.02% EDTA solution before passaging NOK cells. NOK were seeded with a fresh i3T3 feeder layer in the new cell culture flask.

Isolation of primary normal oral fibroblasts

Normal oral fibroblasts (NOF) were isolated from the connective tissue of the biopsy. The connective tissue, remaining after NOK isolation, was finely minced using a surgical scalpel and incubated at 37 °C in a 5% CO_2 humidified incubator for 14-18 hours in 10 mL of 0.5% collagenase A. After incubation the collagenase A containing minced connective tissue was centrifuged at 2000 rpm for 10 minutes. The supernatant was carefully removed using a pipette and the cellular pellet (including undigested tissue) was re-suspended in 10% DMEM (Table 2.2 10% DMEM medium). The cell suspension was seeded into a T25 cell culture flask with vented lid.

Normal Oral Fibroblast Culture

NOF cells could be cultured up to and including passage 8. After passage 8 the cell behaviour changed and were no longer used for experiments.

Culturing tissue engineered oral mucosa

Preparation of De-epidermised dermis (DED)

Glycerol treated cadaveric skin was obtained from the Euro Skin Bank (Beverwijk Netherlands) and was stored at 4°C until in required. Skin was washed thoroughly in pre-warmed PBS for two days until all the glycerol had been removed and the skin cells were removed by dehydrating the skin in 1 M sodium chloride for 24 hours at 37 °C. The epithelium was then gently scraped from the surface of the skin and the skin then washed 3 times in PBS. This method removes the epidermis but retained basal membrane proteins such as collagen IV and laminin which aided the subsequent attachment of NOK in the 3D culture. The processed Euroskin, here referred to as de-epidermised dermis (DED), was stored at 4°C in Green's media. This process was very effective at removing cellular material from the skin but retaining structural integrity and basement membrane antigens. Figure 2.1 shows the appearance of the DED post processing demonstrating the extent of the de-cellularisation.
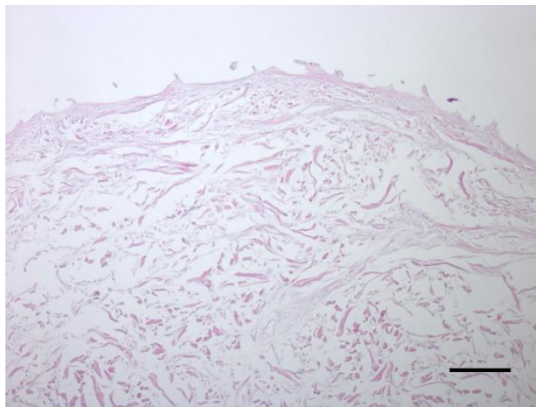
**Figure 2.1 H&E stained section of Euroskin post processing.
Scale bar 200µm.**

Culturing tissue engineered oral mucosa (TEOM)

Processed DED was cut into 2cm x 2cm squares and placed into 6 well plates submerged in Green's media. Chamfered surgical stainless steel rings with an internal diameter of 8mm were pushed onto the DED to provide a liquid tight seal. 1mL of cell suspension containing 5 x10^5 NOKs and 5x10^5 NOFs in Green's media was added into the ring. Green's media was also added outside the ring to stop the cell solution leaking out. Half the media inside the ring was changed each day. On day 3 the DED with cells attached was brought to an air liquid interface using a stainless steel grid. The underside of the model was in contact with Green's

media while the top was exposed to the air to encourage epithelial stratification. Models were cultured for 10-14 days at the air-liquid interface (ALI) (Figure 2.2).
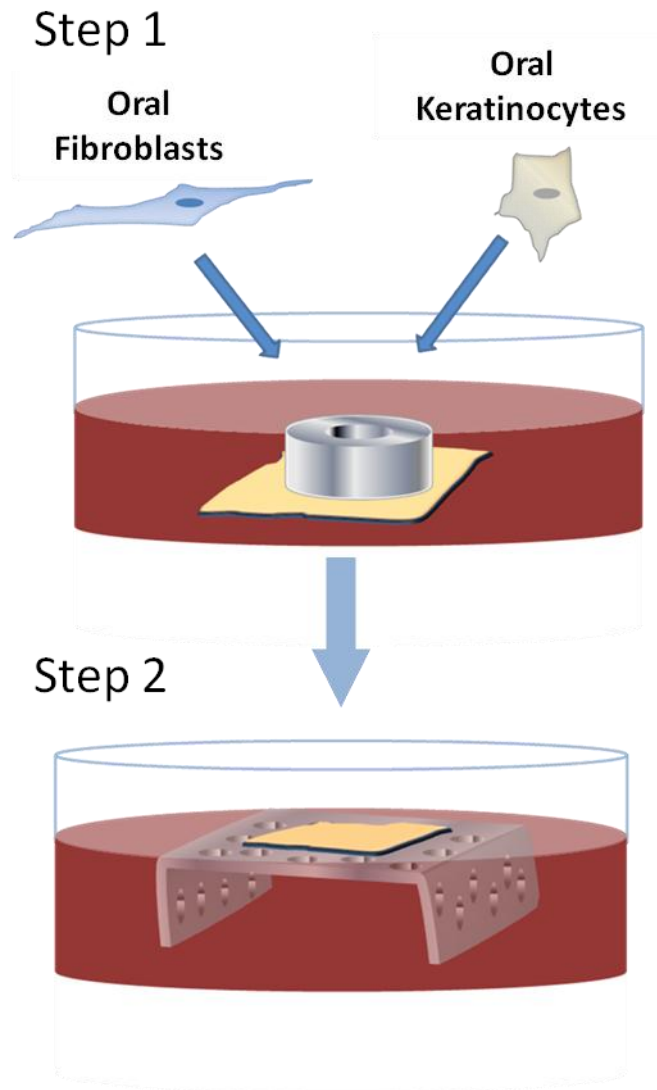
Figure 2.2 Method of culturing 3D TEOM

Culturing 3D models with OSCC cell lines

Eight different cell lines were cultured in 3D tissue engineered models to investigate the pathological appearance of different cell lines when cultured in three dimensions. These models were cultured using a very similar method to that described for TEOM. The Euroskin was processed in the same way as described previously. NOF (5×10^5) and oral cancer cells (2.5×10^5) were seeded onto processed Euroskin (DED) inside a surgical steel ring for 3 days before the models were raised to an ALI. Models were cultured in the cell culture medium corresponding to the cell line used. For details of the cell culture medium used for each cell line see page 72. Models were cultured for 7, 14 and 21 days before being fixed and processed for histological analysis.

Analysis of tissue engineered oral mucosa and 3D models of OSCC

Materials and preparation

3.7 % formaldehyde

37% paraformaldehyde was purchased from (Sigma Aldrich, Dorset, UK) and was diluted 1 in 10 in PBS.

3% hydrogen peroxide in PSB

A 3% hydrogen peroxide solution was made by adding 3ml of hydrogen peroxide to 97ml of PBS.

1M Tri sodium citrate buffer (pH6)

2.94g of tri-sodium citrate (dehydrate) was added to 1 litre of distilled water and mixed to dissolve. The pH was the adjusted to pH 6.0 using 1M HCl. 0.5ml of Tween20 was then added to the mixture which could be stored for up to 3 months at room temperature.

Monoclonal primary antibodies

Primary antibody	Clone	Supplier	Dilution in PBS
Collagen IV	94	Sigma Aldrich, Dorset, UK	1:500
AE1/AE3	AE1/AE3	Dako, Copenhagen, Denmark	1:100
Ki67	MM1	Dako, Copenhagen, Denmark	1:50

Table 2.7
Primary antibodies, suppliers and dilutions.

Secondary antibody

Vectastain® Elite ABC kit (Vector labs, Peterborough, UK) was made up as per the manufacturer's instructions. First a blocking serum was produced with serum from horse. Three drops of horse serum was added to 10ml of buffer in the mixing bottle provided. Next the Biotinylated secondary antibody was made up. Three drops of normal blocking serum stock was added to 10ml of buffer in another mixing bottle with 1 drop of biotinylated secondary antibody stock.

Avidin and Biotinylated horseradish peroxidase macromolecular Complex (ABC)

The Vectastain® Elite ABC solution was made up by adding 2 drops of reagent A to 5ml of buffer in a large mixing bottle. Next 2 drops of reagent B were added to the same bottle and this was mixed before being left to stand for 30 minutes.

3, 3'-diaminobenzidine

3, 3'-diaminobenzidine (DAB) kit (Vector labs, Peterborough, UK) was prepared immediately prior to use according to the manufacturers instructions. Two drops of buffer stock solution

were added to 5ml of distilled water and mixed well. Next 4 drops of DAB stock solution was added and mixed followed by 2 drops of hydrogen peroxide solution.

Fixing Tissue Engineered Models

Samples were washed in PBS and placed directly into 3.7% formaldehyde for at least 24 hours at room temperature prior to histological processing.

Histological analysis of tissue engineered oral mucosa

Samples were processed overnight using a Leica TP1020 benchtop tissue processor (Leica microsystems, Milton Keynes, UK). Samples were processed through the following solutions (Table 2.8 Histological processing schedule).

Solution	Time exposed to solution
10% neutral buffered formalin	1 hour
70% alcohol	1 hour
70% alcohol	1 hour
90% alcohol	1 hour
90% alcohol	1 hour
Absolute alcohol	1 hour
Absolute alcohol	1 hour
Absolute alcohol	1 hour
Xylene	1 hour 30 mins
Xylene	1 hour 30 mins
Paraffin Wax I	2 hours
Paraffin Wax II	2 hours

Table 2.8 Histological processing schedule

Samples were then bisected and embedded in molten paraffin wax using a Leica EG1160 embedding center, dispenser + hot plate (Leica microsystems, Milton Keynes, UK). Samples were embedded perpendicular to the bottom surface of the mould so the samples could be cut in the right orientation. Samples embedded in wax blocks were next cooled on ice blocks for at least 1 hour prior to sectioning using a Leica RM2235 microtome (Leica microsystems,

Milton Keynes, UK) with microtome blades, S35 type (Feather, Japan). Blocks were trimmed using initial slices of 10μm thickness until the sample was fully exposed on the surface of the wax block. Next sections of 5μm thickness were cut and immediately transferred to a water bath set at 38 °C. This allowed the sample to flatten out before samples were mounted onto SuperFrost® Plus slides (VWR International, Lutterworth, UK) and dried under a desk lamp. Samples were stained with hematoxylin and eosin using a Shandon linear staining machine (Department of Pathology, School of Clinical Dentistry, Sheffield, UK) Table 2.9).

Solution	Purpose
Heat	To remove any water from the slide and ensure the section is fully adhered to the slide
Xylene (times 3)	To remove the wax from the section (leaving the tissue section adhered to the slide)
Absolute alcohol	
Absolute alcohol	
70% alcohol	To gradually rehydrate the section
Running tap water	
Harris's Haematoxylin (Shandon) (times 5)	To stain basophilic parts of the section (cell nuclei)
Running tap water (times 2)	To wash off excess Haematoxylin
0.1% HCl in 70 % alcohol	To differentiate the sample helping the sample to take up the red eosin stain
Running tap water	To wash off acidic alcohol
Scott's tap water substitute	To increase the "blueing up" of the heaomtoxylin stain
Running tap water	To wash salt from Scott's tap water substitute off
Eosin Y-aqueous stain (Shandon)	To stain eosinophilic parts of the section (inc. cytoplasmic proteins, collagen and keratin)
Eosin Y-aqueous stain (Shandon)	
Running tap water	To wash off excess eosin stain

95 % alcohol	
Absolute alcohol (times 4)	
50:50 absolute alcohol: xylene	To gradually dehydrate the sample
Xylene (times 2)	

Table 2.9 Staining procedure

Slides were mounted with DPX (Dibutyl phthalate, Polystyrene, Xylene) and coverslips placed on the top of the sample. The DPX on the slides were left to set before being imaged using an Olympus BX51 microscope and Colour view IIIu camera with associated Cell^D software (Olympus soft imaging solutions, GmbH, Münster, Germany).

Immuno histochemistry

Immunohistochemistry was performed on 5µm sections of paraffin embedded samples mounted on SuperFrost® Plus slides (VWR International, Lutterworth, UK). The same method was used for all three antibodies except the dilutions of the three different antibodies (see Table 2.7). Slides were de-waxed in xylene and rehydrated through a series of ethanol dilutions. Endogenous peroxidise activity was next neutralised with 3% hydrogen peroxide in PBS for 20 mins. Slides were then washed in stirring PBS for 5 minutes.

Antigen retrieval was achieved using a sodium citrate buffer. Slides were submerged in pre warmed 0.01 M Tri sodium citrate buffer (pH 6) and the slides in sodium citrate buffer were microwaved on medium heat for 8 minutes and then washed in stirring tap water for 5 minutes. Sections were blocked for non-specific binding using the blocking serum mixture from the Vectastain® elite ABC kit, for 20 minutes at room temperature.

The primary antibody, prepared as described in table Table 2.7, was dropped onto the slides, ensuring the whole section was covered and the slides were incubated for 1 hour at room temperature. Slides were washed for 5 minutes in stirring PBS before the diluted biotinylated secondary antibody solution was added to the slide. Slides were incubated in humidified 37°C 5% CO_2 incubator for 30 minutes with the secondary antibody. Slides were again washed in stirring PBS for 5 minutes. Slides were then incubated with the Vectastain® Elite ABC reagent mixture, made up as described above, for 30 minutes and washed for 5 minutes in stirring PBS. The DAB solution, was mixed well before being added to slides for between 2 and 10 minutes. Colour development was observed under a light microscope to ensure a good staining intensity was obtained. Slides were washed and counter-stained with haematoxylin using the Shandon automatic stainer described in (Table 2.9). Slides were added to the stainer at the water step immediately prior to the haemotoxylin stain. The eosin staining compartments were blocked and slides subject to immunohistochemistry staining were not

stained with eosin. Slides were mounted with coverslips using DPX mount and imaged using an Olympus BX51 microscope and Colour view IIIu camera with associated Cell^D software (Olympus soft imaging solutions, GmbH, Münster, Germany).

Culturing multi-cellular tumour spheroids

Coating of agarose plates

An agarose mixture of 1.5% agarose (type V) in RPMI (for FaDu cells) or DMEM (for other cell lines) (w/v) was autoclaved to sterilise. The autoclaved media and agarose mix was stored at room temperature for up to 3 months before use. The agarose mixture was warmed prior to use using a microwave until it had completely melted. Agarose was poured into a Petri dish and 100µl of agarose and media was pipetted into 96 well plates (Costar, Corning Life sciences, MA, USA) using a multichannel pipette. Care was taken not to get bubbles in the wells as this affected MCTS formation and growth. Agarose was allowed to cool and set before storing upside down in the fridge for up to 6 months. Before culturing spheroids excess condensation on the lid of the 96 well plate was removed using Azo™ sterilising wipes (Synergy Health, Swindon, UK).

Culture of multi-cellular tumour spheroids (MCTS)

The MCTS were grown using the liquid over-lay method first described in (Carlsson and Yuhas 1984). Cancer cells were cultured in cell culture flasks until 80% confluence. Cells were enzymatically detached from the flasks as described on page 78. Cells were then re-suspended in cell culture medium (specific for cell type) and counted. The volume of the cell suspension was adjusted with cell culture media to give a concentration of 1.2×10^5 cells/ml. 100µl of the cell suspension was pipetted into each well using a multi-channel pipette resulting in 1.2×10^4 cell per well of the 96 well plate. This procedure was the same for all cell types as they were tested for MCTS forming behaviour, except different media for each cell type was used (all media and cell types listed on pages 73-77). Unless otherwise stated all MCTS used in subsequent chapters were created from the FaDu cell line.

Cell culture media was replenished every 3-4 days when in culture by adding 100µl of fresh media and then removing and discarding 100µl of media per well. Care was taken not to aspirate spheroids up into the pipette tip during this process.

Culture of MCTS with Fibroblasts

Normal oral fibroblasts were added to MCTS cultures to test if they could promote spheroid formation. 10 ml of cancer cell suspension (1.2×10^5 cells/ml) was mixed with 2.5 ml of NOF cells (1.2×10^5 cells/ml). 125µl of this solution was added to each well of an agarose coated 96 well plate to give a final concentration of 1.2×10^4 cancer cells and 3×10^3 NOFs per well.

Methods for characterising MCTS

Materials

Formalin agarose (0.02g/ml)

2g of Agarose (Sigma Aldrich, Dorset, UK) was dissolved in 90 ml of distilled water and mixed with 10 ml of 40% formaldehyde (Sigma Aldrich, Dorset, UK).

Hypoxyprobe ™-1

Hypoxyprobe™-1 (Chemicon, Nuevo León, Mexico) contains pimonidazole hydrochloride which binds selectively to oxygen starved cells. 100mg of Hypoxyprobe™-1 was dissolved in 1ml PBS (to give a 340mM stock solution) and was stored at -20°C in 30µl aliquots. Immediately prior to use the stock solution was diluted 1 in 200 in pre-warmed serum free medium.

Dako blocking solution

Used as purchased from Dako UK Ltd., Cambridgeshire, UK. Stored at 4°C.

Anti-hypoxyprobe monoclonal primary anti-body

Stored at 4°C.

Bovine Serum Albumin (BSA)

From Sigma Aldrich, Dorset, UK and stored at room temperature.

Brij 35

A surfactant powder purchased from Sigma Aldrich, Dorset, UK. Dissolved in PBS to give final concentration of 0.2%.

Texas red labelled secondary anti-body

Stored at 4°C.

VECTASHIELD Mounting Medium with DAPI

From Vector Laboratories, Peterborough, UK. Stored at 4°C.

Characterisation of FaDu MCTS

Images of MCTS were taken on a Zeiss Axiovert 200M light microscope (Carl Zeiss Inc., Germany) under bright field and images were taken using in integrated high resolution digital camera (AxioCam MRm, Carl Zeiss Inc. Germany) and Axiovision Rel. 4.6 software (Carl Zeiss Inc. Germany). The size of MCTS over time in culture was measured using the Axiovision Rel. 4.6 software. The diameter of at least 5 MCTS per time point was averaged and the standard deviation calculated.

Histological analysis of MCTS

MCTS were washed in PBS and fixed in 3.7% formalin for at least 24 hours at room temperature. MCTS in fixative were placed into the bottom of a cryovial. The fixative was removed being careful not to lose MCTS. 100µl of formalin agarose was added to the MCTS

in the cryovial. The agarose was allowed to set before the MCTS in agarose were placed in histology cassettes and processed as described on page 84. Once processed and embedded MCTS were sectioned and stained as described on page 84.

Biopsies of solid oral cancers

Many thanks to Dr Adam Jones and Dr Helen Colley for allowing me to use their images of *in vivo* tumours stained for Ki67 and hypoxia.

Ki67

Staining for proliferative cells using Ki67 was performed as described for TEOM models on page 86.

Hypoxia staining on wax section

Hypoxia staining on the wax section of tumours was achieved using anti carbonic anhydrase IX (Novis Biologicals, Cambridge, UK) used at a 1:1000 dilution. Immunohistochemistry staining was performed as described on page 86.

Hypoxia staining on frozen section

For visualisation of hypoxia within MCTS the MCTS were incubated with Hypoxyprobe™-1 for 3-4 hours at 37 °C. 10µl of the diluted stock solution was added to each well (which contained 100µl). MCTS were washed in PBS and fixed in 4% paraformaldehyde overnight. MCTS were next frozen in OCT freezing medium (VWR, Lutterworth, UK) at -20 °C in disposable base moulds (Surgipath, Peterborough, UK) and stored at -80 °C. 8µm sections were cut with a Leica Cryostat CM 3050 S (Leica Microsystems, Nussloch, Germany) and transferred onto Superfrost slides (VWR, Lutterworth, UK). Non-specific binding was blocked using DAKO blocking serum for 20 minutes at room temperature. The primary antibody was diluted 1 in 50 in PBS with 0.1% BSA. Slides were incubated with the antibody for 1 hour at room temperature. Slides were then washed twice for 5 minutes with cold PBS with 0.2% Brij 35. Next slides were incubated with the secondary antibody for 30-45 minutes again at room temperature. Another washing step (two washes each for 5 minutes in PBS + 0.2% Brij 35) followed before the slides were mounted using VECTASHIELD Mounting Medium with DAPI. Slides were imaged using a Zeiss Axioplan 2 fluorescent microscope (Carl Zeiss Inc. Germany) with a Q-imaging Retiga 1300R camera (QI Imaging, Arizona, USA) and Image Pro Plus image software (Media Cybernetics, Inc., MD, USA).

Screening of other cells lines for MCTS formation

It was determined whether a cell aggregate or true MCTS had formed from 5 representative images from each plate at each time point over a period of 14 days. Images were taken 1, 2, 6, 8 and 14 days after seeding the cells. Representative images were taken using a Zeiss Axiovert

200M light microscope (Carl Zeiss Inc., Germany) with an integrated high resolution digital camera (AxioCam MRm, Carl Zeiss Inc. Germany) and Axiovision Rel. 4.6 software (Carl Zeiss Inc. Germany).

2.4   Results

Tissue Engineered Oral Mucosa

Production of tissue engineered oral mucosa on DED

The tissue engineered oral mucosa (TEOM) used in this project has built on work previously done in the MacNeil laboratory by Dr. A. Bullock and Dr S. Bhargava. The model used throughout this project has been modified to improve the model's reproducibility and to overcome problems with material availability. The TEOM used here were cultured on an acellular skin scaffold processed from glycerol treated cadaveric skin purchased from Euroskin Bank (Beverwijk, the Netherlands). This was used instead of fresh dermis obtained from surgery as the supply was more reliable and large pieces of skin from the same patient could be obtained improving reproducibility in the thickness and behaviour of the scaffold. No significant difference was seen in models produced on glycerol treated skin compared to fresh dermis obtained from surgery. Cell seeding densities were also increased (compared to the original protocol set out in (Bhargava *et al.,* 2004)) in order to improve the reliability of models.

Epithelium of tissue engineered oral mucosa matures over time

Tissue engineered oral mucosa (TEOM) was cultured using primary human keratinocytes and primary human fibroblasts on a acellular skin scaffold. The length of time the models were cultured at air liquid interface affected the thickness of the epithelium and degree of stratification (Figure 2.3). The length of time a model could be kept in culture was very dependent on the batch of cells which were used. The models shown in Figure 2.3 continued to grow after 14 days and the epithelium continued to thicken. However, models cultured with cells extracted from other biopsies had lost their epithelium after 21 days in culture.

Formation of a differentiated epithelium

Culturing the TEOM at an ALI produced a stratified epithelium after 7 days in culture (Figure 2.3). By 21 days in culture the epithelium was up to 10 cells thick and showed clear signs of organisation and differentiation. Over time in culture the model became more organised and the epithelium became thicker. When the heamotoxylin and eosin (H&E) stained histology sections are compared against healthy oral mucosa biopsy (Figure 2.4), similarities between the tissue engineered model and the human biopsy are apparent. Although the TEOM model

has a thinner epithelium compared to the biopsy the differentiation pattern which is observed *in vivo* can also be seen in our tissue engineered model (Figure 2.4). The basal cells are densely packed with a high number of nuclei in the basal region of the epithelium. Superficially the basal and the supra-basal cells are larger and the nuclei are more dispersed as the cells are beginning to differentiate. The most superficial layer contains cells which are flattened with very few nuclei. These cells are terminally differentiated and have produced a smooth flat surface to the epithelium. Both the human biopsy and the TEOM have rete ridges, the characteristic rounded appearance of the epithelial connective tissue junction. The cells of the epithelium have differentiated in strata (rather than individual cells), a sign that intra-cellular signalling has been involved in the evolution of the epithelium.
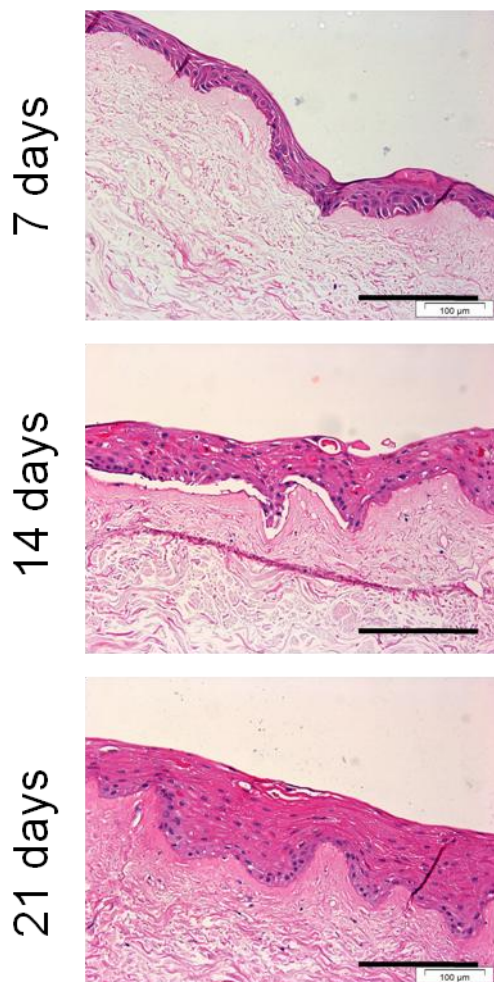
Figure 2.3 TEOM cultured from NOK and NOF cells on DED were exposed to ALI for 7, 14 or 21 days. Representative images n=5
Scale bar = 200μm

Immunohistochemical analysis of TEOM compared to normal human oral mucosa biopsies

The TEOM was compared to a healthy oral mucosa biopsy using immunohistochemistry stains for collagen IV (a protein found in the basement membrane of oral epithelia), AE1/AE3 (a broad spectrum cytokeratin marker) and Ki67 (a cell proliferation marker) (Figure 2.4).

Staining for collagen IV was used to confirm the presence of the basement membrane protein. These proteins are essential for the epithelium to obtain and maintain a strong connection with the connective tissue. The collagen IV staining (brown) on the TEOM was along the epithelial-connective tissue junction, as is seen in the human biopsy (Figure 2.4). The brown collagen IV stain showed continuous staining along the junction as well as staining residual blood vessel structures in the connective tissue.

AE1/AE3 is a broad spectrum cytokeratin stain which stains both high molecular weight cytokeratins and low molecular weight cytokeratins. The broad spectrum stain used here stained throughout the epithelium with staining in both the TEOM and the human biopsy more intense in the basal portion of the epithelium and the most superficial cells (Figure 2.4). Therefore, the presence and distribution of cytokeratins between the two samples appears to be consistent.

Ki67 is an immunohistochemistry stain used to detect the protein which is expressed in the nucleus of cells during the active part of the cell cycle, during cell proliferation. The nuclei of cells undergoing proliferation stain brown. In both the TEOM and the human biopsy those cells which are most proliferative, according to the Ki67 staining pattern are the basal cells (Figure 2.4). This is what would be expected as cells become less proliferative as they differentiate and move superficially in the epithelium. A high level of staining for Ki67 in suprabasal cells would be an indication of the presence of a potentially malignant disorder. More cells stained positive for Ki67 in the human biopsy however, this is most likely due to the greater number of cells in the human biopsy compared to the TEOM.
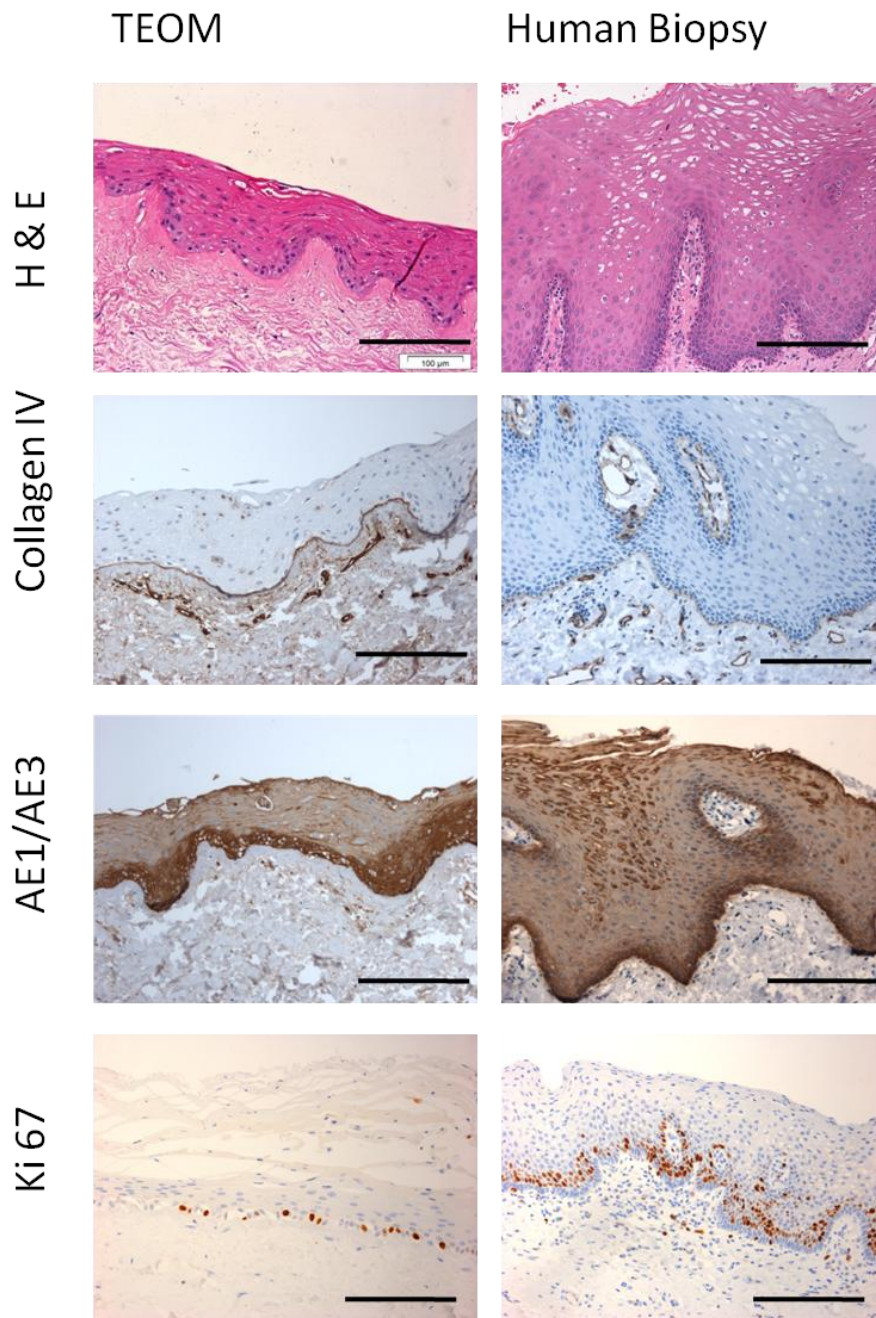
Figure 2.4 Immunohistochemisty analysis of TEOM and a human oral mucosa biopsy.
Scale bar = 200µm
Image adapted from (Colley *et al.,* 2010).

Histology of models cultured from different OSCC cell lines

All the cell lines tested here produced models with distinct architectural and cytological morphology. The following section presents the appearance of each model and compare the features of the models to features seen clinically to determine the ability of our models to recreate different stages of cancer and pre-malignancy. In all of these models normal oral fibroblasts were added. Table 1.1 on page 23 has been used to grade the pathological features.

Particular thanks to Dr. Keith Hunter, consultant oral pathologist at the University of Sheffield for his expert opinion and guidance on this part of the project.
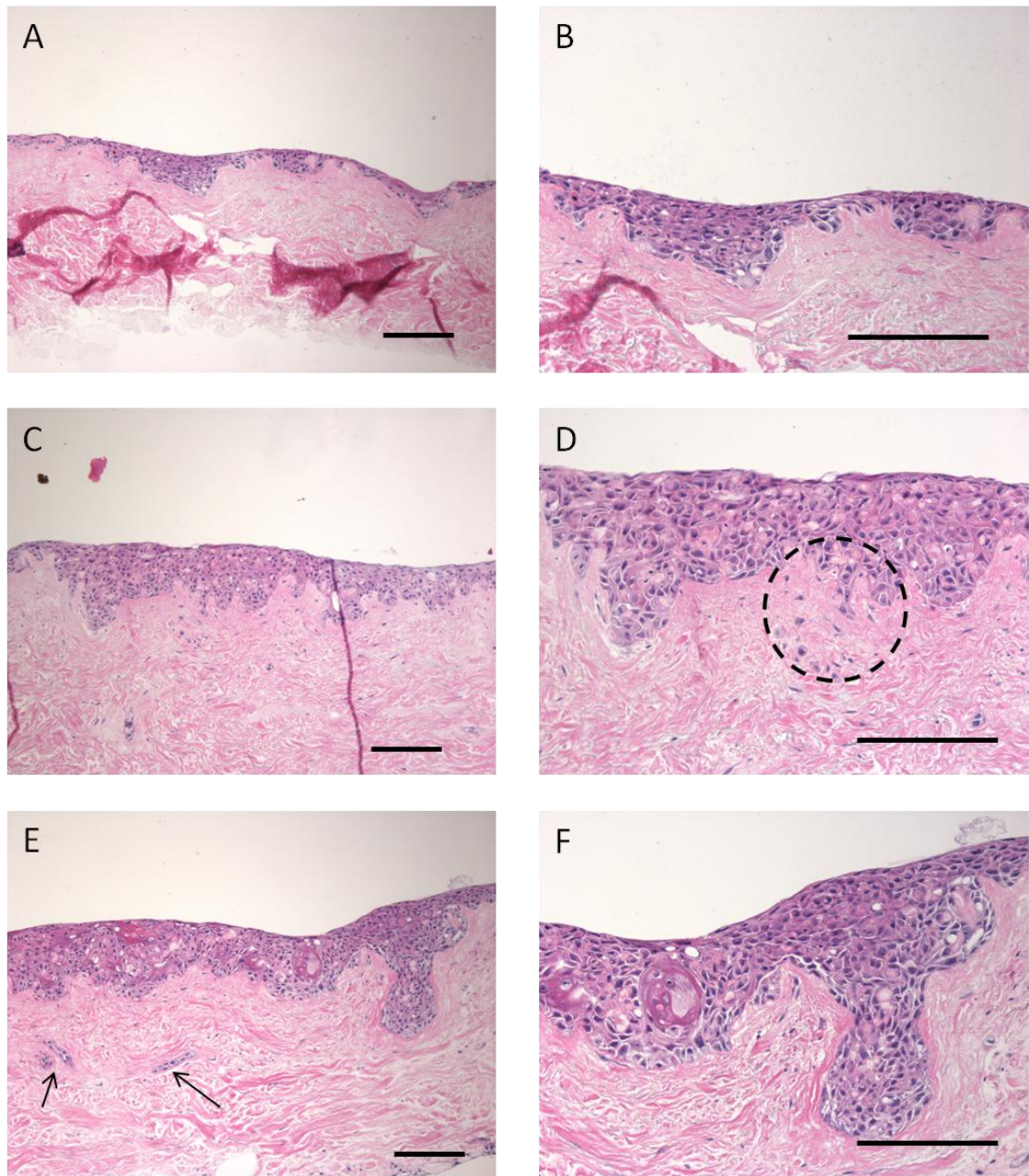
Figure 2.5 Haematoxylin and Eosin stained histological sections of the DOK cell line cultured in three dimensions on DED. Models were grown at an air liquid interface for 7 days (A x10 magnification and B x20 magnification), 14 days (C x10 magnification and D x20 magnification) or 21 days (E x10 magnification and F x20 magnification). Highlighted circle in D shows invading cells. Arrows in E show invaded tumour islands. Scale bar 200µm. n=3
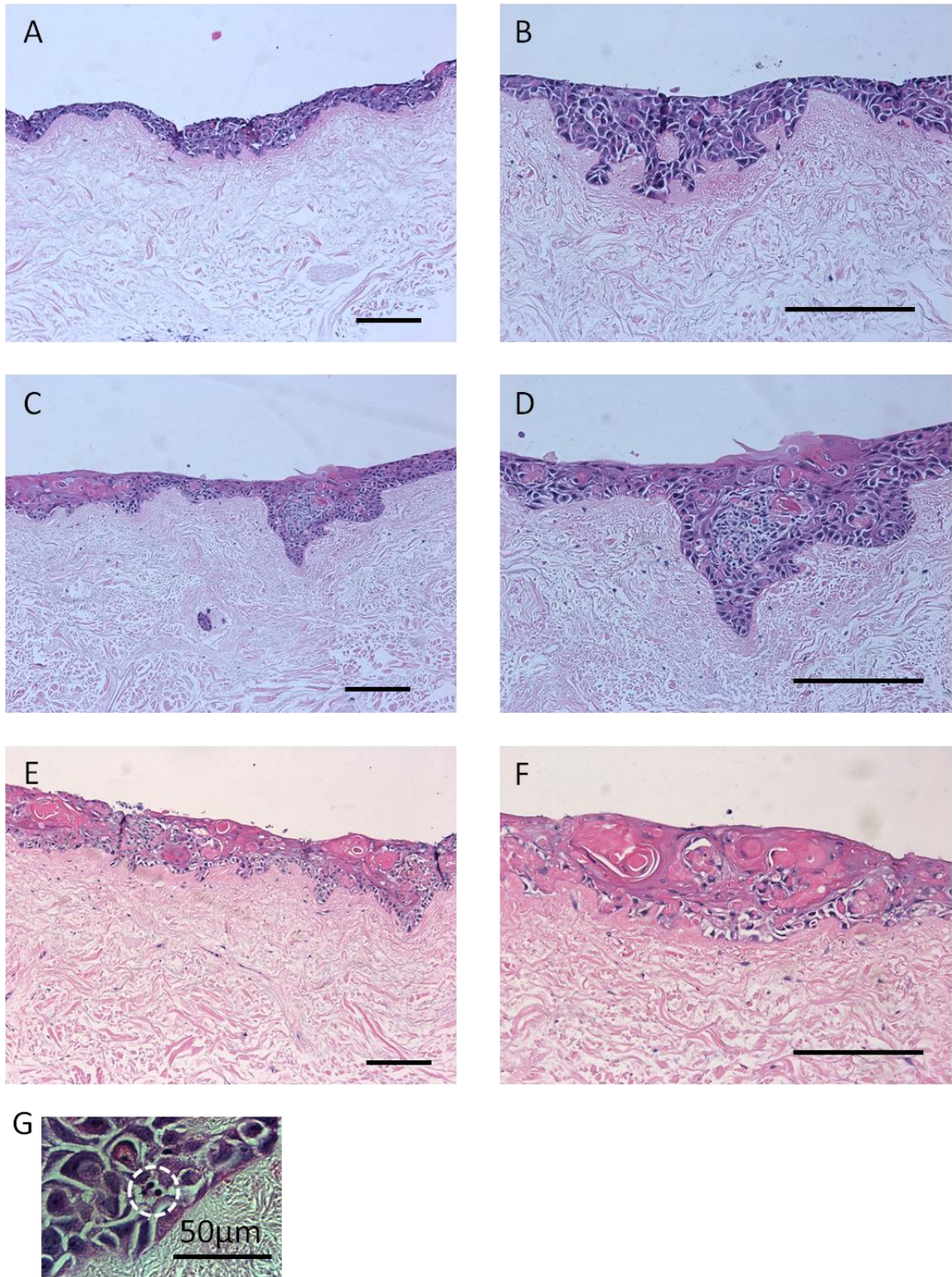
Figure 2.6 Haematoxylin and Eosin stained histological sections of the D20 cell line cultured in three dimensions on DED. Models were grown at an air liquid interface for 7 days (A x10 magnification and B x20 magnification), 14 days (C x10 magnification and D x20 magnification) or 21 days (E x10 magnification and F x20 magnification). Scale bar 200µm. G shows abnormal mitotic figures in model cultured for 14 days (x60 magnification). n=2
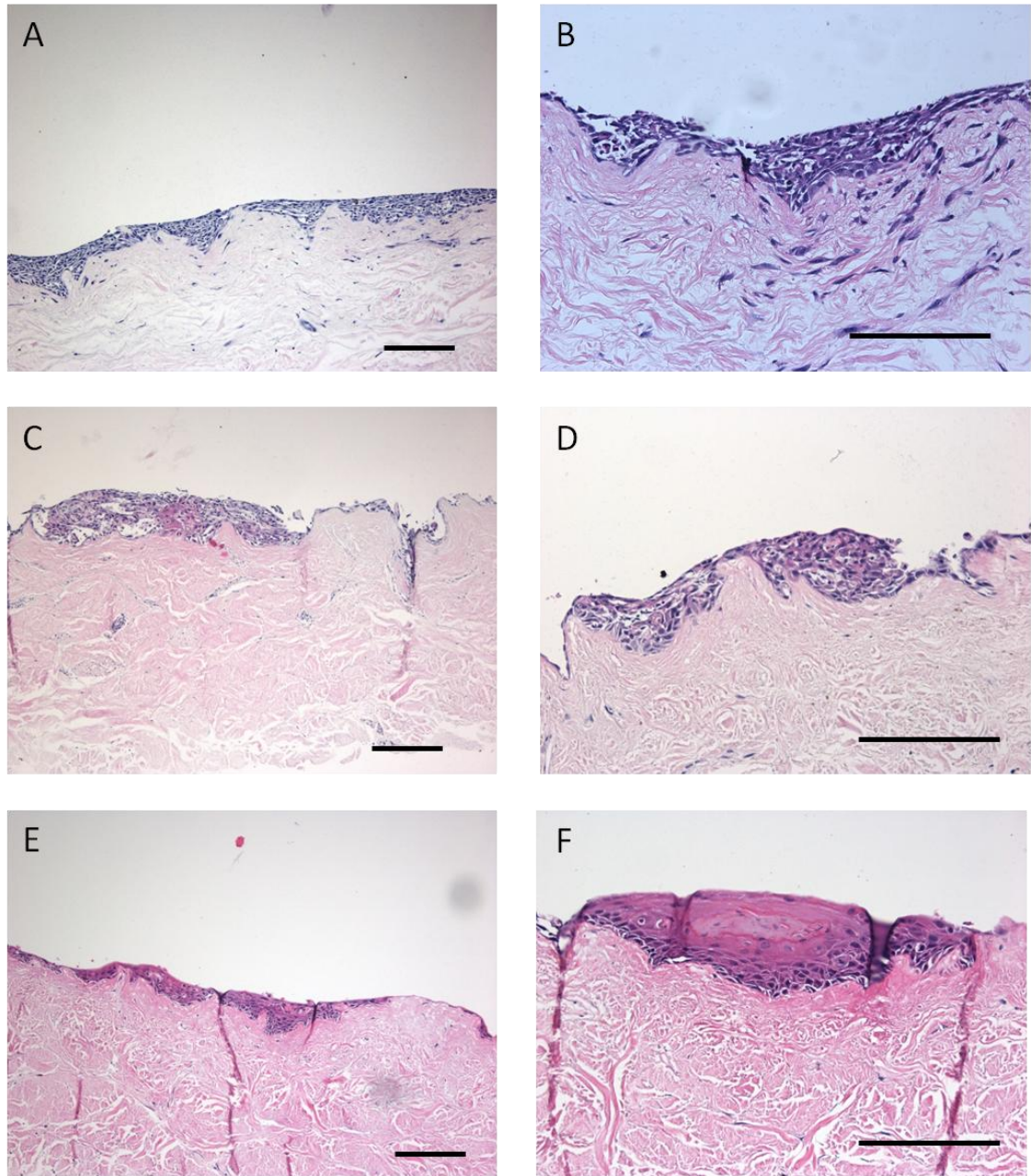
Figure 2.7 Haematoxylin and Eosin stained histological sections of the D19 cell line cultured in three dimensions on DED. Models were grown at an air liquid interface for 7 days (A x10 magnification and B x20 magnification), 14 days (C x10 magnification and D x20 magnification) or 21 days (E x10 magnification and F x20 magnification). Scale bar 200μm. n=2.
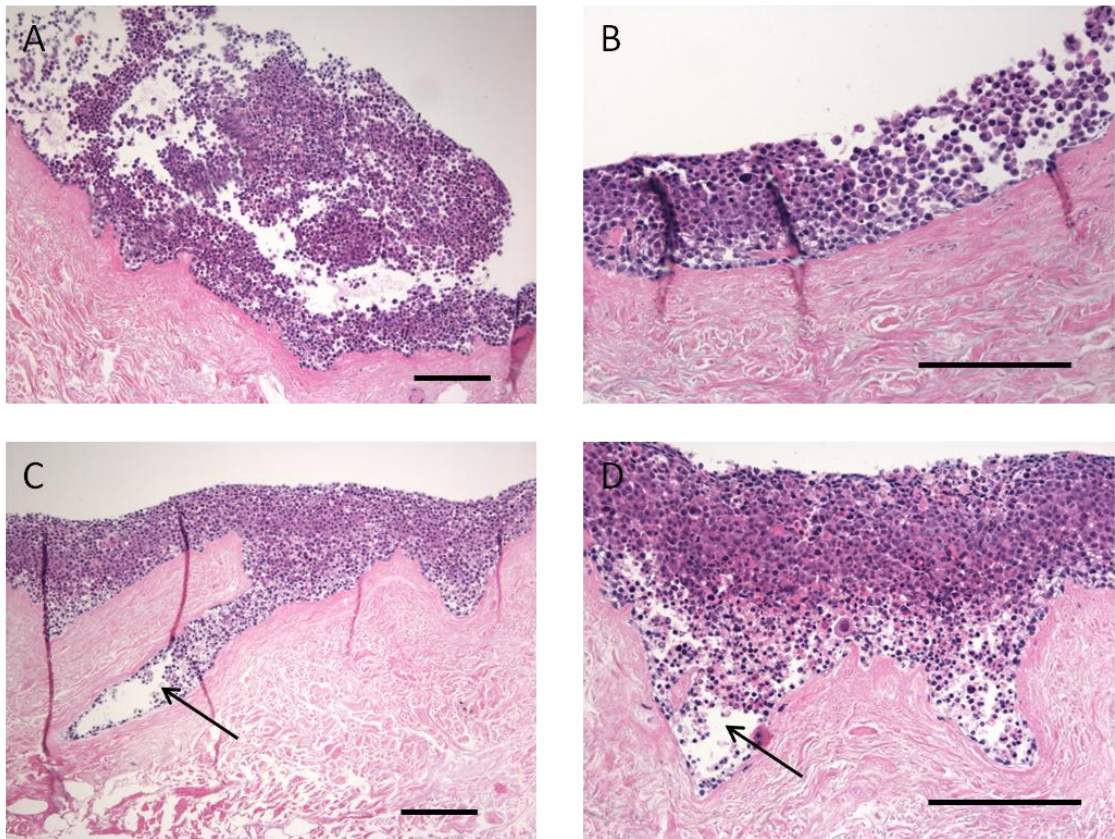
Figure 2.8 Haematoxylin and Eosin stained histological sections of the SCC4 cell line cultured in three dimensions on DED. Models were grown at an air liquid interface for 7 days (A x10 magnification and B x20 magnification) or 14 days (C x10 magnification and D x20 magnification). Arrows in C and D show areas of cell death. Scale bar 200µm. n=2
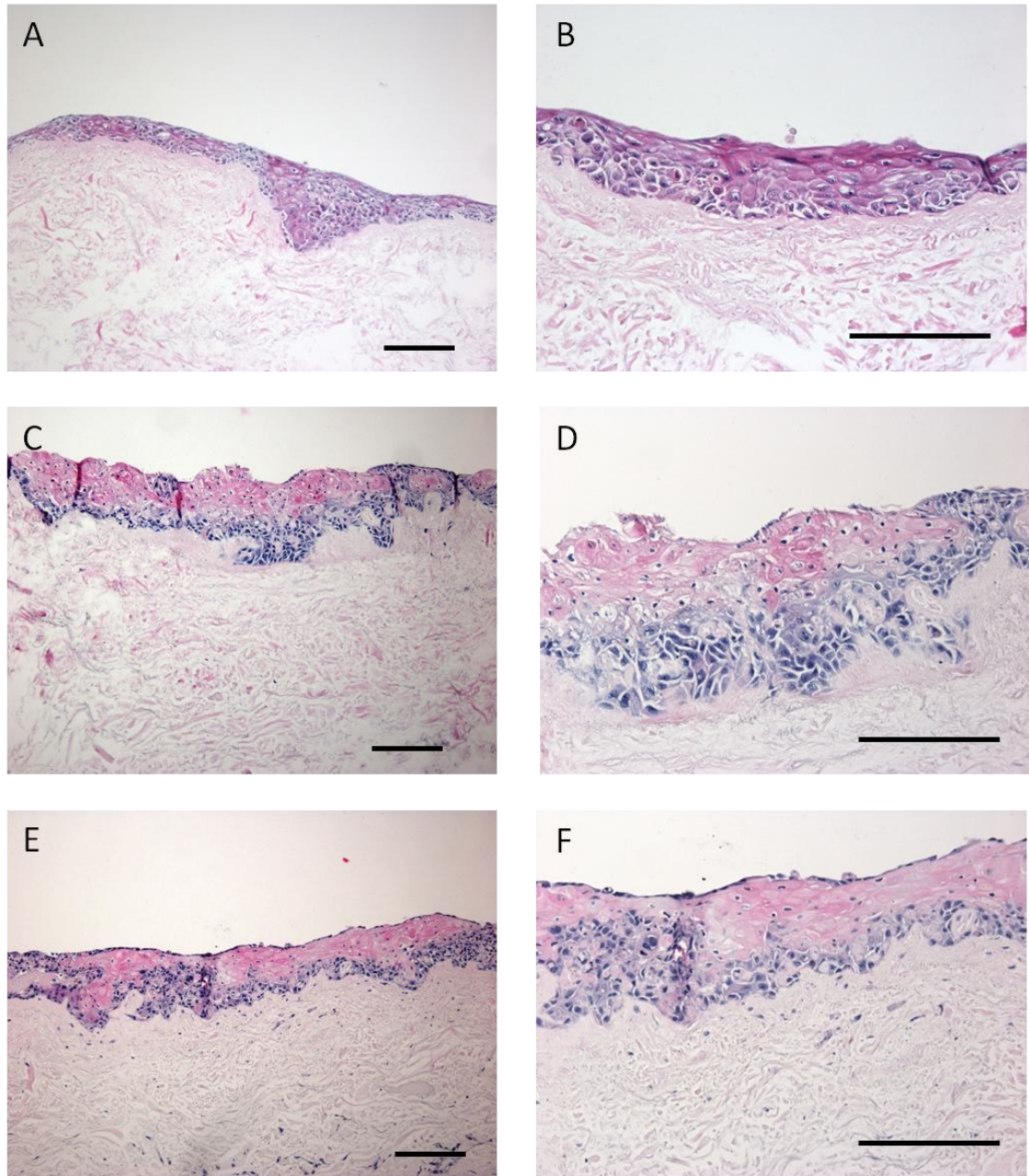
Figure 2.9 Haematoxylin and Eosin stained histological sections of the SCC9 cell line cultured in three dimensions on DED. Models were grown at an air liquid interface for 7 days (A x10 magnification and B x20 magnification), 14 days (C x10 magnification and D x20 magnification) or 21 days (E x10 magnification and F x20 magnification). Scale bar 200µm. n=2
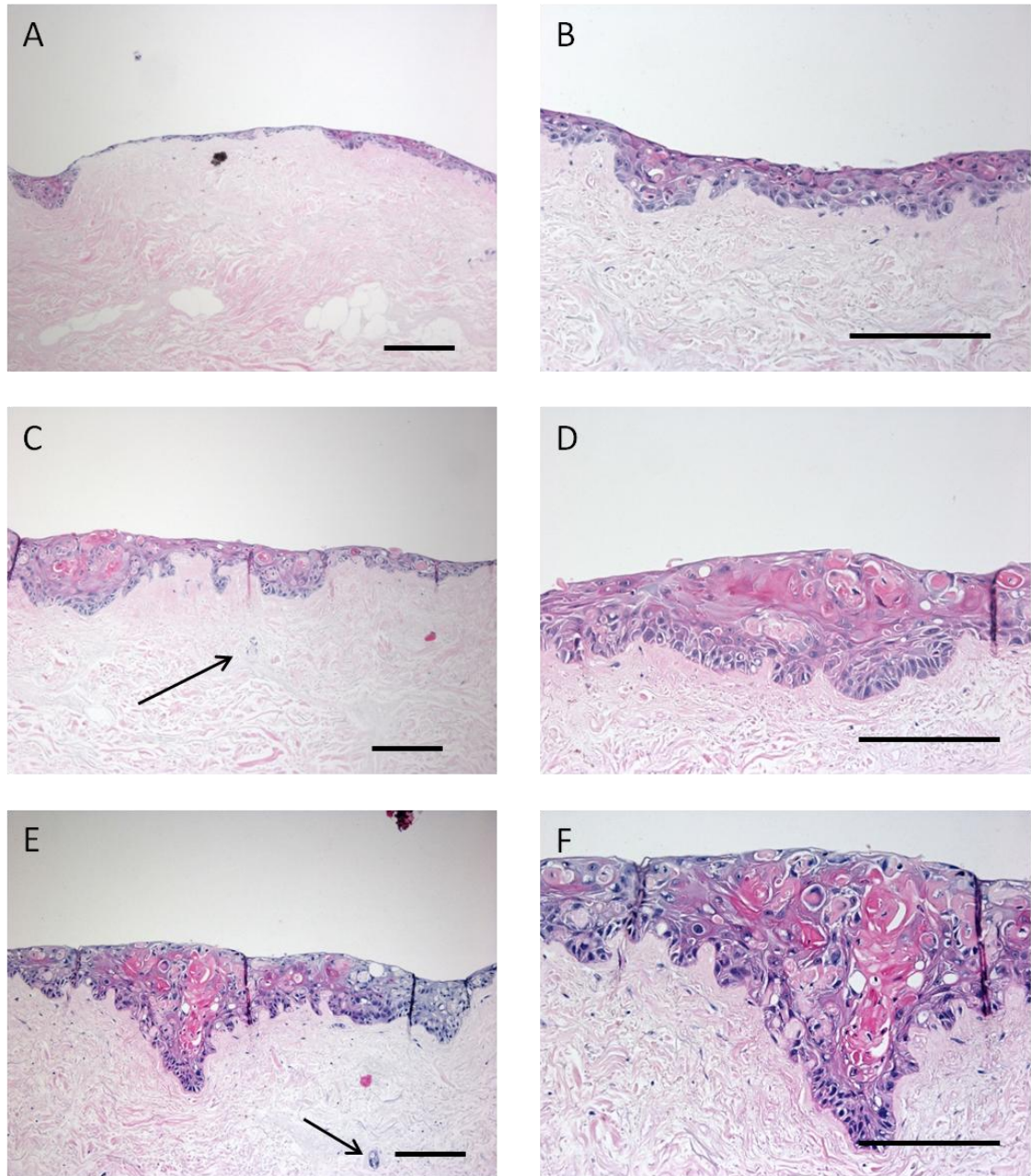
Figure 2.10 Haematoxylin and Eosin stained histological sections of the SCC25 cell line cultured in three dimensions on DED. Models were grown at an air liquid interface for 7 days (A x10 magnification and B x20 magnification), 14 days (C x10 magnification and D x20 magnification) or 21 days (E x10 magnification and F x20 magnification). Arrows show invaded cell islands. Scale bar 200μm. n=2
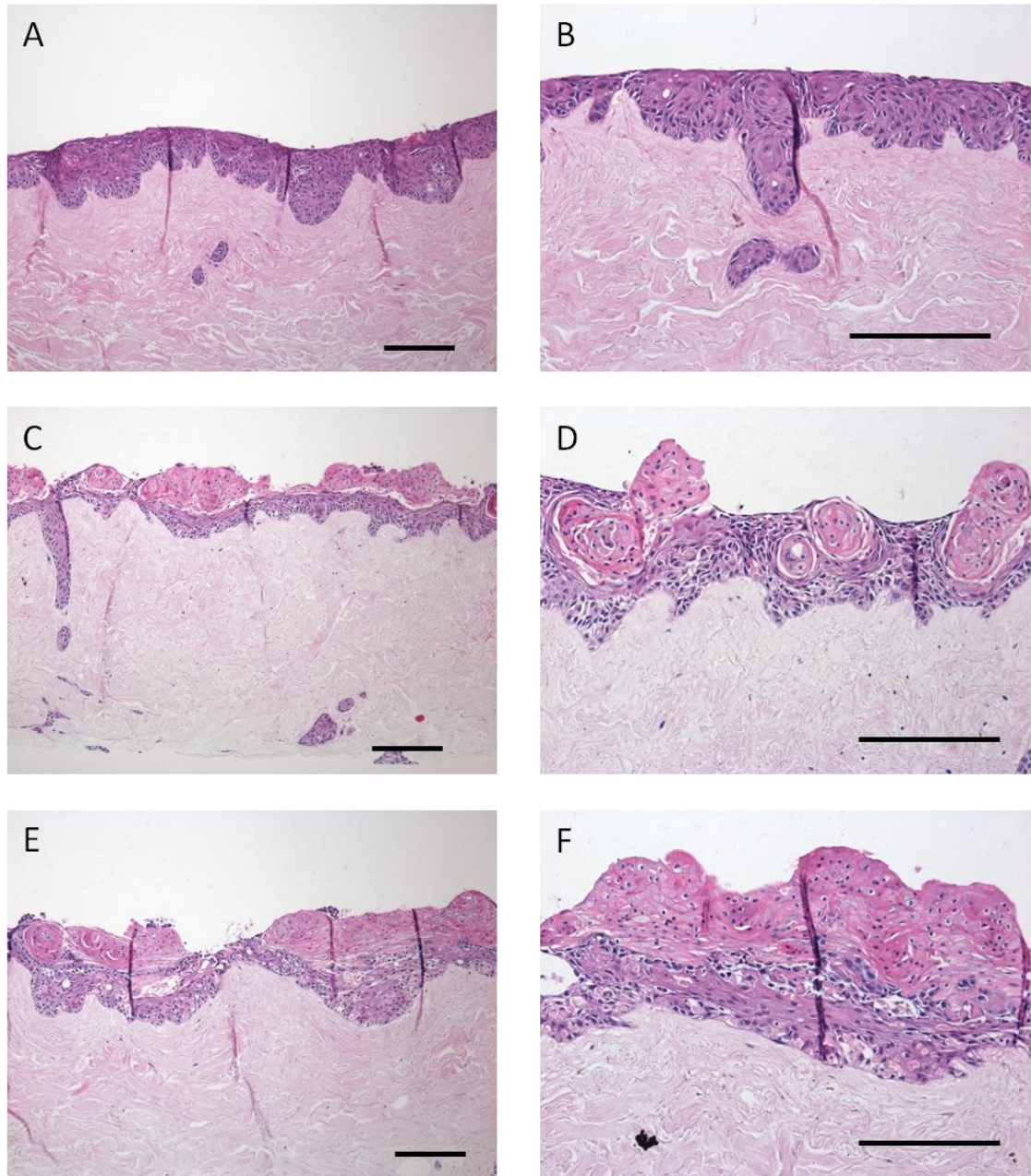
Figure 2.11 Haematoxylin and Eosin stained histological sections of the Cal27 cell line cultured in three dimensions on DED. Models were grown at an air liquid interface for 7 days (A x10 magnification and B x20 magnification), 14 days (C x10 magnification and D x20 magnification) or 21 days (E x10 magnification and F x20 magnification). Scale bar 200μm. n=3
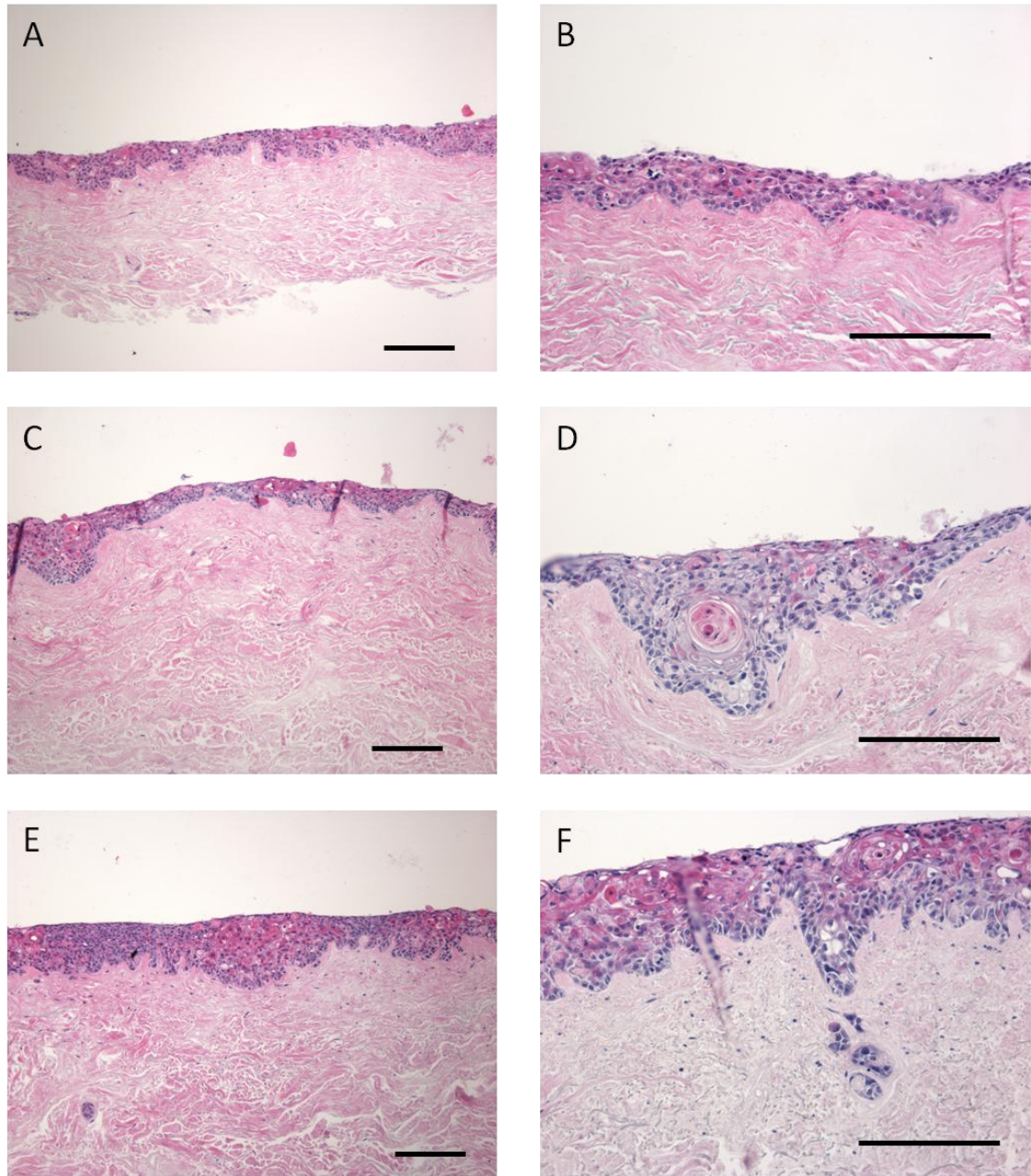
Figure 2.12 Haematoxylin and Eosin stained histological sections of the PE/CA-PJ34 cell line cultured in three dimensions on DED. Models were grown at an air liquid interface for 7 days (A x10 magnification and B x20 magnification), 14 days (C x10 magnification and D x20 magnification) or 21 days (E x10 magnification and F x20 magnification). Scale bar 200µm. n=3
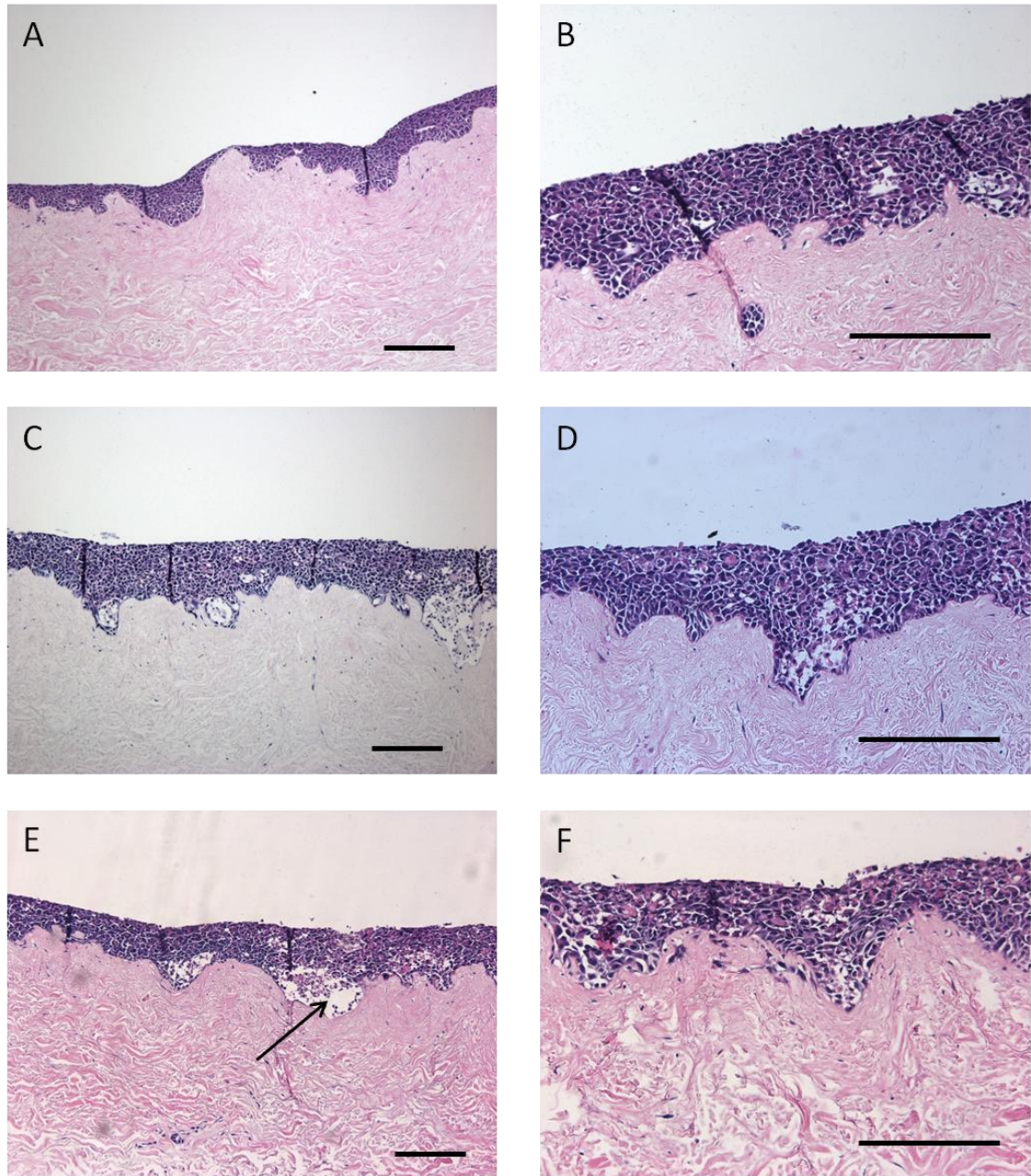
**Figure 2.13 Haematoxylin and Eosin stained histological sections of the FaDu cell line cultured in three dimensions on DED. Models were grown at an air liquid interface for 7 days (A x10 magnification and B x20 magnification), 14 days (C x10 magnification and D x20 magnification) or 21 days (E x10 magnification and F x20 magnification). Arrow in E shows area of cell death. Scale bar 200μm. n=3**

DOK

Figure 2.5 A-F show the development of the 3D tissue engineered models resulting from DOK cells cultured on an acellular skin scaffold. After 7 days in culture at ALI the DOK cells had formed a multi-layer epithelium of between 2 – 10 cells thick. There were areas which showed signs of cell death and the cells had not differentiated into distinct strata (as was seen with the normal cells).

After 14 days in culture the epithelium was thicker than at 7 days and the strata of the epithelium were beginning to show signs of organising themselves. A few of the superficial cells were becoming flattened and the cells adjacent to the connective tissue were in some cases organising in a pattern seen in normal epithelia. There were signs of individual cells producing keratin rather than strata of cells (a sign of dysplasia) along with nuclear pleomorphism throughout the epithelium (an indicator of severe dysplasia or carcinoma *in situ*). There was significant cytological atypia seen in the basal cell which is a feature commonly seen in carcinomas (highlighted region of Figure 2.5 D).

By 21 days in culture the epithelium had a severely dysplastic, carcinoma *in situ* appearance with cytological and architectural abnormalities throughout the epithelium. These included: drop shaped rete peg (bulbous projection into the connective tissue) and keratin pearls (circular formations of keratin, stained with haematoxylin pink) in the middle region of the epithelium. There are islands of cells within the epithelium which have the appearance of epithelial cell invasion. These cells have a different appearance to fibroblasts in the connective tissue as fibroblasts did not cluster in group as the cells seen here did and there is haematoxylin staining around the cells (not seen for the fibroblasts). This could be confirmed using immunohistochemistry staining.

D20

The dysplastic D20 cell line was cultured on a skin scaffold and images of the resulting histological appearance are shown in Figure 2.6 A-F. The D20 cells formed an epithelium after 7 days in culture at ALI which was between 2 and 6 cells thick. The epithelium here had some signs of stratification and keratin was being produced on the surface of the epithelium. The epithelium however, did not appear healthy as there were features of dysplasia present including nuclear and cytological abnormalities. In areas the epithelial connective tissue junction had an interesting appearance. Rather than a smooth junction with an ordered arrangement of basal cells the junction had become rough in appearance with small groups of cells protruding further into the connective tissue than in other regions. This is sometimes seen clinically and is an indicator of severe dysplasia and invading carcinomas.

After 14 days in culture there were drop shaped rete pegs and invaded tumour islands within the connective tissue. The overall structure of the epithelium contained the strata of naturally occurring epithelia; basal cells, a prickle cell layer and flattened keratinised cells in the top layer. However, the epithelium was disordered throughout and there was hyperkeratosis within the epithelium. Nuclear pleomorphism and abnormal mitotic figures could be observed. Abnormal mitotic figures (such as those see in Figure 2.6 D, highlighted by the arrow) are one feature used to grade the severity of dysplasia clinically and are a sign of defects during mitosis. In the case of cancer the rate of mitosis is increased, heightening the chance of abnormalities occurring. These abnormal mitotic figures appear as fragmented multi-ploid nuclei. There was a small amount of epithelial cell invasion with cells growing in islands in the connective tissue.

By 21 days the epithelium had abnormal mitotic figures, signs of cell death and abnormal keratin production. However, in some areas there were still signs of stratification. The epithelial connective tissue junction was still abnormal with cells protruding into the connective tissue.

D19

Figure 2.7 A-F show the models which result from culturing the dysplastic cell line D19 on an acellular skin scaffold for 7, 14 and 21 days. After 7 days in culture at an ALI the D19 models have formed a multilayer epithelium. The D19 cells were more mobile than other cells with cells growing on top and underneath the model. The cells appeared to be unhealthy with poor cell-cell attachments and the cells did not differentiate. Abnormal mitotic figures were seen in these models, a sign of increased proliferation, resulting in mistakes in the mitotic process. The cells seem to be invading into the connective tissue as spindle cells. In Figure 2.7B there are a large number of cells in the connective tissue. These cells have a spindled appearance and seem to have invaded as individual cells rather than forming tumour islands as was seen in some other models. Immunohistochemistry staining would be required to see if these cells are have epithelial or mesenchymal markers.

After 14 days the D19 cells of the epithelium still did not stratify however, there were further areas of invasion within the connective tissue. In some areas the epithelium did not attach well to the connective tissue and some regions of epithelial tissue were lost during processing leaving fragments of cells on the surface adjacent to the basement membrane. The epithelium has no order and there are signs of keratinisation within the epithelium.

After 21 days in culture more of the epithelial cells had become detached however, the regions which did remain post histological processing, were in some cases, well differentiated with some areas appearing relatively normal (Figure 2.7 F). However, the nuclei in these regions

had abnormal morphology. The epithelial connective tissue junction was again disrupted and abnormal with cells protruding into the connective tissue.

SCC4

The SCC4 cells line, when cultured on DED, grew into a multilayer mass of cells (Figure 2.8). There are no signs of stratification and all the cells have the same appearance, size and morphology. In some areas (as seen in Figure 2.8 A) the cells proliferated extensively and produced large masses of cells. There were poor intercellular connections and regions of atrophy (Figure 2.8 C and D) after 14 days. After 21 days in culture the models became fragile and the epithelium became completely dissociated from the connective tissue during processing. The appearance of these models is not one which is seen clinically.

SCC9

SCC9 cells cultured for 7 days on acellular skin showed some signs of differentiation (Figure 2.9). The cells of the epithelium were keratinised towards the surface and the keratin formed in bands associated with many cells rather than single cell keratinisation as was seen in other models. Despite this the epithelium did still have signs of dysplasia with abnormal mitotic figures and irregular cell morphology throughout the epithelium.

By 14 days in culture there were areas of clear differentiation however, other areas showed little or no differentiation. The cells appear in two distinct layers the densely packed nucleated cells basally and the keratinised layer of cells superficially. The basal cells had nuclear pleomorphism, the epithelial connective tissue junction was irregular and the epithelium protruded into the connective tissue in places. The keratinised cells on the top of the epithelium had very small nuclei. These cells had not produced keratin bands and it appeared the keratinisation resulted from single cells rather than strata of cells (a sign of dysplasia).

By 21 days the epithelium was less defined than before and the strata were more disorganised. There were signs of cell death and a cell layer growing on top of the keratinised region of the superficial epithelium (a feature not seen clinically).

SCC25

Figure 2.10 shows the development of the SCC25 model cultured over time. After 7 days in culture the SCC25 cells were starting to form a thin but dysplastic epithelium. The basal cell layer was not well defined and there were some signs of basal cell keratinisation. The epithelium was between 2 and 6 cells thick with signs of abnormal mitotic figures.

After 14 days in culture the cells were beginning to organise into the strata of epithelia. The basal cells were well organised in some areas and a prickle cell layer could be observed superficial to the basal cell layer. This differentiation was more normal looking than in some

models however, the pattern of dysplasia observed here is not one observed clinically. There was individual cell keratinisation, rather than regions of cells forming keratin together. This unusual distribution of keratin exaggerated the abnormality of the tissue which was beginning to stratify and organise into distinct layers of an epithelium. The SCC25 cells here appeared relatively large and the cells had large nuclei suggesting these cells were very active. The models in Figure 2.10 C and E showed some signs of invasion (see arrows) with epithelial islands forming in the connective tissue.

By 21 days in culture the basal cells remained fairly organised in areas while the rest of the epithelium became more abnormal with keratin pearls, keratinisation within the epithelium and significant nuclear pleomorphism.

Cal27

The Cal27 cells produced models which were most comparable to the appearance of clinically occurring dysplasia and carcinoma *in situ* (Figure 2.11). After 7 days in culture the epithelium was well differentiated with a well defined basal cell layer. The differentiation occurred in regions and strata of the epithelium rather than in individual cells indicating some cell-cell interactions. There were epithelial islands within the connective tissue suggesting invasion of the OSCC into the connective tissue.

The models cultured for 14 days were highly keratinised on the surface. This high level of keratinisation is commonly seen on the surface of dysplastic tissues clinically. Figure 2.11 C shows the organised differentiation remaining in areas however, in other places this was disrupted by the extensive keratinisation.

After 21 days in culture the appearance of the histology is less like dysplastic lesions seen clinically as cells had begun to grown over the top of the keratinised areas and the differentiation was mostly lost. This model has the appearance of a squamous cell carcinoma *in situ* with some signs of invasion as early as 7 days at ALI.

PE/CA-PJ34

The models produced by culturing the PE/CA-PJ34 cell line showed little differentiation after 7 days in culture (Figure 2.12). The nuclei were a similar size throughout the epithelium and there was no difference in appearance between the top and bottom of the epithelium. There was a small amount of keratin produced however, not superficially in bands as would be seen in naturally occurring healthy tissue. Hyperkeratisation such as this is a marker of dysplasia.

After 14 days in culture the cells were beginning to organise into differentiated layers. The basal cells had formed an ordered basal cell layer and some keratin had been produced on the most superficial surface. The epithelium was still disordered though, for example there were

keratin pearls which had become incorporated into the mid region of the epithelium in Figure 2.12 D.

After 21 days in culture the differentiation still did not have an appearance comparable to clinically occurring lesion. In many areas the cell nuclei were of equal size throughout the epithelium and the keratin did not form in flattened bands but rather all around individual cells. The model showed signs of invasion with epithelial cells present in the connective tissue and protrusions from the epithelium into the connective tissue at points along the basement membrane.

FaDu

When grown in 3D the FaDu cell line showed no signs of differentiating but instead formed a multilayer homogenous epithelium (Figure 2.13). There are signs of cell death, apoptosis and necrosis, at all three time points. The cells did not attach well to the connective tissue and in some cases the epithelium detached entirely from the connective tissue during processing for histological analysis. After 14 and 21 days there was a large amount of cell death (see arrows on Figure 2.13 E and F). If this level of cell death was seen clinically it would be indicative of a highly aggressive and invasive cancer however, this would not normally be observed in the epithelium but rather in deeply invaded regions of cancerous tissue.

Spheroid formation

The definition for a spheroid or a MCTS is not consistent in the literature (Hirschhaeuser *et al.,* 2010) therefore I will define the term spheroid for use in this project. A spheroid is a mass of cells which when cultured on a non-adherent surface form a spherical solid mass with a well defined border. Cells within the mass are indistinguishable from one another and some of these spheroids expand over time whereas others do not. Spheroids have strong intracellular junctions and good integrity allowing them to be handled with a Pasteur pipette. In contrast to spheroids some cells form aggregates when cultured using the liquid overlay method (Figure 2.14). These aggregates appear as a clump of cells, the border is not well defined and individual cells within the mass can be determined. Aggregates usually fall apart when handled and are often surrounded by cells not incorporated into the aggregate.
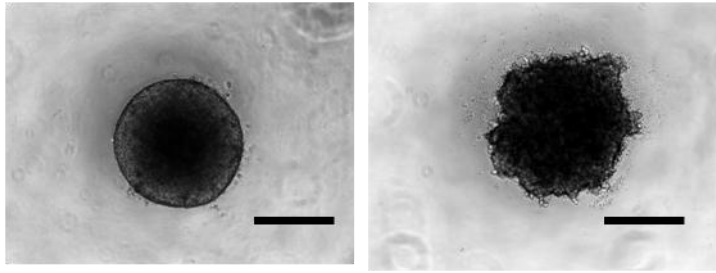
Figure 2.14 Comparison of spheroids and aggregates imaged using light microscopy. Left hand image shows a spheroid (also called MCTS), image on the right shows an aggregate. Scale bar = 400μm

FaDu MCTSFigure 2.15 shows the appearance of FaDu cells cultured on agarose coated plates over 21 days in culture. These cells formed a solid mass of cells after 24 hours. Very few cells could be seen outside the distinct border of the solid mass and individual cells within the spheroid could not be distinguished using light microscopy. This mass of cells became denser over time and by day 6 the spheroid appeared black when imaged using phase contrast light microscopy. The MCTS formed from FaDu cells continued to grow in culture over 21 days. After 1 day in culture the MCTS had an average diameter of 840 μm, this increased almost linearly over the subsequent 14 days and reached a diameter of over 1200 μm after 21 days (Figure 2.15). As the spheroids became larger the size became more varied.

FaDu MCTS compared to *in vivo* tumours

To validate the MCTS model of solid expanding tumours FaDu MCTS were compared to naturally occurring solid oral cancers (Figure 2.16). Proliferation, hypoxia and cell death were compared using immunohistochemistry. Ki67 staining showed the most proliferative cells (brown nuclei) were found in the peripheral cells. The distribution of Ki67 positive cells was similar in our model and in the cancer biopsy. Hypoxia is a common feature of solid tumours as oxygen diffusion is not sufficient to reach the central cell distant from the blood supply. The red staining highlights those cells which are oxygen starved. In both *in vivo* and *in vitro* the cells in the central region are hypoxic. Distance from the blood supply not only leads to hypoxia but also leads to cell death *in vivo* as there is an accumulation of waste products and a lack of cell nutrients. The H&E images show the central region is necrotic, there is a much lower density of nuclei and reduced eosin staining in the centre, demonstrating a lack of cytoplasmic proteins.
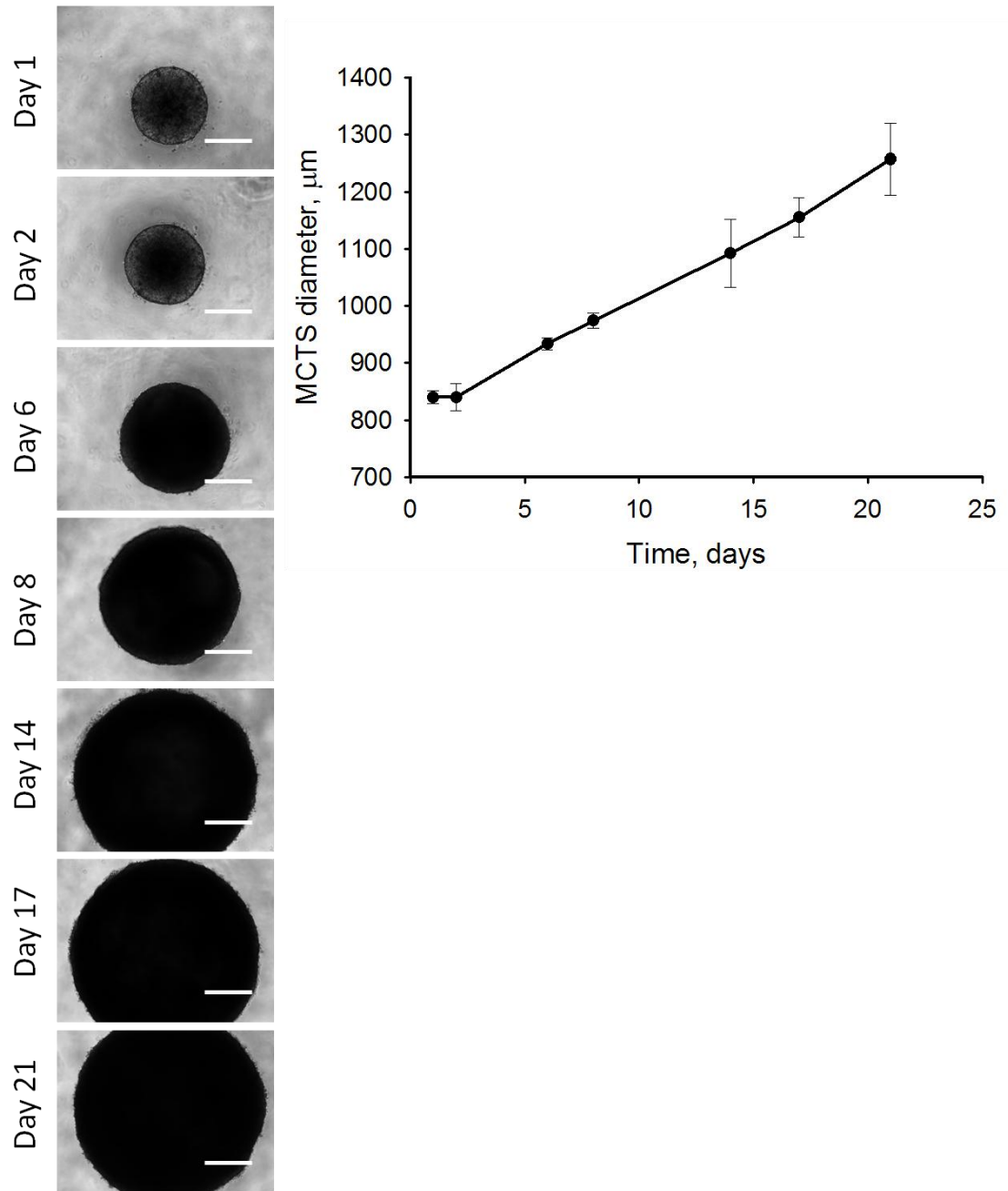
Figure 2.15 Representative images of MCTS cultured from the FaDu cell line.
Growth curve of MCTS cultured over 21 days. Scale bar = 400μm. Error bars = s.d. n=5
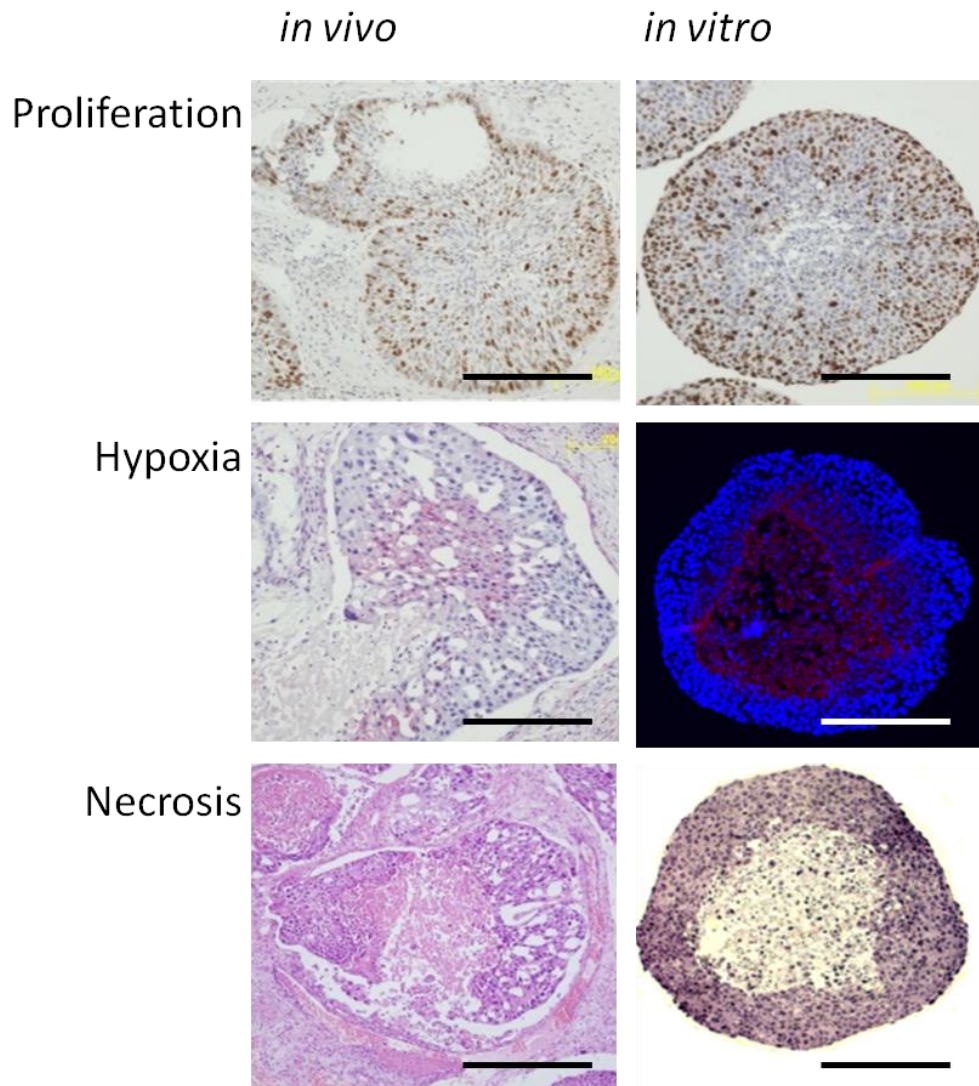
Figure 2.16 Comparing MCTS cultured from FaDu cells to clinical tumours seen *in vivo*. Proliferation measure using Ki67 immunohistochemistry marker. Pink region (*in vivo*), red region (*in vitro*) show areas of low oxygen tension. Necrosis shown using haematoxylin and eosin staining. Scale bar = 200µm.

Which oral cancer cell lines are able to form MCTS *in vitro*?

The FaDu MCTS model is now well established in our laboratory. For drug screening and other applications it would be beneficial to have a larger catalogue of oral MCTS comprised from different OSCC cell lines. Therefore, a number of different cells lines were tested for their ability to form solid expanding tumours *in vitro* including D19, D20, DOK, SCC4, SCC9, SCC25, Cal27, PE/CA-PJ34, and the primary NOK and NOF cells. Cells were cultured using the liquid overlay method in cell culture media specific for that cell type. Figure 2.17 shows the appearance of each of the spheroids formed from each cell line over time. All images were taken using x5 magnification.
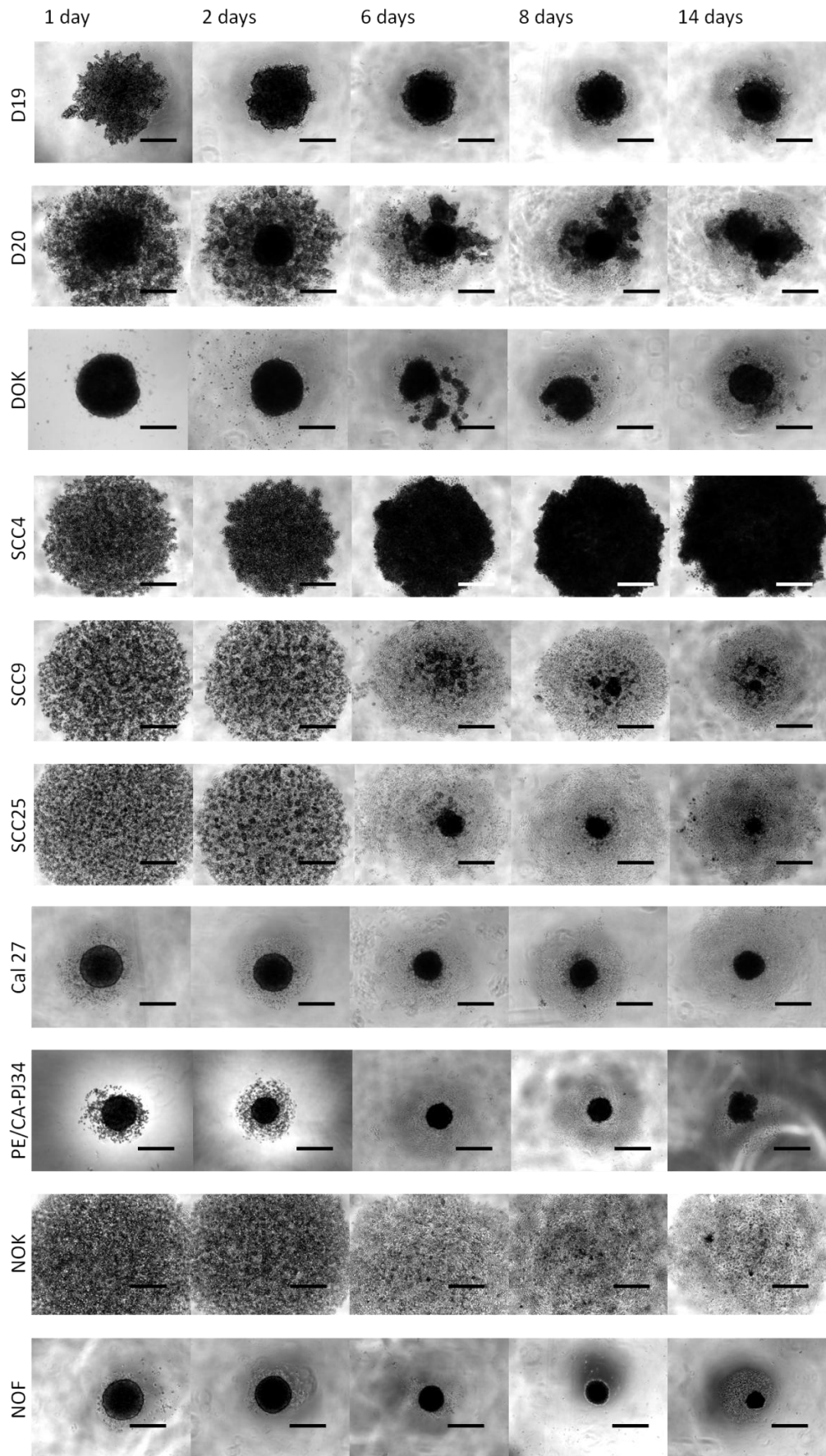
Figure 2.17 Screening of different cell types to test their ability to produce solid expanding MCTS after 14 days in culture.
Scale bar = 400µm. n=3

D19

These cells formed aggregates which compacted over time and resulted in a small aggregate with a large amount of cells surrounding the aggregate after 14 days. The cells within the aggregate were always distinguishable and the border of the aggregate was rough and irregular.

D20

The D20 cells also formed aggregates with a large amount of cells surrounding the aggregate. These aggregates broke apart over the two weeks they were in culture and the aggregates were irregularly shaped.

DOK

The dysplastic cell line DOK formed spheroids after 24 hours. These spheroids had very few cells surrounding them and an average diameter of 610μm. Over time these spheroids reduced in diameter and resulted in spheroids with a diameter of ~440μm after 14 days in culture. Over time the spheroids lost structural integrity, fell apart and resulted in individual cells and a large amount of cell debris surrounding the spheroids.

SCC4

SCC4 cells did not form spheroids. After 24 hours a monolayer could be seen growing on the agarose coated well. Over time the cells proliferated and the monolayer started to clump and the cells appeared to grow on top of one another as they became over confluent.

SCC9

These cells appeared to grow as a monolayer on the agarose for the first two days in culture. These cell monolayers had very small aggregates (of just a few cells) in the monolayer. After 6 days in culture this monolayer appeared less healthy and there was a large amount of cell debris. In the centre of the well there was a very small circular mass of cells however, this could not be classed as a spheroid.

SCC25

The SCC25 behaved in a very similar way to the SCC9 cells. They did not form spheroids initially; however, after 6 days in culture they did form a small spheroid with average diameter 200μm but this reduced in size to just 120μm after 14 days in culture. These spheroids were surrounded by a large amount of cells which were not incorporated into the spheroid and there was no well defined border of this spheroid.

Cal27

Cal27 cells formed spheroids after 24 hours when added as suspension to agarose coated wells. The diameter of these spheroids was ~ 480μm after 24 hours. Some cells could be seen outside the spheroid and the border of the spheroid was almost as distinct as was seen for the FaDu MCTS. Over time these spheroids reduced in diameter from ~480μm after 1 day to ~300μm after 14 days in culture. As time went on more cells could be seen surrounding the spheroid rather than within it. The border also became more "fuzzy" over time when imaged using light microscopy.

PE/CA-PJ34

The PE/CA-PJ34 cell line formed spheroids with a large amount of cells surrounding the central solid mass. The diameter of these spheroids reduced from 405μm after 1 day to 300μm after 14 days in culture. The border was not well defined.

NOK

The appearance of NOK cells cultured on agarose coated plates was very similar to that of the SCC cell lines. The NOK cells grew as a monolayer on the agarose but over time the cells appeared to be dying and there was some cell debris in the well.

NOF

The NOF cells formed spheroids with well defined borders after 24 hours in culture. These MCTS shrank over time in culture. The formation of spheroids by NOF was variable between different batches of NOF cells.

Spheroid Formation with Fibroblasts

Next it was tested whether the addition of primary oral fibroblasts could promote spheroid formation. The resulting appearance is shown in Figure 2.18.

D19 + NOF

When cultured with NOF cells the dysplasic D19 cells formed spheroids with well defined borders. There were very few cells outside the spheroid and the spheroid was dense with cells (appearing black under phase contrast light microscopy). These spheroids shrank over time in culture and by day 14 there were some cells surrounding the spheroid.

D20 + NOF

The D20 cells initially behaved in a similar way to the D19 cells when cultured with NOF cells. The cell mixture formed a large spheroid with a well defined border, no cells could be distinguished within the cell mass. As the spheroids were cultured for longer in culture more and more cells became apparent outside the cell mass and the border of the spheroid appeared rough and irregular.

DOK + NOF

The DOK cells formed larger spheroids after 1 day in culture when they were also cultured with NOF cells (most likely due to the higher total cell number and therefore the greater cell mass per well). These spheroids shrank rapidly over time in culture and the border became irregular and cells outside the spheroid became visible.

SCC4 + NOF

The SCC4 cells were not greatly affected by the addition of NOF cells (compare Figure 2.18 to Figure 2.17). The cell mass did appear denser on the images but the addition of NOF cells did not encourage spheroid formation and the cells still grew as an irregular aggregate.

SCC9 + NOF

Adding NOF to the SCC9 cells caused the cells to form a compact aggregate, as opposed to growing as a monolayer. Over time this aggregate compacted further and after 6 days in culture there was a spherical mass with a well defined border. There was still a large amount of cells not contained within the mass of cells and the spheroid did not grow.

SCC25 + NOF

The SCC25 cells, in contrast to the SCC9 cells, grew in a very similar way with or without NOF.

Cal27 + NOF

The Cal27 cells also grew in a very similar way with or without the NOF cells. The only difference being the Cal27 cells cultured with NOF cells formed slightly larger MCTS, probably due to the higher cell number.

PE/CA-PJ34 +NOF

Culturing the PE/CA-PJ34 cell line with NOF created aggregates which included almost all cells in the well (as opposed to the aggregates created without NOF which had a large number of cells surrounding them). The aggregates formed had irregular borders and reduced in size over time in culture.
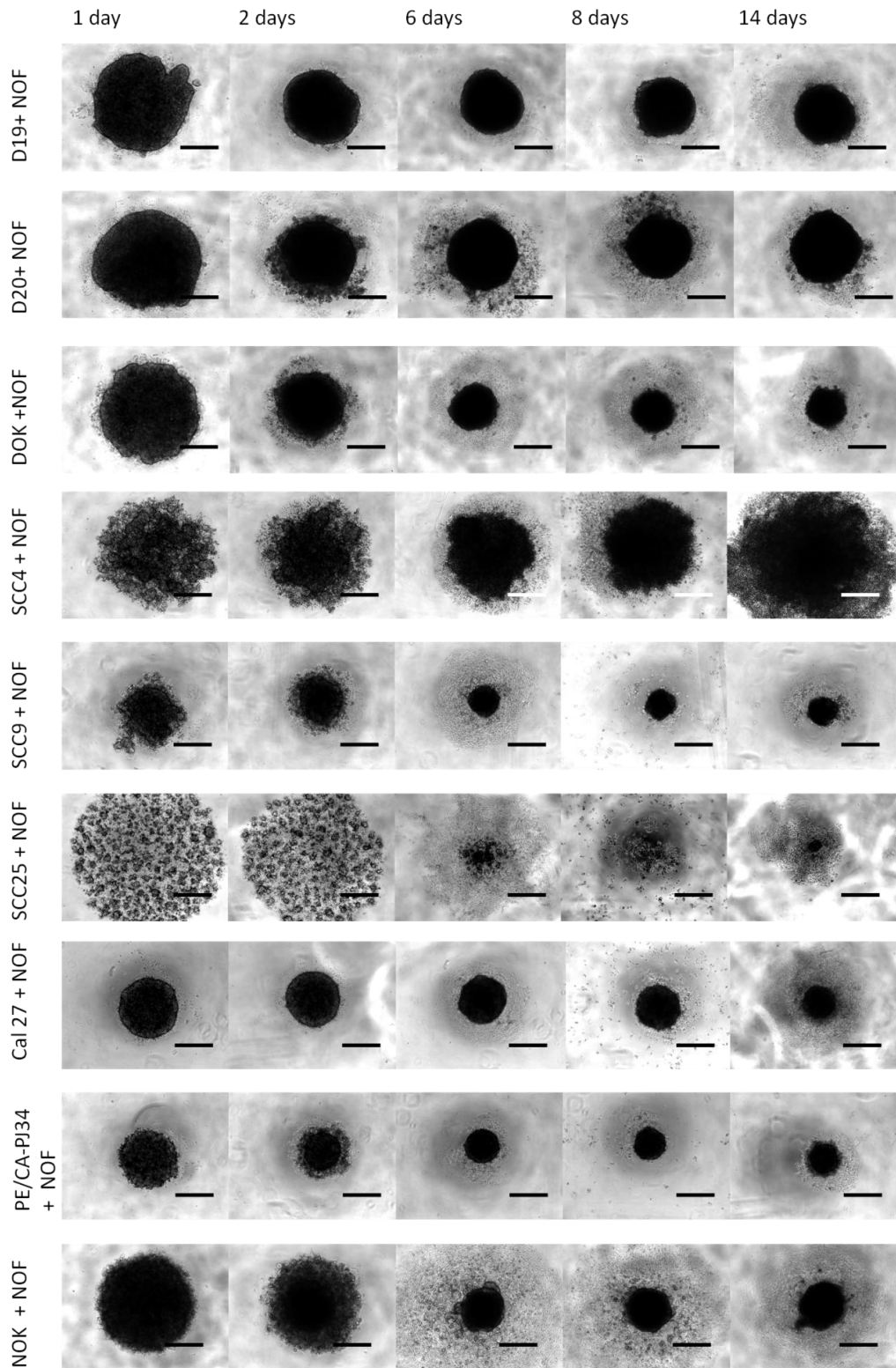
Figure 2.18 Cell lines cultured with NOF cells to test their ability to produce solid expanding MCTS. Cancer cells or NOKs were seeded at a density of 12x10^3 cells/ well plus 3x10^3 NOF cells/ well of a 96 well plate coated with agarose . Scale bar = 400μm. n=3

NOK + NOF

The most dramatic effect from adding NOF cells was the effect these cells had on NOK cultured on agarose coated plates. Instead of growing as a monolayer (NOK monoculture) the NOK cells cultured with NOF cells produced large dense aggregates. These aggregates had an irregular border so could not be defined as a spheroid however, this demonstrates the effect NOF cells can have on the behaviour of NOK cells. Over time the aggregates reduced dramatically in size and many cells were lost from the aggregate.

2.5   Discussion

Currently the majority of new technologies and therapies which reach the patient will previously have been tested in *in vitro* cell monolayer experiments and subsequently in animal models. There is a dramatic difference in the behaviour and response of cells in monolayers compared to the results seen in animal models. Monolayer studies look at the way in which single cells respond to a compound; however, it is now well know that many cells behave differently in 3D culture conditions (Hirschhaeuser *et al.,* 2010). Three dimensional tissue cultures also provide a method by which drug delivery, penetration and distribution within a tissue can also be studied. This is clearly important when investigating the bio-distribution and pharmacokinetics of a drug or drug delivery system.

Animal studies provide a crucial step in the process of novel therapy development. However, animal studies have many disadvantages and any developments which can reduce the need for animal studies or better predict results seen *in vivo* are welcomed by those inside and outside the field. Testing in animals is strictly regulated making the process expensive, time consuming and the experiments which can be performed are limited. It should also be remembered that animal models are not always the best predictor of outcome in humans as the biology of animals is vastly different to humans.

Tissue Engineered Oral Mucosa

The factors mentioned previously have led to researchers to develop 3D tissue engineered models *in vitro* which can be used as a tool to test novel therapies and diagnostics. A TEOM which can be produced in the laboratory from primary human cells provides researchers with an important *in vitro* tool as well as having uses in tissue regeneration (Bhargava *et al.,* 2004; Bhargava *et al.,* 2008). The model presented here is a 3D model of a healthy human oral mucosa. It has been cultured from normal human oral keratinocytes and normal oral fibroblasts from consenting volunteers. As they originate from human tissue these cells are able to model the oral mucosa is a clinically relevant way. When in culture the models are exposed to an air liquid interface which encourages epithelial differentiation and stratification.

These culture conditions resulted in stratified epithelium which thickened over time in culture (Figure 2.3).

Some variation was found between models cultured from different cell batches from different patients. This is the major drawback associated with using primary cells. However, the effects of this can be minimised by keeping good records of the behaviour of different cell batches. Factors including the age of the donor, donor site and condition of the donor site can all affect the behaviour of primary cells which are extracted. The alternative to primary cells would be to use cell lines which have either been transformed in the laboratory to be immortal (such as TURT2 OKF6) or have been isolated from squamous cell carcinomas (such as TR146). Although these cells are of oral epithelial origin their behaviour is different to healthy oral keratinocytes and this makes the model less physiologically relevant. The cancer cell line TR146 is used in the commercially available Human Oral Epithelium (HOE) model from SkinEthic Laboratories. It is clear from Figure 2.19 that this model does not show the stratification seen in the TEOM and does not demonstrate the differential layers of the oral epithelium seen in normal oral mucosa.
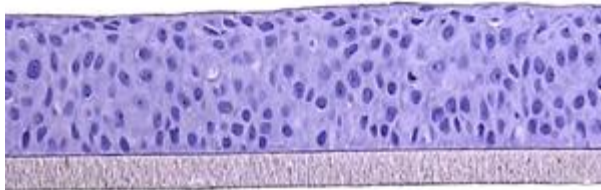
Figure 2.19 Human Oral Epithelium (HOE) model from Skin Ethic Laboratories (Skin Ethic, Lyon, France). Image reproduced from http://www.skinethic.com/HOE.asp

Fibroblasts

Unlike the oral epithelium models discussed in chapter 1 the TEOM model produced here incorporates a mesenchymal element, primary human oral fibroblasts seeded into a connective tissue scaffold. Ralston *et al*., looked at culturing epidermal keratinocytes with and without fibroblasts and found that fibroblasts were required for epithelial cell attachment and differentiation (Ralston *et al.,* 1999). Both keratinocytes and fibroblasts were also required to maintain a continuous and well formed basement membrane (Ralston *et al.,* 1999). It has previously been shown in oral models that fibroblasts are essential to promote oral epithelial thickening, an effect which was also seen with the addition of KGF (Costea *et al.,* 2003). Other features however, could not be induced with the addition of KGF alone. For example co-culture with fibroblasts increased basal cell proliferation and produce a pattern of cell death similar to naturally occurring tissues, suggesting that further signals are released from fibroblasts which are responsible for these changes (Costea *et al.,* 2003). Elsewhere is has been

observed that fibroblasts associated with non-keratinised regions of the oral cavity (such as alveolar mucosa) expressed higher levels of elastin compared to gingival fibroblasts, highlighting the importance of elastin in the keratinisation of tissues (Hsieh *et al.,* 2010).

Connective tissue component

The model presented here included a connective tissue component. The acellular skin scaffold (EuroSkin Bank, Beverwijk, The Netherlands) provide a very physiologically relevant scaffold onto and into which the cells could grow. Connective tissue from the oral mucosa would be optimum however, this tissue is not available in large amounts. Fibroblasts were able to penetrate into the acellular dermal scaffold and keratinocytes adhered well to the upper surface, potentially due to the presence of residual basement membrane proteins after de-cellularisation (Ralston *et al.,* 1999). The protein composition of the acellular skin scaffold is similar to naturally occurring oral connective tissue.

Cell culture medium

It has been noted in the literature that the cell culture medium in which models are cultured affects the resulting characteristics. For example, a medium low in serum and growth factors was used to produce a non-keratinised epithelium model (Kinikoglu *et al.,* 2009). Effects of culture medium were also observed in (Costea *et al.,* 2005) where three different medium types were tested to evaluate their effects on organotypic cultures. The models developed in this project were all cultured in Green's medium (Rheinwald and Green 1975) as it is well established that this culture medium is optimal for keratinocyte growth and proliferation. However, research in this area opens up possible further developments of the model presented here. For example, if non-keratinised areas of the oral cavity were to be modelled, reduced serum and growth factors may enable this.

Immunohistochemical characterisation

Here immunohistochemistry was used to validate our model by demonstrating the similarities between the TEOM and a normal human oral biopsy. The immunohistochemistry staining confirmed our models possessed key features of an oral epithelium including the presence of the basement membrane protein collagen IV, cytokeratin expression and proliferative basal cells.

3D models of OSCC

The aim of this experiment was to screen a number of different cell lines to see which, if any, would make a good model of OSCC which could be used as a model to test novel cancer detection and therapeutic technologies as well as to investigate mechanisms of cancer development. The ideal properties of a model for these applications are reproducibility and characteristics of naturally occurring cancers. If models for all stages of oral cancer from mild

dysplasia through to invading OSCC (Figure 1.4 on page 22) could be produced it would be an incredibly useful tool for *in vitro* studies into oral cancer progression and therapeutics. Nine different models were cultured, each of which have different appearances and many of which show characteristics of naturally occurring tumours and pre-malignant lesions.

Table 2.10 summarises the features seen in each model and if the appearance was comparable to naturally occurring tumours and the clinical grading was shown in the final column. Five out of the nine models had appearances which are not typically seen clinically so no clinical grading was given.

Cell type

There are a number of factors which determine the morphology and behaviour of a tissue engineered model, most importantly the cell types used to culture the model. Figure 2.5 to Figure 2.13 show the diversity of the models created from the oral cell lines tested here.

Cell availability and a desire to improve the reproducibility of models led us to use cell lines, as opposed to primary cells extracted from dysplastic tissues and OSCCs. It has been shown that primary dysplastic keratinocytes from clinical lesions have variable phenotypes when cultured in tissue engineered models due to the heterogeneous populations of cells extracted from lesions (Gaballah *et al.,* 2008). The reproducibility of *in vitro* models is important for them to become a highly utilised model for testing novel technologies. Unfortunately, there are a large number of factors which affect the behaviour of the model which are not all overcome using cancer cell lines. For example, the passage number of the cells (Gaballah *et al.,* 2008) and the exact level of the media in the air liquid interface can affect the resulting phenotype.

It is well established that tumourigenesis is not a result of just epithelial cells but instead results from a combination of epithelial cells and the stromal compartment (Elenbaas and Weinberg 2001). In addition to this, previous findings in our laboratories and others have shown that if models were cultured without fibroblasts, epithelial cells only formed weak attachments to the skin scaffold (Ralston *et al.,* 1999). Therefore, we cultured all of our models with primary oral fibroblasts from healthy patients. Variation between batches of fibroblasts from different donors was observed which is not surprising given fibroblasts and their released factors affect epithelial cells in many different way including cell adhesion, cell proliferation and cell behaviour (Costea *et al.,* 2006). There is now growing interest in the effect fibroblasts extracted from tissues around lesions, areas of dysplasia and carcinomas can have on model morphology. Dysplasia associated fibroblasts have been shown to induce morphological changes in normal oral keratinocytes when co-cultured together, which was not seen with fibroblasts from healthy tissue (Gaballah *et al.,* 2008). Dysplasia associated fibroblasts also secreted higher levels of hepatocyte growth factor (HGF), expressed matrix

metallopeptidase 9 (MMP9) and increased the dysplasia scores of the models cultured with them.

These models studied the level of invasion seen when epithelial dysplastic and cancer cell lines were cultured with fibroblasts and a stromal compartment (which retained basement membrane antigens from the de-epidermisation process (Ralston *et al.,* 1999)). Studies looking at the invasive behaviour of melanoma cell line (Eves *et al.,* 2003) found the addition of keratinocytes and fibroblasts to models cultured with three different strains of melanoma altered the invasive behaviour of these cells. It would therefore be interesting in the future to investigate what effect the addition of normal oral keratinocytes would have on these models and the invasion of these cell lines.

Fibroblasts associated with areas of carcinoma *in situ* are often referred to as myofibroblasts. These myofibroblasts behave differently to normal fibroblasts and it is thought their transformation to myofibroblasts may be in part due to cytokines released by epithelial tumour cells (Elenbaas and Weinberg 2001). Myofibroblasts release different levels of growth factors and ECM proteins aiding the initiation, growth and invasion of epithelial cancers (Elenbaas and Weinberg 2001). It would be interesting to look at whether any of the fibroblasts in our models had myofibroblastic properties such as expression of α-smooth muscle actin, smooth muscle myosin heavy chain or vimentin.

Features of the OSCC models

The majority of clinically familiar features modelled here are those associated with severe dysplasia and carcinoma *in situ* (see Table 2.10) because the abnormalities were present throughout the epithelium. For some applications it would also be of benefit to be able to model mild and moderate dysplasia. For this the epithelial changes associated with OSCC are only observed in the basal 1/3 or 2/3 of the epithelium respectively (see Table 1.1 on page 23). It may be possible to model this by culturing the cancer cells lines with healthy primary oral keratinocytes or by culturing a healthy oral epithelium and inducing dysplasia using external factors.

Cell type	Nuclear pleomorphism	Cell death	Abnormal mitotic figures	Single cell keratinisations	Abnormal keratinisation	Loss of basal polarity	Invasion	Bulbous/ drop shaped rete pegs	Clinical grade
FaDu	■	■					■		
SCC4		■				■		■	
SCC9	■		■		■			■	Severe dysplasia
PE/CA-PJ34				■			■	■	
D19	■		■		■				
SCC25	■		■	■					
Cal 27	■		■						Invasive carcinoma
DOK	■	■		■		■			Severe dysplasia/invasive carcinoma
D20	■	■	■		■		■		Invasive carcinoma

Table 2.10
Features of OSCC models cultured with different cell types. Shaded square shows features present. Cell lines are arranged in order of increasing abnormalities.

Potentially malignant lesions (PML), including leukoplakia, erythroplakia, mild dysplasia and moderate dysplasia, are of particular interest to oral medicine specialists. An ability to predict which of these PML was most likely to become malignant could enable earlier detection of carcinogenesis and could reduce unnecessary biopsies for those patients who have lesions with a very low chance of becoming malignant. Models of PML would have great value in testing agents able to prevent malignant transformation, understand the mechanisms which drive PMLs to become malignant and to test novel diagnosis technologies aimed to detect PMLs.

Of the nine models produced here three had the appearance of invasive carcinoma, one had the appearance of severe dysplasia and the remaining five models had some features of dysplasia and carcinoma however, their overall appearance was not one that is seen clinically (Table 2.10). Many of the cells cultured in the models appeared to behave as single cells rather than as a communicating group of cells. This is not usually seen clinically and was apparent where there was single cell keratinisation and no polarity between the basal and superficial regions of the oral epithelium.

Some models displayed different features as they were cultured for longer periods. For example the SCC9 model cultured for 7 days showed relatively normal stratification however, after two weeks in culture the epithelium had a severely dysplastic appearance. The D19 cells were particularly interesting. The appearance of the model after 7 days in culture was significantly different to the model after 21 days in culture (Figure 2.7). This stark difference in morphology is most likely due to much of the epithelium becoming detached by 21 days and the areas which remained could have resulted from a different sub-population within the D19 cell line as the D19 cells used here were at a low passage number.

The D19 cells also showed an interesting feature after 7 days, many spindle like cells had invaded into the connective tissue. The spindle like cell morphology of the D19 cells which invaded (Figure 2.7) suggests the cells may have undergone epithelial mesenchymal transition (EMT). In EMT epithelial cells change their characteristics and become more like mesenchymal cells. EMT has been proposed as a factor involved in oral submucous fibrosis as well as invasion and progression of OSCC (Yanjia and Xinchun 2007). Epithelial cells undergoing EMT lose epithelial morphology and markers (including cell-cell adhesion and cytokeratins) in favour of mesenchymal phenotypes (including cell motility and α- smooth muscle actin) (Yanjia and Xinchun 2007). Signs of EMT have been found to correlate with poor prognosis and tumour progression. The presence of EMT could be confirmed by immunohistochemistry staining for mesenchymal markers. It is worth noting that in all of these studies normal oral fibroblasts were present. If EMT could be confirmed this model could have value in studying inhibitors of EMT and as a model to study the process by which EMT occurs in dysplastic oral cells.

The origin of the Cal27 cell line has recently been put into question in (Jiang *et al.,* 2009). However, in these experiments the Cal27 cells produced a model of carcinoma *in situ* which behaved in a similar way to a squamous cell carcinoma, suggesting the Cal27 cell line used in our laboratory is of squamous cell carcinoma origin rather than adeno-carcinoma as was proposed by Jiang *et al*., (Jiang *et al.,* 2009). The Cal27 models were the most representative of naturally occurring carcinomas. Although the cells were invasive at all time points the severity of dysplasia increased over time as more keratin was produced and the nuclear and cytological pleomorphism became more pronounced.

In some cases the models cultured in this project were also invasive which required the cancer cells to cross the basement membrane. Eves *et al*., (2003) showed that the presence of a basement membrane affected melanoma cell pigmentation, location within the epithelium and invasive behaviour demonstrating the importance of including a basement membrane within a model of invasion (Eves *et al.,* 2003).

Eves *et al*., also demonstrated that there was a dynamic relationship between keratinocytes, fibroblasts and melanoma cells which together dictated the invasiveness of melanoma cells (Eves *et al.,* 2000; Eves *et al.,* 2003). Matrix metalloproteinase (MMP) enzyme activity was not seen to increase in melanoma cells, however, MMP activity was activated in the adjacent epithelial and stromal cells (Eves *et al.,* 2003). This data suggests melanoma cells were able to cross the basement membrane by utilising the collagenolytic enzyme activity of the surrounding cells.

Work by Colley *et al.,* has shown invading oral cancer models had disrupted collagen IV expression along the basement membrane (personal communication). An ability to prevent tumour invasion clinically would be hugely advantageous to stop tumour metastasis and the formation of solid tumours deep within tissues. This model could provide a useful tool to study the mechanisms of invasion. It also enables research to look at whether novel drug formulations are able to reach all cancer cells including those which have passed into the connective tissue.

3D models of OSCC have great value in studying the mechanisms involved in tumourigenesis. Factors which contribute to the development of this disease can be examined in isolation to enable a complete picture of how the disease progresses and provides useful information which can be utilised in the development of future treatments and therapies.

Gaballah *et al*., investigated the influence of factors in the cell culture medium (EGF and KGF) which affected the appearance of models (Gaballah *et al.,* 2008). They found culturing models with EGF increased the level of dysplasia (increasing suprabasal proliferation and increasing architectural and cytological features throughout the epithelium) (Gaballah *et al.,* 2008). This finding is in agreement with high expression of EGF receptors (EGFR) being

linked to poor patient prognosis (Psyrri *et al.,* 2005), indicating the important role of EGF in tumour progression. On the contrary, culturing with KGF resulted in models with features associated with a healthy epithelium including basal cell proliferation and no epithelial hyperplasia (Gaballah *et al.,* 2008).

Spheroid formation

To accurately model oral squamous cell carcinomas it is important to develop a model which incorporates as many features of a naturally occurring tumour as possible. This model also needs to be reproducible and it would be advantageous to develop a model which can be produced in large quantities for high throughput experiments of novel agents. The main characteristic of solid tumours which can be modelled in 3D tumour spheroid models are the distribution of proliferating and necrotic cells (periphery and core respectively), the diffusion gradients of nutrients and waste products and the intra-cellular connections (Ivascu and Kubbies 2007).

The MCTS model cultured from the FaDu cell line, derived from a hypo-pharyngeal cancer, is a well established model in our laboratory as a model for solid expanding oral cancer tumours. The same FaDu MCTS have also recently been employed by Hirschhaeuser *et al*., to evaluate the efficacy of a novel anti-cancer antibody therapeutic (Catumaxomab) (Hirschhaeuser *et al.,* 2010).

FaDu MCTS are reproducible and continue to expand over 21 days in culture. Figure 2.15 shows FaDu spheroids expand from around 840μm in diameter after 24 hours to over 1mm in diameter after 21 days. These MCTS have been compared against solid expanding oral cancers seen *in vivo* (Figure 2.16). Characteristics of naturally occurring tumours including the proliferative outer cells, a hypoxic central region and necrotic cells in the centre were all comparable *in vitro* and *in vivo* (Figure 2.16).

The proliferative cells on the periphery of these solid tumour regions are the cells responsible for tumour growth. These cells are adjacent to blood supplies enabling them to obtain the nutrients required to proliferate. Therapies which are able to reduce the proliferative ability of these cells can slow tumour growth.

The central regions of tumours above a certain size become hypoxic. These cells are further from the blood supply and have poor oxygen diffusion resulting in a lower oxygen tension in this region. From a therapeutic point of view the hypoxic region presents a major challenge to treatment as it is this region which is most resistant to radiotherapy (Ljungkvist *et al.,* 2000). The central region is not well served by vasculature meaning drugs administered systemically have to diffuse a long way though tissues in order to act on these cells. This means chemotherapy is also less effective on these cells. Regions of hypoxia are often an indicator of

poor patient prognosis clinically. The presence of these features in the MCTS make it an especially useful model to study novel therapies which are able to treat these chemo- and radio-resistant cells.

The cells in the very centre of the tumour undergo cell death as waste products accumulate and nutrient supply is limited. The distance from the blood supply is the main driver for this cell death. Both cell death and hypoxia can be seen in the FaDu MCTS model (Figure 2.15Figure 2.16) making it a clinically relevant model. This model can be produced quickly and cheaply in large numbers making it a useful tool for high throughput screening of novel drugs (Friedrich *et al.,* 2009).

The FaDu MCTS provide us with a very useful tool to study the behaviour of novel therapeutics on solid tumours. A number of different oral cell types were investigated to determine if other oral MCTS models could be produced for testing therapeutic technologies. Extending the variety of MCTS which are able to be used in *in vitro* studies should improve the predictability of the behaviour of novel compounds *in vivo* and make testing on MCTS a more robust and commercially useful testing method.

We tested 10 different cell types including dysplastic cell lines (D19, D20 and DOK), OSCC cell lines (SCC4, SCC9, SCC25, Cal27 and PE/CA-PJ34) and primary cells (NOK and NOF) to see if they were able to spontaneously form MCTS when cultured on a non-adherent agarose surface. Anchorage dependant cells are usually cultured on surfaces on which they are able to adhere. By culturing them on a non-adherent surface these cells are encouraged to adhere to one another to grow. Four of the 10 cell types tested here were able to form spheroids. The DOK, Cal27, PE-CA-PJ34 and NOF cells all produced spherical solid masses of cells with well defined borders (Figure 2.17). In comparison to the FaDu cells (Figure 2.16) these MCTS did not expand over time and some of them fell apart in culture. For a model to be useful in the screening of novel chemotherapeutic agents a predictable growth of MCTS is important to assess the ability of a compound to slow or retard growth of a tumour. Other cell types, including the OSCC cells and NOK cells, did not show any sign of aggregating or forming spheroids when cultured in this way.

It is well known that only some cell lines have the inherent ability to produce spheroids in culture using the liquid overlay method. Friedrich *et al*., tested the 60 human epithelial cell lines included in the National Cancer Institute Developmental Therapeutics Programme (NCI-DTP) human tumour cell line screen (Friedrich *et al.,* 2009). These cell lines make up the standardised catalogue of cells for testing novel anti-cancer treatments. Of these 60 cells, which include cells derived from lung, colon, brain, ovary, breast, prostate, and kidney cancers as well as leukaemia and melanoma (DTP), only 26 formed MCTS. Nine of the 26 MCTS did

not grow once formed but the maximum diameter of those which did grow was between 500-1000 μm (Friedrich *et al.,* 2009).

A number of different techniques have been tested to encourage MCTS production from cell lines which do not spontaneously form these spheroids in culture. The hanging drop method has been employed by Kelm *et al.,* to form spheroids from cell lines which did not form MCTS using the liquid overlay method (Kelm *et al.,* 2003).

Here we tested the effect of adding NOF cells to the MCTS culture to test if NOF cells could aid MCTS formation. As discussed previously, it is well known that tumourigenesis is a result of the interactions between epithelial and stromal cells. Stromal cells, namely fibroblasts, also produce large amounts of ECM proteins. Therefore we investigated whether adding NOF to the cancer cells would enable MCTS formation from the cell lines which did not form or expand previously.

Some cells showed little or no difference when cultured with or without NOF cells. These cells included SCC4, SCC25 and Cal27. In other cases the addition of NOF initially encouraged spheroid formation however, none of these went on to expand in culture and many fell apart when cultured for longer times. The NOK cells without NOF cells did not aggregate at all. When NOF cells were added the NOK cells did aggregate but these aggregates were not spheroids and fell apart over time in culture. The dysplastic cell lines (D19 and D20) formed spheroids when cultured with NOF rather than aggregates. The other dysplastic cell line (DOK) formed larger spheroids when cultured with NOF but still did not expand.

There are many different factors which influence whether or not cells form MCTS in culture. These include the components of the cell culture medium, the method used to initiate MCTS formation and various other factors. These factors include the tissue type from which the cells originate, the age and differentiation of the cells as well as the cell density used (de Ridder *et al.,* 2000). Extrinsic factors including temperature, rotation speed (if used) and the ions present in the culture medium have all been shown to effect MCTS formation (de Ridder *et al.,* 2000). The method by which cells are detected from monolayer culture surfaces can effect the morphogenic capacity. de Ridder *et al.,* avoided the use of enzymes such as collagenase and trypsin as these alter the surface of the cells, but instead used mechanical detachment (de Ridder *et al.,* 2000).

Ivascu and Kubbies looked at the cell adhesion molecules involved in spheroid formation with eight different breast cancer cell lines (Ivascu and Kubbies 2007). Different cell lines showed dependence on different adhesion molecules for spheroid formation and tight cell packing demonstrating the complex interactions between many different cell surface proteins which are involved in the establishment of 3D cell culture models *in vitro.*

Cell adhesion molecules which were seen to have a role in spheroid formation included E-cadherin, N-cadherin and the interaction between collagen I and integrin β1. In cells from other cancers and fibroblasts, integrin β1-fibronectin interactions have also been identified as being important (Salmenpera *et al.,* 2008). It may be the relative expression of these cell-cell interaction proteins and cell-matrix interactions which contribute to whether or not cells spontaneously form solid MCTS. It is well documented that cells behave differently *in vitro* compared to *in vivo*, therefore the expression of cadherins and integrins is likely to be different when cells are cultured *in vitro* affecting spheroid formation. Further studies into the expression of these integrins and cadherins would be interesting in the cell lines tested here to establish whether these are responsible for the pattern of spontaneous MCTS formation.

Cell-cell interactions and cell-matrix interactions have also been proposed to be involved in drug resistance clinically. These features are seen in MCTS models enabling *in vitro* research into ways to overcome the drug resistance seen in tumours and MCTS (also called the "multi-cellular resistance" effect) (Green *et al.,* 2004). This highlights a clear advantage of using MCTS over traditional two-dimensional cultures as only MCTS exhibit the "multi-cellular resistance" to cytotoxic agents (Green *et al.,* 2004). Green *et al*., have also demonstrated that by targeting these cell adhesions in multicellular tumours and MCTS it may be possible to sensitise them to respond better to anti-cancer agents (Green *et al.,* 2004).

A number of studies have looked at adding extrinsic and artificial additives and matrices to cancer cells to promote MCTS formation. For example Ivascu *et al*., tested the addition of reconstituted basement membrane (rBM) on breast cancer cells to induce MCTS formation (Ivascu and Kubbies 2006). However, it is important to remember the addition of external factors may alter the behaviour of cell lines, changing cell growth, protein expression and potentially altering responses to drugs (Friedrich *et al.,* 2009).

Some of the cells tested here were able to form MCTS (DOK, Cal27, PE-CA-PJ34 and NOF) but these did not expand over time in culture. This could be due to a number of factors such as the effect spherical culture has on the proliferation of the outer most cells and the level of cell death experienced in the central core of the MCTS.

Correlation between MCTS formation and invasion

All the cell lines tested in this study were genetically and phenotypically distinct from one another and this was apparent in the appearance of the 3D models cultured on DED with fibroblasts and the appearance of cells when cultured on a non-adherent surface.

Table 2.11 shows the correlation between spheroid formation (with and without fibroblasts) and the invasive behaviour of the cells when cultured on DED with fibroblasts. There is a

strong correlation between those cells which formed spheroids in the presence of fibroblasts and those which invaded into the 3D model. All six cell lines which were tested for spheroid formation with fibroblasts and the FaDu cell lines invaded. Interestingly, the correlation is not as strong when comparing those cell lines which formed spheroids without fibroblasts and those which invaded (as not all invading cell lines formed spheroids in monoculture). This data further supports the hypothesis that invasion and cancer progression are the result of a combination of factors from the epithelial and stromal compartments. Used in combination these models could provide a useful tool to study factors which determine invasiveness of tumours and the relationship between epithelial cancer cells and fibroblasts.

Cell type	Formed spheroid	Formed spheroid in co-culture with fibroblasts	Invasive in 3D model
DOK			
Cal27			
PE/CA-PJ34		late	
SCC25	late	tiny	
D20			
D19			
FaDu		Not tested	
SCC4			
SCC9			

Table 2.11
Correlation between invasion in 3D model and spheroid formation. Shaded squares show positive result. Cells listed in order of correlation.

Chapter 3: Novel therapeutic technologies

3.1   Aims

To produce nano-sized polymersomes using the polymers 2-(methacryloyloxy)ethyl phosphorylcholine)-poly(2-(diisopropylamino)ethyl methacrylate) (PMPC-PDPA) and poly(ethylene oxide)-poly(2-(diisopropylamino)ethyl methacrylate) (PEO-PDPA) and to study the behaviour of these polymersomes in three dimensional tissue engineered models *in vitro*.

3.2   Introduction

In order for chemotherapy outcomes and patient tolerance to significantly improve, highly potent anti-cancer drugs need to be delivered with better specificity to sites of disease. Improving bio-availability of drugs in target areas and reducing drug delivery to other locations will reduce side effects, which are often dose limiting, and will therefore improve therapeutic outcomes. The bioavailability of drugs and control over their delivery can be achieved using drug delivery vectors, reviewed in chapter 1 on page 29.

Delivery systems enable better delivery of drugs which exhibit poor tissue penetration and enable targeted drug delivery both passively, *via* the EPR effect, and actively *via* targeting moieties. Drug delivery vectors can also have drug release profiles tailored to the application. In the most part these alterations can be achieved without altering the drug's structure or therapeutic action.

This chapter evaluates the properties of the amphiphilic block co-polymers PMPC-PDPA and PEO-PDPA.   These self-assembling block co-polymers have previously been demonstrated to produce membrane-enclosed vesicle structures (polymersomes) in aqueous solutions (Du *et al.,* 2005; Massignani *et al.,* 2009). The polymersomes are non-toxic and rapidly taken-up by a large selection of primary cells and cell lines (Massignani *et al.,* 2009) (Figure 3.1). Capable of encapsulating DNA, RNA, antibodies and proteins (Lomas *et al.,* 2007; Massignani *et al.,* 2010) these polymersomes have huge potential in the field of drug delivery for many different diseases.
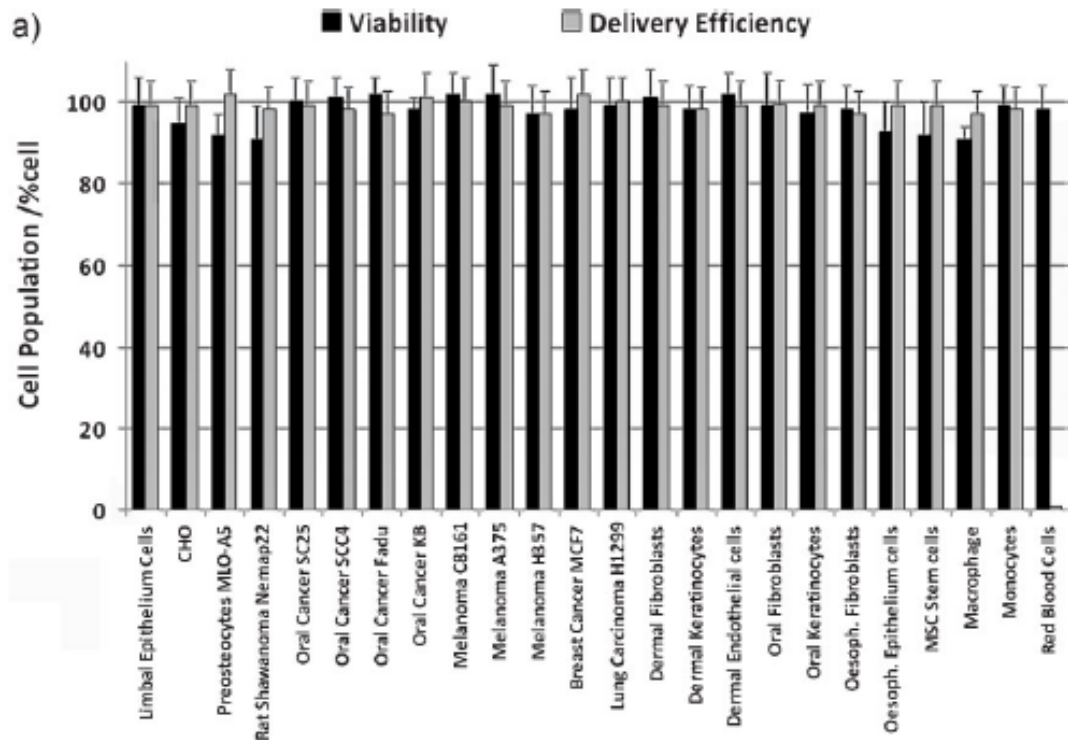
Figure 3.1 Viability and uptake of PMPC-PDPA after 24 hours exposure with many different cell types.
Graph from (Massignani *et al.,* 2009)

The polymersomes investigated here are pH sensitive. The PDPA block (poly(2-(diisopropylamino)ethyl methacrylate) present in both polymers is pH sensitive. At low pH (below pH 6.4) the PDPA polymer block is hydrophilic. Raising the pH causes the PDPA block to become deprotonated and causes it to become hydrophobic (Figure 3.2). The PMPC and PEO blocks on the other hand are not pH sensitive so remain hydrophilic at low and high pH. Therefore the change in pH causes the block co-polymer to shift from entirely hydrophilic (at low pH) to amphiphilic (part hydrophobic, part hydrophilic). The hydrophobic effect causes the amphiphilic block co-polymers to self assemble into membrane-enclosed vesicles. This configuration is energetically favourable as the hydrophobic regions are shielded from the aqueous solution by the hydrophilic blocks of the polymer.
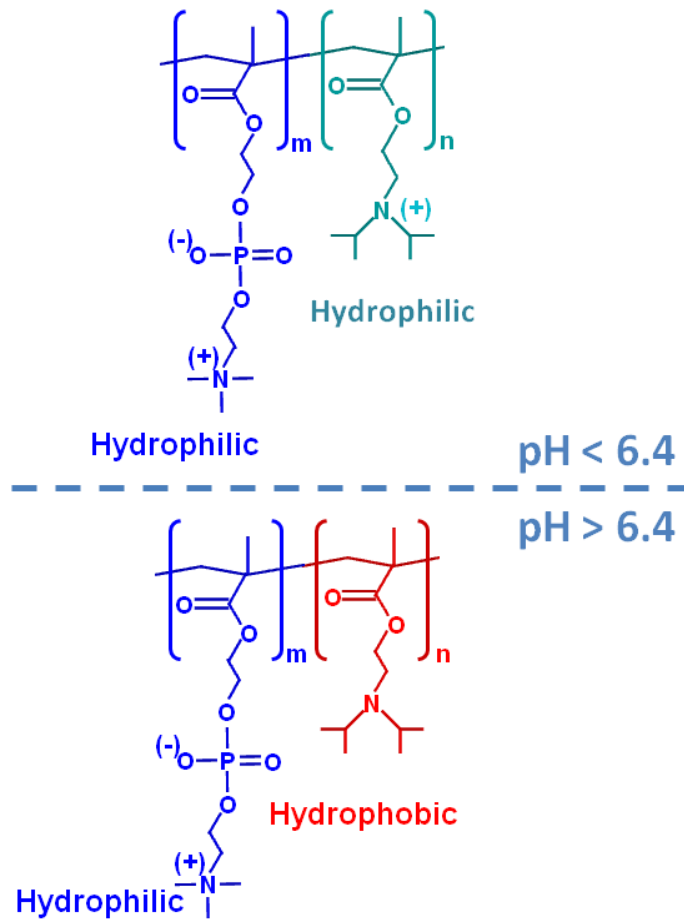
Figure 3.2 pH sensitive PMPC-PDPA.
Below pH 6.4 the block co-polymer is hydrophilic. Above pH 6.4 the polymer is amphiphilic.
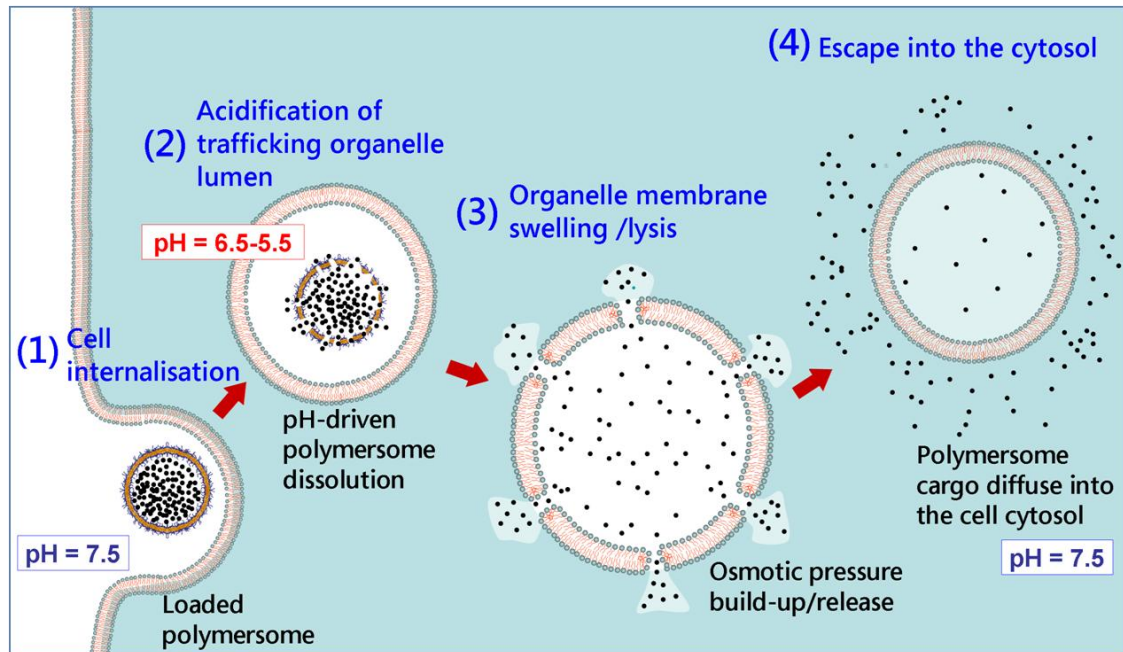
Figure 3.3 Proposed mechanism for the escape of polymersomes from the endolysosomal pathway and the release of polymersome encapsulated cargo into the cell's cytosol. Reproduced from (Massignani *et al.,* 2010)

This pH sensitivity is thought to have a role in the delivery of encapsulated cargo into the cytosol of cells (Massignani *et al.,* 2010) (Figure 3.3). The endosomal vesicles which deliver and traffic materials endocytosed by the cell into the endolysosomal pathway have a lower pH compared to the rest of the cell. The pH in these endocytic vesicles is below pH 6.4 causing any polymersomes which enter these vesicles to disassemble as the PDPA block becomes hydrophilic. This results in an osmotic shock as one particle (the polymersome) disperses into many thousands of polymer chains and the cargo is released. This osmotic shock is sufficient to lyse the endocytic vesicle membrane and the material within the endocytic vesicle (including encapsulated polymersome cargo) is released into the cytosol thus escaping the endo-lysosomal pathway.

Before polymersomes can be utilised clinically their behaviour *in vitro* and *in vivo* must be understood. Here the behaviour of these polymersomes was studied, in a range of oral cancer cells and primary oral cells grown in monolayers. The uptake of polymersomes by these cells and the toxicity profile associated with polymersome exposure was investigated. Next the behaviour of polymersomes in three dimensional tissues *in vitro* was examined and their ability to penetrate into 3D tissues was evaluated. This was tested using the tissue engineered models described in the previous chapter of solid oral cancer tumours (MCTS) and healthy oral mucosa (TEOM). This information is clearly important in the development of polymersome mediated therapies for the treatment of oral cancer and for transmucosal

delivery. Delivery to the basal epithelial cells and the central regions of solid tumours is particularly difficult due to the penetration barrier of the oral mucosa and the distance from a blood supply respectively. These areas are particularly desirable to deliver to as the centres of solid tumours are often resistant to radiation and chemotherapy.

If it can be demonstrated that polymersomes can cross the oral mucosa membrane intact and deliver their payload into the circulation then polymersome mediated therapy could provide an alternative to parenteral delivery. For chronic diseases parenteral delivery by injection is not well accepted by the patient and requires administration by a healthcare professional (except in the case of diabetes). Therefore, self-administered transmucosal therapy which is able to deliver treatment directly to the circulation could significantly improve treatment of a number of chronic conditions. On the other hand a technology which was able to deliver its payload across the penetration barrier and into the epithelium of the mucosa would be beneficial for a number of mucosal diseases including OSCC. The MCTS models are used here to test if polymersomes could enable drug delivery into the avascular areas of tumours which are typically harder to treat because of poor drug penetration and radiotherapy resistance.

The behaviours of these polymers *in vivo* has been tested in (Murdoch *et al.*, 2010). This paper demonstrated a good safety profile and acceptable bio-distribution of PEO-PDPA and PMPC-PDPA polymersomes.

3.3 Materials and Methods

Production of polymersomes

Materials

PMPC$_{25}$-PDPA$_{70}$, PEO$_{23}$-PDPA$_{15}$ block co-polymer and rhodamine 6G conjugates PMPC$_{30}$-PDPA$_{60}$ block co-polymers
Block co-polymers were kindly synthesized by Paul Topham, Jeppe Madsen, Nick Warren and Adam Blanzas in Professor S Armes' laboratory in the Department of Chemistry, University of Sheffield. The synthesis of the polymers used in this work is described in (Hearnden *et al.,* 2009); (Massignani *et al.,* 2009). Chemical structures of both polymers and the PMPC-PDPA conjugated with rhodamine 6G are shown in Figure 3.4.

Rhodamine B octadecyl ester perchlorate dye
Purchased from Sigma Aldrich, Dorset, UK, dissolved in chloroform to give a concentration of 1mg/ml, protected from the light and stored at -20°C in a spark-free freezer (Figure 3.4d).

Sodium hydroxide(NaOH)
Made up to a concentration of 1M using distilled water. Filter sterilised prior to use and stored at room temperature.

Hydrochloric acid (HCl)

Made up to a concentration of 1M using distilled water. Filter sterilised prior to use and stored at room temperature.

Sonicator
From Sonicor Instruments Corporation, New York, USA.

Sepharose 4B
Purchased from Sigma Aldrich, Dorset, UK and stored in methanol at 4°C.

Preparation of block co-polymer film

890nM of $PMPC_{25}$-$PDPA_{70}$ or PEO_{23}-$PDPA_{15}$ were dissolved in a glass vial in 2:1 chloroform: methanol solution. For rhodamine labelled samples, 5% (molar %) rhodamine labelled polymer (rho-$PMPC_{30}PDPA_{60}$) was added to the polymer solution.

For internalisation experiments on cell monolayers an amphiphilic rhodamine B octadecyl ester perchlorate dye (Sigma Aldrich, Dorset, UK) was encapsulated into polymersomes (Figure 3.4d). 100μl of the stock solution of the dye (1mg/ml rhodamine B octadecyl ester perchlorate dye) was added to 20mg of the PMPC-PDPA polymer dissolved in the solvents (or per 4mg of PEO-PDPA). A co-polymer film was formed by evaporating the solvent in a vacuum oven at 40°C for 2-3 hours, or until all solvent was removed.
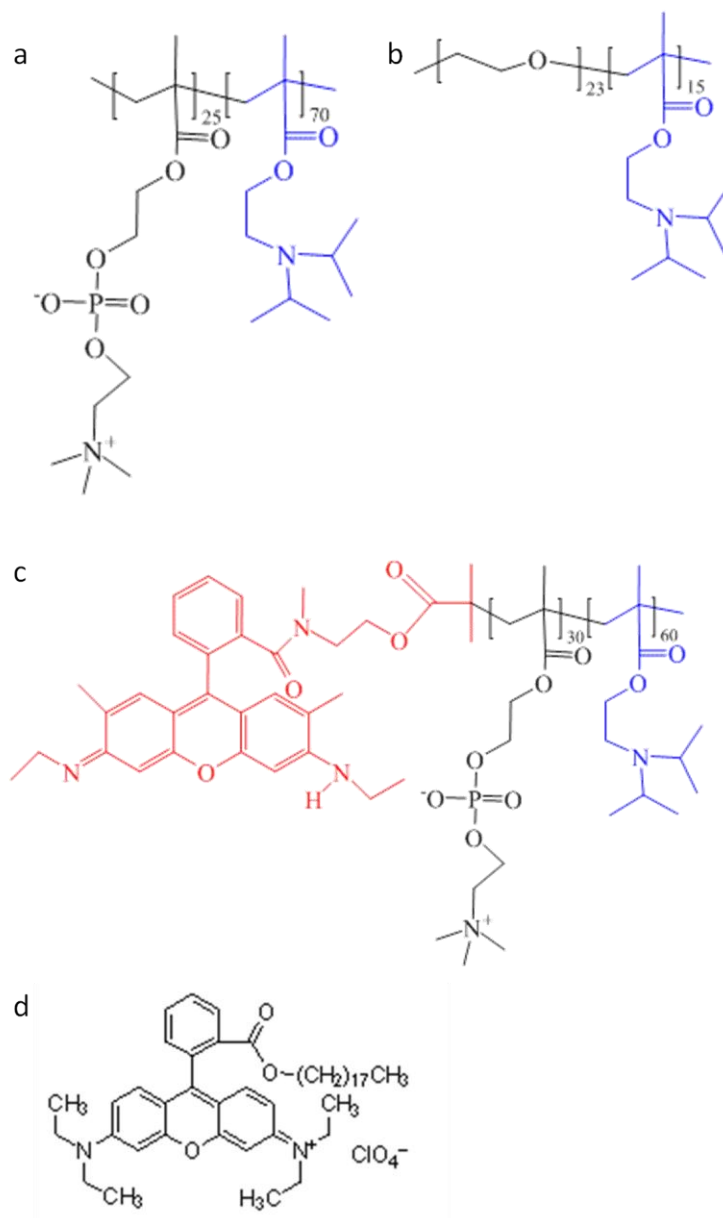
Figure 3.4 Chemical structures of PMPC₂₅-PDPA₇₀ (a), PEO₂₃-PDPA₁₅ (b), Rho- PMPC₃₀-PDPA₆₀ (c) and rhodamine B octadecyl ester perchlorate (d).

Polymersome production: pH increase method

The film was then rehydrated using 2 ml of pH 2 PBS (100mM) giving a co-polymer concentration of 0.2mM (10mg/ml for PMPC-PDPA and ~2mg/ml for PEO-PDPA) (Figure 3.5). Once the polymer had dissolved and the solution was completely clear the pH was raised very gradually using 1 M sodium hydroxide (NaOH). The NaOH was added drop wise into the polymer solution while the solution was being mixed. Vortexing and sonication were used throughout the pH increase to remove any precipitates which occurred. Once the solution reached pH 7.4 the polymersome solution was sonicated for 20 minutes in icy water to create a more evenly dispersed solution of polymers with single membranes and of a similar size (Figure 3.5).

Preparation of gel permeation chromatography column

Gel permeation chromatography (GPC) columns were prepared with Sepharose 4B. Sepharose was packed into a column, 300mm in length. The column, containing sepharose, was shaken once packed to remove any bubbles which may have formed. GPC columns were sterilised prior to use by autoclaving or with 70% IMS. Once the IMS had run through the column the column was washed three times with sterile PBS to remove all the alcohol. Columns were stored at room temperature, upright and the sepharose was always kept submerged in PBS or IMS to prevent it from drying out and creating bubbles in the column. The sepharose was replaced monthly and resterilised periodically.

Purification of polymersome solution by GPC

Once the polymersome solution had been brought to pH 7.4 using sodium hydroxide and the solution had been sonicated, the solution was passed through a GPC column to remove free rhodamine, micelles or polymer which was not incorporated into the polymersomes. In GPC the largest molecules travel fastest as the sepharose allows them to travel around the sepharose particles. Smaller materials are able to pass both around and through the sepharose, creating a slower more convoluted route which enables the separation of large macromolecules from smaller molecules. The polymersome solution was added to the top of the column 2ml at a time. Once the polymersome solution had entered the sepharose the column was washed through with PBS and fractions were collected (Figure 3.5). Those fractions with the highest turbidity were retained while the rest were discarded.

Checking for removal of free rhodamine

One ml fractions from the GPC column were collected, diluted 1 in 10 with PBS and the fluorescence of 1 ml of this solution measured using a fluorescence spectrophotometer (Varian Cary Eclipse, CA, USA) with excitation set at 540nm and emission at 560nm.
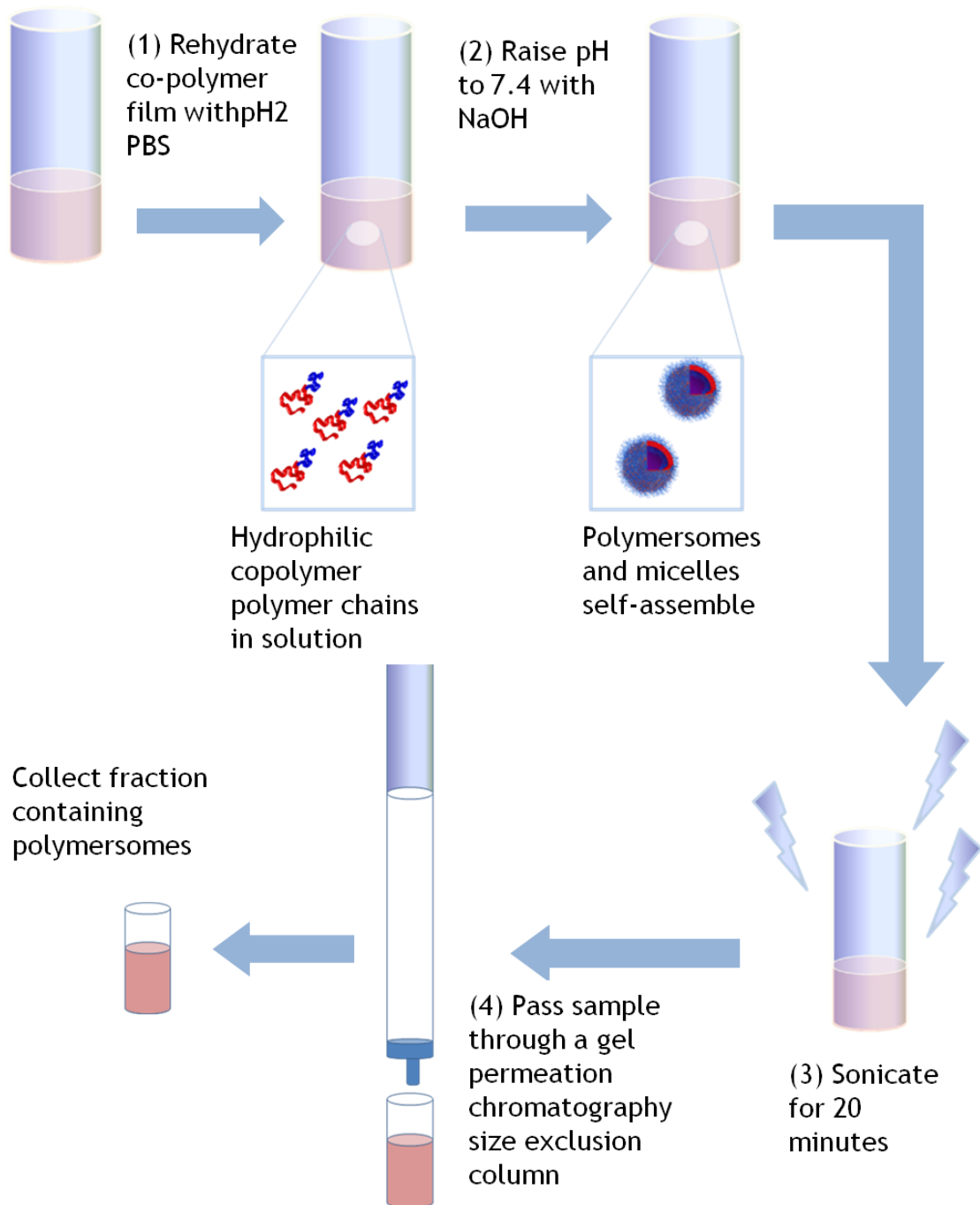
Figure 3.5 Method for making polymersomes
(1) The co-polymer film is rehydrated at pH 2 making a solution of unimers. (2) The pH is increased and the block co-polymers become amphiphilic. Macromolecular structures such as polymersomes and micelles form. (3) The solution is sonicated to encourage all polymer to form unilaminar vesicles as the membranes are broken and reform. (4) The solution is passed through the GPC column to extract large structures (polymersomes), from smaller structures (such as micelles and unimers).

Characterisation of polymersomes

Transmission Electron Microscopy (TEM)

For TEM analysis, samples of polymersome solution were mounted onto pre-carbon-coated copper grids. These grids were firstly glow discharged for 40 seconds, and then submerged into the polymersome solution for 60 seconds. The grids were then blotted dry and submerged into a phosphotungstic acid solution (0.75 w/v %, made up using distilled water) for 20 seconds, before being blotted dry, and then briefly dried under vacuum. Imaging was performed on a Philips CM100 instrument operating at 80 kV equipped with a Gatan 1k CCD camera.

Cell monolayer and polymersomes

Materials and Preparation

MTT Solution

MTT (3-(4,5-dimethylthiazol-2-yl)-2,5 diphenyl tetrazolium bromide) powder was purchased from Sigma Aldrich, Dorset, UK. MTT solution was made up in PBS at a concentration of 0.5mg/ml. MTT powder is mutagenic if inhaled and was therefore always weighed in a fume cupboard. MTT solution, once prepared, was kept at 4°C for up to one week, protected from the light.

Acidified isopropanol

Isopropanol (Fisher Scientific, Leicestershire, UK) was acidified using 125μL of 10M HCl per 100ml isopropanol.

Paraformaldehyde solution

Paraformaldehyde powder (Sigma Aldrich, Dorset, UK) was weighed in a fume cupboard and dissolved into a 100mM PBS solution to give a final concentration of 3-4% (wt %). The paraformaldehyde powder in PBS was stirred and gently heated to 37 °C on a stirring plate for several hours. 5M HCl was then added to the solution drop-wise until the paraformaldehyde powder had completely dissolved and the solution was clear. The paraformaldehyde solution was then cooled and the pH was adjusted to pH 7.4 using sodium hydroxide. Paraformaldehyde was frozen in aliquots and thawed immediately prior to use.

Cell monolayer exposure to polymersomes

Cells were seeded in 24 well plates (Costar, Buckinghamshire, UK) for toxicity and flow cytometry experiments. Cells were seeded at a density of 30,000 cells per well and incubated for 24 hours prior to polymersome exposure in humidified incubators (37°C, 5% CO_2). Prior to polymersome exposure an equal number of cells were seeded in each well and were checked under phase contrast microscopy to ensure cells had adhered well. 5mg/ml polymersome solutions were diluted in fresh cell culture medium to give the desired concentration. For

toxicity studies polymersome concentrations of 0.1mg/ml, 1mg/ml and 2mg/ml were used. For control wells fresh cell culture medium was diluted with PBS so the concentration of cell culture medium was equivalent for all samples. For flow cytometry experiments a polymersome concentration of 1mg/ml was used.

Existing cell culture medium was removed and discarded into bleach. The polymersomes, or PBS, in cell culture medium were then added to the cells and cells were incubated for the desired length of time. For toxicity experiments, cells were incubated for 24 or 48 hours. For flow cytometry experiments looking at the uptake of polymersomes, time points of 2,5, 10, 30, 60, 180, 480, 1440 minutes were analysed.

MTT assay for metabolic activity

The mitochondrial metabolic activity of cells was measured using MTT (3-(4,5-dimethylthiazol-2-yl)-2,5 diphenyl tetrazolium bromide) and was used as an indicator for cell viability (Mosmann 1983). Monolayers were washed 3 times in 100mM PBS and incubated for 40min, with MTT solution (0.5 mg/ml MTT in PBS, 0.5ml per well in 24 well plate) at 37 °C with 5% CO_2. After 40 minutes, the unreacted MTT solution was removed and the purple intracellular formazan salt (produced by dehydrogenase reduction of MTT) was solubilised and released from cells using acidified isopropanol (125µl of 10M HCl in 100ml isopropanol). The eluted dye was transferred to a 96 well plate. The optical density of the solution was measured at 540nm with a reference at 630nm, using a spectrophotometer (Tecan). All optical densities were normalised to a control sample of untreated cells.

Flow Cytometry

Cells monolayers were washed 3 times using PBS and detached using 0.5ml trypsin EDTA per 24 well as previously described on page 78. Trypsin EDTA was neutralised using cell culture medium containing FCS and the cell suspension from each well was transferred into 1ml eppendorf tubes. Eppendorfs containing samples were spun at 6000rpm for 2 minutes using a bench top centrifuge. The supernatant was removed and cells were resuspended in 3% paraformaldehyde (w/v) to fix the cells. Fixed cells were stored in the fridge for up to a week before flow cytometry analysis. Fixed cell solutions were added to a 96 well plate and fluorescence at 543nm was measured using a BD FACSArray™ Bioanalyzer (BD Biosciences, California, USA). Cell populations were gated using forward scatter (FSC) and side scatter (SCC) measurements. Cell debris was excluded from the measurements (see Figure 3.6a). A threshold for positively fluorescent cells was set using untreated control cells (see Figure 3.6). All samples were run in triplicate and the experiment was repeated twice.
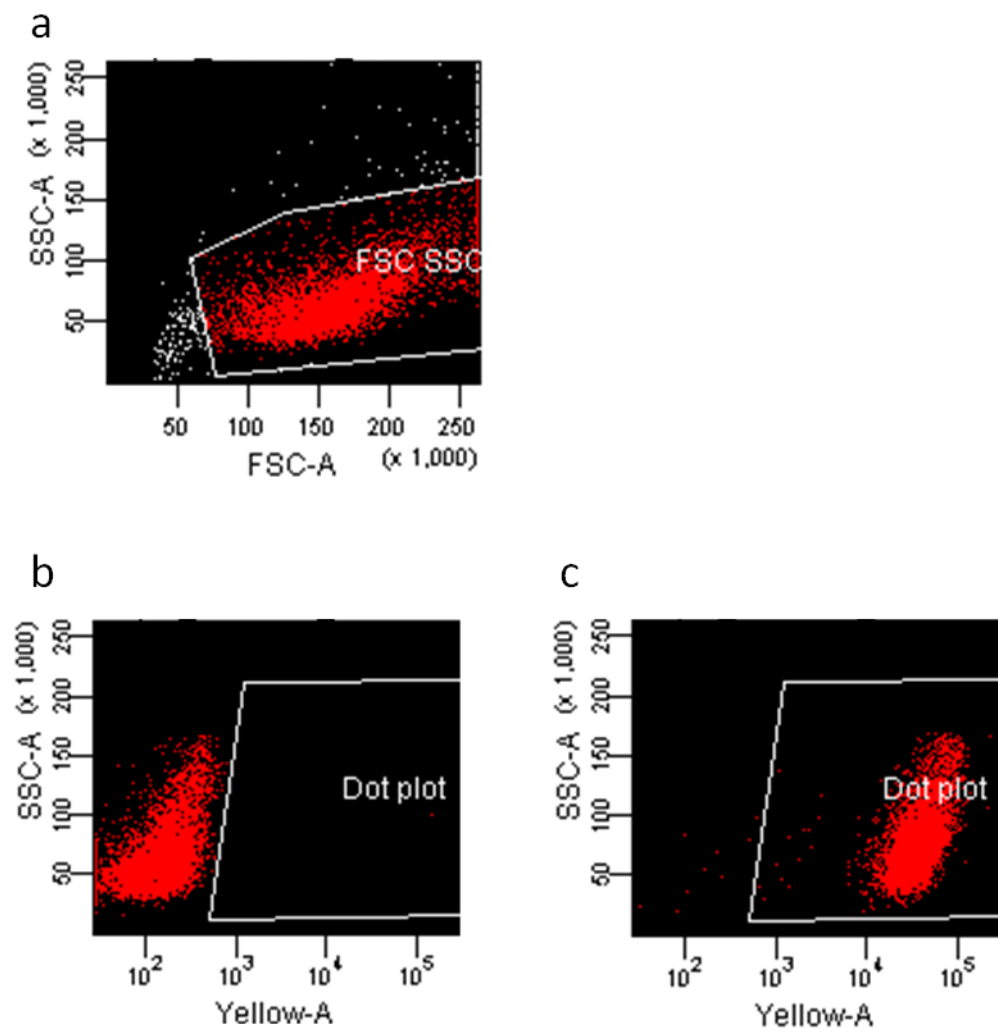
Figure 3.6 Example of FACS dot plots.
(a) Red dots indicate cells gated to be included in analysis (white dots indicate cell debris not included). (b) Untreated control sample used to determine non fluorescent population using dot plot and (c) Cells within white lines classed as positively fluorescent.

Statistics

The standard deviation (error bars) and significance values were calculated from the normalised values of cell viability. Microsoft Excel 2007 was used to calculate mean, sum and standard deviation of data. All measures of statistical significance were determined using Student's t-test. To perform Student's t-test Microsoft Excel 2007 was used. A parallel t-test on SigmaPlot v10 was also done to confirm the results. An unpaired two tailed t-test was performed and homogeneity of variance was assumed.

Polymersomes + MCTS

Adding polymersomes to FaDu MCTS

MCTS were cultured 7 days prior to polymersome exposure. PMPC-PDPA polymersomes were added to the MCTS to give a final concentration of 0.02mM in cell culture medium.

Polymersomes, labelled with conjugated Rho-PMPC-PDPA were mixed with cell culture media and administered when the cell culture media was replenished on the cells. This cell culture media remained on the cells for the duration of the polymersome exposure.

Dissociation of multi-cellular tumour spheroids for flow cytometry analysis

MCTS are clearly visible by eye once formed and can be removed from a 96 well plate using a Pasteur pipette. MCTS were washed three times with PBS and placed in a clean 12 well plate. 1ml Trypsin/0.02% EDTA solution was added to the MCTS and incubated for 10 minutes, or until all cells in the MCTS had dissociated. The cell suspension was then centrifuged and re-suspended in 3% para-formaldehyde for flow cytometry analysis and stored in the fridge for up to 5 days. FACS analysis was performed as described for cell monolayers on page 140. One spheroid per 96 well was measured and all samples were measured in triplicate or more.

Frozen sections

For visualisation of polymersomes within MCTS the MCTS were frozen in OCT freezing medium (VWR International, Lutterworth, UK) at $-$ 20 °C in disposable base moulds (Surgipath, Peterborough, UK) and stored at $-$ 80 °C (Figure 3.7). 8μm sections were cut with a Leica Cryostat CM 3050 S (Leica Microsystems, Nussloch, Germany) and transferred onto Superfrost slides (VWR, Lutterworth, UK). The sections were labelled with DAPI mounting medium (Vectashield, Vector Laboratories Ltd., Peterborough, UK) and cover-slipped.

Fluorescence imaging

Frozen sections were imaged using a fluorescent microscope (Zeiss Axioplan 2) with a Q-imaging Retiga 1300R camera (QI Imaging, Arizona, USA) and Image Pro Plus image software (Media Cybernetics, Inc., MD, USA).
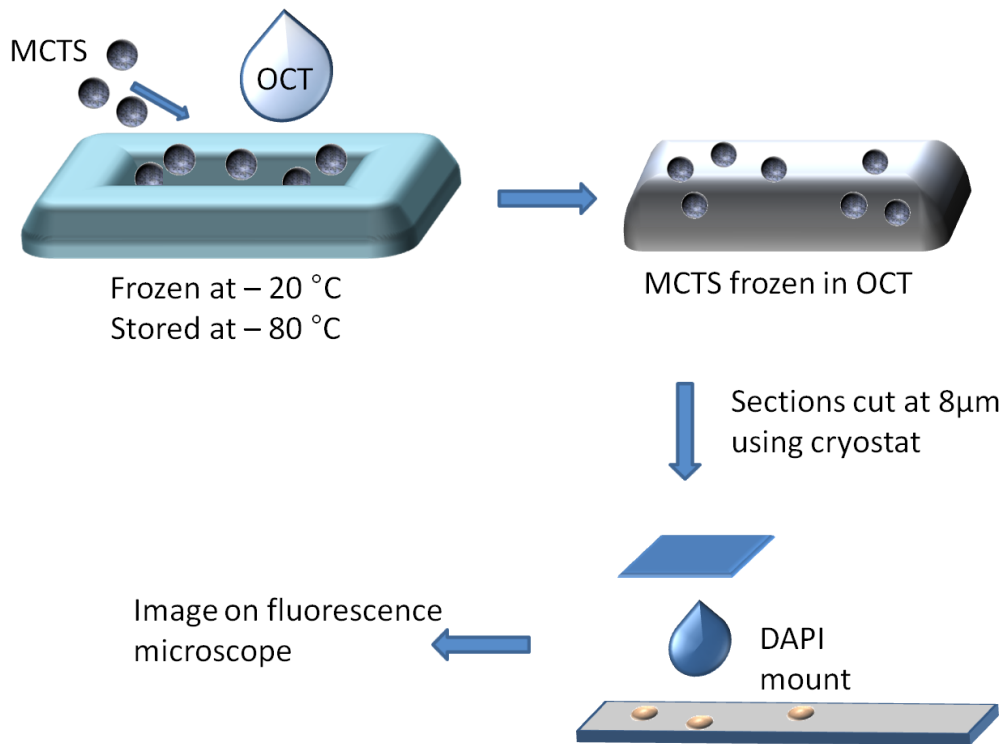
Figure 3.7 Analysis of MCTS using cryo-sectioning.

Polymersomes and TEOM

Exposure of TEOM to Polymersomes

TEOM were cultured for 10 days at ALI prior to polymersome exposure. Polymersomes were added to the superficial surface of the TEOM at a concentration of 0.2mM (10mg/ml for PMPC-PDPA, 2mg/ml PEO-PDPA) inside a plastic ring pushed gently onto the top surface of the TEOM (Figure 3.8). Cell culture medium remained under the TEOM for the duration of the experiment.

Freezing of samples for fluorescence histology

Samples were washed thoroughly in PBS and fixed in 3% paraformaldehyde overnight at room temperature. Samples were coated in OCT freezing medium and snap frozen by dipping the TEOM into liquid nitrogen. Frozen samples were stored at -80°C, sectioned, stained and imaged as described above for MCTS frozen sections (page 142).
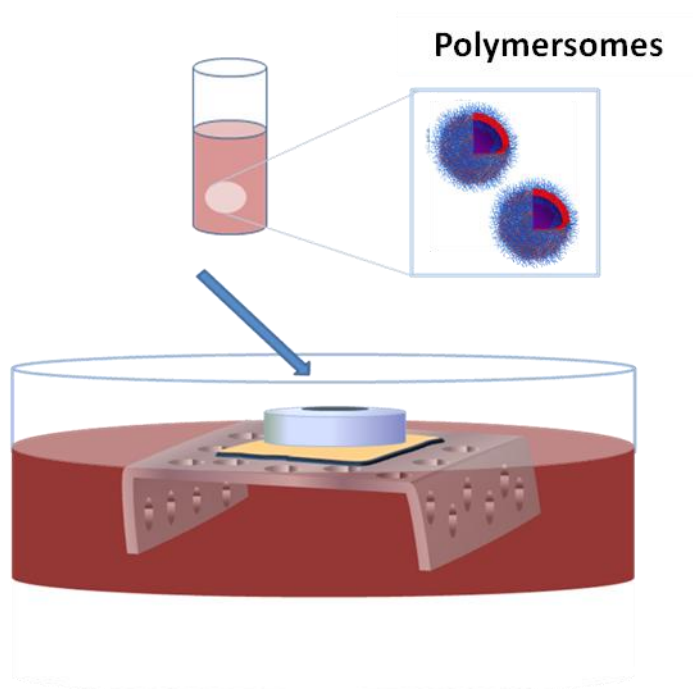
Figure 3.8 Application of polymersomes to surface of TEOM.

Confocal laser scanning microscopy (CLSM)

TEOM samples exposed to polymersomes were washed thoroughly in PBS and left submerged in PBS in a 6-well plate for CLSM imaging. All CLSM images were obtained using Zeiss LSM 510 META Upright Laser Scanning Confocal Microscope (Carl Zeiss Inc., Germany) with corresponding LSM 510 META Software (Carl Zeiss Inc., Germany).

Determining autofluorescence from TEOM

To successfully image polymersome penetration into the TEOM a fluorescent dye which was excited at a wavelength which did not result in a large amount of autofluorescence was required. To assess the best wavelength to use, TEOM were exposed to 488nm and 543nm excitation and the emission spectra detected using lambda stack mode on the confocal. The resulting emission spectra was detected between 500nm and 700nm, using a multi-channel detector consisting of 32 photo-multiplier elements enabling an emission fingerprint to be detected across a range of wavelengths.

Detecting fluorescently labelled polymersomes within TEOM

Samples were washed 3 times in PBS prior to imaging and samples were submerged in PBS throughout imaging and then imaged using an Acroplan x40 dipping lens (Carl Zeiss Inc., Gemany). All samples were imaged fresh and unfixed. Three dimensional images of 200μm x 200μm x 100-200μm were obtained using the z-stack function. These images are made up of 50-100 images 2μm apart.
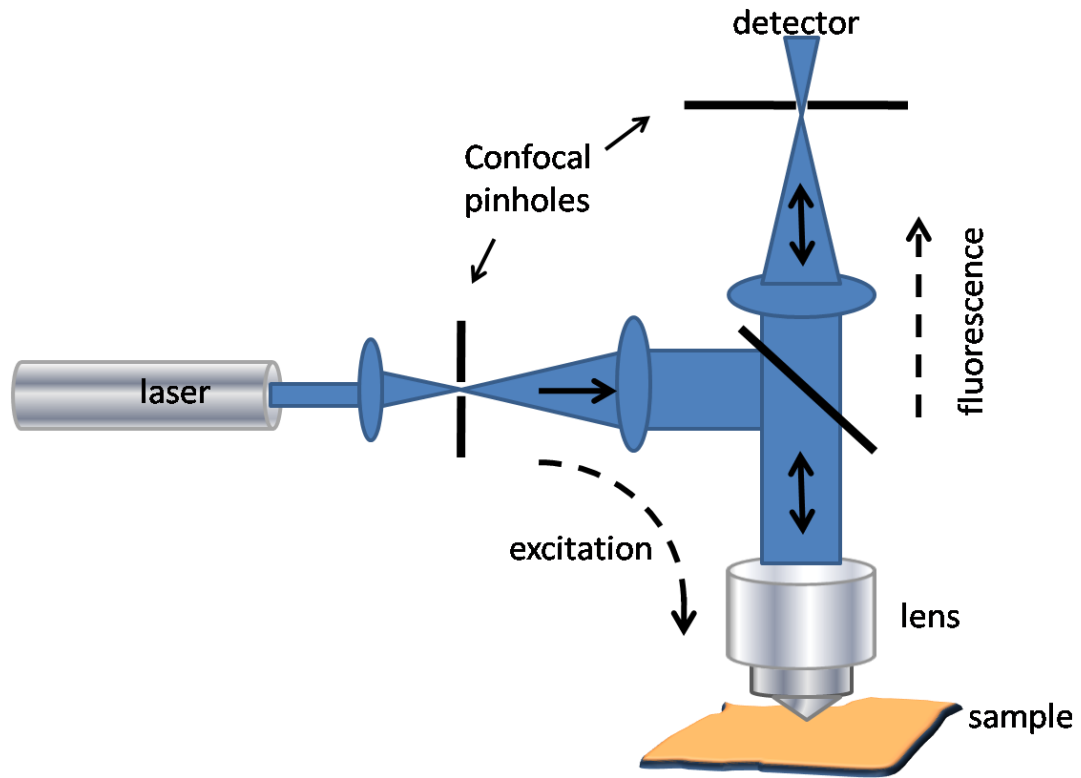
Figure 3.9 Diagrammatic representation of CLSM

3.4 Results

Characterisation of polymersomes
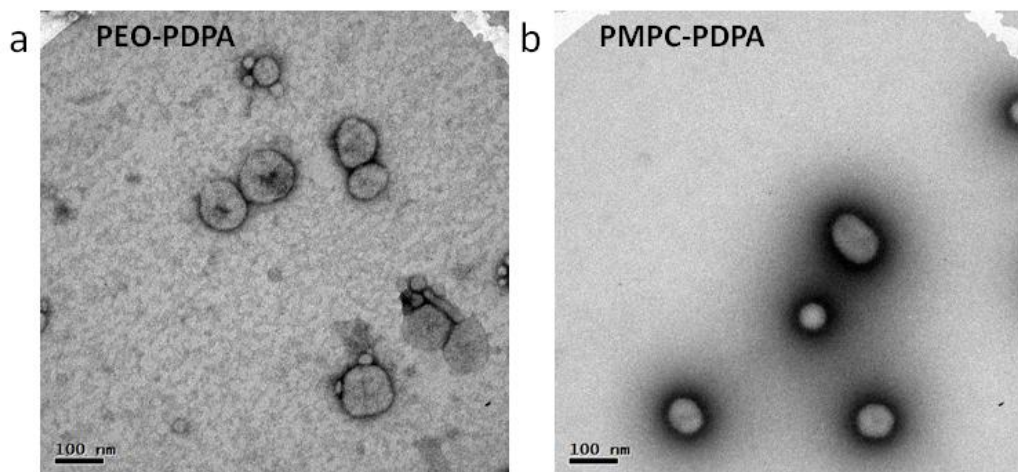
Figure 3.10 Transmission electron microscopy (TEM) images of PEO$_{23}$-PDPA$_{15}$ (a) and PMPC$_{25}$-PDPA$_{70}$ (b).

Imaging of polymersomes

To confirm the presence of polymersomes we imaged polymersome samples using transmission electron microscopy. Spherical polymersomes with diameters ~100nm can be observed in samples of both the PEO_{23}-$PDPA_{15}$ and $PMPC_{25}$-$PDPA_{70}$.

Removal of free rhodamine using gel permation chromatography (GPC)

Two methods were used to fluorescently label the polymersomes. In the first method PMPC-PDPA conjugated to rhodamine 6G (Rho-PMPC-PDPA) was mixed with either PMPC-PDPA or PEO-PDPA polymer solutions before the film was produced. 5% of Rho-PMPC-PDPA was added to label the polymer (molar %). A second method was implemented, which resulted in higher fluorescence intentisites. An amphiphilic rhodamine dye (Rhodamine B octadecyl ester perchlorate dye) was encapsulated within the membrane of the polymer vesicles.

The method used to conjugate or encapsulate these dyes into polymersomes always resulted in some free rhodamine being present in the sample. To remove any non-conjugated rhodamine or non-encapsualted amphiphilic rhodamine, polymersomes were passed through a GPC column. Fractions were collected every 1ml and the fluorescence profile was measured using fluorescence spectroscopy. Fractions 2ml-5ml after the first fraction were used for experiments as these showed the highest rhodamine fluorescence, were turbid and contained polymersomes. Due to its small size the free rhodamine left the GPC column after 16ml (Figure 3.11), un-encapsulated rhodamine was also removed in this way.
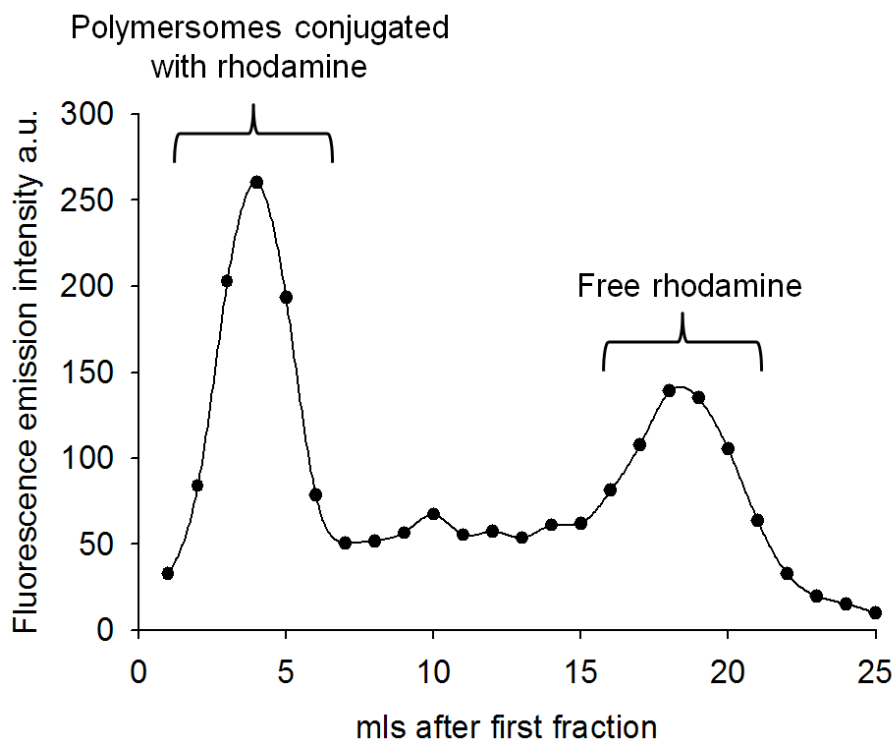
Figure 3.11 Removal of free rhodamine from polymersome solution using GPC column

Effect of Polymersomes on Cell Viability

PMPC-PDPA

The mitochondrial activity of six different cell lines was tested and used as a method to determine relative viability of cells after 24 and 48 hours of polymersome exposure. PMPC-PDPA polymersomes were added to cell culture medium at concentrations of 0.1mg/ml, 1mg/ml and 2mg/ml. After 24 hours there was no significant reduction in viability in any of the cell types at 0.1mg/ml PMPC-PDPA (Figure 3.12). Some cells types were affected after 24 hours exposure to 1mg/ml PMPC-PDPA (oral and skin fibroblasts) and all cell types except the SCC4 cell line showed significant toxicity when exposed to 2mg/ml of PMPC-PDPA for 24 hours. After 48 hours exposure there was no significant reduction in viability when 0.1mg/ml of polymersomes was added. The longer exposure time however, caused significant toxicity to all cell types at 2mg/ml and all cell types except Cal27 and normal oral keratinocytes at 1mg/ml (Figure 3.12).

PEO-PDPA

The viability of cells exposed to PEO_{23}-$PDPA_{15}$ was tested on 3 different cell types (Figure 3.13). Normal oral fibroblasts (NOF), normal oral keratinocytes (NOK) and the cancer cell line FaDu were exposed to 0.02mM or 0.01mM for 24 or 48 hours. The concentration 0.02mM is the molar equivalent to 1mg/ml of $PMPC_{25}$-$PDPA_{70}$.

The PEO-PDPA was not tested at the equivalent of 2mg/ml concentration however, at 0.02mM the PEO-PDPA did not affect the viability of these cells as significantly as the PMPC-PDPA (Figure 3.13). The NOK cells were affected at 0.02mM after 24 hours exposure. After 48 hours NOK cells were not significantly affected, likely due to the high variability in the control samples. The FaDu cells were significantly affected after 48 hours, at the higher concentration (0.02mM).
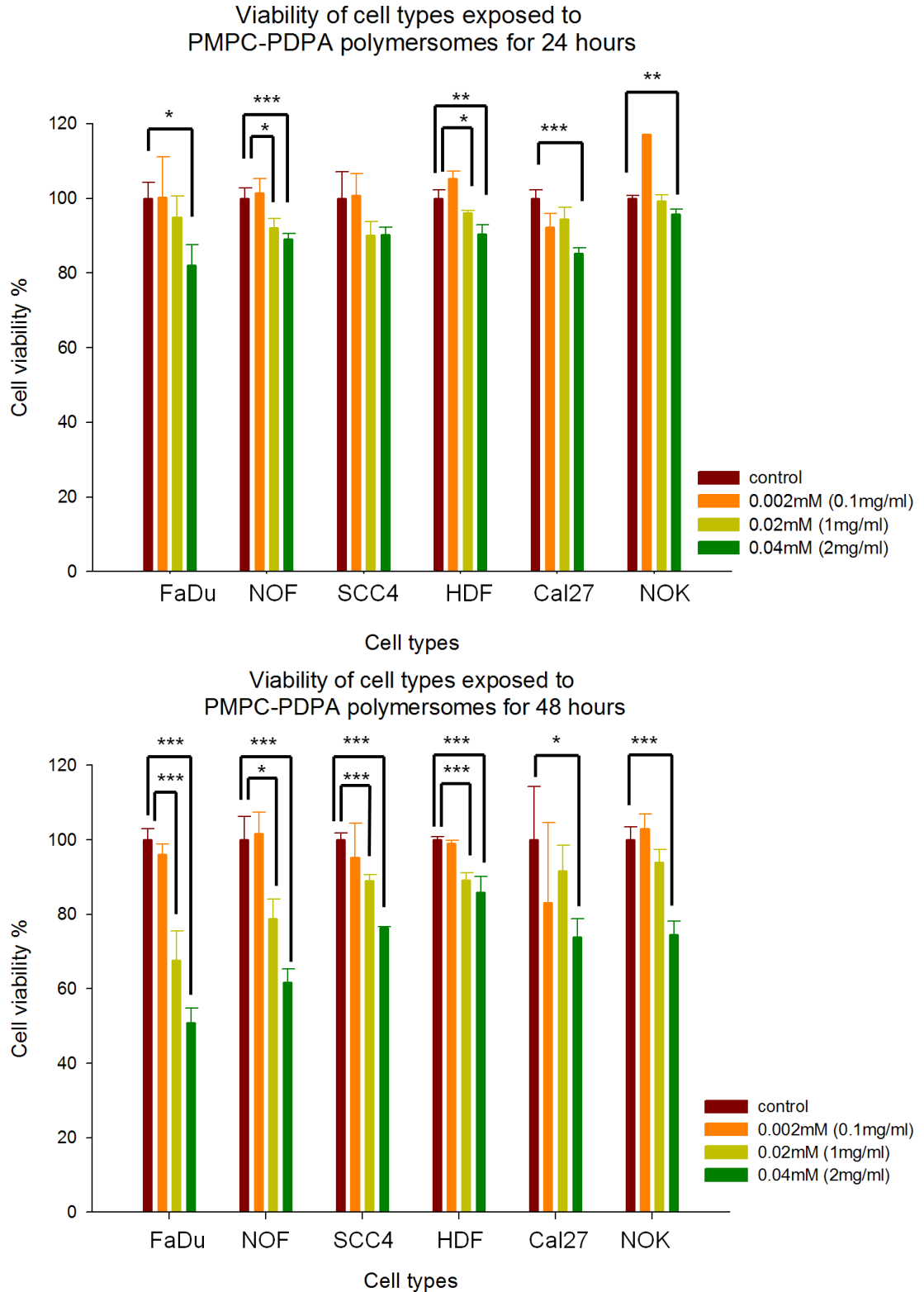
Figure 3.12 Viability of cell monolayers exposed to PMPC-PDPA polymersomes at various concentrations.

Error bars= s.d. FaDu = OSCC cell line, NOF = normal oral fibroblasat, SCC4 = OSCC cell line, Cal 27= OSCC cell line, NOK = normal oral keratinocytes and HDF = human dermal fibroblasts. * $p < 0.05$, ** $p < 0.01$, *** $p < 0.005$ Representative of one experiment n=3

Figure 3.13 Viability of cells exposed to PEO$_{23}$-PDPA$_{15}$ polymersomes.
***= p< 0.05, *** = p < 0.005. Representative of 1 experiment n=3.**

Kinetics of Polymersome Uptake

Effect of Cell types of PMPC-PDPA Polymersome Uptake

Polymersomes containing the amphiphilic rhodamine dye, rhodamine B octadecyl ester perchlorate, were added to a variety of cell lines and the uptake of polymersomes by these cells was measured over time using flow cytometry. The FaDu cells took up the PMPC-PDPA polymersomes very rapidly (Figure 3.14). After 2 minutes exposure over 70% of FaDu cells contained detectable levels of polymersomes. The Cal27 cancer cell line showed the next fastest uptake with SCC4 cells showing a similar rate of uptake. These cancer cell lines showed faster uptake when compared to the primary cells in terms of the percentage of cells which contained detectable levels of rhodamine. The oral keratinocytes took up polymersomes faster than oral and dermal fibroblasts. Virtually one hundred per cent of all cell types had taken up polymersomes after 3 hours exposure (Figure 3.14).

The amount of polymersomes taken up by each cell type over time was measured using the fold increase of fluorescence compared to the control cells. Fold increase was used as a measure of fluorescence to account for the differences in autofluorescence occurring from the different cell types before polymersome exposure (Figure 3.14).

For all cell types this increased over time, and continued to increase for the whole time the cells were exposed to polymersomes (24hours). After 100% of cells had taken up polymersomes the increase in intensity appears to be linear.

The cells which took up the most polymersomes per cells (highest fold increase in fluorescence intensity) were the FaDu cell line; with the least polymersomes taken up by the oral fibroblasts.
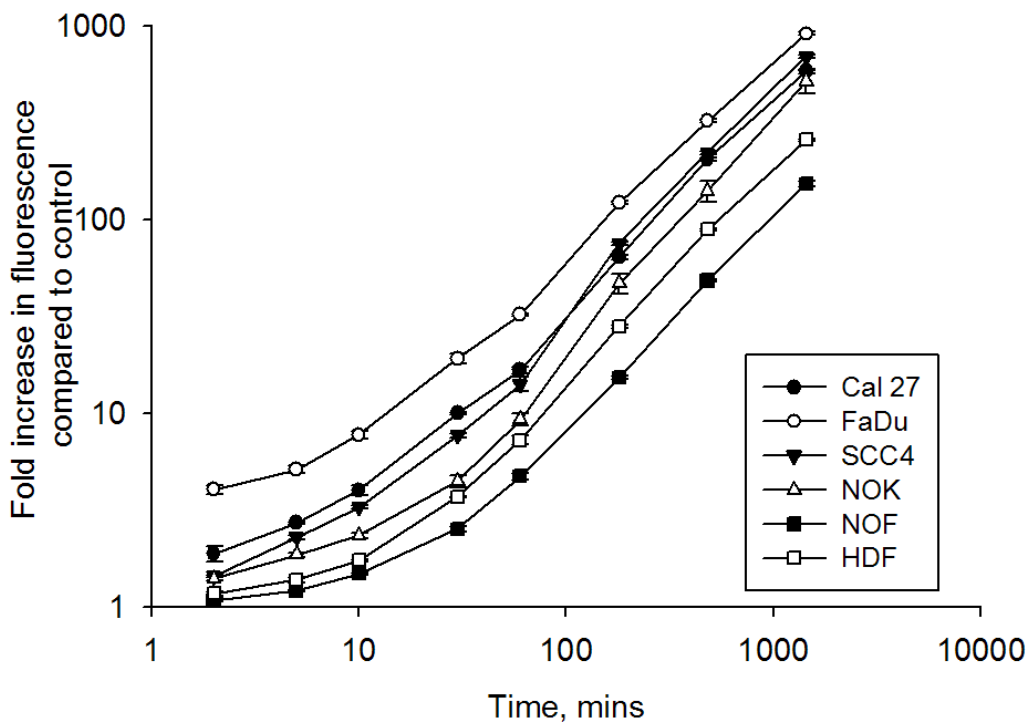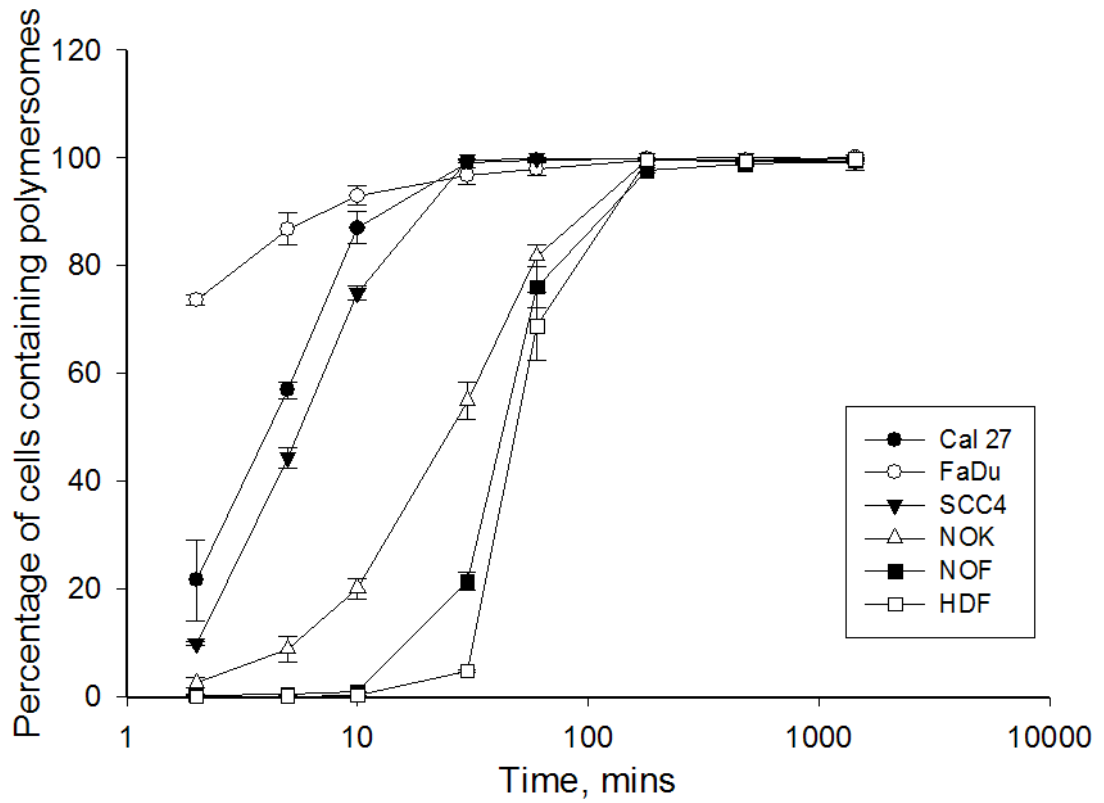
Figure 3.14 Uptake of PMPC-PDPA Polymersomes by monolayers of various cell types. Percentage of population positive for polymersomes (detected by flow cytometry, see Figure 3.6) and fold increase in fluorescence compared to control. n=3

PMPC-PDPA Polymersome Uptake is Concentration Dependant

PMPC-PDPA polymersomes labelled with encapsulated amphiphilic rhodamine were added to FaDu cells at two different concentrations (0.1mg/ml and 1mg/ml) and analysed by flow cytometry. The percentage of cells which contained a detectable amount of polymersomes was significantly higher in the samples exposed to the higher concentration of polymersomes (1mg/ml) for 1 hour compared to 0.1mg/ml (Figure 3.15). By 3 hours exposure over 90% of cells, in both the high concentration and low concentration samples, had taken up a detectable amount of polymersomes.   The intensity of fluorescence, and therefore amount of polymersomes per cell, increased at a similar rate in both samples once the uptake of polymersomes could be detected in the majority of cells (1-3 hours). The reason for this is probably because before this point the samples exposed to lower concentrations were taking up polymersomes however, the fluorescence was below the detection limit until around 1 hour exposure. After 1 hour the intensity of fluorescence and therefore amount of polymer was 10 times higher in the cells exposed to the higher concentration (Figure 3.15) compared to the lower concentration. This indicated the uptake of polymersomes is concentration dependant as the difference in concentration between the two samples was 10 times.
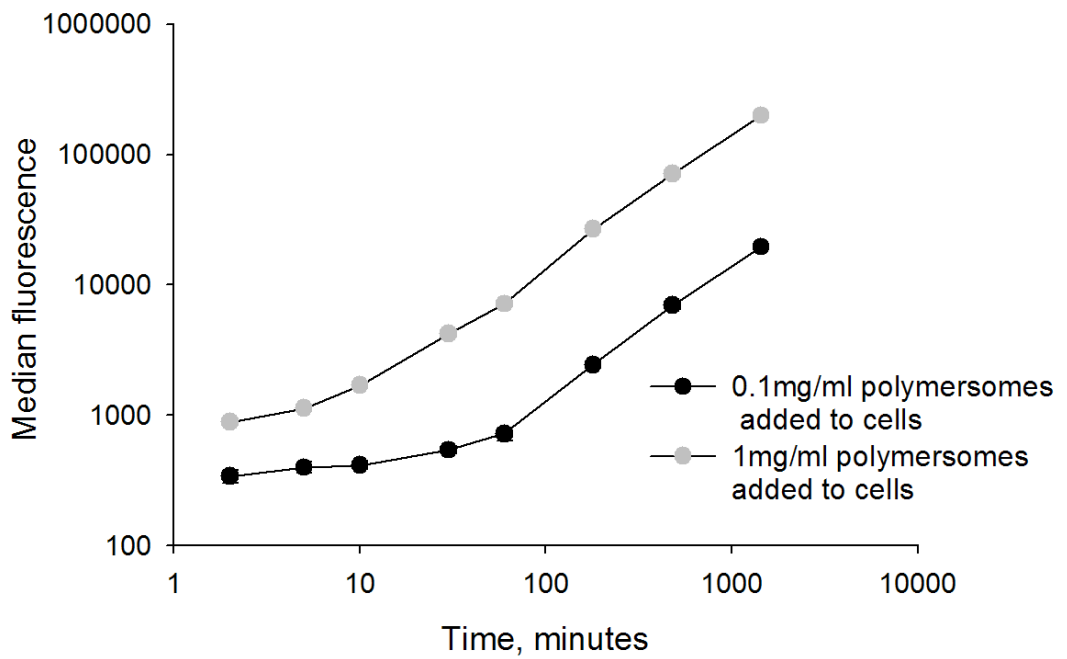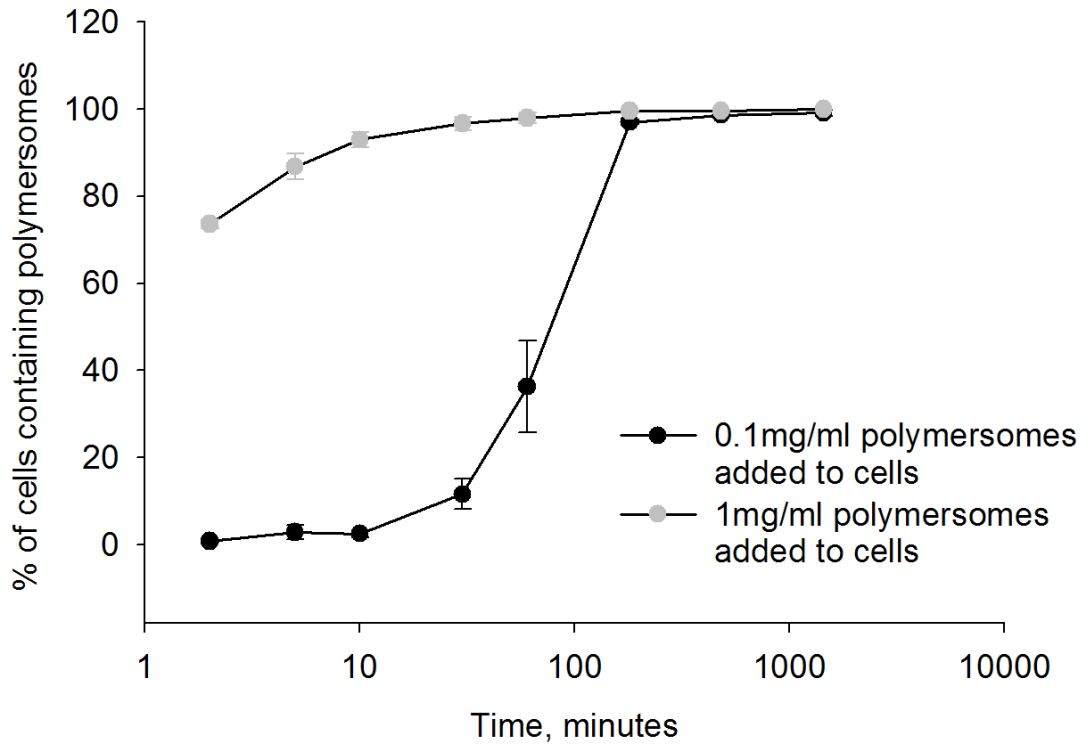
Figure 3.15 Concentration dependant uptake of PMPC-PDPA polymersomes encapsulated with amphiphilic rhodamine in FaDu cells. n=3

Penetration of Polymersomes into TEOM

Delivery of drugs and therapeutic agents into and across the oral epithelium is desirable for the treatment of many conditions. The penetration capacity of fluorescently labelled polymersomes (containing 5% rho-PMPC-PDPA) through the oral epithelium was assessed using the TEOM model, described in the previous chapter. Initially TEOM models exposed to polymersomes were examined using frozen sections, counter stained with DAPI. The control samples were exposed to PBS instead of polymersomes. Figure 3.16 shows the frozen sections of TEOM after 6 and 30 hours exposure to polymersomes.
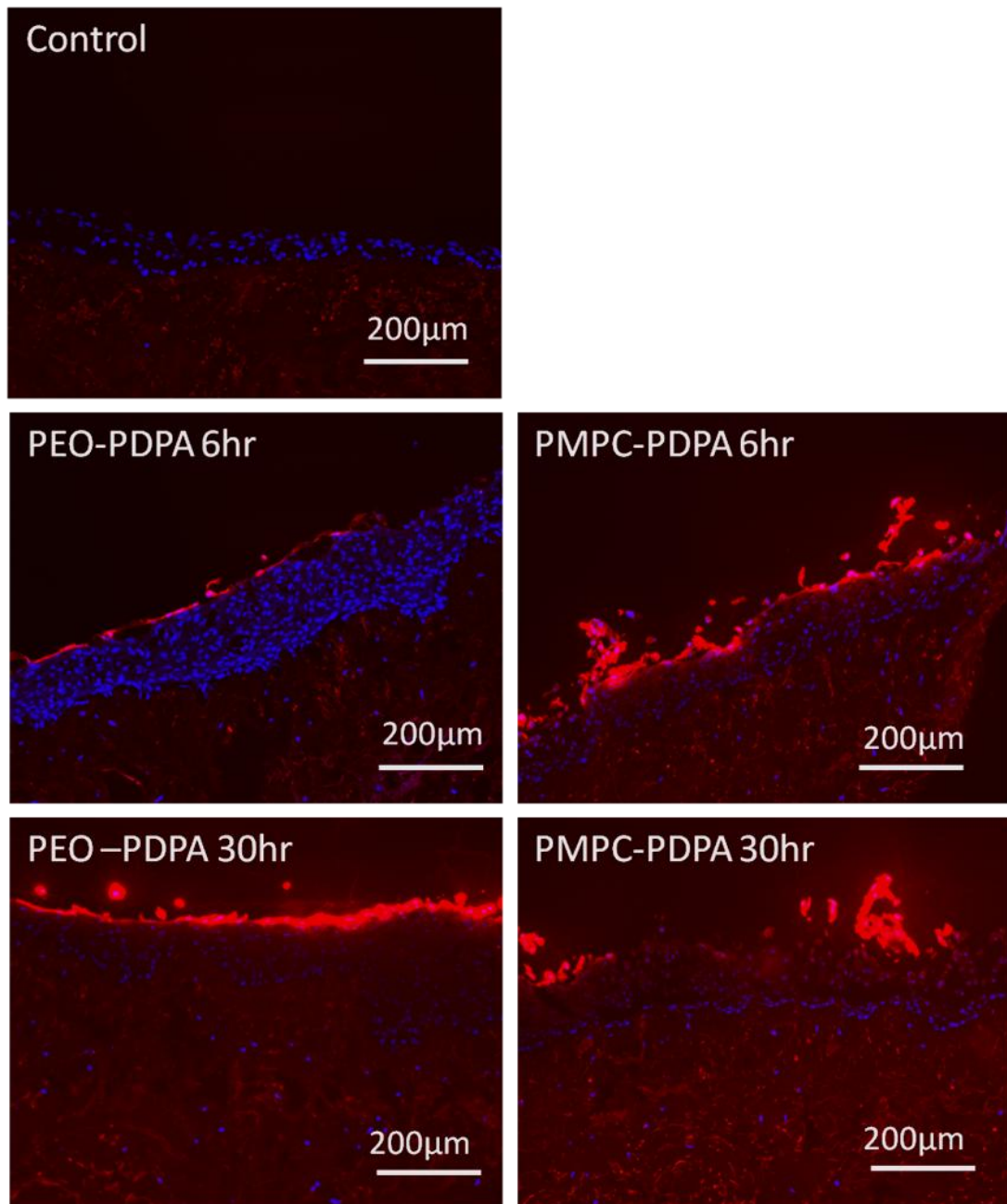
Figure 3.16 TEOM exposed to polymersomes with encapsulated amphiphilic rhodamine. Blue fluorescence is DAPI a marker for cell nuclei. Representative image, n=3.

The fragile nature of the models once they had been snap frozen and the autofluorescence signal from the tissue lead to confocal microscopy being used for future experiments.

Avoiding the autofluorescence of TEOM

In order for the TEOM and polymersomes to be imaged effectively the autofluorescence from the tissue needed to be avoided. Figure 3.17 shows the emission spectra of the oral mucosa model when excited at 488nm and 543nm. Both spectra were taken using the same settings and the same excitation intensity.   There is a broad fluorescent emission from TEOM autofluorescence when the TEOM was excited at 488nm (Figure 3.17a) but very little when excited at 543nm (Figure 3.17b). The autofluorescence comes predominantly from the extra-cellular matrix (ECM) proteins (Schenke-Layland *et al.,* 2006). To avoid the autofluorescence as far as possible we used rhodamine 6G which is excited at 543nm, to label the polymersomes.
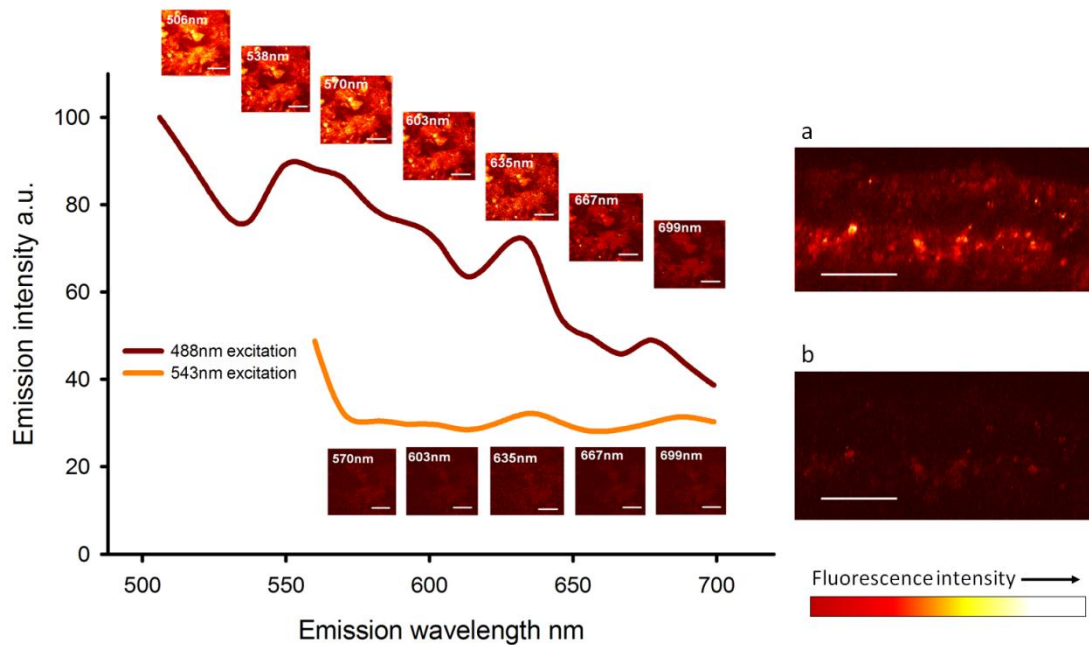
Figure 3.17 Emission spectra of TEOM without polymersomes when excited with 488nm and 543nm lasers.
z-x section of TEOM excited at 488nm (a), and at 543nm (b). Scale bar 50µm.

After the TEOM was exposed to rhodamine labelled polymersomes the emission spectra arising from 543nm excitation changed dramatically demonstrating the presence of polymersomes (Figure 3.18a). Figure 3.18b shows a confocal image of TEOM excited at 488nm and 543nm after 48 hours exposure to polymersomes while Figure 3.18c shows the control model without polymersome exposure. The 488nm channel (autofluorescence) was used to locate the model during CLSM imaging and was useful to orientate the epithelium.

Combining both excitation channels gives a composed image. A negative control of unlabelled polymersomes also showed no fluorescence in the 543nm channel.
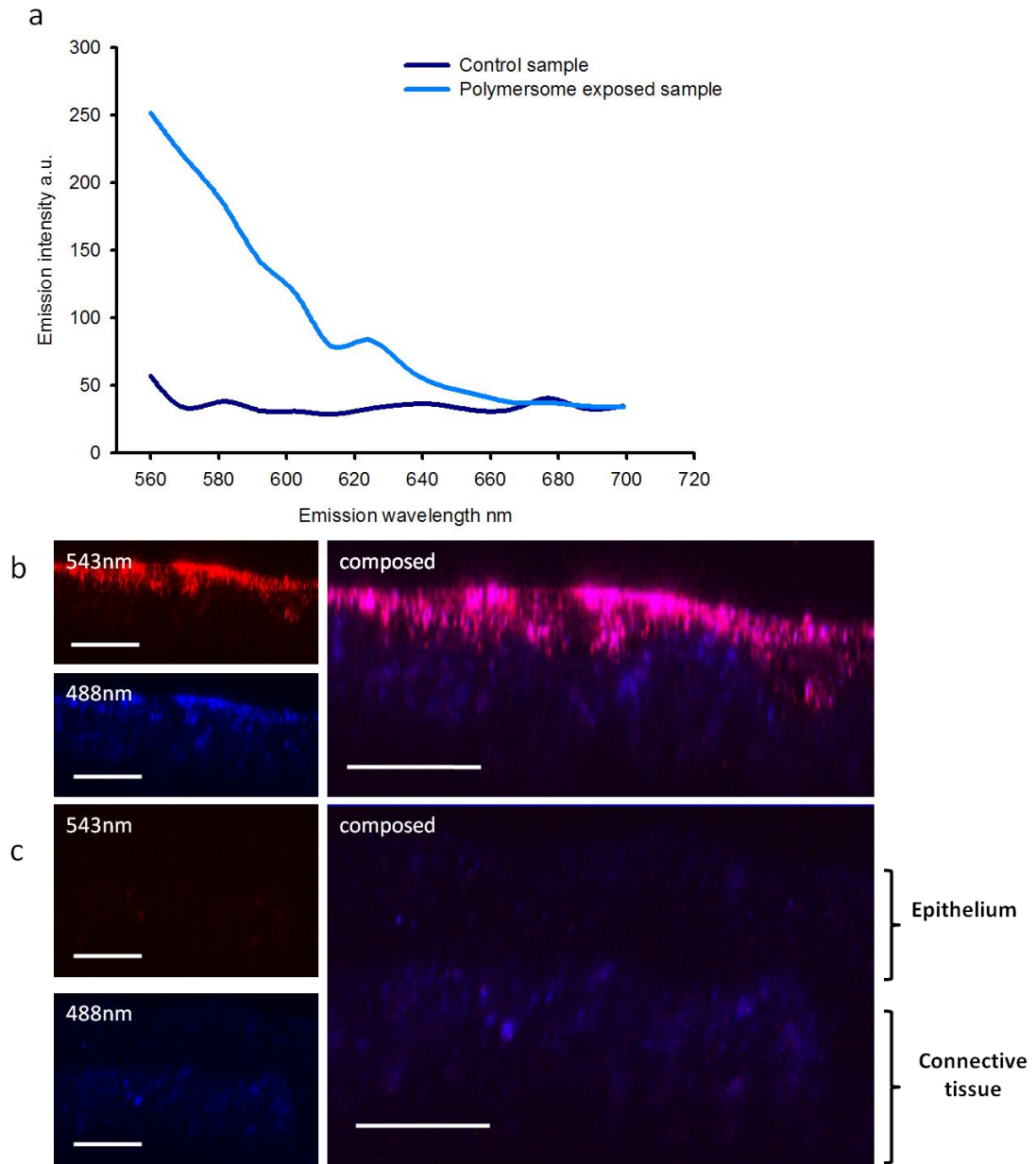
Figure 3.18 Emission spectra of tissue engineered oral mucosa after exposure to rhodamine labelled polymersomes excited at 543nm.
(a) z-x section of TEOM exposed to $PMPC_{25}$-$PDPA_{70}$ polymersomes for 48 hours (b) z-x section of TEOM with no polymersome exposure. Blue= 488nm excitation. Red= 543nm excitation. Scale bar 50µm.

Figure 3.19 examined the location of the PMPC-PDPA and PEO-PDPA polymersomes over 48 hours using CLSM. The diffusion of both PEO-PDPA and PMPC-PDPA polymersomes into the TEOM was time-dependant. In Figure 3.19 the z-x plane shows a cross section through the

full thickness model. While the x-y plane shows a representative horizontal slice through the model and the image on the right shows a 3D reconstruction of the TEOM. After 6 hours exposure to both formulations of rhodamine labelled polymersomes (PEO-PDPA and PMPC-PDPA), rhodamine (red) fluorescence could be seen in the most superficial epithelial layers of the model (Figure 3.19b,e). The position of the polymersomes in respect to the epithelial/connective tissue interface can be judged from the relative positions of the red fluorescence of the polymersomes and the blue autofluorescence of the connective tissue. The basal region appears dark suggesting the polymersomes have not penetrated into the basal cells. There was more wide spread uptake of polymersomes by the superficial epithelial cells for the PMPC-PDPA polymersomes than the PEO-PDPA (Figure 3.19c & f). After 48 hours exposure to PMPC-PDPA it appears that all cells within the epithelium contain polymersomes (Figure 3.19d) and display high levels of fluorescence. There is no dark region between the upper epithelium and connective tissue component in Figure 3.19d suggesting polymersomes have diffused down to the epithelial/connective tissue interface and have been internalised by basal, as well as more superficial epithelial cells. The TEOM exposed to PEO-PDPA for 48 hours expressed high levels of polymersome uptake and fluorescence in the upper layers of the epithelium, but less uptake and fluorescence in the deeper layers of the epithelium compared to PMPC-PDPA polymersomes (Figure 3.19 g). The PEO-PDPA polymersome diffusion pattern is less uniform and appears in patches. However, this may be due to differences in fluorescence intensity between the two polymersome formulations rather than an inherent difference in polymersome behaviour of the two formulations (see appendix 2).
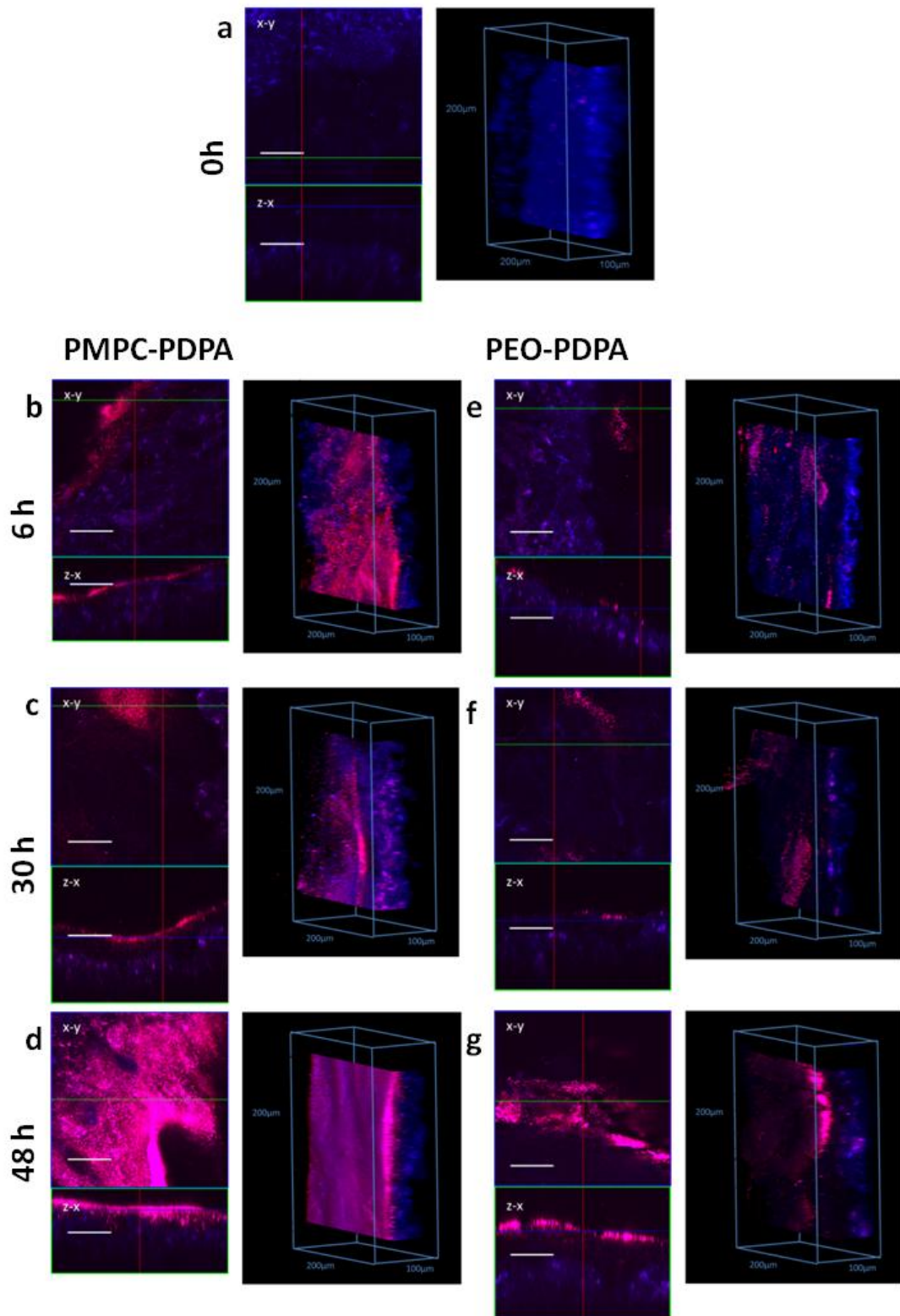
Figure 3.19 Tissue engineered models were exposed to rhodamine labelled PMPC$_{25}$-PDPA$_{70}$ or PEO$_{23}$-PDPA$_{15}$ polymersomes for 6, 30 or 48 hours.
(a) shows control sample, no exposure to polymersomes. CLSM images of TEOM exposed to PMPC$_{25}$-PDPA$_{70}$ for 6 hours (b), 30 hours (c) or 48 hours (d). TEOM exposed to PEO$_{23}$-PDPA$_{15}$ polymersomes for 6 hours (e), 30 hours (f) or 48 hours (g). Images on the left show x-y and x-z sections. Images on the right are three-dimensional projections of these models. Scale bar 50µm. n=2

158

Confocal images were also used to obtain quantitative information about the penetration of the two polymersome formulations into the TEOM. Zmax was calculated by measuring the greatest depth of red fluorescence in the TEOM at different time points (Figure 3.20a). The depth of penetration was greater for the PMPC-PDPA compared to the EPO-PDPA but not significantly different. PMPC-PDPA reached a depth of over 50μm after 48 hours (Figure 3.20b).
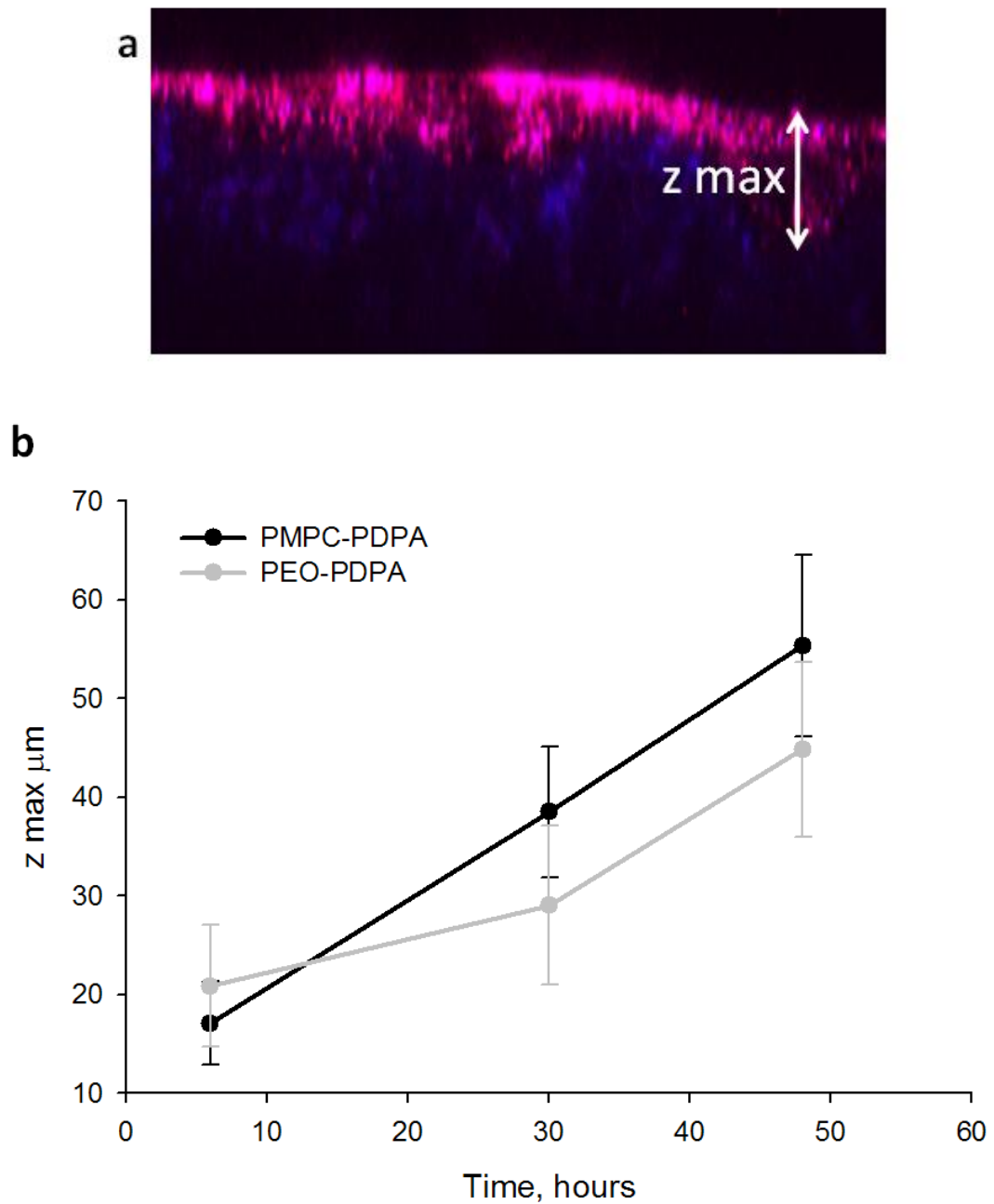
Figure 3.20 Depth of penetration (z$_{maz}$) for PMPC$_{25}$-PDPA$_{70}$polymersomes into the model as measured by analysing the x-z and y-z projections (a). Depth of penetration over time for the two different polymersome formulations (b). n=3

Polymersomes and MCTS

Effect of polymersomes on viability and growth of MCTS

FaDu MCTS were cultured for 7 days before being incubated with fluorescently labelled PMPC-PDPA polymersomes. The effect of polymersomes on MCTS growth and viability was measured using the MTT viability assay (Figure 3.21) and microscopy (Figure 3.22). No significant effect could be seen on the viability of MCTS when incubated with 0.1mg/ml PMPC-PDPA or 1mg/ml PMPC-PDPA for up to 11 days. The growth curves of all spheroids, unexposed control spheroids, spheroids exposed to 0.1mg/ml and 1mg/ml of PMPC-PDPA were very similar (Figure 3.22). This is in comparison to the FaDu cell monolayers which were affected by 48 hours exposure to 1mg/ml. This demonstrates the difference in the behaviour of cells in 2D and 3D.
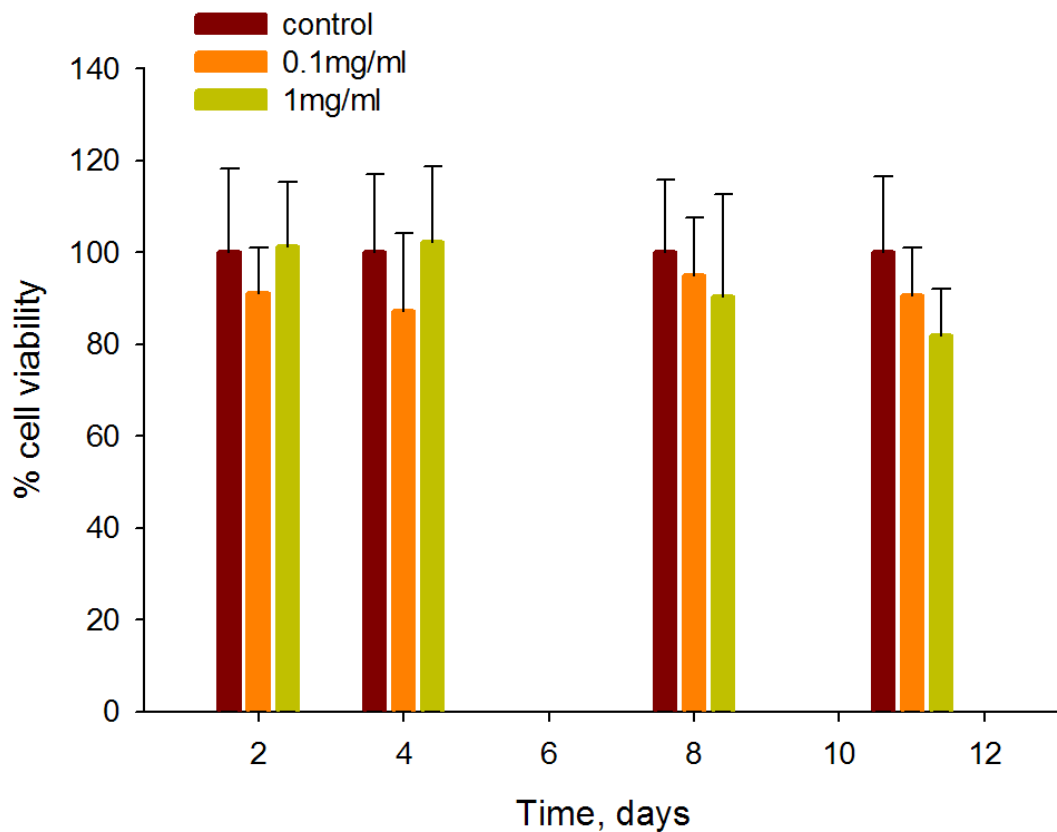
Figure 3.21 Viability of cells exposed to PMPC-PDPA polymersomes for up to 11 days. n=5
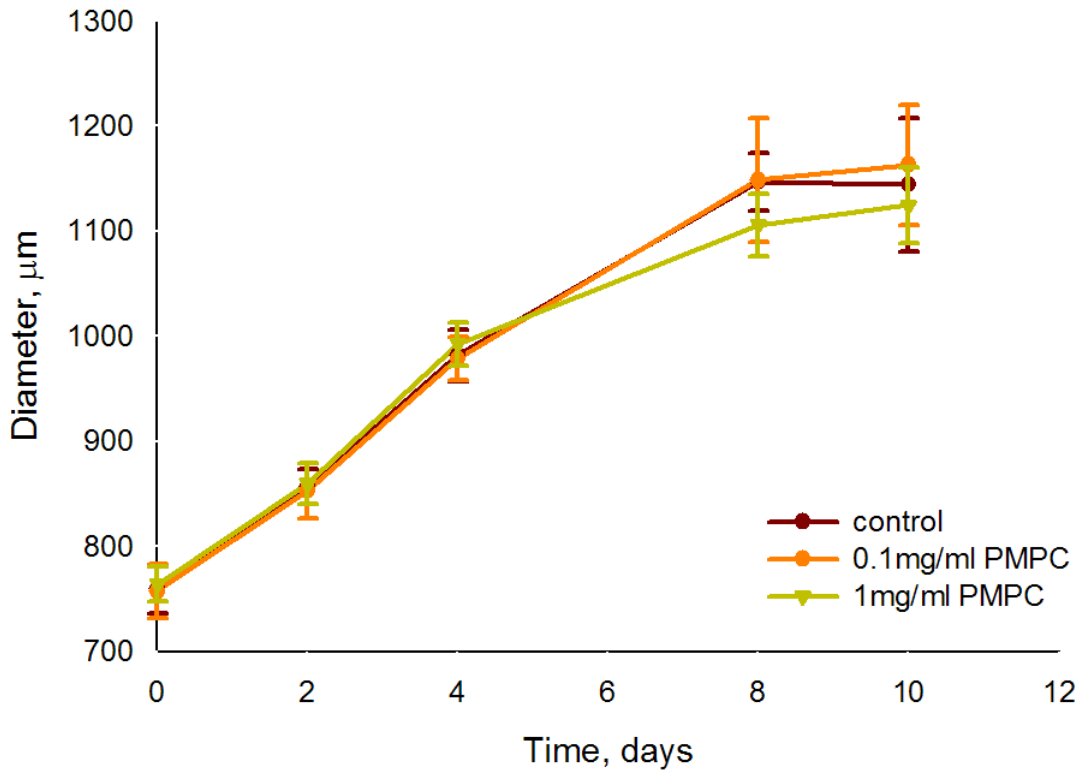
**Figure 3.22 Growth curve of MCTS exposed to PMPC-PDPA polymersomes.
Day 0 indicates time of polymersome addition. n=5**

Uptake of Polymersomes by MCTS

MCTS were incubated with fluorescently labelled PMPC-PDPA polymersomes for 6, 24 or 48 hours before being frozen, sectioned and stained with DAPI to show up the cell nuclei. These frozen sections show that polymersomes penetrated into MCTS in a time dependent manner (Figure 3.23). After 6 hours exposure the polymersomes had entered the most superficial cells of the MCTS. After 24 hours the outer most 2-3 cells contained polymersomes (labelled with Rho-PMPC-PDPA) and after 5 days (120 hours) the whole MCTS appeared to contain PMPC-PDPA polymersomes as the whole MCTS was strongly fluorescent in the red channel.

To quantify the uptake of polymersomes by cells, MCTS were dissociated and analysed by flow cytometry. After 24 hours exposure polymersomes had been taken up by around 20% of cells within the MCTS (Figure 3.24). By 120 hours exposure the polymersomes had been internalised by 80% of the cells and the intensity of fluorescence per cell increased over the 120 hours of polymersome exposure (Figure 3.25).
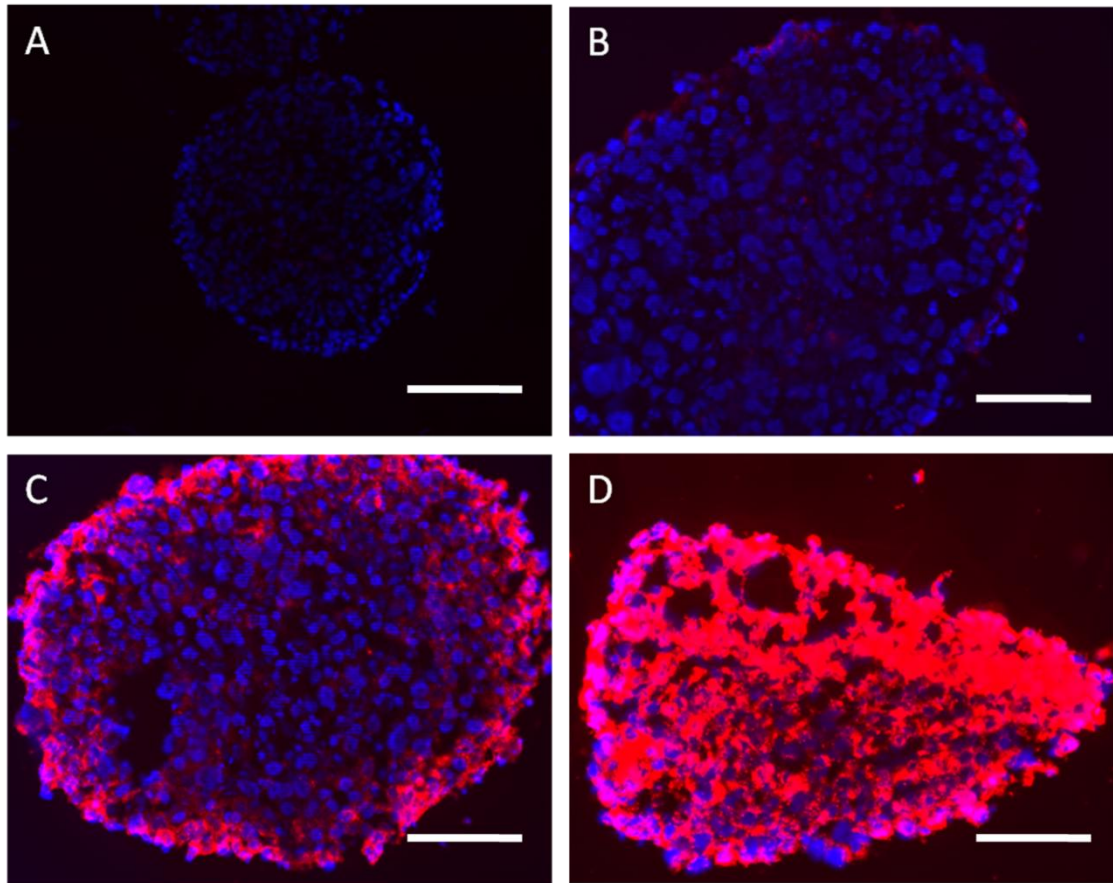
Figure 3.23 Diffusion of rhodamine labelled PMPC-PDPA polymersomes over time.
(a) control, no polymersomes, (b) 6 hour, (c) 24 hour and (d) 120 hour incubation with
polymersomes. Blue = DAPI stained cell nuclei Red= Rhodamine fluorescence. NB the
differences in size of MCTS are due to where the MCTS slice was taken. Scale bar = 100μm.
Representative images n=3
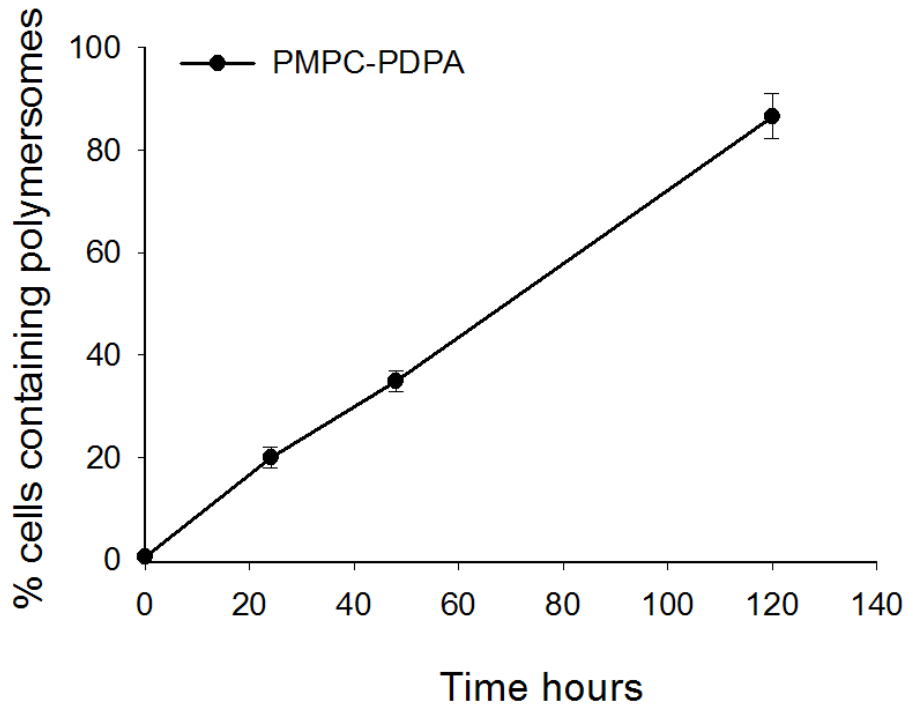
Figure 3.24 Percentage of cells in MCTS which took up polymersomes as measured by flow cytometry on dissociated MCTS. n=3
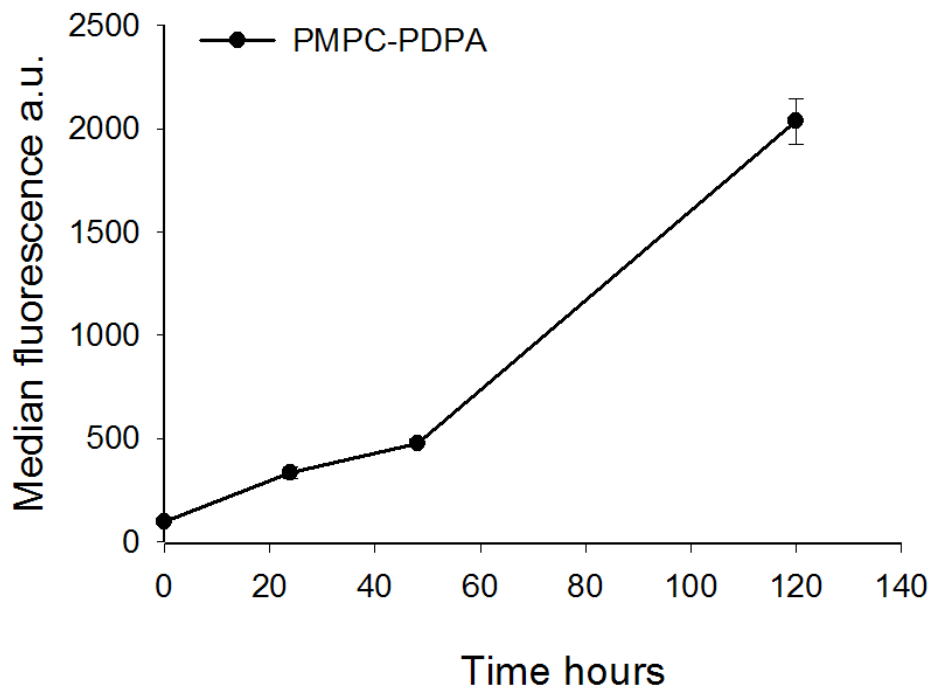
Figure 3.25 Median fluorescence of cells within MCTS exposed to polymersomes labelled with rho-PMPC-PDPA over time. n=3

3.5   Discussion

Characterisation of Polymersomes

Analysis of polymersomes using TEM indicated the presence of polymersomes in the turbid solutions for both polymers (PEO-PDPA and PMPC-PDPA). This is in agreement with previous studies involving polymersomes made from these polymers (Massignani *et al.,* 2009). To study polymersome location in cells and other *in vitro* settings requires a marker and fluorescence is one of the most common labelling techniques used in bioimaging. Polymersomes have been fluorescently labelled in two different ways, described on page 135.

Figure 3.11 shows the removal of free rhodamine which remained after synthesis. Using GPC the small free rhodamine molecules could be separated from the polymersomes. The same method was also used for the removal of rhodamine B octadecyl ester perchlorate which had not been encapsulated. This meant tracking of polymersome location could be achieved using these dyes, as the only dye remaining after GPC purification was associated with the polymersomes.

Effect of Polymersomes on Cell Viability

For polymersomes to be utilised in a clinical setting they must be non-toxic and not stimulate an immune or inflammatory response when administered to a patient. Despite previous studies showing minimal or no toxicity (Figure 3.1 (Massignani *et al.,* 2009)) in this study it appears that for longer incubation times polymersomes can effect mitochondrial activity in some of the cell types looked at here. MTT has been used as an indicator for cell viability because MTT salts are only reduced by cells with active mitochondria (Mosmann 1983).

The reduction in cell viability seen in this project is not desirable. However, it may not pose a problem for the applications proposed in this research. Cells grown *in vitro* in monolayer culture are an artificial representation of cells which are present within the body. It has been shown previously (Sun *et al.,* 2006) that cells grown in two-dimensions behave differently compared to cells grown in three dimensions. In the study by Sun *et al*., the same cells cultured in 3D were able to withstand much higher concentrations of silver and hydrogen peroxide than cells grown in monolayer. It is also very likely that cells in 3D within the complex environment of the human body will be more able to withstand potential cytotoxic agents because of blood perfusion of the tissues which will rapidly reduce the concentrations of agents added. In a clinical scenario it is very unlikely that a population of cells would be continuously exposed to such high concentrations of polymersomes for 48 hours due to the nature of drug delivery and clearance. It is more likely the cells will be exposed for a short

period of time, during the drug administration, but would then have the opportunity to excrete the polymer between administrations.

The most significant toxicities were found after 48 hours of exposure which could be due to a number of factors. The damage to the cells may not be caused instantly but instead may be a result of prolonged polymersome-cell interaction. The cells may also be tolerant to a certain amount of polymer material within the cytosol but may become damaged when the concentration within the cell reaches a threshold. As can be seen in Figure 3.14, the cells continued to take up polymersomes steadily over 24 hours.

As a result of these findings subsequent monolayer studies were carried out for 24 hours and concentrations of 1mg/ml or less were used.

Internalisation of Polymersomes by Monolayers

The uptake of polymersomes by a variety of primary cells and oral cancer cell lines was measured using PMPC-PDPA polymersomes with rhodamine B octadecyl ester perchlorate encapsulated within them. Flow cytometry was used to determine how many cells had taken up polymersomes over 24 hours. The cell population was classed as positive for polymersomes when it was above the detection threshold for the flow cytometry machine. Figure 3.6 shows how the control and fluorescent populations were set using a dot plot of fluorescence intensity *vs*. side scatter.

The faster uptake of polymersomes by the cancer cells (Figure 3.14) may provide a method to passively target polymersomes to cancer. Interestingly, the cancer cell lines, in particular FaDu, took up the polymersomes more rapidly than the primary cells. From a therapeutic point of view this is beneficial as higher uptake of cytotoxic agents by cancer cells with a relatively lower uptake by healthy cells could dramatically increase tumour killing and reduce unpleasant and dose limiting side effects. There are a number of factors which may be responsible for this increased uptake including preferential binding of polymersomes to the surface of cancer cells, faster metabolic rate of cancer cells and higher levels of endocytosis.

The quantity of polymersomes taken up by each cell type increased over 24 hours at a similar rate however, the quantity taken up by FaDu cells was the greatest throughout. There does appear to be some connection between the rate and quantity of uptake by cells and their viability post exposure. The uptake of fluorescently labelled PMPC-PDPA polymersomes, as measured by flow cytometry showed that the FaDu cells took up the polymersomes fastest. After 10 minutes over 90% of the cell population contained some fluorescently labelled polymersomes and had more polymersomes per cell compared to other cell types. It was the FaDu cell line, which showed the lowest viability after 48 hours exposure for the two highest

concentrations 1mg/ml and 2mg/ml (Figure 3.12). This could be due to the quantity of polymer present in the cells or the response of FaDu cells to polymersomes.

The uptake of polymersomes was concentration dependant, as shown in Figure 3.15. This is important to know when taking polymersomes to the clinic and considering dosing of polymersome mediated therapy.

Penetration of Polymersomes across TEOM

Developing drug delivery systems that can carry a wider array of therapeutic agents across the epithelial permeability barrier, in particular biological agents and genes, and deliver them with high efficiency either into basal keratinocytes or directly into the connective tissue where they can be taken up by the blood supply, would open up a broad spectrum of more effective therapeutic tools for treating many oral mucosal diseases.

The aim of this study was to explore the use of TEOM as a convenient *in vitro* surrogate for normal oral mucosa to examine the penetration of two novel forms of polymersomes through healthy oral mucosa using CLSM. As these polymersomes are being developed to deliver drugs, proteins or genes into tissues for future clinical use, information on their penetration into tissues is clearly an important part of their development.

Initial experiments showed that it was possible to track rhodamine labelled polymersomes using CLSM as the wavelength used to excite the rhodamine (543nm) did not result in autofluorescence from the TEOM. The 488nm autofluorescence was used as a reference to orientate the oral mucosa. Figure 3.19 shows time-dependent penetration of polymersomes comprised of PEO-PDPA or PMPC-PDPA into the epithelium of a TEOM model over 48 hours. The TEOM used in this study closely resembled normal oral mucosa with epithelial cell differentiation and stratification, minimal keratinisation of superficial epithelial layers and a well attached epithelium on a collagenous connective tissue containing fibroblasts (Figure 2.4 on page 93).

The $PMPC_{25}$-$PDPA_{70}$ polymersomes appear to penetrate the epithelium faster and over a more widespread area than the PEO_{23}-$PDPA_{15}$ polymersomes. By 48 hours the fluorescence generated by the $PMPC_{25}$-$PDPA_{70}$ polymersomes appeared to follow the contours of the basal epithelial cells which reside along the basement membrane, strongly suggesting that these polymersomes diffuse as far as the basal cells. The diffusion of the PEO-PDPA polymersomes compared to the PMPC-PDPA did not appear to be as widespread and penetration was higher for PMPC-PDPA polymersomes compared to PEO-PDPA polymersomes, but not significantly so (Figure 3.20).

Unfortunately, whether or not the differences in cell membrane adhesion and polymer-cell interactions caused the distinct distribution profiles seen for each polymer cannot currently be

confirmed as there were significant differences in the fluorescence intensity between the two types of polymersomes (see appendix 2). The difference may be due to the fluorescence detection limit of CLSM rather than the behaviour of the polymers.

The penetration of both polymersome formulations was over 50μm which corresponds to at least 5 cell layers. Models with a thicker epithelium, closer to naturally occurring oral epithelium (which can be over 500μm in thickness (Nanci 2003)) or an *in vivo* model would be needed to further test whether polymersomes can reach the basal cells of these thicker epithelia.

The bilayer membranes of polymersomes are highly deformable enabling them to pass through gaps between cells in tissues, such as the oral epithelium, that are smaller than their own diameter (Discher *et al.,* 1999). For a bilayer membrane to be ultra-deformable there must be a certain level of flexibility within the membrane which enables the molecules to redistribute themselves within and between the bilayers (Cevc and Gebauer 2003). Re-distribution within membranes reduces the volume-stress created by the deformation. The deformation capability of polymersomes has been demonstrated (Discher *et al.,* 1999) using micropipette aspiration of giant sized (20-50 μm) polymersomes.

It is hoped this flexibility and the encapsulation potential of polymersomes may enable efficient trans-epithelial delivery of several therapeutic agents. The diffusion of polymersomes across the oral epithelium may not be driven by a concentration gradient as for other materials but rather *via* a hydration gradient across the different layers (Cevc and Gebauer 2003). In the epithelium the hydration gradient pulls the carriers through the relatively dehydrated keratinized layer until they reach the viable epithelium where there is a higher level of hydration. These rather bulky carriers are then pushed through the lower layers of the epithelium by more carriers which are drawn into the epithelium by the hydration gradient (Cevc and Gebauer 2003).

For transmucosal applications, the ability to deliver intact polymersomes containing their therapeutic loads would be incredibly beneficial. To test if polymersomes were able to cross the epithelium intact polymersomes encapsulating a cargo (usually impermeable to the oral epithelium) should be applied to the surface of the TEOM and detection of the cargo underneath can then be measured. Whether or not polymersomes cross intact depends on the route by which they traverse the epithelium and its permeability barrier. From the current data we are unable to determine which path is taken by either PMPC-PDPA or PEO-PDPA polymersomes. However, there are two possible routes: (i) the intercellular pathway where material passes through lipid rich domains around the cells and (ii) the trans-cellular pathway where material passes in and out of the cells in each layer (Sood *et al.,* 2005).

As discussed in the previous chapter the permeability of TEOM could not be measured with the equipment available. A previous study of tissue engineered skin, with a similar composition to the TEOM, found trans-epithelial potential was comparable to a split thickness skin graft (Bullock *et al.,* 2007). However, similar studies have not been undertaken for TEOM.

Despite this, preliminary experiments did show the TEOM was less permeable to dextrans with molecular weights of 20kDa and 40kDa compared to dextrans with molecular weights of 4 and 10 kDa. Naturally occurring oral epithelia have been shown to be impermeable to dextrans of 20kDa and greater (Selvaratnam *et al.,* 2001).

The data presented here demonstrates the potential for polymersome mediated therapies to be delivered for topical delivery to the oral mucosa in the future. There are still many aspects to consider including how to deliver high enough concentrations of therapeutic agents topically to the oral mucosa for long enough periods of time to obtain a therapeutic effect. Polymersomes may need to be formulated into mucoadhesives or gels to enable sustained release. These and other formulations for drug delivery to the oral mucosa are reviewed in (Hearnden *et al.,* in preparation).

Penetration of Polymersomes into MCTS

The viability and growth of FaDu MCTS were not affected by exposure to polymersomes for 11 days (Figure 3.21 and Figure 3.22). The same FaDu cells were previously seen to be significantly less viable when grown as monolayers and exposed to the same concentration of PMPC-PDPA (1mg/ml) for 48 hours (Figure 3.12). It has previously been shown that cells are more resilient when grown in 3D compared to monolayers and it is referred to as the "multicellular effect" in (Green *et al.,* 2004). Green *et al*., (2004) showed MCTS and solid tumours were less sensitive to cytotoxic anti-cancer agents compared to cell monolayers. Possible reasons for this include the proportion of cells exposed to the agent (peripheral cells in 3D compared to all cells in 2D), the difference in cell metabolism in 3D compared to 2D or the way in which cells respond to cyto-toxic agents when in contact with other cells. The stark difference between viability in 2D and 3D highlights the value of using MCTS and other 3D models to test novel agents prior to further studies.

The MCTS model here is a valuable model which enabled us to investigate the penetration of polymersomes through a solid tumour. The model includes necrotic and hypoxic regions as well as the penetration barrier, created by the 3D arrangements of cells. The uptake of polymersomes by cells within the MCTS shows promise for delivering anti-cancer drugs to those cells not often reached by chemotherapeutic agents delivered in a conventional manner. By using polymersomes labelled with Rho-PMPC-PDPA we were able to see that 80% of calls

within the MCTS took up polymersomes over 5 days, which correlated well to the images of the frozen sections.

Though this experiment shows the location of the polymer it does not allow us to determine whether or not the polymersomes were able to reach the central region intact. To test this we would need to deliver an encapsulated agent (not able to penetrate alone), such as a DNA plasmid to see if the agent reached the central region of the MCTS or whether its delivery was restricted to the superficial cells. As discussed previously for the penetration into the TEOM, whether or not the polymersomes are intact depends on the route by which the polymersomes penetrate (trans-cellular or intercellular).

The uptake of polymersomes by the cells within the MCTS was dramatically slower compared to the FaDu cells grown as monolayers. The increase in polymersomes per cell increased linearly over the 5 days of polymersome incubation (Figure 3.24). Polymersomes were internalised by 80% of cells within the MCTS. In the future it would be interesting to see if the remaining 20% of cells which did not internalise these polymersomes were non-viable, not metabolically active or if the remaining 20% of cells could be reached with longer exposure times.

Preliminary work *in vivo* has shown polymersomes are able to penetrate throughout a tumour from the injection site (Murdoch *et al.,* 2010). Polymersomes were found within the cytosol of cancer cells throughout the tumour after intra-tumoural injection (Murdoch *et al.,* 2010). Polymersomes were also found in the spleen and liver associated with macrophages. It is well known that tumours *in vivo* are populated by immune cells such as macrophages which phagocytise cell debris and necrotic cells so it is not surprising that these cells came into contact with and took up polymersomes. It would be interesting to see if the macrophages phagocytised polymer with or without encapsulated cargo. This *in vivo* study examined polymersomes which were fluorescently labelled but delivered no cargo. The effect this uptake by macrophages may have clinically (especially if delivering cytotoxic agents) will need to be considered before taking polymersome therapy to the clinic.

Chapter 4: Novel Diagnostic technologies

4.1 Aim

To test novel diagnostic technologies for diagnosis of potentially malignant lesions and oral cancer using tissue engineered models.

4.2 Introduction

A non-invasive oral cancer diagnostic technology could dramatically improve patient care and enable widespread screening of at risk patient groups. This could enable oral cancer to be detected earlier and thus improve survival rates. The current gold standard for oral cancer diagnosis is histopathological examination of surgical biopsies taken from lesions with a suspicious appearance. Histopathlogy is a well established method which produces reliable diagnoses, in the hands of expert pathologists, for numerous diseases. However, as with any technique, there are disadvantages associated with surgical biopsies and their subsequent analysis. It is hoped new technology could reduce the amount of biopsies which need to be taken and help clinicians to biopsy those parts of a lesions that will provide the most valuable diagnostic and prognostic information.

From biopsy to diagnosis is a time consuming process which requires the expertise of the dentist, histology staff and pathologists before a patient can be told the outcome. In the case of cancer this delay can cause significant stress and anxiety for the patient. The procedure for performing a biopsy on a patient can be painful and if longitudinal monitoring of a suspicious lesion is required sequential biopsies must be taken. The continuous biopsying of suspicious lesions potentially has other consequences. In an area of abnormal tissue taking repeated biopsies will cause considerable trauma, inflammation and damage in that area which could speed up disease progression or exacerbate problems faced by the patient. Kinsukawa *el al*., showed the presence of cancer cells in the circulation after taking a biopsy of a squamous cell carcinoma increasing the risk of metastasis (Kinsukawa *et al.,* 2000).

Of the suspicious lesions which are biopsied just 5% require treatment. In the interests of time, money and patient satisfaction a technique which could achieve real time non-invasive imaging and diagnosis of suspicious lesions would be hugely beneficial. Another problem faced by clinicians is choosing the best area to biopsy which will give the most reliable result as only a small section of tissue can be analysed at a time in this way (Oliver *et al.,* 2004). Technologies which improve this and reduce sampling errors could help earlier more accurate diagnosis of oral cancer to be achieved.

Here four different techniques for detecting OSCC were investigated *in vitro* using the tissue engineered models, described in chapter 2. The first technique used an exogenous marker for cell metabolism to determine whether cancer cells could be distinguished from normal cells using an inherent difference in metabolic activity (Skala *et al.,* 2007). The second technique was impedance spectroscopy (described on page 56) a method which measures changes in bioimpedance of different tissues when a current is applied to the tissue. FTIR was the next diagnostic technique evaluated. FTIR is a spectroscopy method which can detect specific bonds within a tissue by measuring IR radiation absorbed by bonds within a sample. Finally, optical coherence tomography (OCT) was investigated. OCT is a form of imaging which detects differences in the optical scattering and reflectance properties of tissues up to 2-3mm deep (described on page 58).

4.3   Materials and Methods

Metabolic stain for cancer detection

Materials

C_{12} resazurin cell metabolic assay
A stock solution of Vybrant Cell metabolic assay kit with C_{12} resazurin (Molecular probes, Invitrogen, Paisley, UK) was made as per the manufacturer's instructions. Kit components were allowed to warm to room temperature before a 10mM stock solution was prepared by dissolving 1 vial of C_{12} resazurin into 20µl of DMSO. To ensure all the C_{12} resazurin was fully dissolved the solution was sonicated briefly in an ultrasonic water bath.

CellTrace™ Far Red DDAO-SE
One vial of CellTrace™ Far Red DDAO-SE (Molecular probes, Invitrogen, Paisley, UK) was dissolved in 20µl of pre-warmed DMSO (Sigma Aldrich, Poole, UK). The solution was mixed gently with a Gilson pipette until fully dissolved. Twenty µl of dissolved CellTrace™ in DMSO was next added to 5ml of pre-warmed serum-free DMEM media.

DAPI (4',6-diamidino-2-phenylindole) Cell nuclear stain preparation
Ten mg of DAPI powder was dissolved in 10ml of PBS to make a concentration of 1mg/ml. This was then stored in 10µl aliquots at -20°C and protected from the light. Immediately prior to use 10µl of the DAPI stock solution was defrosted and diluted in 10ml of PBS to give a final concentration of 1µg/ml and kept protected from the light until used.

Exposure of cell monolayers to C_{12} – Resazurin metabolic indicator

Three x 10^4 cells were seeded onto glass coverslips (19mm diameter) (Menzel Gläser, Braunschweig, Germany) in 12 well tissue culture plates. Cells were cultured for 48 hours prior to being exposed to C_{12} resazurin. The stock solution of Vybrant Cell metabolic assay

kit with C_{12} resazurin (Molecular Probes , Paisley, UK) was diluted in DMEM cell culture medium (without serum) to give a concentration of 10µM. Cells were incubated with 300µl of 10µM C_{12} resazurin solution for 15 minutes in fresh 12 well plates. Coverslips with cells on were washed three times in excess PBS and imaged submerged in PBS on the confocal microscope.

Confocal Laser Scanning Microscopy of cell monolayers exposed to C_{12} – Resazurin metabolic indicator

Models were imaged on a Zeiss LSM 510 META Laser Scanning Confocal Microscope (Carl Zeiss Inc., Germany) with corresponding LSM 510 META Software (Carl Zeiss Inc., Germany) using the 543nm laser and an Achroplan x40 magnification, 0.8 numerical aperture, water dipping objective (Carl Zeiss Inc., Germany).

Image analysis

Five fields of view were chosen at random from each sample and imaged using identical settings. Images were quantified using the Image J software (version 1.43u, National Institute of Health, USA). The median intensity of fluorescence from each image was measured by drawing around each cell or cell colony on each image. The median intensity was chosen instead of the mean as some areas of the images were over exposed which would make the mean value unrepresentative (Figure 4.1).
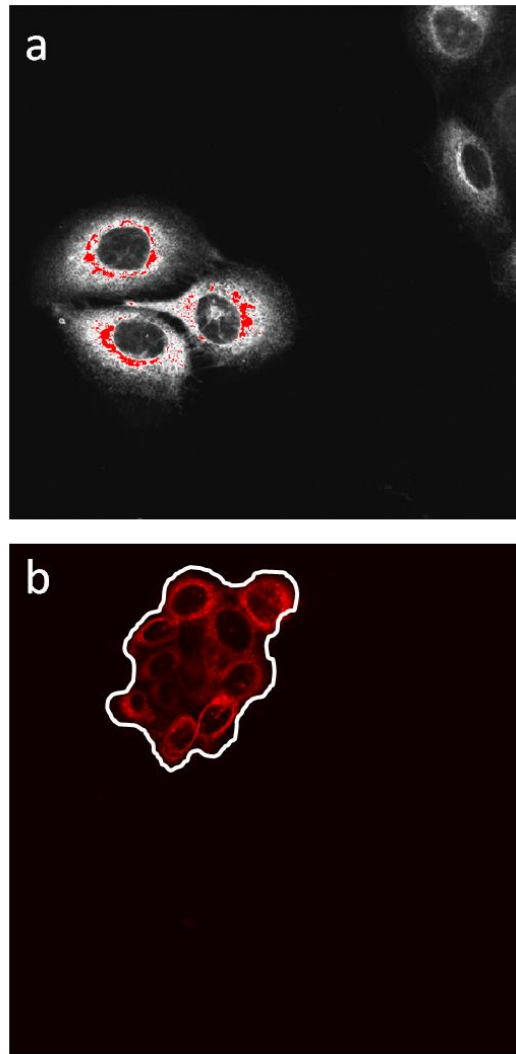
Figure 4.1 Method to quantify fluorescence intensity of cells exposed to C$_{12}$ resazurin.
(a) Example where area of image was over exposed. Image re-coloured with LSM Image browser software (Carl Zeiss Inc., Germany) to show over exposed regions in red.
(b) Diagram to show how cells were selected prior to quantification by Image J software. Area inside the white line border was measured for median fluorescence intensity.

Statistics

The distribution of fluorescence intensity values was not normally distributed so the median of these values was calculated (rather than the mean). The median values of each area measured from the 10 fields of view (from two experiments) were combined and the median value and inter-quartile ranges were calculated using SigmaPlot v10. A Mann-Whitney Rank Sum Test was performed to determine the statistical significance of the variation in fluorescence intensity between different cell types using SigmaStat v2.03.

Culture of DOK + NOK 3D Model

Models were cultured with a mixture of normal oral keratinocytes and the dysplastic cell line DOK. Prior to seeding onto the 3D model the DOK cells were labelled with CellTrace™ Far

Red DDAO-SE (Molecular probes, Invitrogen, Paisley, UK). 5ml of CellTrace™ solution was added to a sub-confluent T75 flask of DOK cells and incubated for 45 minutes. Cells were then washed thoroughly with PBS before being enzymatically detached using trypsin-EDTA, counted and seeded onto the 3D model.

To culture the model with DOK and NOK cells, models were first seeded with NOF and NOK cells as for TEOM described on page 81. After 5 days at ALI 2.5 x 10^5 labelled DOK cells were added to the model in a stainless steel ring. The model was cultured submerged with DOK cells inside the ring for 48 hours during which time cell culture medium within the ring was half replenished after 24 hours. After 48 hours the model now with NOK and DOK cells, was raised to ALI and cultured for a further 6 days at ALI before being imaged.

Labelled DOK cells were seeded into a separate 6 well plate to observe the intensity of CellTrace™ in the DOK cells throughout the experiment (Figure 4.2a).

Culture of Spheroid model

Models of carcinoma *in situ* were cultured as previously described in (Colley *et al.,* 2010). Briefly, TEOM models were cultured as described on page 81. Seven day old FaDu MCTS were added onto the upper surface of the TEOM after 6 days at ALI using a Pasteur pipette. 5-6 spheroids were added onto each model and cultured at ALI for 6 days.

Exposure of 3D models to C_{12} – Resazurin metabolic indicator

Models were placed onto a 6 well tissue culture plate and 1ml of C_{12} – resazurin solution at a concentration of 10µM (prepared as described on page 171) was added to each well to fully submerge the 3D model. The tissue engineered models were then incubated for 15 minutes before being washed 3 times in 4ml of PBS and then submerged in DAPI nuclear stain solution for imaging. DAPI was used to help orientate the models during confocal imaging.

Confocal Laser Scanning Microscopy of 3D models exposed to C_{12} – Resazurin metabolic indicator

Models were imaged on a Zeiss LSM 510 META Laser Scanning Confocal Microscope (Carl Zeiss Inc., Germany) with corresponding LSM 510 META Software (Carl Zeiss Inc., Germany) and a Achroplan x40 magnification, 0.8 numerical aperture, water dipping objective (Carl Zeiss Inc., Germany). Z-stacks of 20-40 slices with 2µm between slices were obtained. Models were imaged using the following excitation/emission filters.

Laser (excitation wavelength)	Emission filter	Stain imaged
543nm	BP 565-615nm	C_{12} – resorufin (Vybrant™ cell metabolism assay kit)
Ti:Sa multi-photon laser (780nm)	BP 390-465nm	DAPI nuclear stain
633nm	BP 650-710nm	CellTrace™ Far Red

Table 4.1
Confocal conditions used to image C_{12} experiment

Quantification of 3D models using Image J

Four slices from each z stack were used to quantify the intensity of the fluorescence signal from resorufin (the fluorescent reduced product of C_{12} – resazurin) and therefore the metabolic activity of that area of tissue measured. Z-stack slices were chosen at 4 distinct points throughout the thickness of the tissue (slices which had no cells in focus on that slice were ignored) (Figure 4.3). For the DOK + TEOM model the areas measured were those which were fluorescent in the red (resorufin) and the far red (CellTrace™) channels. The intensity of just the red channel was quantified and the far red channel was used as a guide to which areas contained DOK cells labelled with CellTrace™ (Figure 4.2b). For the MCTS + TEOM models it was clear which areas resembled the normal oral mucosa and which were the FaDu spheroid regions because of differences in cell morphology and nuclear to cytoplasmic ratios compared to the TEOM (Figure 4.2 c and d). Only regions which had the features of MCTS were used to quantify the intensity of fluorescence from the FaDu spheroid regions. Intensity of resorufin fluorescence from TEOM was calculated from TEOM only models exposed to C_{12} – resazurin.
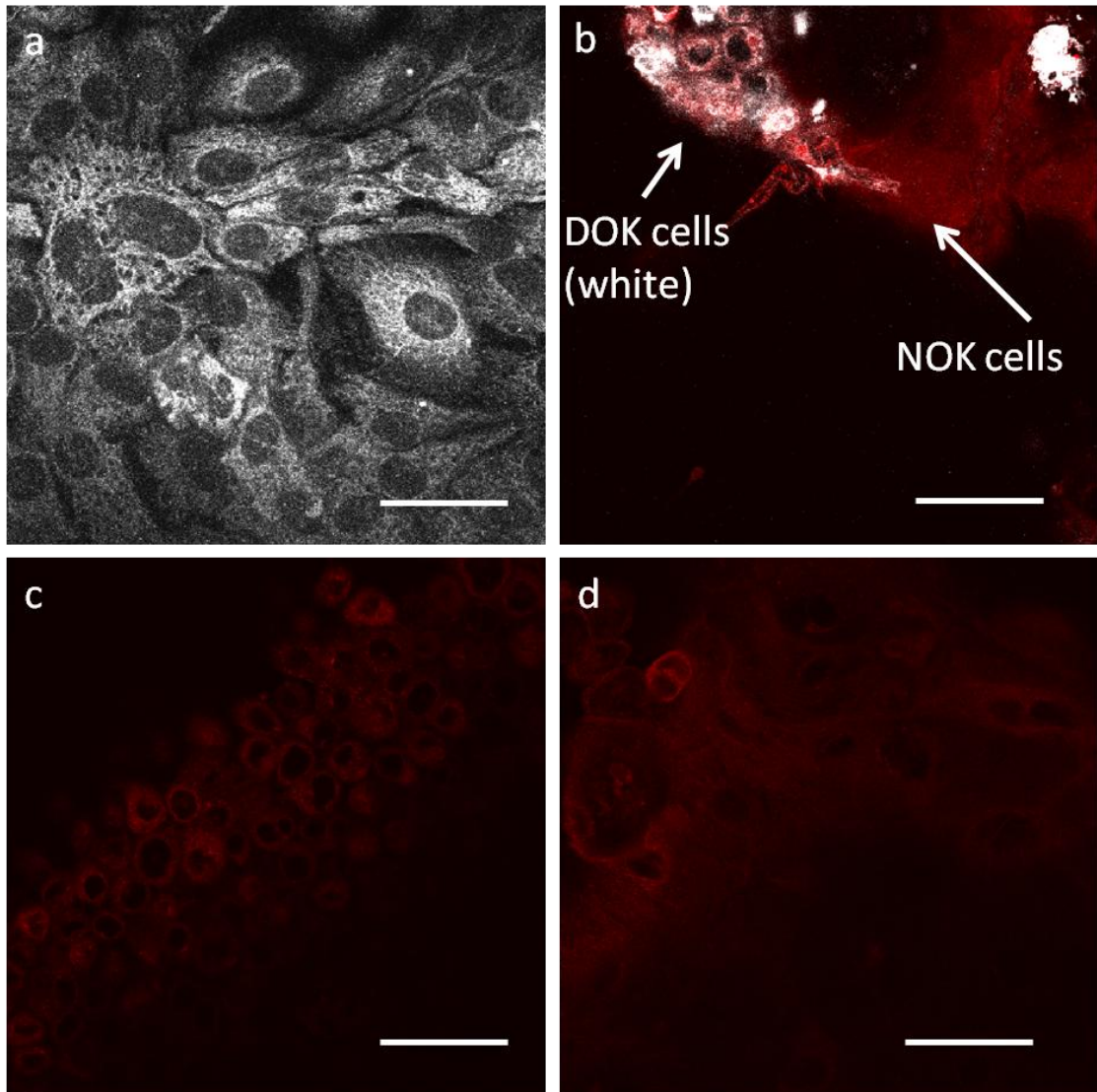
Figure 4.2 Method to quantify fluorescence of different cell types within 3Dmodels
(a) Fluorescence of DOK cells labelled with CellTrace™ was confirmed by imaging cells in monolayer using CLSM. (white= CellTrace™ far red DDAO-SE). (b) Slice of CLSM z-stack showing DOK cells in white and all cells containing resorufin fluorescence (red). Representative images of FaDu spheroids on the MCTS + TEOM model (c), and of normal epithelium on TEOM (d). Scale bar = 50µm.
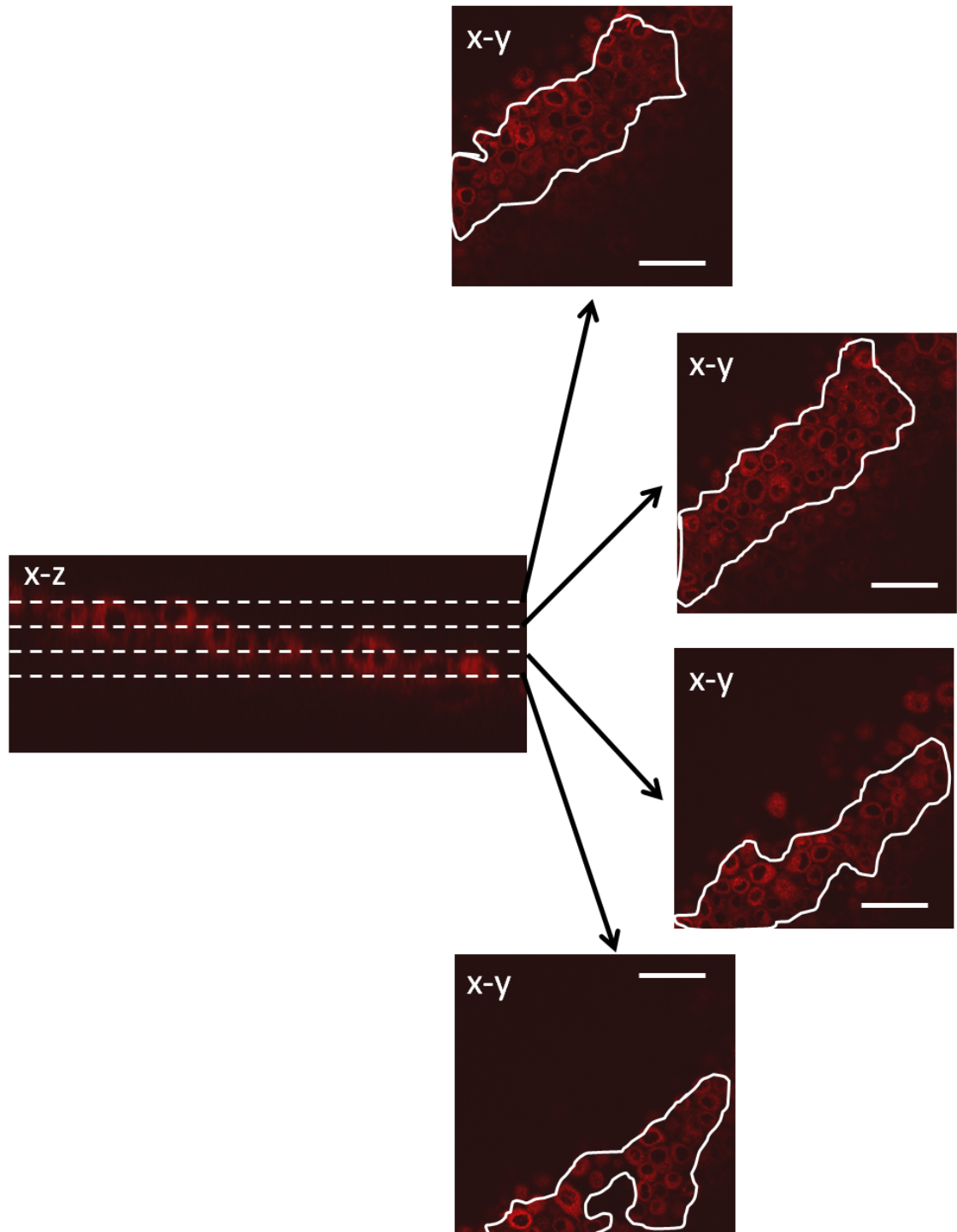
Figure 4.3 Method for quantifying 3D models exposed to C$_{12}$ – resazurin.
Areas of slice which contain cells in focus were highlighted and the area within the line measured using Image J software.

The Image J software (version 1.43u, National Institute of Health, USA) was used to quantify fluorescence of the red channel, corresponding to the reduced product of C_{12}-resazurin, resorufin. The median intensity of fluorescence from each image was measured by drawing around the areas which contained cells in focus on that slice (Figure 4.3). The median fluorescence intensity for the highlighted areas of the four slices over the three experiments were combined and the statistics were performed as described on page 173.

FTIR

Materials

FTIR Spectroscopy Device
The device used for this study was the Spectrum 2000 (Perkin Elmer, Cambridgeshire, UK).

Slides
Low 'e' MirrIR slides (Kevley Technologies, Ohio, USA) were used. These slides were coated with layers of silver so there was no absorption in the range of wavenumbers used (400-4000cm^{-1}).

FTIR on tissue engineered models

Tissue engineered models produced as described on page 81 were used to test the ability of FTIR to distinguish between healthy oral mucosa (TEOM) and three different models of OSCC (FaDu, DOK and SCC9).

Initially, it was attempted to measure the FTIR spectra from models fixed in formalin or fixed in formalin and subsequently dehydrated in ethanol. Unfortunately, this technique was unsuccessful due to high noise levels in the spectra because of the presence of water which absorbs in the mid IR range and the thickness of the samples (samples above 15µm in thickness can cause spectral saturation).

For these reasons further studies were performed on paraffin embedded samples sectioned and mounted onto MirrIR slides. Sample processing and sectioning was performed as described on page 84. Instead of heamotoxylin and eosin staining the slides were dewaxed using xylene (2 minutes immersed in xylene) and dried prior to FTIR analysis.

The reflective nature of the slides meant the transflection mode on the FTIR device was used. Sixteen scans were taken per sample, spectra from at least three samples of each cell type from three separate experiments were measured, spectra from the same cell type were averaged and the data was analysed and graphed in MATLAB.

There were significant differences in signal intensities from the different samples due to the differences in the size of the section on each slide. To overcome this, the spectra were aligned based on points on commonality to enable comparison between spectra to be performed.

Impedance spectroscopy

Materials

An impedance spectroscopy device was kindly provided by Peter Highfield (Zilico Ltd, Sheffield, UK). The probe was an APX100, designed for the clinical investigation of cervical tissue. Figure 4.4 shows the device and the tips used as well as the electrodes on the end of the disposable tips. These tips were sterilised prior to use by submerging in 70% IMS and then washed twice in excess PBS. The measurements were downloaded onto a personal computer (PC) using Cervical Probe Applications Software (CPAS), revision 1.03 (Triteq, Berkshire, UK).

Impedance spectroscopy on tissue engineered models

The sterilised disposable probe tip was connected onto the device and the tip placed in contact with the epithelial surface of the tissue. In built software within the probe was used to tell when the measurements were completed. At least 5 measurements were taken per model and each individual measurement was an average of 8 measurements, averaged by the probe. Different regions of the model were measured and an average of the measurements from the whole model was calculated. Photographs of the device and the tip are shown in Figure 4.4.

OCT imaging

Four different OCT imaging devices were used in this project. The specification of each machine is shown in Table 4.2.

All samples were imaged by OCT in the 6 well tissue culture plates in which the models had been cultured, with the exception of the Optovue® system. Samples were kept sealed, sterile and at an ALI (on a stainless steel grid with cell culture medium in contact with the bottom of the sample) for imaging. Care was taken to ensure that the level of media was low enough that no moisture remained on the top surface of the sample because liquid causes strong reflective signals when imaged using OCT. Condensation which occurred on the inside of the lid of the sample was removed using a hairdryer on the warm setting. The Optovue® system has been developed for ocular application so the samples were placed in a $9cm^2$ Iwaki petri dish (Sterilin Ltd., Caerphilly, UK) with no cell culture media and clamped perpendicular (vertically) to the lens using a bench top clamp and stand. For the Optovue® system, samples were not in contact with cell culture media; however, the imaging was very rapid (less than 3 minutes for 4 images) avoiding substantial damage to the cells. Models were sacrificed for histological analysis and compared to the OCT images.
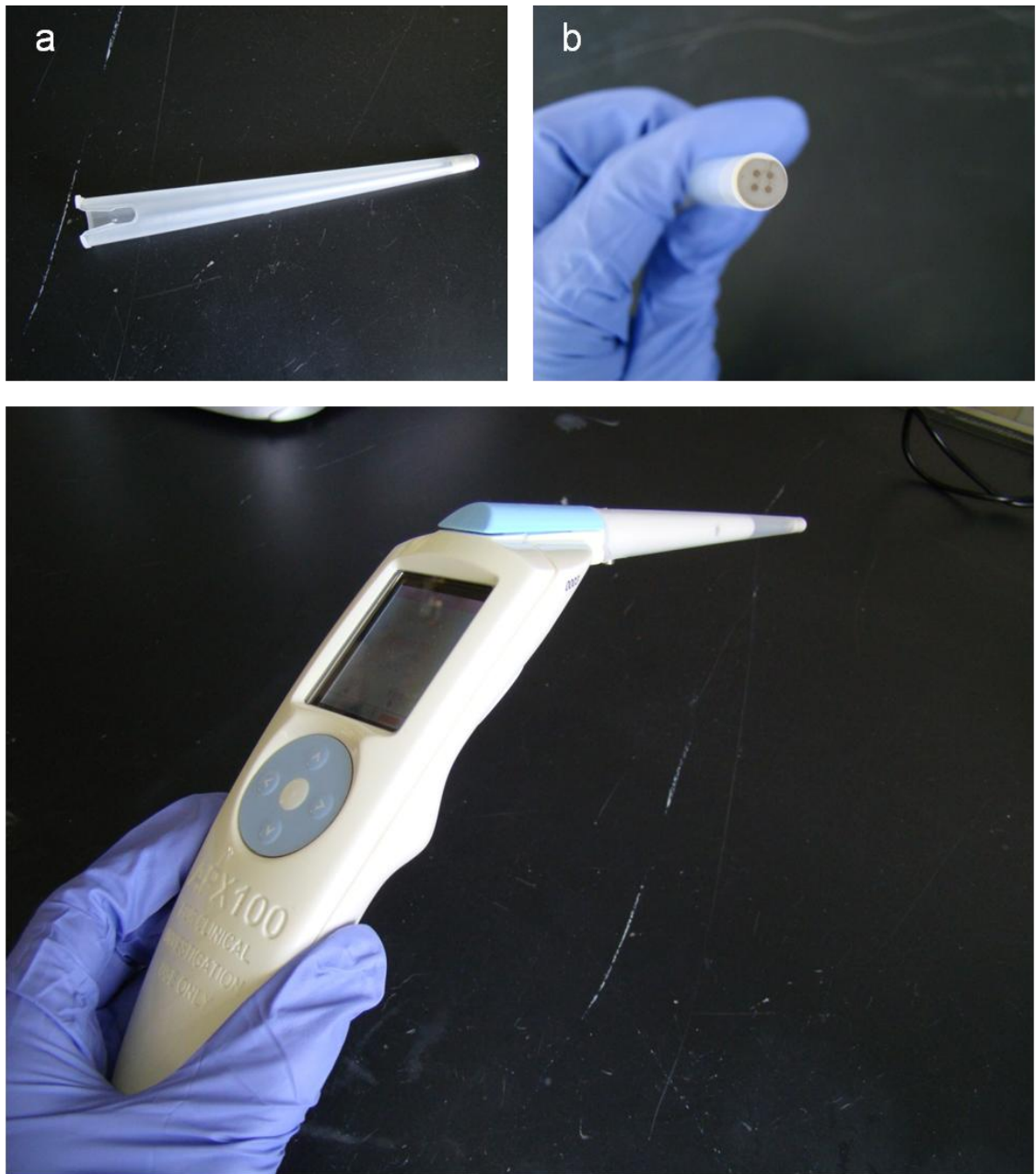
Figure 4.4 Impedance spectroscopy device.
(a) Disposable tip, (b) end of disposable tip (electrodes), (c) the hand held impedance spectroscopy device.

OCT Device	Optovue® (RTVue®)	TD OCT 1.25 μm system	FDOCT	MD SS-OCT^
Time domain or Fourier domain	Fourier domain	Time domain	Fourier domain	Fourier domain
Wavelength of light source	840nm ±10nm	1250nm	800nm	1305nm ±15nm (Sweep range 150nm)
Type of light source	In-built light source	SLED #	Broadlighter D890-HP, Superlum, Russia	Santec HSL-2000-10 wide sweep laser
OCT device commercially available	From Optovue Inc. (Fremont, CA, USA)	No	No	Parts available from Michelson Diagnostics
Number of scans averaged for final image	10	1	1	5
A-scans/ second	26,000	80	1000	10,000
Depth (axial) resolution in tissue	5μm	9 μm	5-6 μm (with 2x SLED 2-3um)	10μm
Transverse resolution	15μm	17 μm	17 μm	25μm
Depth in TEOM*	~500μm	~850μm	~500μm	~850μm
Scan length	6mm	3mm	2mm	4mm

* Estimated depth calculated from images obtained for this project

^ MD SS-OCT = Michelson Diagnostics Swept Source Optical Coherence Tomography

 # SLED = Superluminescent Light Emitting Diode (Produced in EPSRC Centre for III-V technologies, Sheffield)

Table 4.2
Specifications for OCT devices used in this project.

4.4   Results

Using C_{12} –resazurin to detect areas of dysplasia and carcinoma *in situ*.

Can Cancer and dysplastic cell lines be distinguished from normal oral cells in cell monolayers using a metabolic activity marker?

A Vybrant™ cell metabolic assay kit with C_{12} –resazurin (Molecular probes, Invitrogen, Paisley, UK) was used to measure the metabolic activity of a number of different cells (primary normal cells, dysplastic cells and cancer cell lines) in monolayer culture. The active ingredient of Vybrant™ cell metabolic assay kit is resazurin, a non-fluorescent, non-toxic molecule which can be reduced by metabolically active cells. The reduced product, resorufin, can be detected using fluorescence (excitation 530nm, emission 590nm). The resazurin used here is a lipophilic C_{12} –resazurin which exhibits better cell retention and shorter exposure times compared to resazurin without the carbon chain, commonly known as alamarBlue® (AccuMed International, Inc.) (Probes 2001). The different cell types were all exposed to C_{12} –resazurin for 15 minutes and the intensity of resorufin fluorescence was imaged using CLSM. Figure 4.5 shows representative images of the different cell lines and primary cells post C_{12} – resazurin exposure.

Figure 4.6 shows the median intensity of fluorescence resulting from the different cell types cultured in monolayers. Figure 4.6 (a) shows that the cell lines PE/CA-PJ34, SCC9, SCC25, D20 and D19 had a statistically higher median fluorescence compared to NOK cells. The highest fluorescence was shown by the dysplastic cell lines D19 and D20 implying these cells were the most metabolically active. The Cal27 cell line showed statistically lower median fluorescence compared to the NOK cells and the FaDu cells were similar to NOK. When compared to NOF (Figure 4.6b) all cell lines except Cal27, FaDu, SCC4, PE/CA-PJ34 and DOK showed significantly higher fluorescence and therefore had an increased metabolic rate compared to NOF. However, while these results achieved statistical significance (due to the high n number) the extent of the difference in fluorescence intensity between the different cell lines was small.
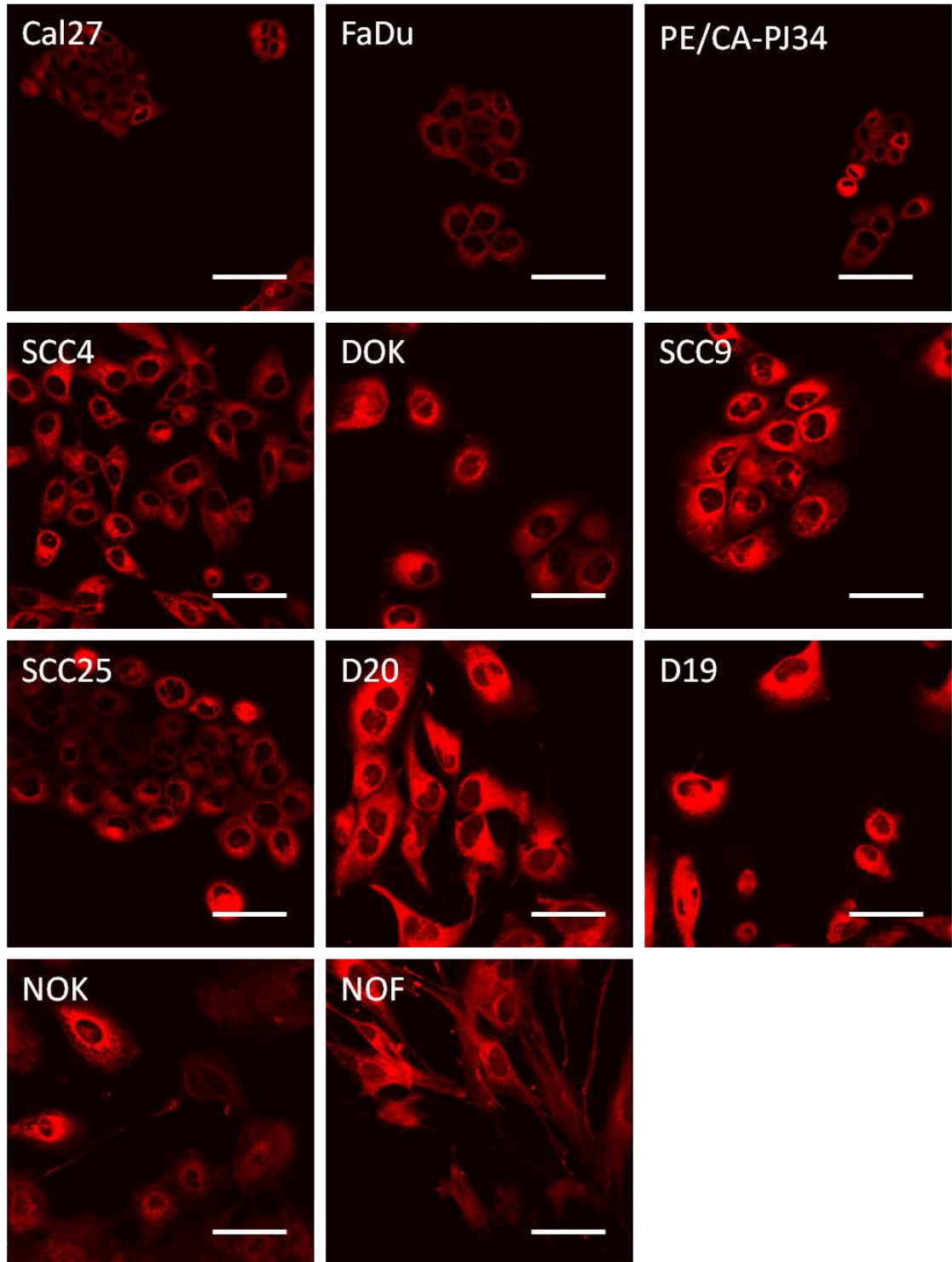
Figure 4.5 Representative images of cell lines and primary cells exposed to C$_{12}$ -resazurin. Scale bar= 50µm. n=2
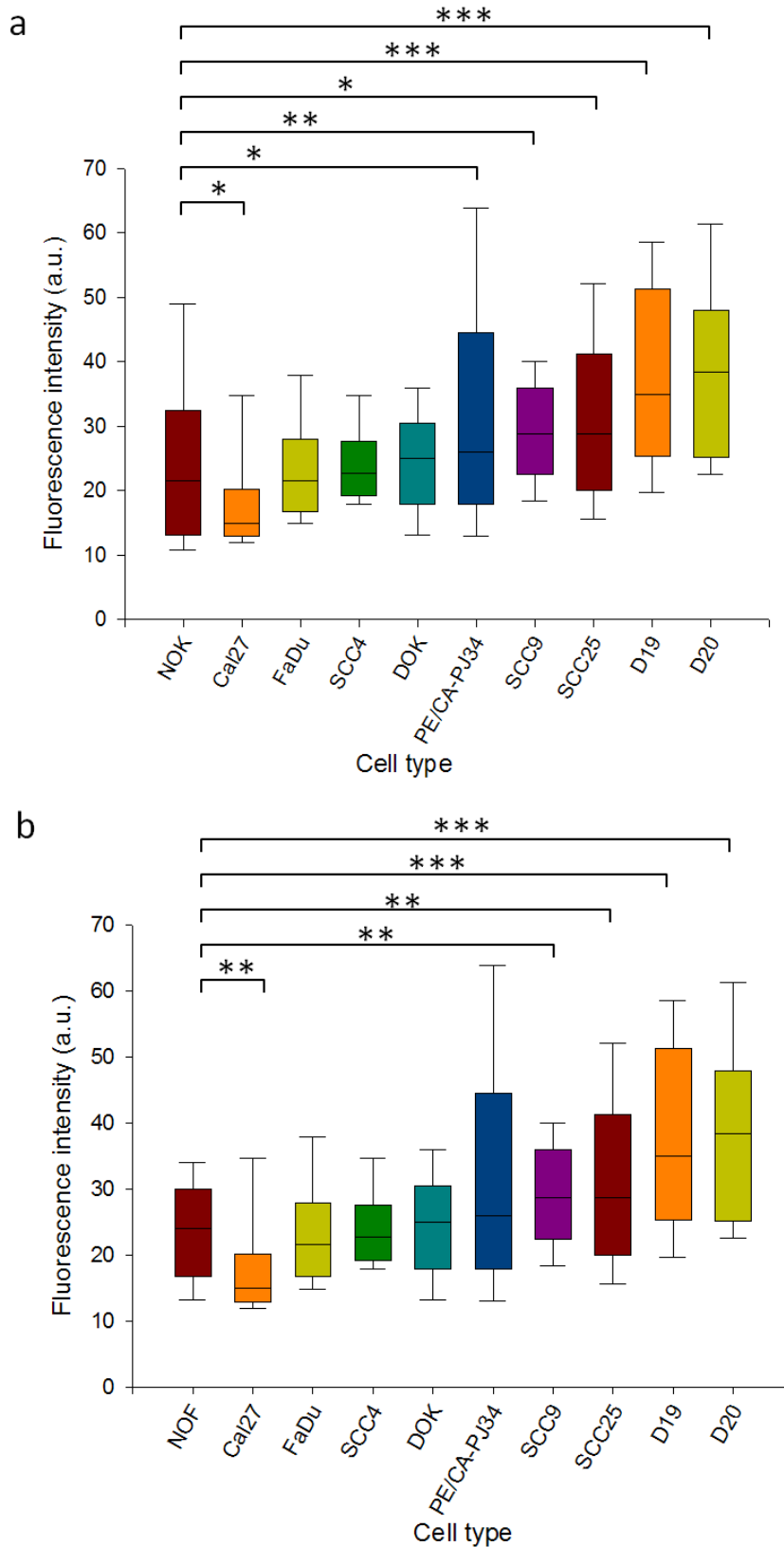
Figure 4.6 Median fluorescence of different cell types exposed to C12-resazurin compared to NOK (a) and compared to NOF (b). Box plot shows data between 25th and 75th percentiles. Error bars show 10th and 90th percentiles. * = p<0.05, **= p<0.01, ***= p<0.005. n=2

Detecting regions of Carcinoma *in situ* and dysplasia in TEOM using a cell metabolic activity indicator

Three different 3D tissue engineered models were used here as models to test if the C_{12} − resazurin cell metabolic activity marker could be used to detect regions of carcinoma or dysplasia within an epithelia. Histology for each of these models is shown in Figure 4.7.
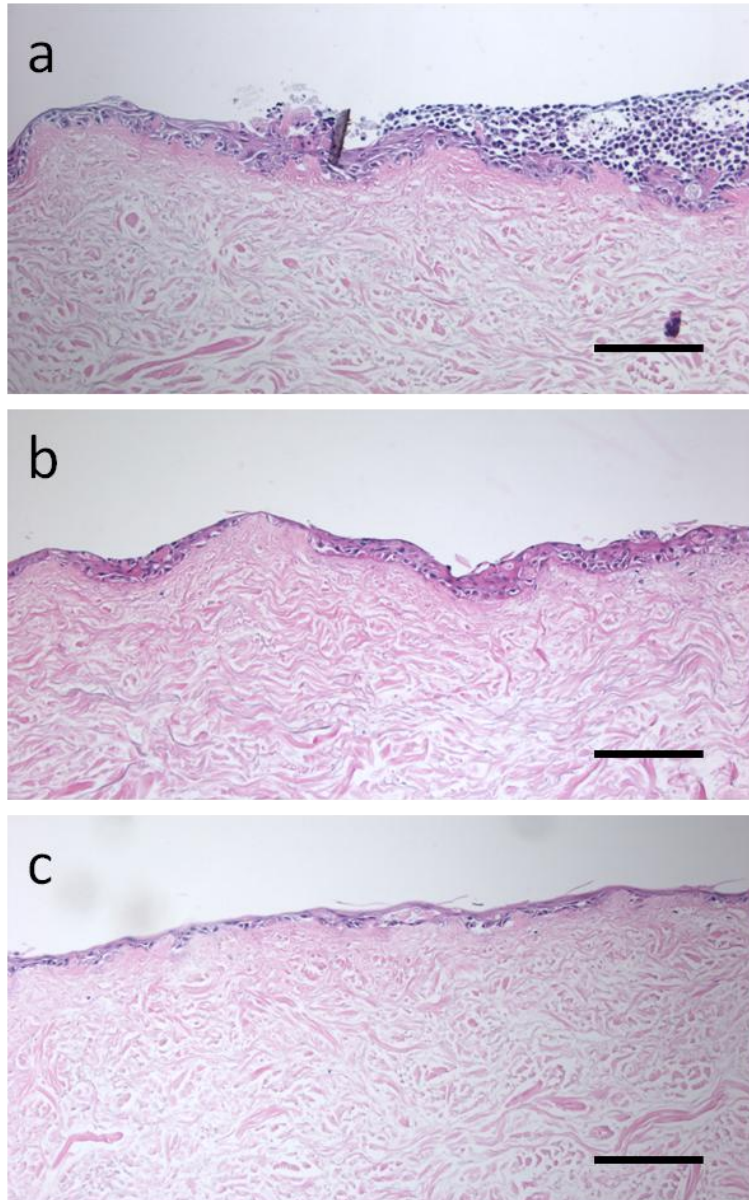
Figure 4.7 Histological appearance of 3D models used to test the ability of C_{12}- resazurin to detect regions of cancer within tissue engineered models.
(a) MCTS + TEOM, region with MCTS on the right, normal mucosa on the left. (b) DOK + TEOM epithelium comprised of both NOK and DOK cells. (c) TEOM (note: epithelium thinner compared to previous chapters as cultured for shorter time at ALI). n=3. Scale = 200μm

The first model was the MCTS + TEOM model which comprised of a healthy epithelium with regions of carcinoma *in situ*. This model was made by culturing FaDu MCTS on the surface of the TEOM once the TEOM was raised to ALI. This model of carcinoma *in situ* had healthy regions of mucosa adjacent to areas which resembled carcinoma with necrosis and abnormal cell morphology (Figure 4.7) also described in (Colley *et al.,* 2010). The second model was DOK+ TEOM. This model was initially cultured the same way as the TEOM model; however, after 3 days at ALI dysplastic DOK cells which had been previously labelled with CellTrace™ were added to the models. As a healthy control the TEOM model of healthy epithelium was used.

Figure 4.8 shows representative slices from a CLSM *z*-stack of images for each of the different models after they had been exposed to C_{12}- resazurin for 15 minutes. The three different models showed different patterns of fluorescence when imaged using CLSM (Figure 4.8). The areas which contained the FaDu MCTS had a dense distribution of cells which was distinct from the regions of NOK cells. The DOK cells were labelled with CellTrace™ so could be distinguished from the NOK cells using fluorescence in the far red range. The appearance of these cells was in many cases different to the NOK cells but both cell types were interspersed in this model. Figure 4.8 demonstrates the difference in the appearance of the TEOM exposed to C_{12}- resazurin at the upper most surface (d) and deeper into the epithelium (c).

Differences in nuclear morphology and nuclear to cytoplasmic ratios could also be seen using CLSM. The TEOM had an even distribution of fluorescence throughout the cell cytoplasm with dark regions where the nuclei were, in all but the most superficial slices which appeared spotty. There were fewer nuclei per field of view and the area of each cell was large when compared to the FaDu and DOK cells in the other models. The upper most surface of the models showed the characteristic pattern seen in Figure 4.8 (d) when the TEOM had been cultured for over a week. This pattern was not seen in the models cultured for less than 1 week where the cells were less differentiated.

When the images from the three models were quantified (Figure 4.9) the normal oral mucosa models (TEOM) showed a statistically higher (p< 0.001) fluorescence signal after C_{12}- resazurin exposure compared to the DOK + TEOM models and the MCTS + TEOM models. The models with cancer cells present were approximately 30% less fluorescent than the control model of healthy oral mucosa.
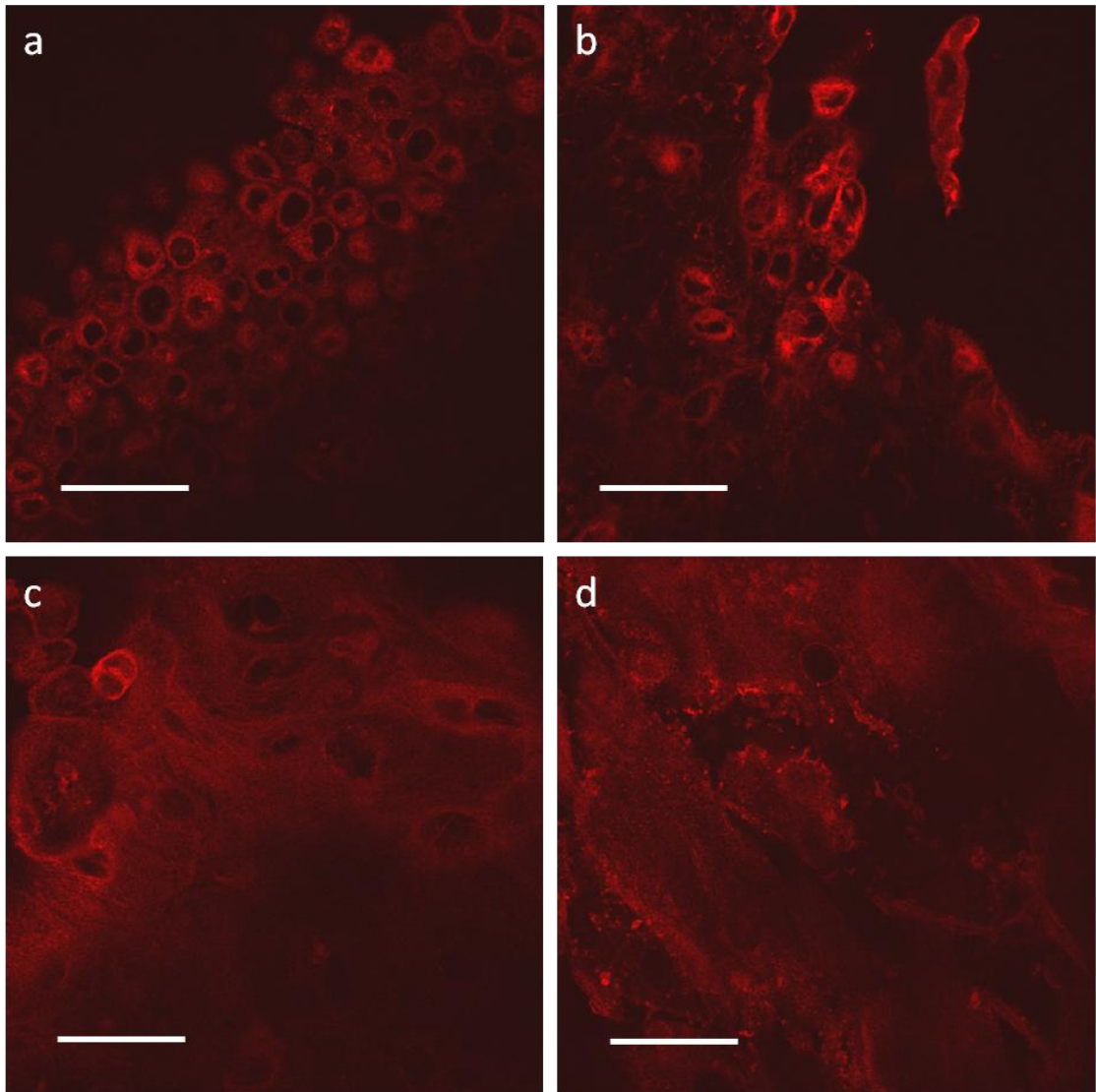
Figure 4.8 Representative images of 3D models exposed to C_{12}- resazurin imaged using CLSM.
Red = resorufin fluorescence from metabolically active cells. Models exposed to C_{12}-resazurin for 15 minutes (a) MCTS + TEOM, (b) DOK + TEOM. (c) Shows TEOM ~20- 30μm deep (d) shows most superficial surface of TEOM. Scale bar =50μm. n=3
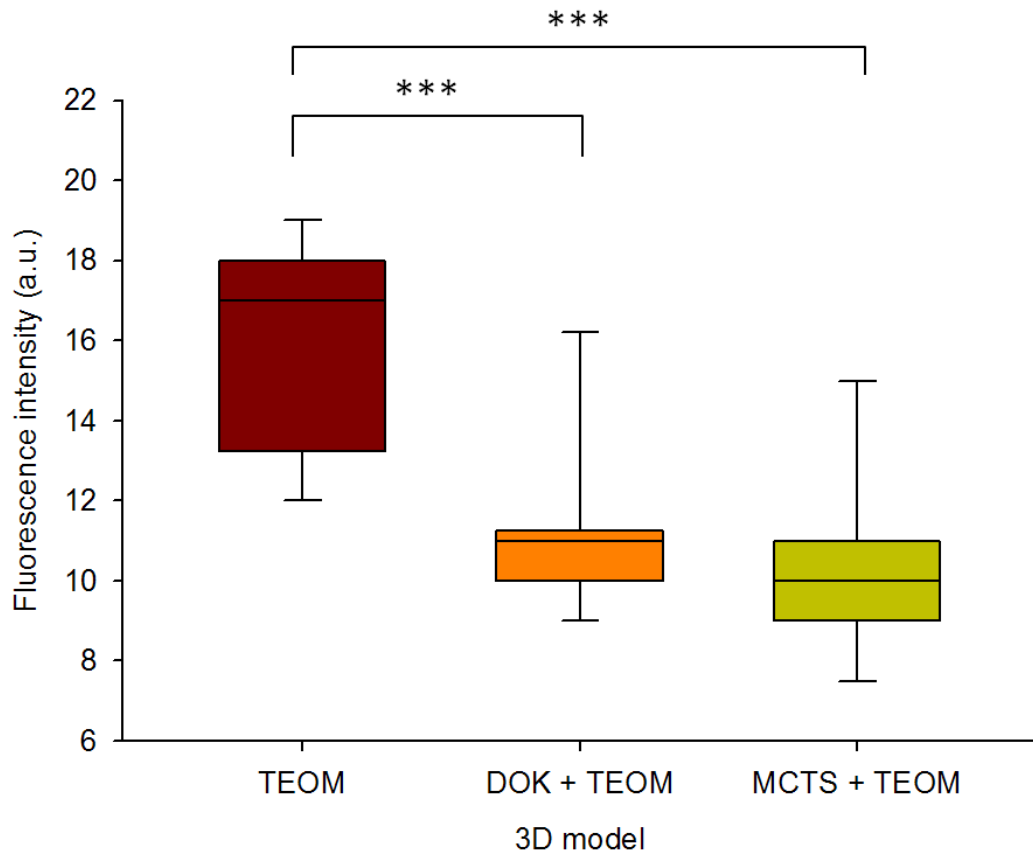
Figure 4.9 Median intensity of resorufin fluorescence.
Resorufin is a marker of cell metabolism. TEOM = Tissue engineered oral mucosa, model of healthy epithelium. DOK + TEOM = model of dysplasia, MCTS + TEOM = model of Carcinoma *in situ*. *** = p< 0.001. Error bars = s.d. n=3.

Impedance spectroscopy: TEOM vs cancer models

Tissue engineered models cultured from five different cancerous or dysplastic cell lines were cultured for at least 7 days at ALI before their impedance values were measured. The histology of these models can be seen in Figure 4.7 on page 185.

The models cultured from cancer cell lines on DED were compared to DED alone and TEOM cultured with normal oral keratinocytes. The average impedance measurements are shown in Figure 4.10. The impedance values at different frequencies were relatively similar for all models except the TEOM. De-epidermised dermis (DED) demonstrated the lowest impedance to the current applied, as would be expected since impedance is created as the electrical current is impeded by the cells. The models cultured from the PE/CA-PJ34 cell line showed the highest impedance, with FaDu also showing slightly higher impedance compared to the other models. No significant differences were seen between the TEOM and the cancer cell models as the variation between measurements, even on the same model, were large (standard deviations, not shown on graph for clarity, but were in some cases over 100 Ohms).
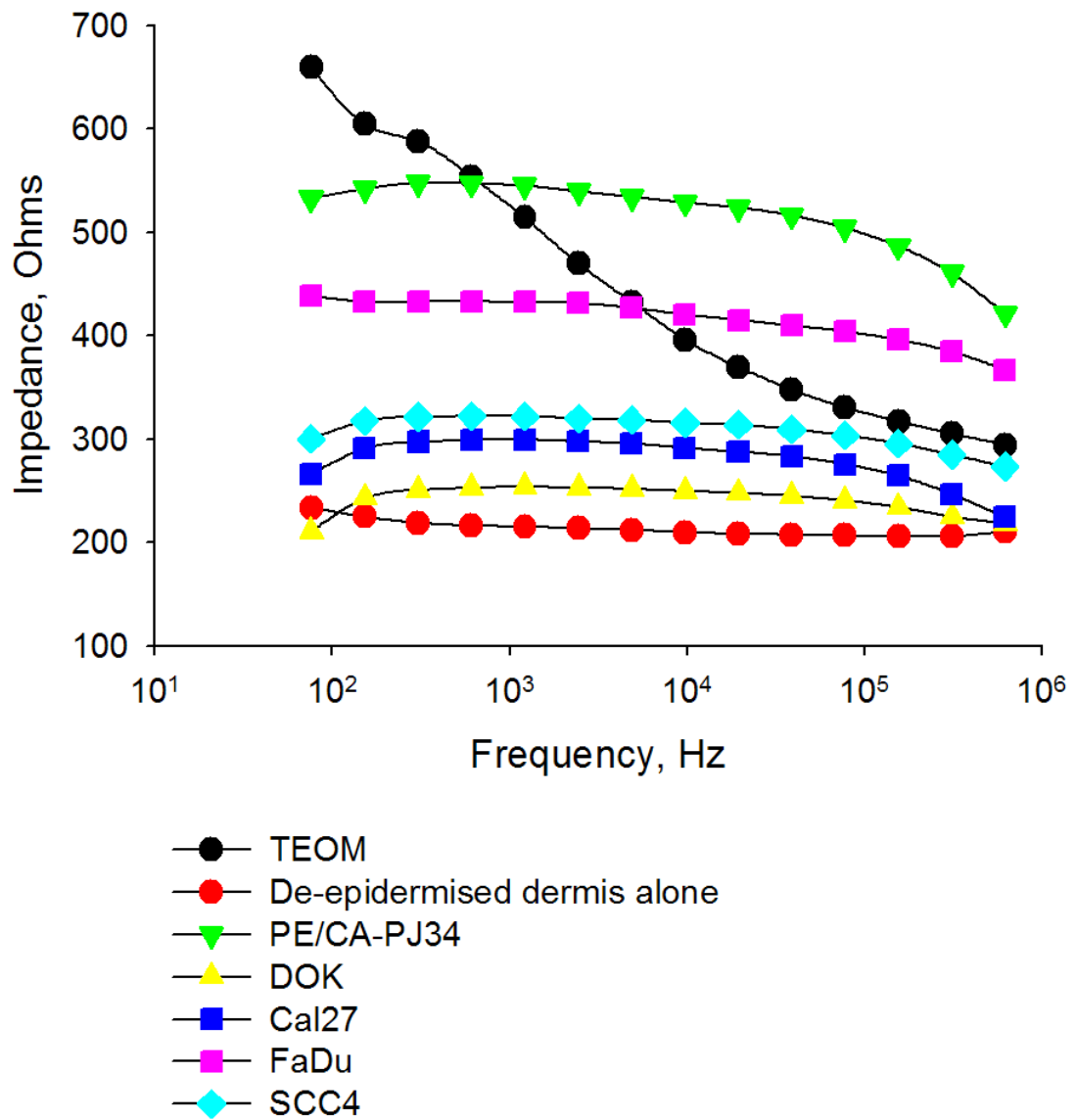
Figure 4.10 Comparison of difference impedance values from different tissue engineered models cultured from normal cells and cancer cell lines on DED. n=1 for all except TEOM n=5.
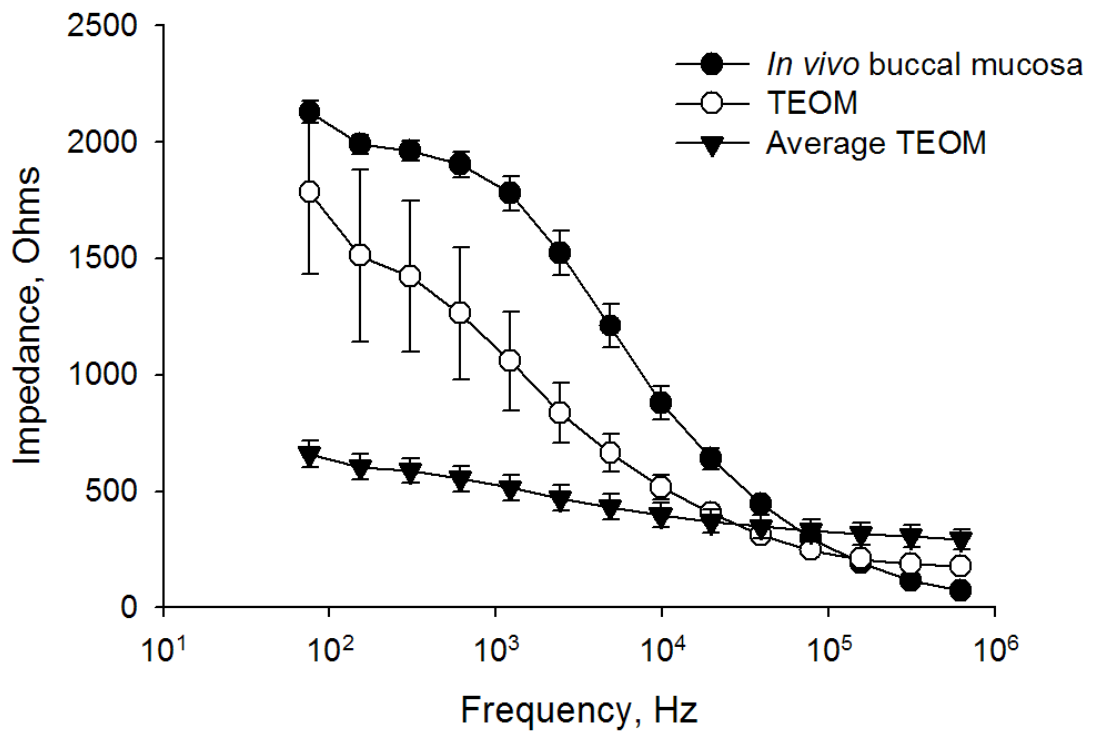
Figure 4.11 Comparison of impedance from TEOM and *in vivo* buccal mucosa.
White circles show one measurement taken, black triangles show the average of all TEOM readings.   Error bars = s.d.

Impedance spectroscopy: TEOM vs *in vivo* buccal mucosa

Figure 4.11 shows the impedance values for the average of all TEOM models (black triangles). The black circles show the impedance values obtained from *in vivo* measurements of a healthy buccal mucosa. There is a large difference in the values obtained from the tissue engineered models and the naturally occurring tissue.   The white circles show the readings from one TEOM model.   The data obtained here were more similar to the values obtained *in vivo* however, this result was not reproducible.

In vivo impedance measurements
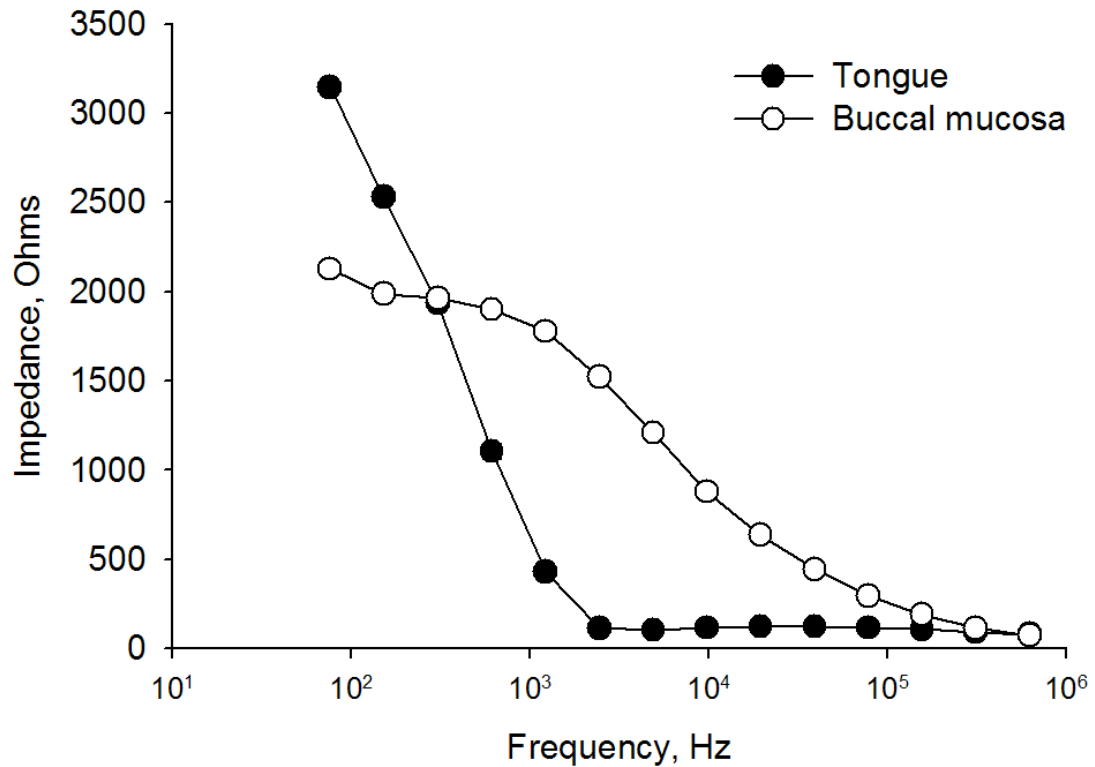
Figure 4.12 *In vivo* impedance measurements of buccal mucosa and tongue. Average of 16 readings from one volunteer. n=1

Impedance spectroscopy: Buccal mucosa vs tongue *in vivo*

Impedance was measured on the tongue and the buccal mucosa of a healthy volunteer. The impedance values obtained from a single healthy volunteer varied depending on the area of the mouth the measurement was obtained from (Figure 4.12). For example the impedance value at 2.4 kHz is 114 Ohms for the tongue and 1522 Ohms for buccal mucosa. Differences can be seen at almost all frequencies except for measurements at 300Hz and at the highest frequencies. The variation between measurements from the same region of the mouth was very small although it should be noted this data was from only one volunteer. There may be person to person variation.

FTIR on models of OSCC

The FTIR spectra obtained from sections of four different tissue engineered models are shown in Figure 4.13. MirrIR slides mounted with tissue sections were exposed to MidIR radiation (500-4000 cm^{-1}). The four different models showed some areas of commonality, representing bonds found in our models of healthy, precancerous and cancerous tissues. However, there were however, areas of each spectra which differed between samples. The following peak assignments from Movasaghi *et al*., have been used to determine the bonds which are represented by each peak (Movasaghi *et al.,* 2008). The main peaks discussed here are listed in Table 4.3, for a full list of all bonds and their respective wavenumbers see (Movasaghi *et al.,* 2008).

Wavenumber (cm^{-1})	Band representation
1238	Amide III
1240	Amide III
1337	Collagen CH$_2$ wagging
1403	CH$_3$ of collagen and of methyl groups of proteins
1455	Methyl groups of skeletal proteins CH$_3$ of proteins C-O-H
1462	Paraffin
1470	CH$_2$ in lipids
1549	Amide II
1644	Amide I
2848	Cholesterol, phospholipids, creatine
2916	Cholesterol, phospholipids, creatine
2955	CH
3200-3500	Water

Table 4.3
Peak assignments of the FTIR spectroscopy bands used in this study (Movasaghi *et al.,* 2008).
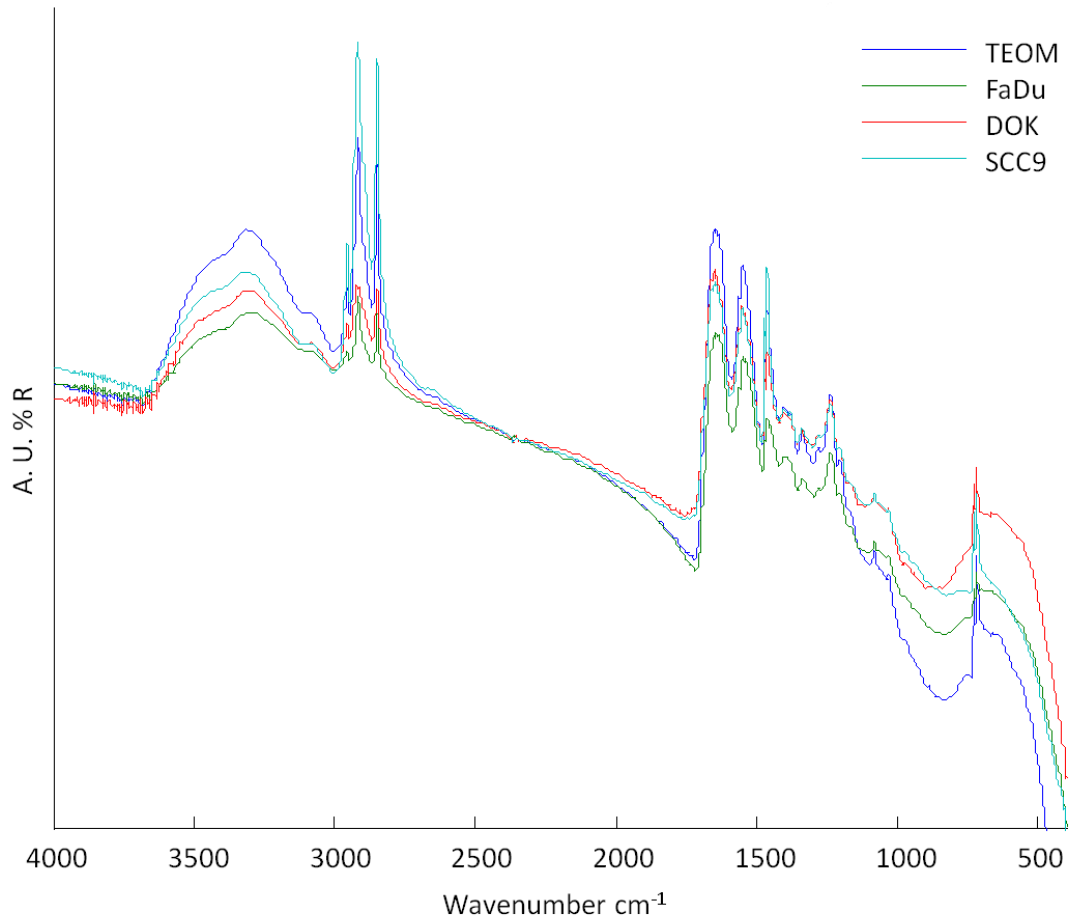
Figure 4.13 Average FTIR spectra of four different tissue engineered models TEOM, FaDu, DOK and SCC9, aligned according to commonalities. n=2
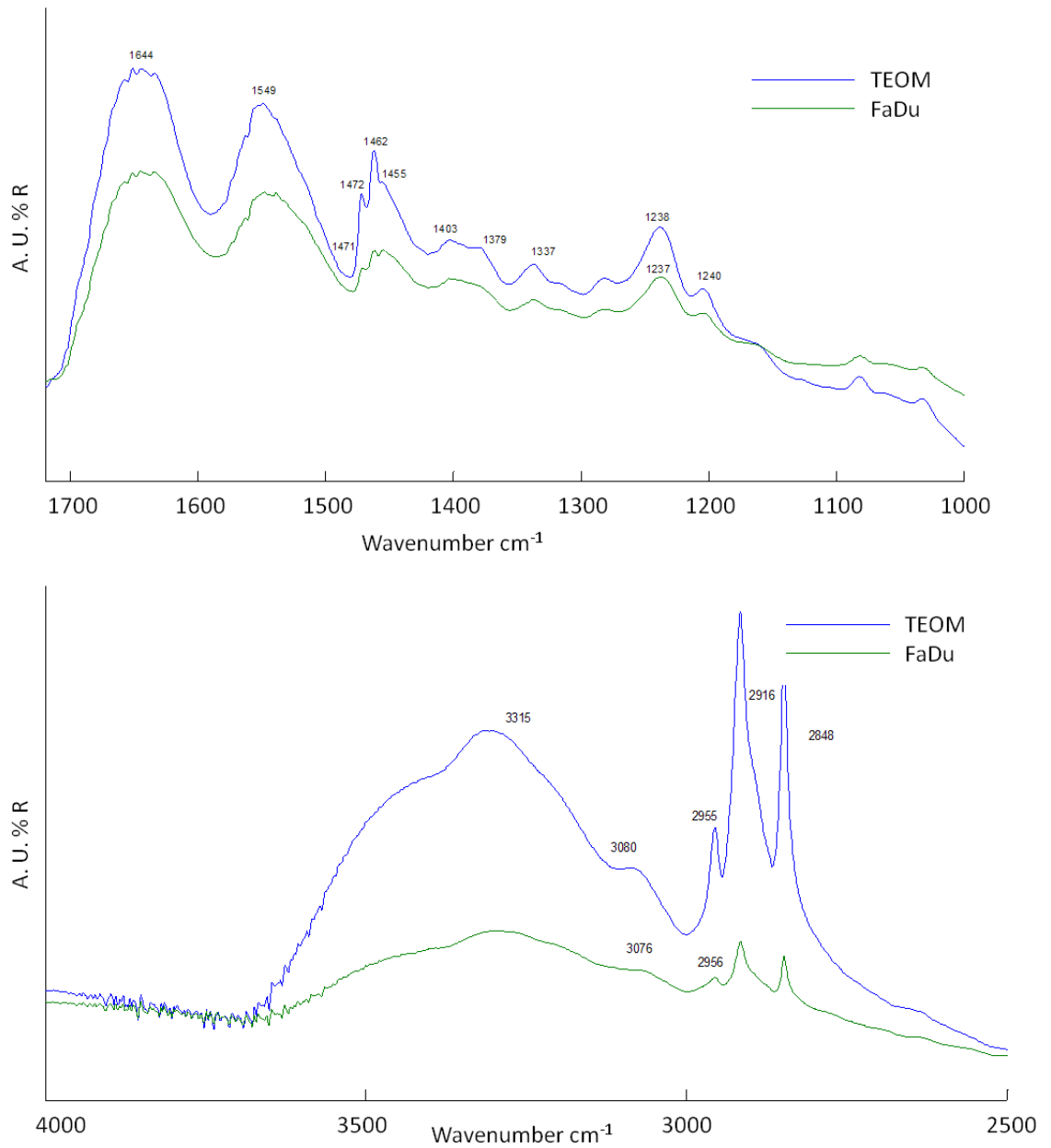
Figure 4.14 Comparison of FTIR spectra resulting from TEOM and FaDu models. (No peaks visible between 1700 and 2500 cm^{-1}).
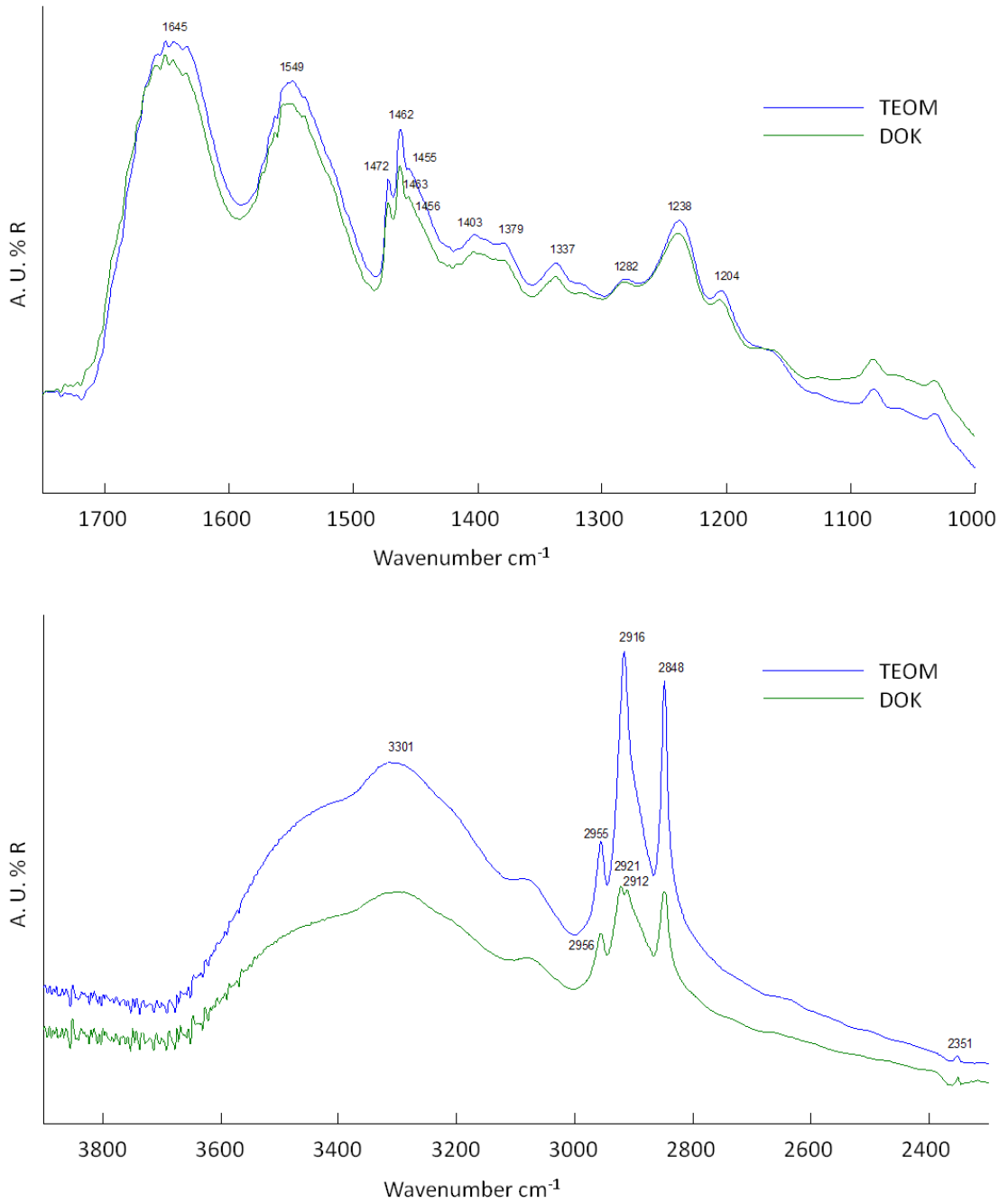
Figure 4.15 Comparison of FTIR spectra resulting from TEOM and DOK models.
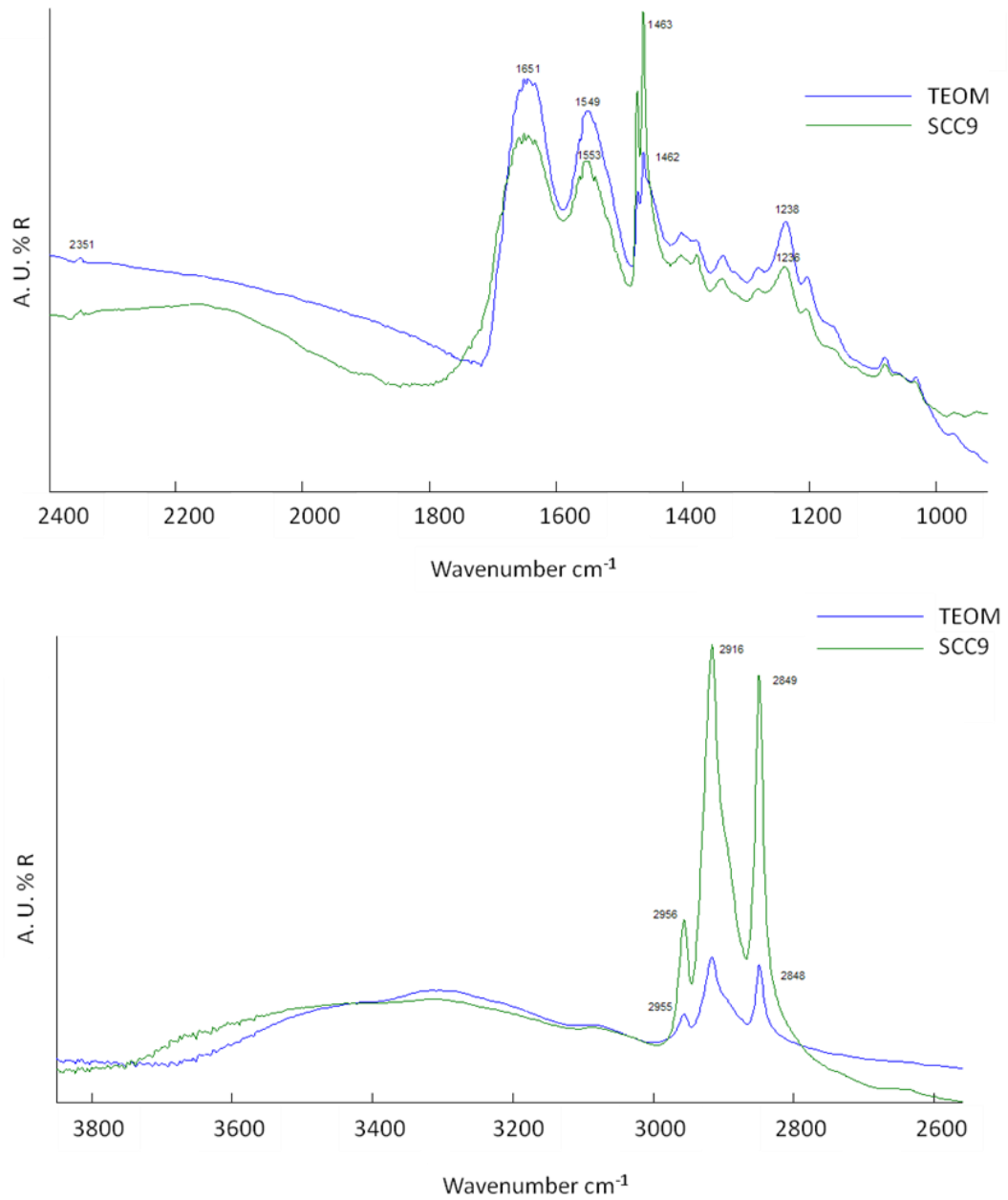
Figure 4.16 Comparison of FTIR spectra resulting from TEOM and SCC9 models

Figure 4.14 compares the spectra from TEOM models and the models of OSCC cultured with FaDu cells. For images of the histological appearance of these models see Figure 2.3 and Figure 2.13. Comparing the spectra resulting from analysis of the TEOM and the model cultured with FaDu cells (Figure 4.14) reveals several differences in specific peaks. The peak at 2955 cm^{-1} which corresponds to a C-H bond was far more pronounced in the TEOM compared to the FaDu model. The peaks at 2916 cm^{-1} and 2848 cm^{-1} were also more pronounced in the TEOM; these bonds correspond to stretching vibrations of CH_2 and CH_3 bonds found in cholesterol, phospholipids and creatine. Peaks at 1644 cm^{-1}, 1549 cm^{-1}, 1238 cm^{-1} and 1240 cm^{-1} (representing amides) were all more pronounced in the TEOM spectra compared to the FaDu model. Peaks at 1644cm^{-1} and 1549cm^{-1} corresponding to amide I and amide II respectively, were higher in the TEOM model compared to the FaDu model's spectra.

Comparing the spectra of TEOM and spectra from the models cultured with DOK cells (Figure 4.15), showed very similar peaks in the 1000 cm^{-1} and 1700 cm^{-1} range. However, the peaks at 2916 cm^{-1} and 2848 cm^{-1}, both corresponding to cholesterol, phospholipids and/or creatine were elevated in the TEOM model compared to the DOK model (the same trend was seen for the FaDu model). Peaks at 1644cm^{-1} and 1549cm^{-1} corresponding to amide I and amide II were also slightly higher in the TEOM. There was a 1cm^{-1} shift although this may be due to the detection accuracy of the machine rather than a change in the bonds present.

The spectra from the SCC9 models (Figure 4.16) showed the opposite trend with higher peaks at 2916 cm^{-1} and 2848 cm^{-1} compared to the TEOM implying there were higher levels of cholesterol, phospholipids and or creatine in the SCC9 model than were in all the other models. There was also a larger peak at 2955/6 corresponding to the C-H bond.

The region between 3000 and 3500 cm^{-1} varied between spectra however, this region is affected significantly by water so it was not analysed. The peak at 1462 cm^{-1} corresponds to paraffin.

OCT on models of OSCC

The ability of optical coherence tomography (OCT) to non-invasively image tissue engineered models of healthy oral mucosa and OSCC was next investigated. Four different OCT systems were tested and their ability to clearly image beneath the surface of the epithelium was compared. Details of the four different OCT systems and their specifications can be found in Table 4.2. The tissue engineered models used were cultured as described in chapter 2. Figure 4.17 gives a brief guide to interpreting OCT images.

Figure 4.18 shows the SCC9 model imaged with all four systems. All four systems showed a distinct difference between the epithelium and the connective tissue and showed the topography of the surface of the models. The MD SS-OCT and TD-OCT systems were able to

obtain a signal from deeper into the tissue compared to the other two systems as these systems had a higher wavelength light source compared to the FD-OCT and the Optovue® systems. Non-homogenous human tissues such as the oral mucosa exhibit high light scattering properties, reducing the depth of penetration of light. Light of longer wavelengths is able to penetrate further into tissues as it experiences less scattering, this is why near IR light is used for OCT devices. Axial resolution was best when using the FD-OCT and Optovue® systems and clearer images of the epithelial/connective tissue junctions could be obtained. By averaging several images the signal:noise ratio could be increased, as demonstrated in the Optovue® system images where 10 scans were averaged. Due to relative similarities in images obtained with the different systems and the ongoing development of the TD-OCT and the FD-OCT systems, it was decided that only the Optovue® system and the SS-OCT would be used for the remainder of the project.

Reflection from liquid on the surface of the tissue engineered model

Dark region likely to relate to epithelial-connective tissue junction

Depth of tissue where signal is no longer strong enough to be detected

Grid on which the models are cultured (surgical stainless steel)
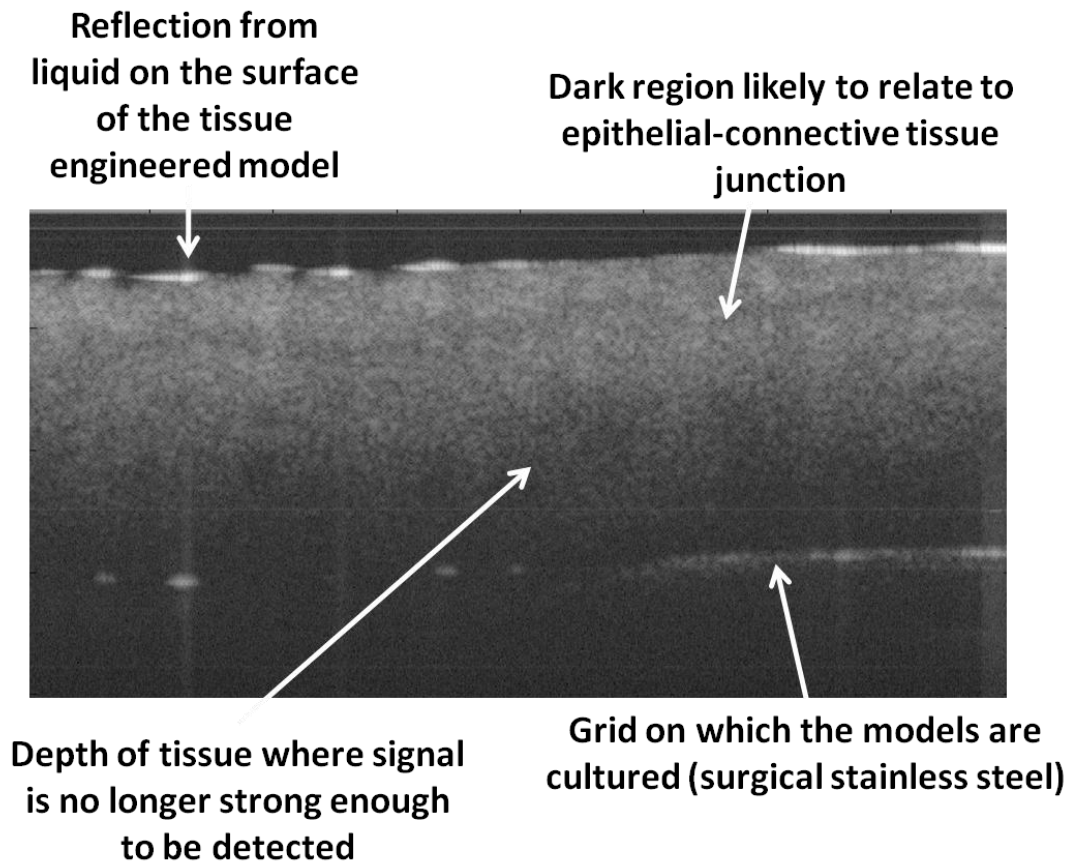
Figure 4.17 A guide to interpreting OCT images.
Grey scale images were obtained on all OCT systems. White spots on the surface result from reflection of liquid on the surface. The whitest signals result from the areas of tissues which reflect the greatest amount of light. Different shades of grey come from tissues with different light scattering and reflection properties. The black areas show where no signal can be obtained. Image 4mm x 2mm

OCT images of TEOM and OSCC

Six different tissue engineered models were imaged using OCT. OCT images obtained from the SS-OCT system and the Optove® system for all 6 models are shown and compared to the histology of the corresponding model (Figure 4.19 to Figure 4.24). All figures show representative images. The experiment was repeated between 1 and 3 times, depending on the model and the OCT device.
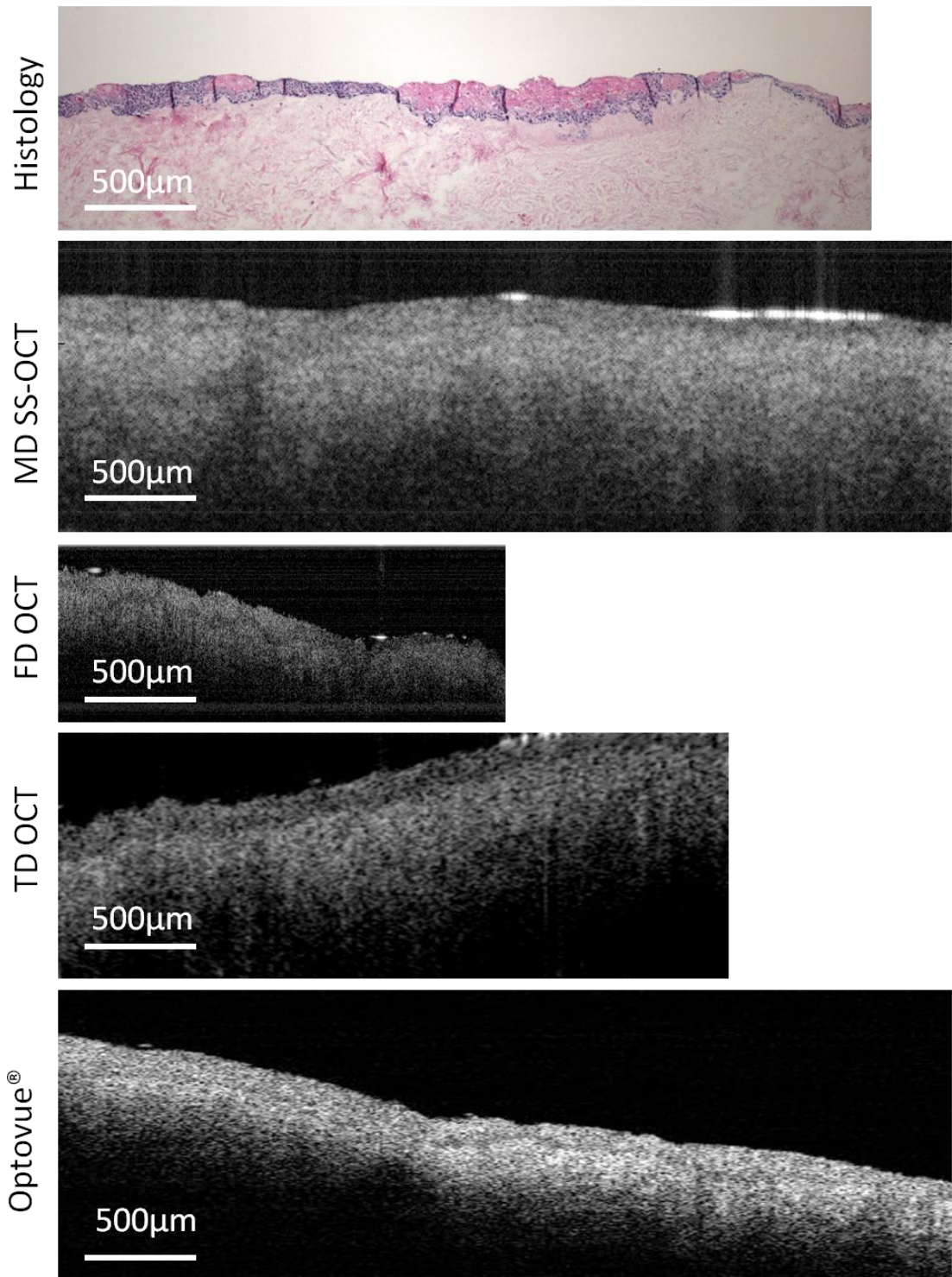
Figure 4.18 OCT images of 3D model cultured from SCC9 cells for 3 weeks at ALI resulting from four different devices, compared to histology.
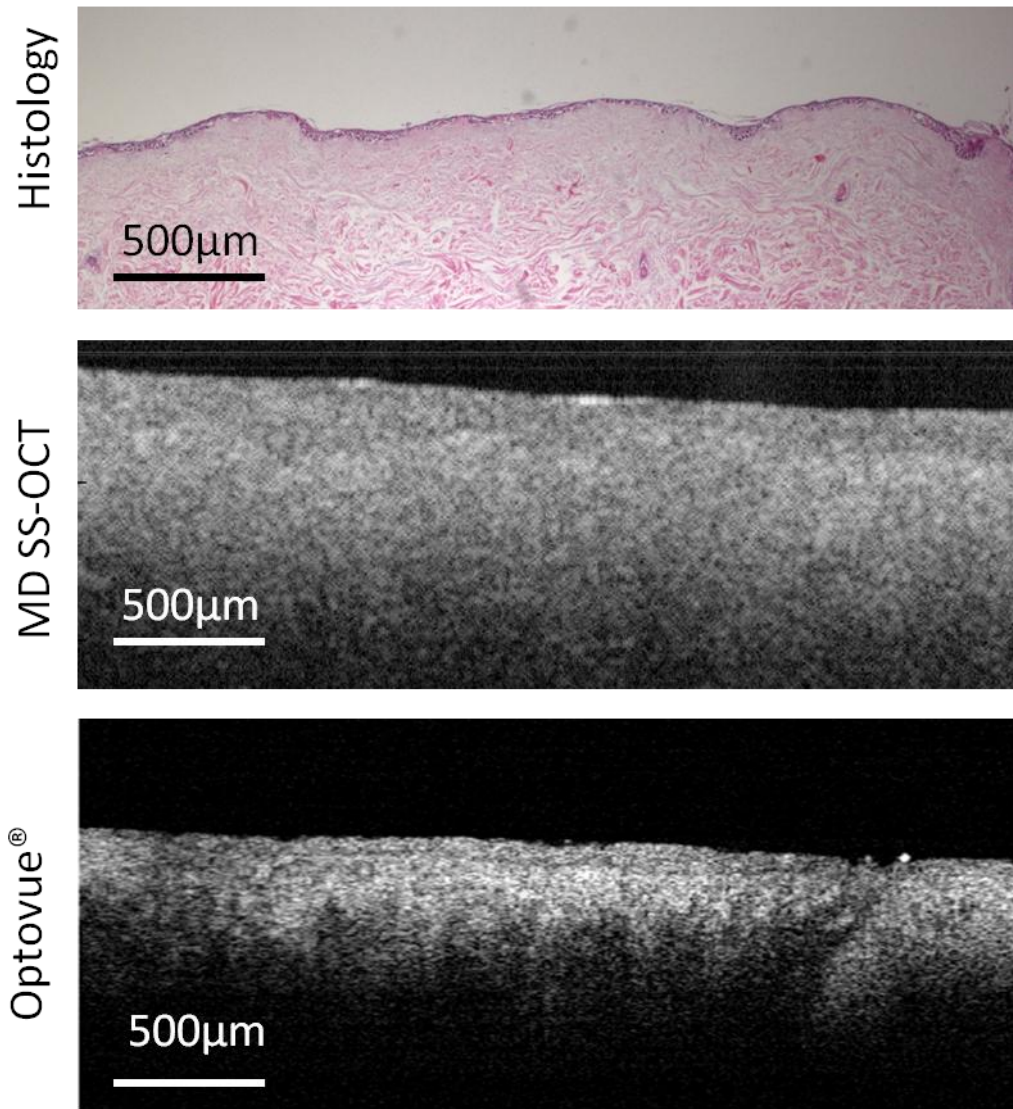
Figure 4.19 OCT image of TEOM.
NB images are from different areas on the model.

TEOM

Figure 4.19 shows the TEOM imaged using OCT. Unfortunately, the models cultured during the time of these experiments had a relatively thin epithelium compared to models cultured at other times. Despite this the epithelium was still able to be distinguished from the connective tissue. The images from both OCT systems clearly show the epithelial connective tissue junction in the models. The epithelium is darker compared to the underlying connective tissues implying that the level of light reflected and scattered from the epithelium is less than for the connective tissue. The epithelium appears thinner in the histology image. However, it should be remembered that samples shrink (around 30%) during histological processing. The image from the Optovue® system gives better resolution and less noise compared to the SS-OCT system.
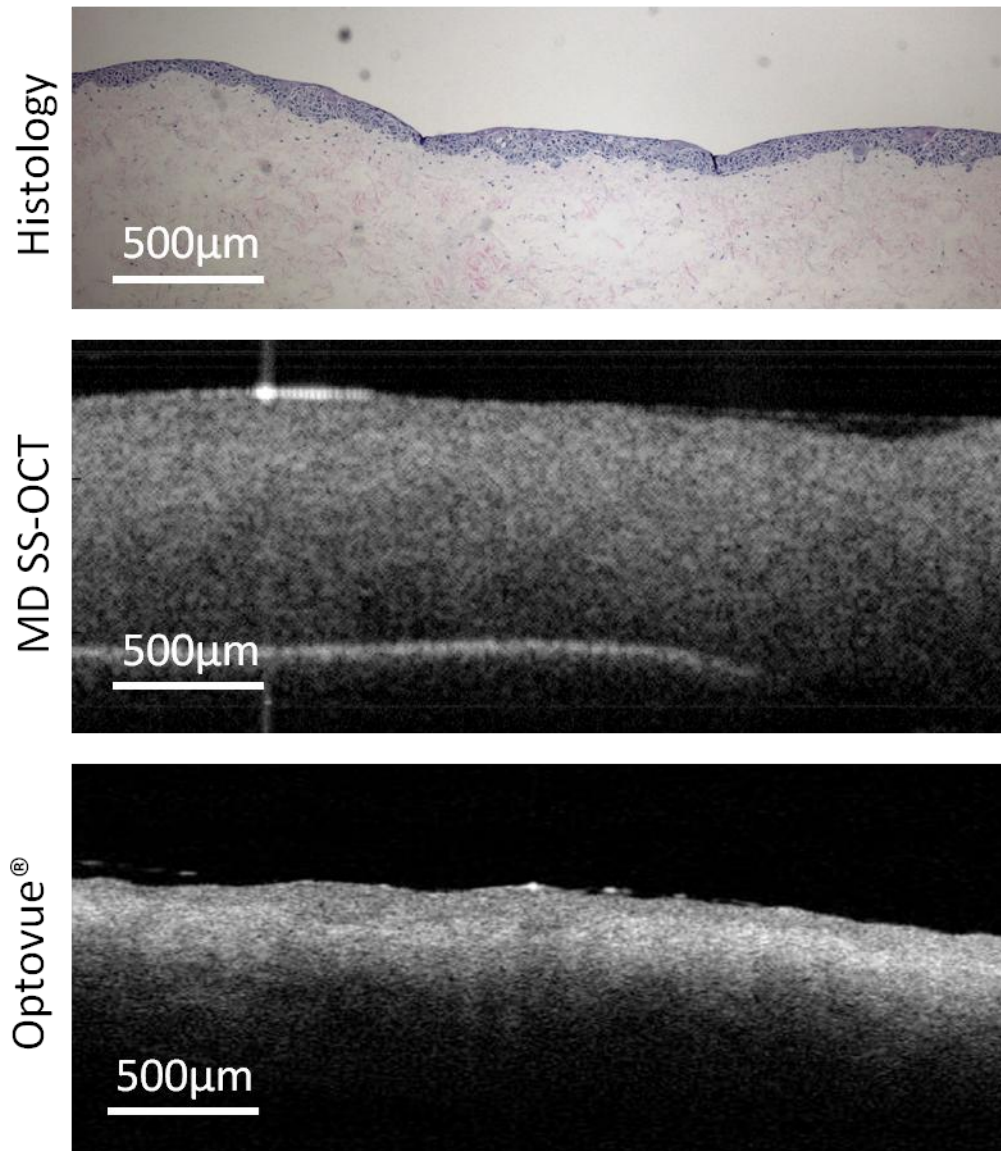
Figure 4.20 OCT image of DOK model

DOK

The epithelial connective tissue junction is clearly visible in the image of the DOK model obtained from the Optovue® system but it is difficult to distinguish a clear boundary between the epithelium and the connective tissue in the SS-OCT image (Figure 4.20). The SS-OCT image has a dark superficial region which probably corresponds to the epithelium. In the Optovue® image the axial resolution is better giving more detailed information regarding epithelial connective tissue junction morphology. As with the TEOM, the epithelial region appears darker than the underlying connective tissue.
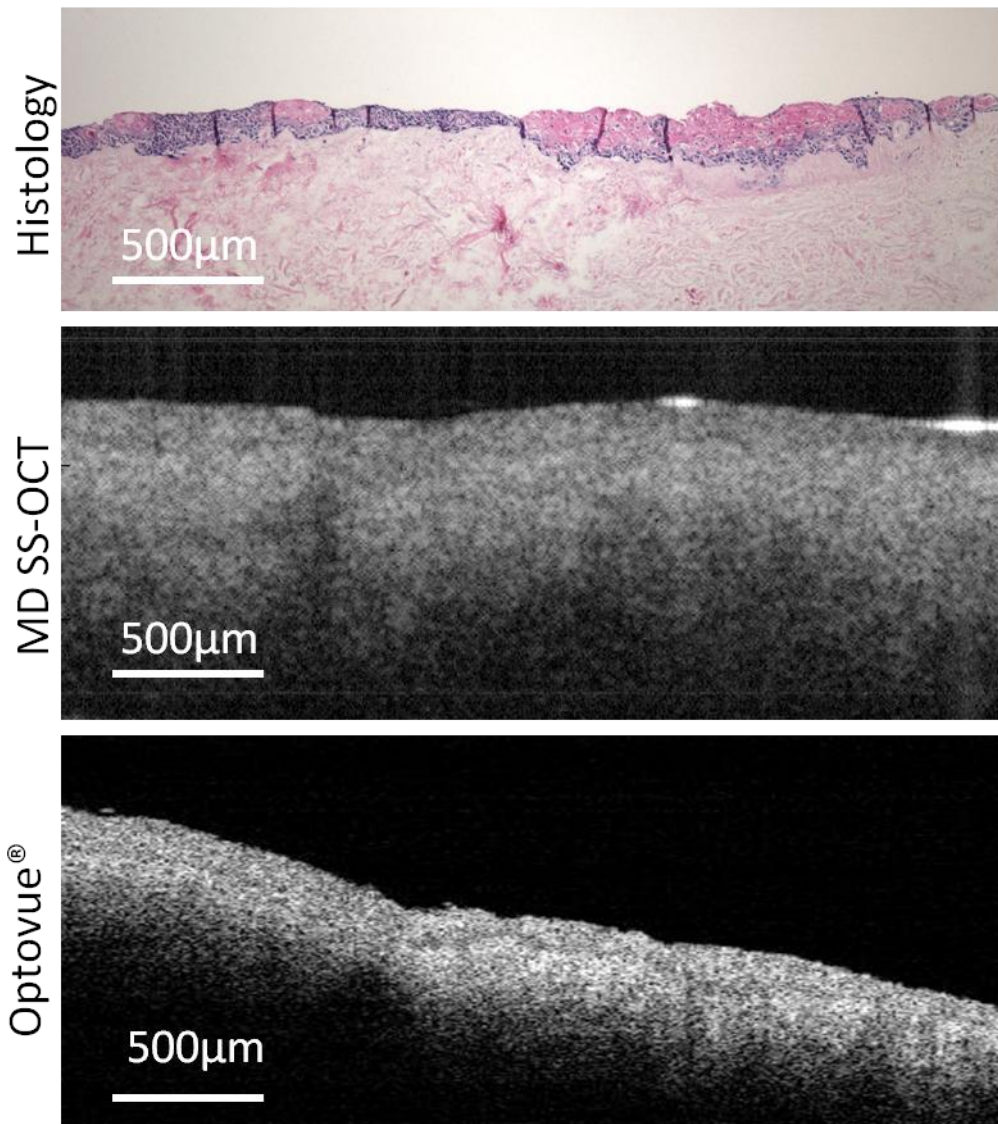
Figure 4.21 OCT image of SCC9 model

SCC9

The histology of the SCC9 model showss large amounts of extracellular proteins, stained in pink, most likely keratin, in distinct regions of the epithelium (Figure 4.21). In the images from Optovue® system the epithelium is as bright as the connective tissue in areas. This is in contrast to the other epithelia which had relatively dark epithelia compared to the connective tissue. This could be due to the higher reflective or scattering properties of the keratin. Higher light back scattering or reflective properties of a tissue region show as a brighter region in the image. The brightness of the epithelium in the image obtained from the SS-OCT system was more uniform suggesting that the difference between cells and keratin cannot be distinguished when using this system.
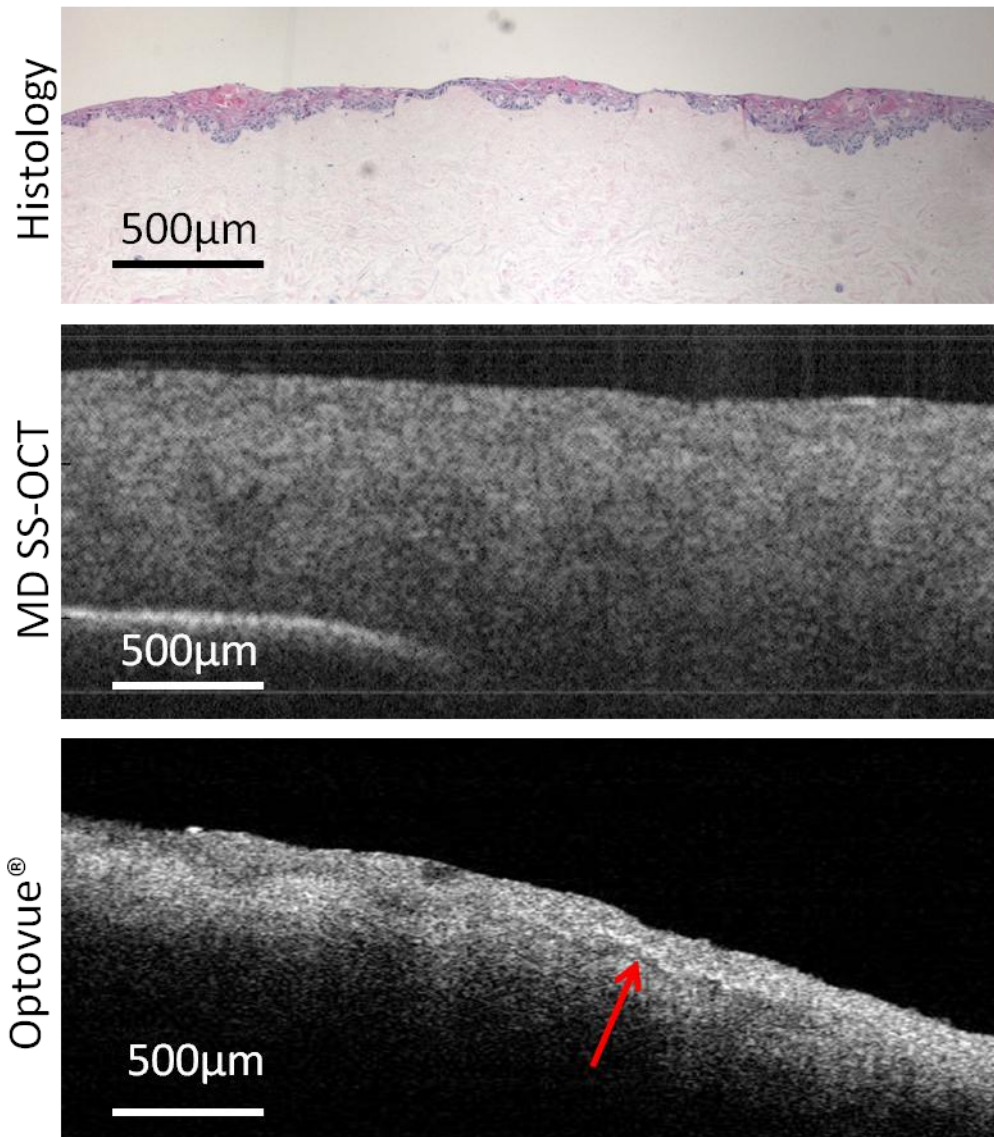
Figure 4.22 OCT image of SCC25 model.
Red arrow shows white line, possibly keratin.

SCC25

The SCC25 models also contain large amounts of ECM proteins, most likely keratin, in areas of the epithelium. The range of brightness in the epithelium in images from the Optovue® system was clearly apparent for the SCC25 models. In the Optovue® image in Figure 4.22 there is one area where there is a bright white line (arrow on figure) a few microns superficial to the dark line of the epithelial connective tissue junction. This bright white line could indicate the junction between keratin and cells in the SCC25 epithelium (arrow on Figure 4.22).
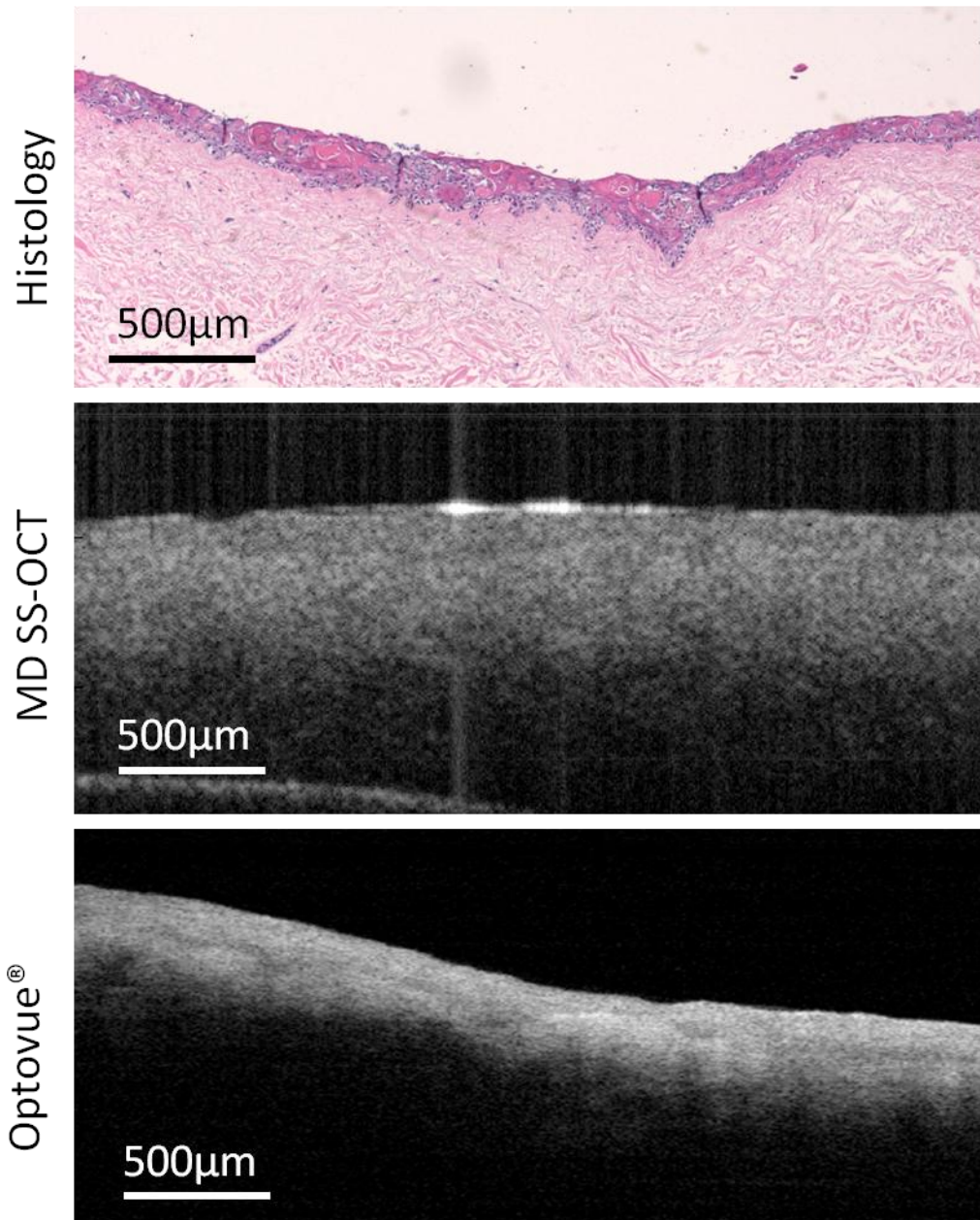
Figure 4.23 OCT image of D20 model

D20

There was very little difference in the brightness of the epithelium compared to the brightness of the connective tissue in the D20 models imaged with both the SS-OCT system and the Optovue® system (Figure 4.23).   Despite this, there is a dark region where the epithelial connective tissue junction lies suggesting the scattering and reflective properties of the epithelial connective tissue junction proteins is different to the optical properties of the tissue.
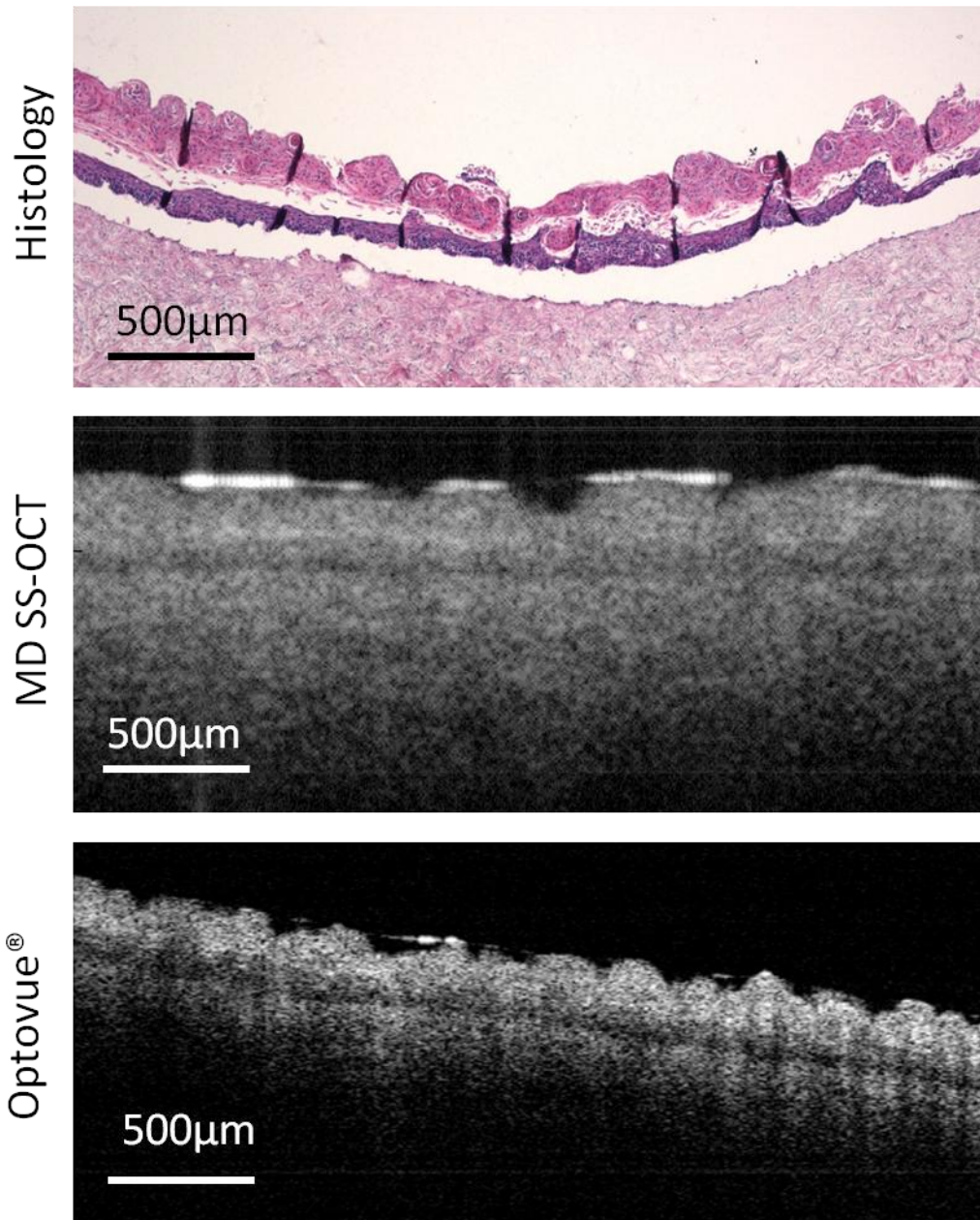
Figure 4.24 OCT image of Cal27 model

Cal27

The appearance of the Cal27 model was severely dysplastic and the epithelium formed two distinct layers. There was a layer of dysplastic cells adjacent to the epithelial connective tissue junction and superficially to this a layer of highly keratinized cells (Figure 4.24). The models also had an unusual surface topography, not flat or smooth as in the TEOM but rather a lumpy surface created by the pattern of keratinisation. The surface topography could easily be determined using OCT, with a clearer image obtained using the Optovue® system compared to the SS-OCT system. The two layer structure of the model could also be determined in the Optovue® system. The superficial keratin layer was brighter than the underlying epithelium.

The portion of the epithelium which is made from non-keratinized cells appeared as a dark band below the bright keratin. A boundary can also be seen between the dark band and the underlying connective tissue, corresponding to the epithelial connective tissue junction. The highly reflective and back scattering keratin appears to cause a "banding" deeper in the image. This appearance of these white bands is similar to that seen if there is moisture on the surface of the model. This banding was also described by Wilder-Smith *et al.,* (Wilder-Smith *et al.,* 2009) in OCT images of cancer *in vivo* (see Figure 1.16 on page 67).

In vivo OCT imaging of human oral mucosa

Figure 4.25 shows an OCT image obtained by the Optovue® system of the inner mucosal surface of the lower lip of a healthy volunteer and compares it to the histology of this region of the oral cavity. The OCT image clearly shows a distinction between the epithelial layer and the underlying connective tissue. The connective tissue portion is brighter than that seen in the tissue engineered models, most likely due to the high water content of the connective tissue *in vivo*. Within the connective tissue structures such as the minor salivary glands and blood vessels could be made out (features not present in these tissue engineered models). The Optovue® system was able to image roughly 500μm deep into the tissue with good resolution. The epithelium appears smooth and has uniform brightness throughout.
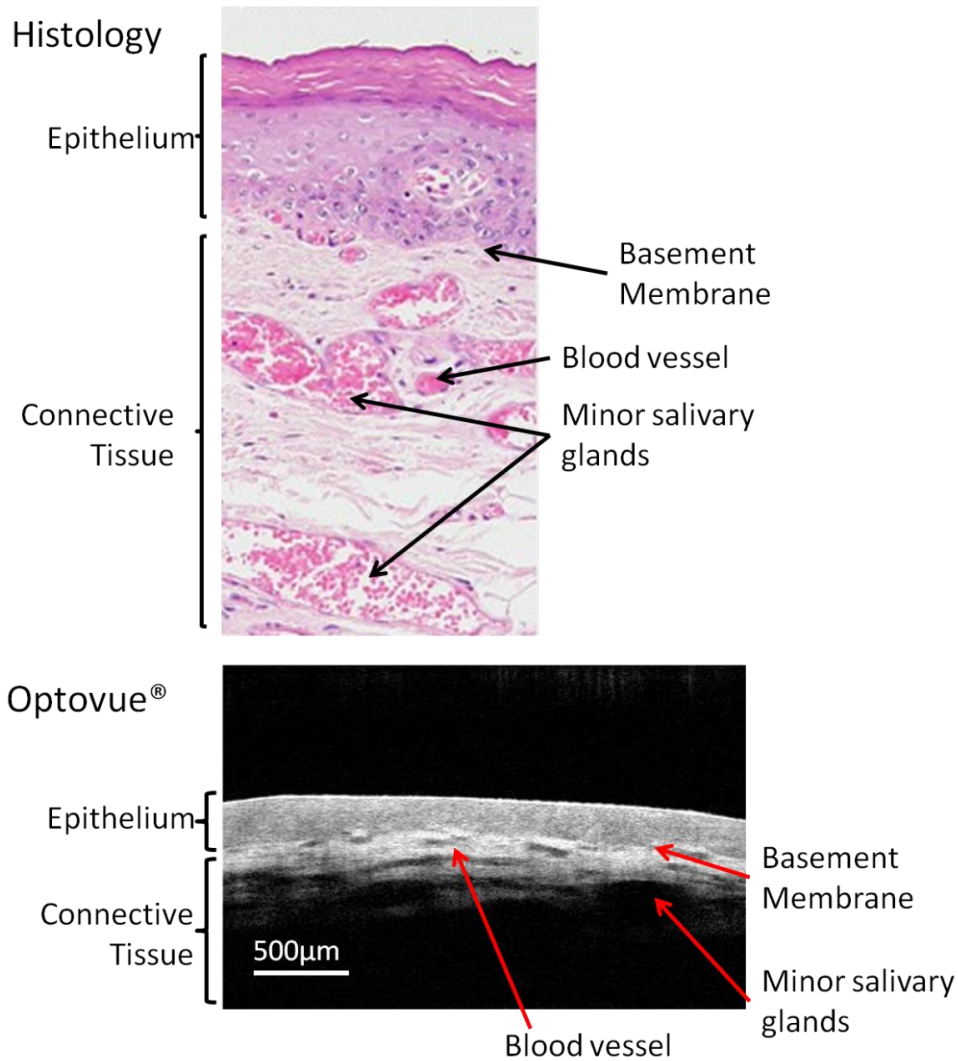
Figure 4.25 Histology of the mucosal surface of the lower lip from (Slomianka 2009) and OCT of the mucosal surface of the lower lip, *in vivo* in a healthy volunteer. n=1

4.5   Discussion

An ideal novel detection device for use in the diagnosis of oral cancer should:

- be non-invasive,
- be simple to use,
- enable point-of-care real-time diagnoses,
- be affordable for general dental practices as well as hospitals,
- have high specificities and sensitivities,
- have good patient acceptability.

Here we evaluated the potential of four different methods for potentially malignant lesion diagnosis using tissue engineered models.

C $_{12}$ – resazurin as a marker for cancer

C $_{12}$ – resazurin is a tool used in cell culture to measure the metabolic activity of cells in culture. It is well known that cancer cells demonstrate higher metabolic activity compared to healthy tissue surrounding them. The non-toxic, short exposure time and fluorescent nature of this marker (Vybrant™ cell metabolic activity kit with C $_{12}$ – resazurin) led to the simple hypothesis; could a fluorescent metabolic marker be used as a tool to aid the diagnosis of oral lesions, and could it differentiate between healthy, premalignant and cancerous tissues?

Monolayers

The C $_{12}$ – resazurin metabolic marker was reduced by all cell types tested here after 15 minutes exposure. The cell stain remained in the cells when washed and cell monolayers on glass cover-slips could clearly be imaged using CLSM. Different cell types exhibited different intensities of fluorescence. Despite the overlapping variances the differences between many of the cancer cell lines and the primary cells were statistically significant due to the very large n number (2 experiments, 5 images per cell type in each experiment and 1-5 areas of each image quantified depending on the amount of cells and cell colonies per image). All cell lines except the Cal27 and FaDu cells showed higher fluorescence intensity, and therefore metabolic activity, compared to the normal oral keratinocytes. It was expected that the cancerous and dysplastic cell lines would all show higher metabolic activity compared to the normal oral keratinocytes. However, this was not the case in 2D cell culture conditions. It should be noted that the differences in intensity were mostly in the order of 10-50% between the cell lines and NOK cells. NOKs are also known to be highly metabolically active *in vivo* as they continually replenish the cells of the oral epithelium. The 2D *in vitro* environment is an artificial one and this experiment had many limitations.

The intensity of fluorescence seems to relate to the rate of proliferation that different cell types undergo. It has been observed in the laboratory that the D19 and D20 cell lines proliferate faster than other cell types. These two cell lines were the most metabolically active when measured using the C$_{12}$- resazurin metabolic activity kit. It is logical to expect that metabolic rate and proliferation are connected as cell proliferation and division are some of the most metabolically demanding processes which the cell undergoes (Skala *et al.,* 2007). The Cal27, FaDu and PE/CA-PJ34 cell lines proliferated slowest in culture (observations from culturing these cell lines in the laboratory) and these gave the lowest intensities of resorufin fluorescence and therefore metabolism.

The values obtained from NOK metabolic activity varied greatly between batches of keratinocytes from different individuals and different experiments.

In conclusion, these experiments showed that C_{12}-resazurin can be used as a marker for metabolic activity and is well retained by the cells and can be imaged easily using CLSM. The majority of cell lines tested did show significantly greater metabolism compared to NOK and NOF. However, the actual differences in intensities were small and varied greatly. The intensity of fluorescence does appear to be related to cell proliferation but a specific experiment testing proliferation alongside resorufin intensity would be needed to confirm this. This metabolic marker is non-toxic and the short exposure time, 15 mins, means that practically it has potential. However, the variation in normal cells make this a very inaccurate method to identify malignant cells and this method would detect any cells which had an increased metabolic activity rather than specifically cancer cells. This would include cells involved in wound healing or non-malignant disease processes involving increased proliferation of oral keratinocytes e.g. oral lichen planus, papilloma virus infected cells etc. There was also a large variation in the intensity of fluorescence between samples so for a clinician to be able to correctly distinguish healthy tissue from tissue with increased metabolic activity would be challenging as there will be patient to patient variation as well as sample to sample variation.

In 3D models of oral cancer and dysplasia

The 3D models of normal oral mucosa (TEOM), dysplasia (DOK+ TEOM) and carcinoma *in situ* (spheroid +TEOM) gave different patterns of fluorescence and different fluorescent intensities post C_{12}- resazurin exposure. Confocal microscopy was able to image resofurin at depths of up to 30μm. Although limited, this depth of imaging was enough to visualise the metabolic activity of the most superficial layers of cells. The limited penetration could be due to several factors including penetration of the C_{12}- resazurin stain across the epithelial permeability barrier with just 15 minutes exposure, the scattering effect of the tissue on the light and the physical limitations of 543nm wavelength light penetration through biological tissues. Further studies could include a time course experiment to see if increased exposure time resulted in better penetration.

Clinically, the restricted depth of imaging could be problematic as the most metabolically active cells are the proliferative basal keratinocytes. The most superficial cells of the healthy epithelium are not metabolically active as these cells are terminally differentiated and some cells lose their nuclei. Furthermore, early dysplastic change in the oral epithelium is evident first in the basal 1/3 of the epithelium.

Vybrant™ Cell Metabolic Assay Kit shows better cell retention compared to alamarBlue® and this results in clear imaging of individual cells within an epithelium in 3D (Probes 2001). The most superficial surface of the TEOM showed strong and spotty staining for resorufin. The most superficial cells would not be expected to be metabolically active however, the cells on

the uppermost layer of the TEOM model may not have fully differentiated at the time of C_{12}-resazurin exposure and therefore the cells would still have some metabolic activity. In deeper cells the staining did not have this spotty distribution but was uniformly stained across the cytosol. This superficial spotty pattern could be due to resorufin becoming bound to the keratin in the sample or due to cell damage.

Although many of the cancer cell lines tested in monolayer gave higher median fluorescence intensity compared to normal cells (Figure 4.6), the cells used here to model cancer in 3D did not. The FaDu cells had slightly, but not significantly, lower fluorescence than NOK and the DOK cells were more fluorescent compared to NOK but not significantly so in the previous monolayer studies.

In 3D the TEOM was significantly more fluorescent compared to the DOK + TEOM and the MCTS + TEOM models. This could be due to NOK cells having a higher metabolism in 3D compared to cancer cells. It could also be due to a limitation of this method for quantifying the fluorescence in the 3D models. The ratio of nucleus to cytoplasm in the TEOM model was much lower than in the other two models (Figure 4.6). The high proportion of nuclei included in the measurements of the DOK +TEOM and spheroid + TEOM models could have caused a reduction in the median fluorescence of the areas measured as the nuclear region of the cell did not take up the stain and was therefore not fluorescent distorting the values. The brightly fluorescent spots seen on the TEOM models (potentially due to the keratin) may have also affected the values.

The original aim of this experiment was to see if the C_{12}- resazurin measure of metabolic activity could be used as a quantitative marker for cancer in an oral epithelium. It was hoped more metabolically active cancer cells would be distinguishable from healthy epithelium using this marker. The differences in fluorescence in 3D have actually proved to be opposite to the initial expectation possibly due to the reasons outlined above. The differences in fluorescence intensities were small making the C_{12}- resazurin metabolic marker not clinically useful when looking at the difference in intensity of fluorescence between cell populations. Despite this, the C_{12}- resazurin may be useful for looking at the morphology of cell populations in a patient's epithelium. The current gold standard for oral cancer detection is histology. This is a qualitative method which looks at the morphology of cells, their nuclei and the arrangement of cells throughout the epithelium. When resorufin (the reduced product of C_{12} – resazurin) is retained within cells it clearly shows the morphology of the cell, the size, shape and distribution of cell nuclei and the cytoplasm to nuclear ratio. This could be of benefit clinically for imaging changes in cell and nuclear morphology in the most superficial cells. These occur in severe epithelial dysplasia and carcinoma *in situ*. Unfortunately, confocal microscopy combined with this stain were not able to penetrate into the deeper layers of the

epithelium and would therefore not be able to detect changes when they occur in the basal regions of the epithelium, as are seen in moderate and mild dysplasia.

While it may be useful as a marker for highly proliferative and aggressive carcinoma, the greatest need is for a marker for early stage tumours which need to be distinguished from suspicious benign lesions which do not require treatment. This approach is unlikely to be useful for this purpose.

Slow imaging capture rates also make this method impractical *in vivo* as movement artefacts, resulting from patients moving during image acquisition, make accurate imaging not feasible without an anaesthetic. This along with the complexity, cost and time consuming nature of this type of imaging make it unlikely to be taken up widely for screening of at risk patient groups for the detection of oral cancer.

Impedance spectroscopy

Impedance spectroscopy is a non invasive method which is able to detect changes in bioimpedance, which in turn give information about the electrical properties of the tissue in contact with the probe. Many factors affect the electrical properties of a tissue including cell density inter-cellular junctions and cell type. These factors are all affected in cancer progression. The probe applies a current to the tissue and changes in the impedance to the current can be detected in different tissues. The impedance spectroscopy system used here has been shown to be able to distinguish not just cervical cancer from normal cervix but can also distinguish between different cervical intraepithelial neoplasia (CIN) grades of cervical dysplasia (Abdul *et al.,* 2006). A simpler system than the one used here has recently been reported as being under investigation for detection of tongue cancer (Sun *et al.,* 2010). Sun *et al.,* have shown in that cancerous regions of the tongue, which are disordered with less tight inter-cellular junctions could be distinguished from healthy tissue as cancerous regions, and had lower impedance at low frequencies (20Hz and 50kHz) (Sun *et al.,* 2010). The impedance values are lower in cancerous regions as it is easier for the current to pass around disordered cancer cells compared to healthy oral epithelium where the cells were very well organised with strong inter-cellular junctions. The differences were not seen at higher frequencies (1.3MHz and above) as the current is able to pass through cells as well as around them at these frequencies (Sun *et al.,* 2010).

This chapter presents data obtained from a quick study to evaluate differences between cancer and healthy oral mucosa *in vitro*. Unfortunately, the tissue engineered model system used here failed to show a significant difference between the models cultured from the cancer cell lines and the TEOM. There was a large amount of variation between readings. The only obvious difference was that the TEOM impedance values varied between different frequencies whereas the impedance values from the cancer models were not dependant on frequency.

There was a large variation in the measurements obtained from the tissue engineered models. This could be due to a number of factors including the fragile nature of the cultured epithelium, differences in epithelial thickness in different areas and differences in the thickness of the DED onto which the epithelium was cultured. The process of taking the measurement may have damaged the epithelium, affecting the impedance values. The method of measuring needs to be refined as currently there could be differences in the level of pressure applied to get the probe into contact with the model, the temperature of the model and the moisture on the surface of the model.

It was hoped that this technique would allow us to demonstrate the similarities between TEOM and naturally occurring buccal mucosa. Unfortunately, for the most part there was a large difference in values obtained from these samples, except in one (non-reproducible) case (Figure 4.11). Unfortunately, for these reasons it appears that the tissue engineered models here are not suitable for testing this technology and testing in patients and volunteers will provide more robust data and information on this technology.

The readings, taken *in vivo* of buccal mucosa and tongue, showed very different patterns of impedance depending on the area of the mucosa. It would be interesting to study this further and look at the impedance of all areas of oral mucosa including the palate, floor of the mouth, buccal, gingivae and tongue. Comparing these to histology images for the corresponding region of tissue would enable us to gain a better understanding of how the epithelia thickness and morphology affected the impedance values. The variation in impedance in different areas of the mouth (apparent in Figure 4.12) means criteria for diagnosing oral cancer in different anatomical locations needs to be site specific and the usefulness of this technology may be limited to some regions. The value of impedance spectroscopy for determining tongue OSCC has already been demonstrated (Sun *et al.,* 2010) and suggests more *in vivo* testing of healthy and diseased tissues could further prove the value of impedance spectroscopy for clinical diagnostics in the oral cavity.

Impedance spectroscopy has the advantage that it is simple to perform, non-invasive and practical for oral applications. The accuracy for determining the borders of potentially malignant lesions is limited by the electrode spacing on the tip of the probe which may be one of the limitations of impedance spectroscopy in the future.

FTIR

FTIR is a method of spectroscopy which enables specific bonds within a sample to be determined using IR radiation. The spectra taken here are preliminary data which have been used to develop an effective method to measure tissue engineered oral models spectra to evaluate the potential of this technology.

In this study, FTIR was not able to get meaningful spectra from live or fixed tissue which had not been sectioned due to water absorption of IR radiation and the spectral saturation of samples thicker than 15µm. However, it was possible to collect spectra from wax embedded paraffin sections and all the spectra shown in this project were collected this way. This highlights the potential for this technology to be used alongside the current method of diagnosis, histopathological analysis of surgical biopsies. FTIR could provide adjunctive objective information regarding the chemical make up of a biopsy to improve diagnoses which currently rely on subjective opinions of morphological appearances. Many diagnostic procedures also require immunohistochemical staining of specific proteins. Although this procedure is very well established and reliable it is time consuming and subject to personal interpretation. A method such as FTIR which could determine the biomolecular composition quickly and accurately could be of benefit in these cases.

The small sample size and differences in sample area on each slide may have altered the results. However, some differences could be seen which could be of interest in the diagnosis of oral cancer and pre-malignancy. Higher peaks at $2848cm^{-1}$ and $2916cm^{-1}$ which were seen in FaDu and DOK compared to TEOM (but not SCC9). These peaks which result from stretching vibrations in CH_2 and CH_3 bonds found in cholesterol, phospholipids and creatine, have previously been identified as peaks which differ in cancer compared to normal cells (Huleihel *et al.,* 2002). Huleihel *et al*., attributed this difference to levels of creatine (a cell metabolite) which are higher in healthy cells and has previously been shown to inhibit cancer cell proliferation in mouse models of human colon adenocarcinoma (Huleihel *et al.,* 2002).

Meurens *et al*., found a strong correlation between amide I and II and density of cancer cells and the absorption bands in breast cancer tissue (Meurens *et al.,* 1996). The cause of this is not yet known. The bands corresponding to amide I and II bonds were higher in the TEOM compared to FaDu and SCC9 models (the opposite trend to that seen in (Meurens *et al.,* 1996)).

The real aim for improved diagnostics of oral lesions would be a method which was able to non-invasively diagnose a lesion. Novel technology such as attenuated total reflectance (ATR) and fibre optic spectroscopy enabled Wu *et al*., to measure FTIR spectra from freshly excised tissue without any prior tissue preparation (Wu *et al.,* 2001).

ATR FTIR enables imaging of tissues even in the presence of strong IR absorbers such as water. In ATR FTIR the IR light source is directed through a crystal which is transparent to IR and has a high refractive index. This high refractive index creates total internal reflections within the crystal enabling the tissue in contact with the probe to be measured despite the presence of water (Kendall *et al.,* 2009).

Wu *et al*., demonstrated that FTIR with ATR could be used to differentiate between normal and cancerous tissue in recently excised tissue samples. The wavenumber peak which appeared the most useful for distinguishing between normal and malignant oral tissue in (Wu *et al.,* 2001) was at 1745 cm^{-1}. They attribute this band to the vibration of carbonyl in ester groups found in fat cells. This peak was not seen in any of the sample's spectra. However, this is most likely due to the loss of lipids during histological processing. Special fixation with potassium dichromate, for over 3 weeks is required to retain fat in paraffin sections (Chou 1957). It is also likely that the tissue engineered models used here do not have the same distribution of fat cells compared to naturally occurring tissues. If the spectra obtained from freshly excised salivary gland tissue and the spectra from our tissue engineered models are compared (Figure 4.13 on page 193) there are some common peaks. However, much more work needs to be done in order to fully evaluate this technique and the effect bonds present in samples have, not only on the size of the peak, but also to shifts in the wavenumber of peaks. It will also be interesting to see if FTIR can be performed in live patients without requiring tissue excision.

This initial study into using FTIR for cancer diagnosis is promising. However, a substantial amount of further work is needed to develop this technology into a clinically useful, non-invasive, fast method to diagnose oral lesions.

OCT imaging for cancer diagnostics

The ability of OCT to image differences in tissue engineered models of OSCC was evaluated in this study. The images obtained from the different OCT devices tested here varied and their clarity was dependant on a number of factors including the light source (axial resolution), wavelength of light source (depth of penetration) and the number of images averaged, to reduce noise, and give the final image. Depending on the application it is possible for different parameters to be adjusted in order to obtain the most useful information from a sample. The SS-OCT device and the TD-OCT system were able to image deeper into the tissue but the resolution (axial and transverse) of the commercially available Optovue® system was better overall and gave a clearer image.

Of the four devices tested, all were able to show the epithelial connective tissue junction and distinguish between epithelium and connective tissue, thus giving information on the thickness of the epithelium. The surface topology could also be clearly seen. Within the epithelium and connective tissue specific cells or features could not be determined but regions of keratinised cells did appear brighter than non keratinised cells making them distinguishable in the SCC25 model.

The thickness of naturally occurring oral mucosa epithelium is between 75- 550μm (Nanci 2003) and the systems tested here were able to image to depths of 500μm or greater (systems

described in the literature have been able to image to depth of over 2mm (Georgakoudi *et al.,* 2008)). This means the imaging of mucosal diseases is feasible with this technology.

While OCT imaging of these *in vitro* models has real value in the development of OCT systems for oral lesion diagnosis, there are limitations. Tissue engineered models such as these were able to give clear images of some features of the epithelium and the boundary of epithelium and connective tissue. However, images taken *in vivo* (Figure 4.25) appeared clearer and more features (many of which were not present in tissue engineered models) were visible. It has been previously noticed that *ex vivo* and *in vitro* samples do not give as clear OCT images compared to *in vivo* images (Smith *et al.,* 2010). Hsiung *et al*., looked at the image quality degradation over time post excision and found a reduction in signal intensity over time, most likely due to a loss of blood, cell lysis and subsequent changes in the tissue's microstructure (Hsiung *et al.,* 2005).

For clinical applications this is not a problem as real time non-invasive imaging is the ultimate aim; however, this may explain the difference in image quality obtained from tissue engineered models compared to *in vivo* tissue. Tissue engineered models may still have use in OCT development, for example, as a tool to test novel contrast agents or to image specially designed models with specific features (for example cancer cell invasion or models with altered cell densities) to enable researchers to examine the appearance of these features with OCT before clinical trials.

Figure 4.25 shows the real potential for using this technology clinically. Further clinical studies need to be undertaken to study, in more detail, the different appearances which arise from OCT imaging of different stages of OSCC and other potentially malignant mucosal conditions as well as testing the specificities and sensitivities which can be achieved. OCT devices are still a relatively new technology and for the most part have been optimised for ocular applications. OCT development directed for oral applications may further improve the images which can be obtained.

Pathologically, the appearance of the epithelial connective tissue junction is important when diagnosing a number of different conditions, not just OSCC. Many mucosal diseases including lichen planus affect this junction adjacent to basal cells and the diagnosis of these conditions may also benefit from OCT investigation. The ability to visualise not just the epithelium but also the adjacent connective tissue including blood vessels, ducts and minor salivary glands may mean OCT has just as much, or more, potential for diagnosis of non-malignant or diseases e.g. oral ulcerative conditions, Sjögren's syndrome, vascular anomolier, superficial cystic lesions, submucous fibrosis, orafacial granulomatosis, lichen planus etc.

The data emerging in the literature from OCT imaging of suspicious oral lesions clinically is encouraging (Figure 1.16 on page 67). This has been reviewed in Chapter 1. With the ever

improving technological advances in OCT combined with the desperate need for a faster, simpler and non-invasive method to detect early changes in oral epithelia OCT could soon become commonplace in dental surgeries. Image acquisition from OCT is very rapid and could in the future be used to screen at risk patient groups for oral cancer, aiding early diagnosis before symptoms appear and improving survival rates. Currently the gold standard of oral cancer diagnosis is by invasive surgical biopsy. This, while accurate and well established, could never be used in the screening of patients at risk with no signs or symptoms. OCT has the advantage of being able to obtain data from the same area over several years to get longitudinal information on a patient's condition, an advantage to this technique which has already been adopted by ophthalmologists (Bechtel 2010).

OCT may in the future help to define surgical margins and provide direct evaluation of the effectiveness of cancer treatments (Wilder-Smith *et al.,* 2009). OCT can also be used to image the whole oral cavity of a patient with a malignant lesion and find other areas of malignancy in the oral cavity which may not be observable by the naked eye. OCT can locate these secondary malignancies in the oral cavity and give the clinician further information which helps them to biopsy the area which is most advanced and thereby helping to determine the best treatment for that patient based on a more accurate diagnosis of the severity of the patient's disease (Keller 2010). It can also be used for long term monitoring of lesions that are being kept under observation and may avoid the necessity for regular repeat biopsy of lesions. Another major advantage over biopsy is the ability to produce real time, point of care images of the tissues that can be discussed with the patient and enable efficient treatment planning and decision making without the need for a repeat visit as is needed following a biopsy.

As shown in (Wilder-Smith *et al.,* 2009) this imaging technique is relatively easy to use, with observers being trained in just 2 hours. Observers obtained sensitivities and specificities of 0.931 and 0.931 when diagnosing OSCC and carcinoma *in situ* from healthy tissue, far higher than those obtained from methods such as Toludene blue described in the introduction (page 54). Tsai *et al*., devised a technique which could be used to quantify data obtained from OCT images removing the subjective nature of diagnosis and determining standardised diagnostic parameters (Tsai *et al.,* 2009).

One hurdle which was highlighted in Fujimoto's article in Nature Biotechnology is the length of time it takes for biomedical technology, such as this, to reach the clinic (Fujimoto 2003). Many stages must be overcome before biomedical technologies can reach the clinic including: initial research, prototype development, clinical feasibility studies, clinical trials, regulatory approval, demonstration of clinical efficacy and sales into the clinical community (Fujimoto 2003). The first *in vivo* retinal imaging using OCT was demonstrated in 1993 and by 2003 OCT was rapidly becoming the standard of care in ophthalmology (Fujimoto 2003). Now, in

2010, OCT is commonplace in ophthalmology and its benefits have extended from the retina to other areas of the eye (Bechtel 2010). With OCT imaging for oral lesions gaining momentum in the research community it is hoped that OCT for oral applications may follow on from the success of retinal OCT imaging and have a real positive effect on the early diagnosis of oral cancers and subsequently survival rates.

Table 4.4 summarises the pros and cons of the four techniques tested here and the next steps needed for their development.

Technique	Pros	Cons	Potential for Development?	The next step
C_{12} resazurin	• Can image cell morphology using the stain and CLSM	• Difference in fluorescence intensity between normal, and malignant cells not great enough to have diagnostic value • High magnification imaging not suitable for *in vivo* imaging	No	• Find an alternative marker which is more specific to malignancy
Impedance spectroscopy	• Non invasive • Affordable • Simple to use • Potential for real time point of care diagnostics	• Size of the probe limits the spatial sensitivity	Yes	• A clinical trial to determine the values of impedance for each grade of tissue (healthy, potentially malignant and benign) in all different regions of the oral cavity has recently been funded under the NIHR i4i program.
FTIR	• Gives quantifiable data of the chemical composition	• Affected by the presence of water • Data currently must be obtained from biopsy sections, not *in vivo*	Yes	• Retrospective study of the FTIR spectra resulting from biopsies of a range of oral lesions to determine the bonds with diagnostic potential • Use tissue engineered models to develop FTIR technology so it is possible to image live tissues which contain water
OCT	• Non-invasive • Non-ionising radiation • Depth of imaging 2-3mm • Fast, imaging • Already in use in ophthalmology • Longitudinal monitoring possible • Adequate resolution	• Light sources expensive • Optimised for retinal imaging not oral • Detection limits not currently sensitive enough for many cancers	Yes	• Clinical trials imaging clinical lesions to test the ability of OCT to distinguish potentially malignant lesions from benign lesions and other oral conditions • Use tissue engineered models to develop contrast agents and to optimize the technology for oral use • Investigate the potential of OCT for imaging other conditions of the oral mucosa

Table 4.4
Table to summarise advantages and disadvantages of the four techniques tested here. This table highlights some of the developments which are needed for these techniques to have real diagnostic value clinically and the potential for use of tissue engineered models in the future of their development.

Chapter 5: Future work and conclusions

This project initially demonstrated the ability to create physiologically relevant tissues in the laboratory and then demonstrated some of their potential applications in the development of medical technologies. The models of normal oral mucosa created from primary human oral cells (fibroblasts and keratinocytes) were cultured on an acellular skin scaffold creating a model which comprised of epithelial and connective tissue components. This model was characterised using immunohistochemistry and was shown to have many components seen in physiologically normal oral mucosa including basement membrane proteins (collagen IV), cytokeratins and proliferative basal cells. This model was used in this project to test the ability of polymersomes, a novel drug delivery vector, to cross the oral epithelium and as a control for testing non-invasive diagnostic technologies. In the future this model could be developed further by incorporating endothelial or immune components. One drawback of this model was the variation seen between different batches of primary cells. However, this is commonly experienced when using primary cells. To overcome this immortalised cell lines could have been used but these cells do not have a normal phenotype and have been modified to become immortal. Hence despite the convenience of using cell lines (as are used in several commercial models) these lack the full range of physiological responses .

The method for culturing normal oral mucosa was next adapted to test whether it was possible to culture dysplastic or malignant epithelium. While some of the cell lines tested here produced epithelia with appearances unlike anything seen clinically, we were able to create models of dysplastic epithelia using normal oral fibroblasts cultured with DOK cells and SCC9 cells. These models contained features of dysplasia including cytological and architectural abnormalities (see Table 2.10 for details). Other models, cultured from D20 and Cal27 cells, showed more severely pathological appearances which more closely resembled early invasive carcinomas. All these models could be used in a number of future *in vitro* applications for example, as a model to study factors which cause and are able to inhibit cancer progression. This project demonstrated that these models could be useful in testing novel diagnostic technologies while future applications could include using these to test therapeutic technologies and novel drug delivery vehicles. It would be interesting to culture the cell lines used in these models in co-culture with normal oral keratinocytes to see how the normal and malignant cells interact and whether less severe dysplasias could be modelled.

There were signs of early tumour cell invasion of the connective tissue in the models cultured from the DOK, D20, D19, Cal27, PE/CA-PJ34 and FaDu cell lines. Interestingly, when these same cell lines were co-cultured with fibroblasts and screened for their ability to form multi-

cellular tumour spheroids when cultured on agarose coated plates they did form spheroids. The cells which did not invade (SCC4 and SCC9) were the cells which did not form spheroids when co-cultured with fibroblasts. This correlation was not seen when the cell lines were screened for MCTS formation in mono-culture. It is well known that epithelial cell invasion is influenced by both epithelial cells and mesenchymal cells. This correlation further suggests fibroblasts may be involved in the establishment of solid tumour islands within the connective tissue, once the cells have invaded. These models will lend themselves to investigations of epithelial/stromal interactions in particular.

The MCTS model cultured from the FaDu cell line modelled many features seen in the intra-vascular regions of solid expanding tumour islands. These included the hypoxic centre, caused by insufficient oxygen diffusion into the central region of the tissue. The central region also showed signs of necrosis as a result of an accumulation of waste products in the central region of the tissue. The outer cells were proliferative and the MCTS expanded over time. This project used the MCTS model to test the ability of polymersomes to penetrate into the central region of the MCTS, and thus model the drug delivery vehicle's ability to diffuse into the hard to treat core of solid expanding tumour islands. Polymersomes were able to reach 80% of the cells within the MCTS and could be seen throughout the MCTS after 5 days exposure. The uptake of polymersomes by cells within multi-cellular tumour spheroid was slower than the uptake seen in cell monolayers, demonstrating the importance of testing drug delivery systems in 3D models as well as in monolayer studies.

One of the most interesting applications for the MCTS is for high-throughput screening of potential therapeutic agents before *in vivo* testing. It has been shown that MCTS are a better predictor of clinical success compared to *in vitro* monolayer studies. A number of different cell types were tested for their ability to form MCTS with the aim of expanding the library of MCTS models available for the testing of novel therapies against OSCC. Unfortunately, none of the cell lines tested (except the FaDu cell line) were able to form solid expanding tumour spheroid models using the liquid overlay method. Some cells formed spheroids but these did not expand over time limiting their usefulness as a model to test the anti-cancer capacity of novel therapies.

The uptake and diffusion of polymersomes were tested in 2D and 3D. When the relative uptake of polymersomes was compared between primary cells (fibroblasts and keratinocytes) and cancer cell lines (FaDu, SCC4 and Cal27) both the rate and quantity of polymersomes taken up by the cancer cells (FaDu in particular) was significantly greater than the uptake by the primary cells. This is interesting as a potential form of passive targeting to cancer cells *in vitro*. There are many different possible reasons for this including faster metabolism or increased endocytosis by cancer cells but the study of the cell metabolism marker C_{12}-resazurin in chapter 4 showed very similar levels of cell metabolism between the NOK cells

and the FaDu cells. The proposed mechanism of polymersome uptake is *via* endocytosis (Figure 3.3) therefore it would be interesting to see if FaDu cells had a higher rate of endocytosis compared to the primary cells or to see whether the polymersomes bound more readily to the surface of the cancer cells compared to the primary cells. It is possible the polymersome endocytosis is receptor mediated although the identity of the receptor is currently unknown. If polymersome endocytosis is receptor mediated our data suggests that head and neck cancer cells may express this receptor more than normal oral keratinocytes and fibroblasts.

The data emerging from polymersome studies here and elsewhere in the Battaglia laboratory is encouraging. However, a large amount of further work is needed before the true clinical value of this drug delivery technology can be realised. Data presented in this thesis show that polymersomes were able to reach the basal cells of the tissue engineered oral mucosal model and the central region of the MCTS but it is currently unknown whether the polymersomes reach these cells intact. It will be interesting to next investigate whether the polymersomes are able to deliver an encapsulated cargo into these cells and whether polymersomes are capable of transmucosal delivery right across the epithelium and into the blood supply. If both these were achievable using these polymersome formulations, the clinical benefits seen from their use could be far reaching. The synthetic nature of the polymer from which these polymersomes are made also increases their versatility; enabling the addition of targeting moieties to the external surface and alterations to the polymer changing release profiles, flexibility and size.

Finally, four different diagnostic technologies were tested using the models developed earlier in the project. The first method for diagnosis which was tested stemmed from a simple hypothesis. Could the enhanced metabolism seen in cancer cells compared to healthy cells be detected using a non-toxic cell metabolism marker such as C_{12} resazurin? When this was tested in three different models (normal oral mucosa, carcinoma *in situ* model and dysplastic epithelium) the opposite result was seen to what was expected. The normal oral mucosa showed the highest intensity and therefore metabolism when exposed to the cell metabolism marker C_{12}-resazurin. This could be due to a number of factors discussed previously but discounts the usefulness of this method for cancer detection clinically.

The second method of detection tested here was impedance spectroscopy. The benefit of this has already been demonstrated clinically as it is able to diagnose and grade cervical neoplasias. Unfortunately, the values obtained from the *in vitro* models using this technique were highly variable and did not correspond to the values obtained *in vivo*. It was therefore concluded that this non-invasive diagnostic technology would be best studied further in clinical trials.

The third diagnostic technology was FTIR. Currently, this technology is not able to measure samples which contain water (including the *in vitro* models). However, new developments in

FTIR technology suggest this may be possible in the future. Bonds present in wax embedded sections of our models were measured and a few bonds identified which may be of interest clinically. For this to be developed further it will require the potentially useful bonds to be identified using samples from clinical tissues as our models do not include all the components which are present in cancerous and potentially malignant tissues such as endothelial and immune components. Tissue engineered models may have a use in developing and optimising this technology to be used in the presence of water.

Finally, we imaged tissue engineered models using optical coherence tomography (OCT). This imaging method is rapid and capable of obtaining clear images *in vivo* in live patients without the need for anaesthetic and with little or no motion artefacts. OCT is already making a great difference in the treatment and detection of many ocular diseases but using OCT for oral diagnostics is a relatively new idea. The data we obtained from the tissue engineered models was promising and clearly demonstrated the ability of OCT to image the epithelial connective tissue junction. The ability to see this junction could enable detection of epithelial hyperplasia and disruptions to the basement membrane which are features of potentially malignant lesions as well as other diseases of the oral mucosa. The images obtained from the different tissue engineered models were for the most part similar to one another except for the models cultured from the Cal27 cell line. In this model the epithelium was seriously disrupted and OCT was able to image the abnormal surface morphology of this model. A vertical banding could be seen throughout the image (Figure 4.24), something which was also observed *in vivo* in a squamous cell carcinoma (Figure 1.16). It has previously been observed that the images which can be obtained *in vivo* have better clarity and resolution compared to images taken *ex vivo* and *in vitro*. This was also seen in this project as the images obtained *in vivo* of the mucosal surface of the lower lip using the Optovue® system gave far greater contrast compared to our images of the *in vitro* models. The clear visual appearance of the epithelium, surface topology as well as features in the connective tissue including blood vessels and minor salivary glands (Figure 4.25) highlights the potential of this technology in the diagnosis of many oral diseases. Further developments are required before OCT can be used clinically, for example an endoscopic device is required and the imaging parameters will need to be optimised for oral rather than ocular applications. Once these factors have been considered it will be very interesting to see the results which can be obtained from clinical trials using this technology.

In conclusion, the tissue engineered oral models are a great advance on the use of monolayer cell cultures for a wide range of laboratory studies. They may be particularly valuable in pre-clinical studies to develop and evaluate therapeutic and diagnostic technologies, such as the polymersome drug delivery vehicles and C_{12}-resazurin metabolic stain used here, before they are ready for use in patients. But for more established technologies that have already been

proven safe for use in patients e.g. impedance spectroscopy and OCT, they may not yet be good enough to replace patients in clinical trials. Nonetheless, continuing improvement in tissue engineered models to more accurately replicate the *in vivo* situation will continue to expand the areas of research in which they prove valuable.

Chapter 6: Appendices

6.1 Appendix 1 Polymersomes

Polymersomes are a new technology which is still undergoing significant development and optimisation. Standardised, large scale synthesis of the polymers used here has not yet been achieved, resulting in variation in the polymers synthesised by different members in the Department of Chemistry at different times. The synthesis method used to produce these block co-polymers is complicated and is dependant on many factors including laboratory temperature. Overcoming these many variable factors and identifying the problems took many months to complete. Unfortunately this meant for a crucial period in this project there was a lack of comparable polymers available. For this reason there are some results presented here which would have benefited from substantial amounts of further work and repeats however, this was not possible with the materials available to me in the time frame allowed for this project. The following information has been included for completeness and serves as an illustration of the problems encountered through the project.

Variation between polymer batches

Throughout this project several different polymer batches were used. Table 6.1 shows which polymer was used for each experiment and the properties of the polymer. Figure 6.1 shows the variation in cyto-toxicity resulting from the different batches when tested on NOF cells (Figure 6.1a) and FaDu cells (Figure 6.1b) under the same conditions.

The difference in viability of FaDu cells exposed to the different bathes of PMPC-PDPA is evident in (Figure 6.1b). After 24hours exposed to batch 12 PMPC-PDPA polymersomes the FaDu cells were 51% viable compared to FaDu cells exposed to batch 4 of PMPC-PDPA which were 95% viable. After 48 hours the cells showed lower viabilities for all batches of PMPC-PDPA. The polymer batch JPD70 showed the highest viability with 83% of cells remaining viable after 48 hours. In comparison, 24% of the cells exposed to batch 12 PMPC-PDPA cells remained viable.

As well as cell viability there were also issues surrounding polymersome formation and the precipitation of polymers.

Polymer batch number	Block co-polymer composition (1H NMR)	Date synthesised	Synthesised by	Initiator	Experiments used for in this thesis
Original WEP049023	No data Target PMPC $_{25}$ PDPA $_{70}$	2nd Nov 2007	Biocompatibles UK	No data	TEOM, histology of spheroids with fluorescent Rho
Polymer 1 PTP7 (1st batch cleaned)	PMPC $_{25}$ PDPA $_{67}$	27th June 2008	Dept. Chemistry, University of Sheffield (Dr. Paul Topham)	Azide	Spheroid and Monolayer FACS and toxicity
Polymer 2 PTP7 (2nd batch cleaned)	PMPC $_{25}$ PDPA $_{67}$	28th July 2008	Dept. Chemistry, University of Sheffield (Dr. Paul Topham)	Azide	Spheroid and Monolayer FACS and toxicity
Polymer 3 NWG5	PMPC $_{25}$ PDPA $_{63}$	Summer 2008	Dept. Chemistry, University of Sheffield (Nick Warren)	Morpholino-based initiator (MEBr)	Spheroid and Monolayer FACS and toxicity
Polymer 4	?	Summer 2008	Dept. Chemistry, University of Sheffield	?	Spheroid and Monolayer FACS and toxicity
Polymers 5-20	Variable	2008-2010	Dept. Chemistry, University of Sheffield	Variable	8,10 and 12 toxicity (Figure 6.1). Not used for other experiments because of precipitation and toxicity
JPD-70		Jan 2010	Dept. Chemistry, University of Sheffield (Jeppe Madsen)		Batch testing (DLS trace not polymersomes-precipitation)

**Table 6.1**
Batches of PMPC-PDPA polymersomes
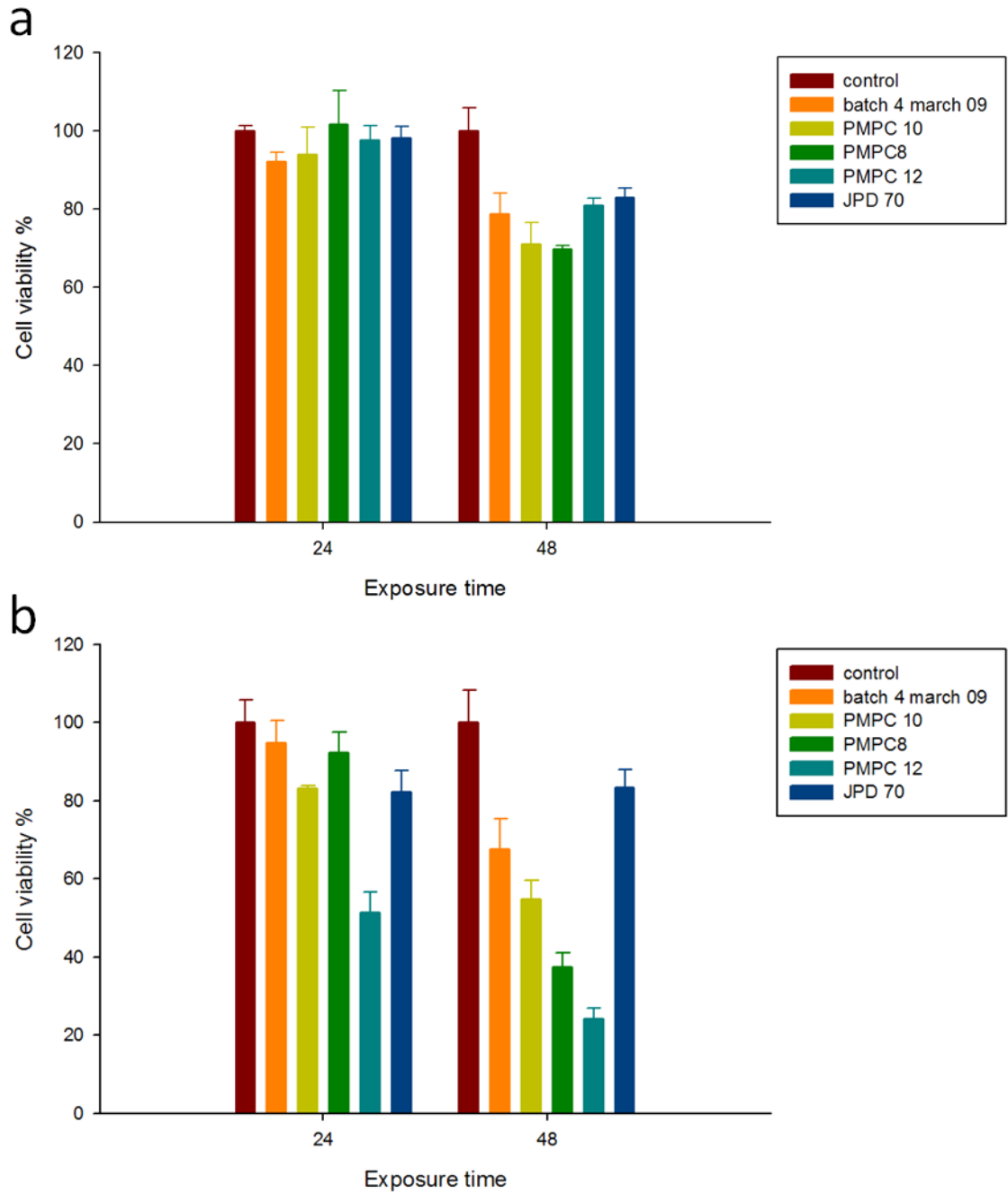
Figure 6.1 Viability of NOF cells exposed to different batches of PMPC-PDPA (a) and FaDu cells exposed to different batches of PMPC-PDPA (b) for 24 and 48 hours.

6.2 Appendix 2 Fluorescence

How to compare the two different polymers

In order for the PMPC-PDPA and PEO-PDPA polymers to be compared against one another they must have comparable detectable characteristics. Throughout this project the polymersomes have been fluorescently labelled in two different ways. The first method of labelling the polymersomes fluorescently was by encapsulating an amphiphilic rhodamine dye (Rhodamine B octadecyl ester perchlorate) within the membrane of the polymersome.

Figure 6.2 shows the uptake of the PMPC-PDPA polymersomes compared to the PEO-PDPA polymersomes in FaDu cells. From this experiment it looks as though the PMPC-PDPA polymersomes were taken up faster and in larger amounts (as determined by FACS analysis looking at the proportion of cells with detectable fluorescence and the median fluorescence intensity of each cell). However, when the fluorescence intensity of the two different polymersome solutions were measured after the column at variable concentrations, using a fluorescence spectroscopy plate reader, it could be seen that the PMPC-PDPA polymersome solution had a much higher fluorescence intensity compared to the PEO-PDPA solution (Figure 6.3). The PMPC-PDPA solution had a fluorescence intensity of 157 a.u when the concentration of the polymersomes was 0.34μM however, the same intensity of fluorescence in the PEO-PDPA sample corresponds to 4.28μM; 12.5 times higher. Therefore the result seen in the FaDu cells exposed to both polymersome solutions is most likely not an inherent difference between the two polymers but instead an artefact created by the difference in fluorescence intensities. One reason for the lower fluorescence intensity is the encapsulation efficiency of Rhodamine B octadecyl ester perchlorate dye by the PEO-PDPA polymersomes as demonstrated in the profile of the fractions eluted from the GPC column. It is clear in Figure 6.4 that the majority of the amphiphilic rhodamine is not encapsulated in the PEO-PDPA polymersomes (fractions 6-10ml after first fraction) but are eluted from the column as free rhodamine in fractions around 25 -30ml after the first fraction.
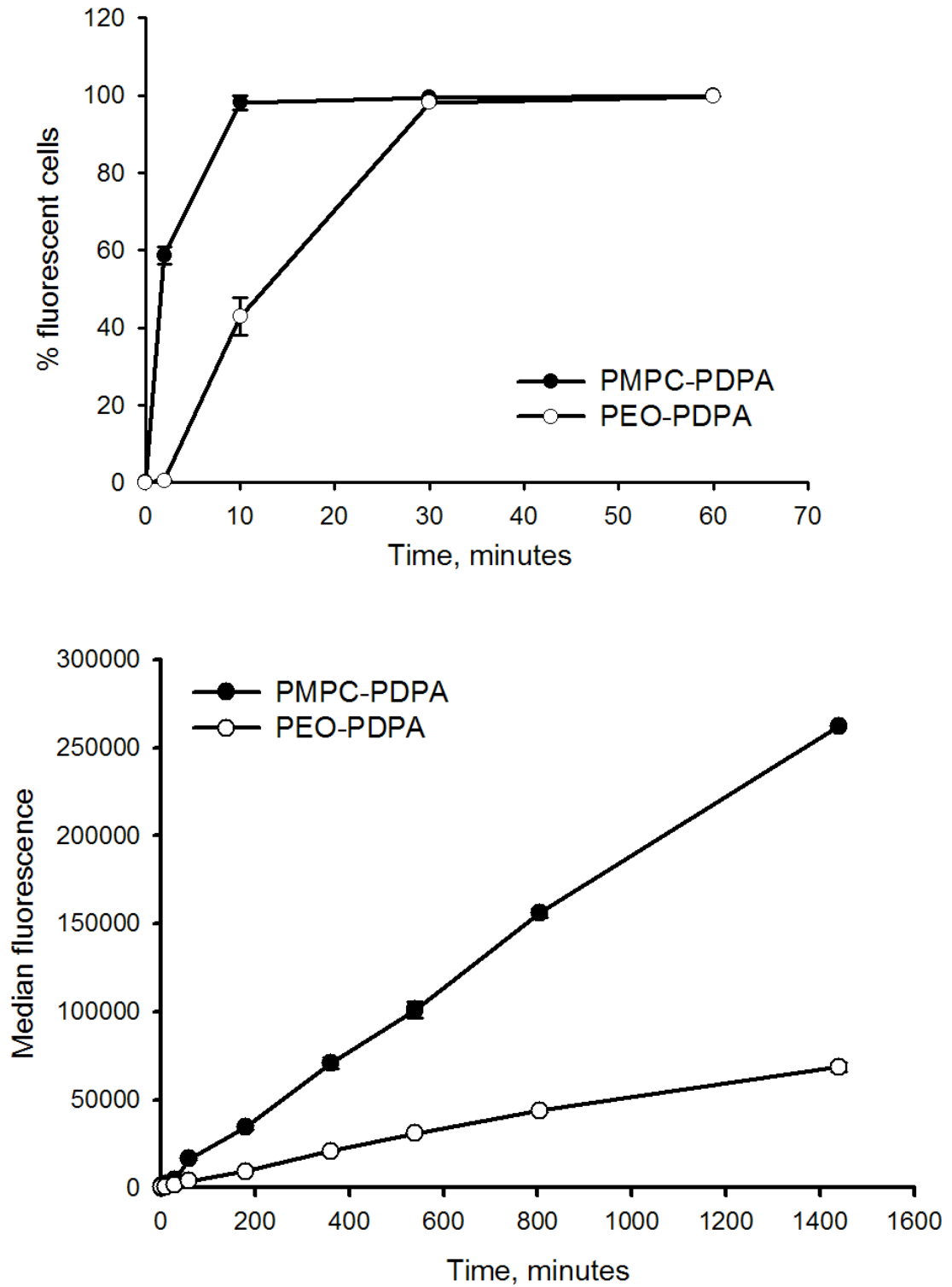
Figure 6.2 Relative uptake of PEO-PDPA and PMPC-PDPA polymersomes labelled with amphiphilic rhodamine by FaDu cells.
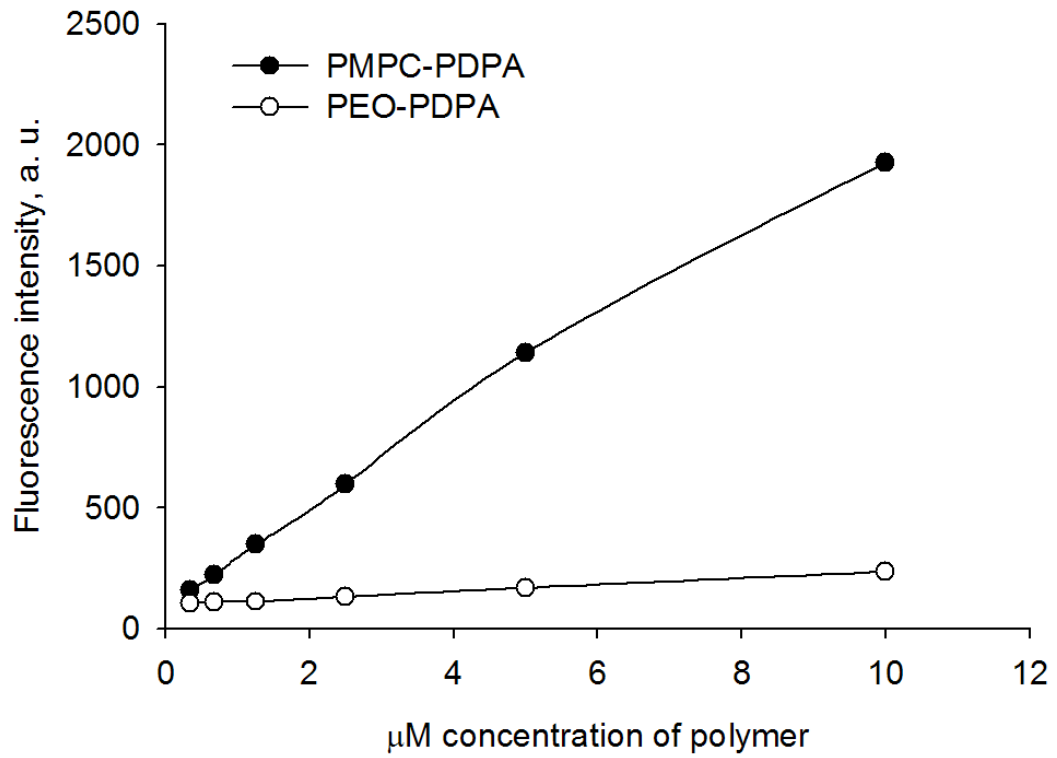
Figure 6.3 Fluorescence intensity of both polymersome formulations with encapsulated amphiphilic rhodamine dye (at various concentrations).
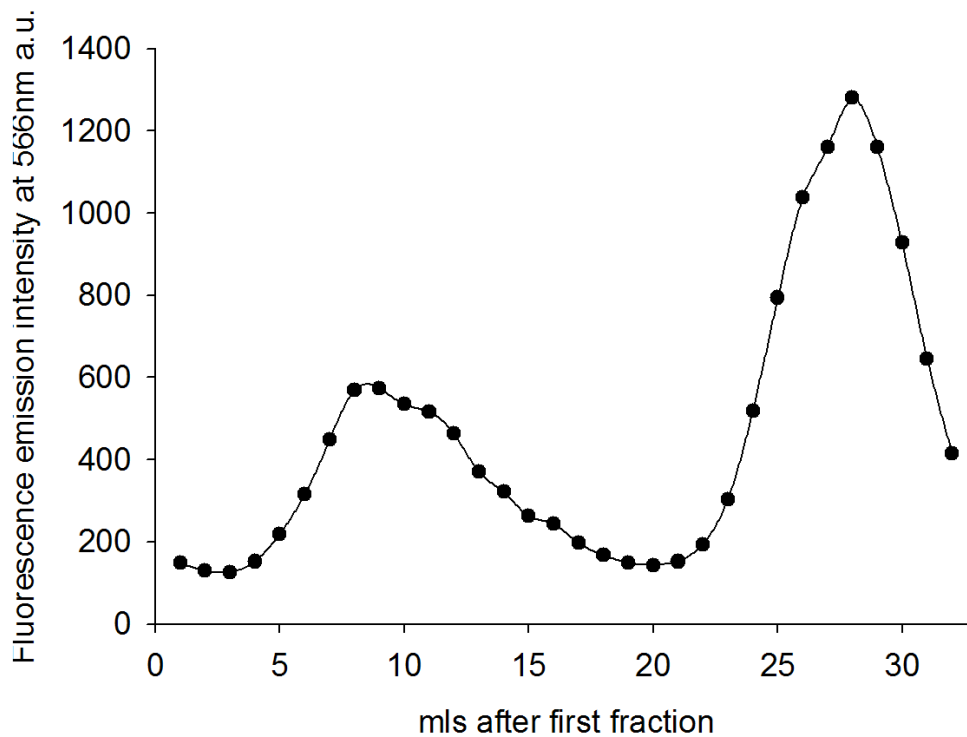
Figure 6.4 Fluorescence profile of fractions leaving the GPC column for PEO-PDPA encapsulating amphiphilic rhodamine dye.

The second method of fluorescently labelling polymersome samples was to use a fluorescently labelled polymer, with rhodamine 6G covalently conjugated to the terminal of the PMPC block

on the PMPC-PDPA polymer chain. The fluorescent polymer chains were added to the unlabelled polymer at a 5% molar concentration. This same PMPC-PDPA polymer could also be added to the PEO-PDPA polymer to label this. When used to label the PEO-PDPA polymersomes the rho-PMPC-PDPA was added to the unlabelled PEO-PDPA at 5 molar %. The fluorescence intensity for the two polymers using this approach was still significantly different (Figure 6.5) however, instead of a 12.5 fold difference the difference was nearer 2.3 (with the same fluorescence intensity corresponding to 1μM of PEO-PDPA compared to 0.432μM of PMPC-PDPA). The drawback of labelling the PEO-PDPA polymersomes in this way is that the influence of Rho-PMPC-PDPA chains within the polymersomes may affect the uptake profile.

Some attempts have been made to quantify the amount of polymersomes within cells in a way which is not as affected by the differences in fluorescence. The method described in (Massignani *et al.,* 2009) involved lysing the cells after exposure to polymersomes. The intensity of this lysate could then be correlated back to a calibration curve of a known quantity of polymersomes in cell debris. Unfortunately this method did not work for the experiments performed in this project, most likely due to the high level of scattering caused by the cell debris and the method used to lyse the cells. In conclusion the method for fluorescently labelling the 2 different polymers needs to be improved before these two can be directly compared
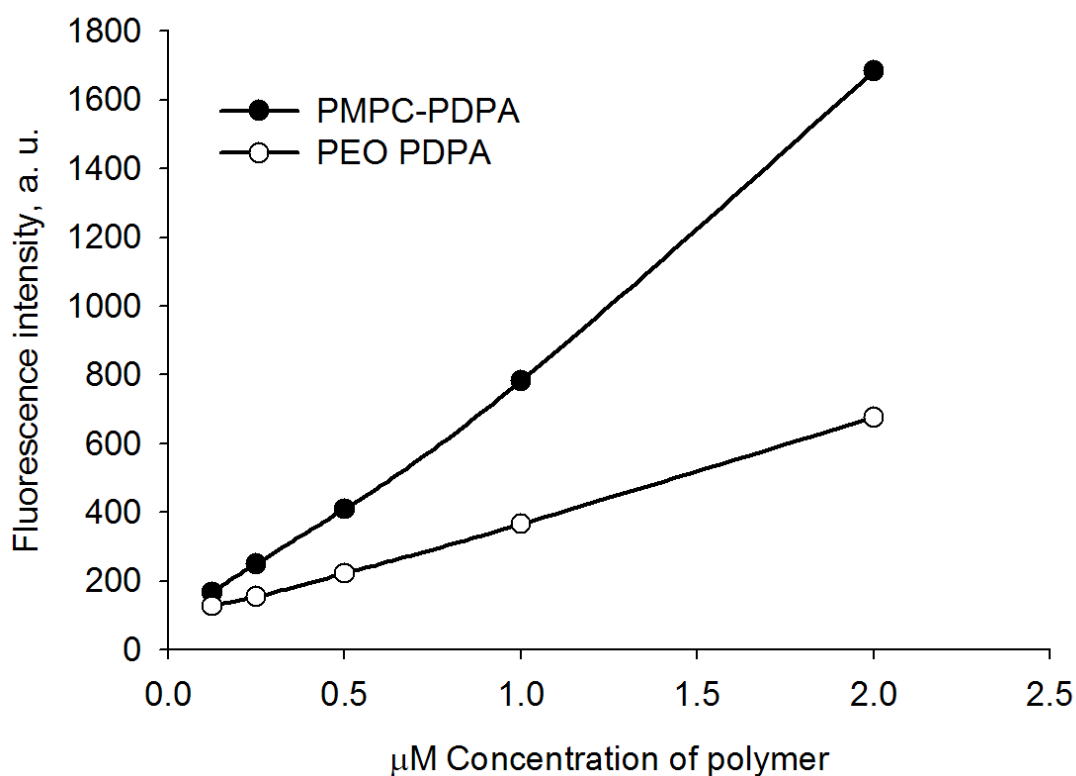
Figure 6.5 Fluorescence intensity of two polymersome formulations with 5 molar % Rho-PMPC-PDPA.

Chapter 7: References

Abdul, S., Brown, B. H., Milnes, P. and Tidy, J. A. (2006). "The use of electrical impedance spectroscopy in the detection of cervical intraepithelial neoplasia." Int J Gynecol Cancer **16**(5): 1823-32.

Ahmed, F., Pakunlu, R. I., Brannan, A., Bates, F., Minko, T. and Discher, D. E. (2006). "Biodegradable polymersomes loaded with both paclitaxel and doxorubicin permeate and shrink tumors, inducing apoptosis in proportion to accumulated drug." J Control Release **116**(2): 150-8.

Ahmed, F., Pakunlu, R. I., Srinivas, G., Brannan, A., Bates, F., Klein, M. L., Minko, T. and Discher, D. E. (2006). "Shrinkage of a rapidly growing tumor by drug-loaded polymersomes: pH-triggered release through copolymer degradation." Mol Pharm **3**(3): 340-50.

Alaminos, M., Garzon, I., Sanchez-Quevedo, M. C., Moreu, G., Gonzalez-Anadres, M., Fernandez-Montoya, A. and Campos, A. (2007). "Time-course study of histological and genetic patterns of differntiation in human engineered oral mucosa." Journal of Tissue Engineering and Regeneraitive Medicine **1**: 350-359.

Alberts, B., Johnson, A., Lewis, J., Raff, M., Roberts, K. and Walter, P. (2002). Molecular Biology of the Cell, Garland Science.

Aranda-Espinoza, H., Bermudez, H., Bates, F. S. and Discher, D. E. (2001). "Electromechanical Limits of Polymersomes." Physical Review Letters **87**(20): 208301.

Argiris, A., Karamouzis, M. V., Raben, D. and Ferris, R. L. (2008). "Head and neck cancer." Lancet **371**: 1695-709.

Arifin, D. R. and Palmer, A. F. (2005). "Polymersome Encapsulated Hemoglobin: A Novel Type of Oxygen Carrier." Biomacromolecules **6**(4): 2172-2181.

Atala, A., Bauer, S. B., Soker, S., Yoo, J. J. and Retik, A. B. (2006). "Tissue-engineered autologous bladders for patients needing cystoplasty." Lancet **367**(9518): 1241-6.

Ballangrud, A. M., Yang, W. H., Charlton, D. E., McDevitt, M. R., Hamacher, K. A., Panageas, K. S., Ma, D., Bander, N. H., Scheinberg, D. A. and Sgouros, G. (2001). "Response of LNCaP spheroids after treatment with an alpha-particle emitter (213Bi)-labeled anti-prostate-specific membrane antigen antibody (J591)." Cancer Res **61**(5): 2008-14.

Bangham, A. D. (1961). "A correlation between surface charge and coagulant action of phospholipids." Nature **192**: 1197-1198.

Battaglia, G. (2005). Amphiphlic polymeric membranes - PhD Thesis. Department of Chemistry. Sheffield, University of Sheffield. **PhD:** 215.

Battaglia, G. and Ryan, A. (2005). "Bilayers and Interdigitation in Block Copolymer Vesicles." J. Am. Chem. Soc. **127**: 8757 - 8764.

Battaglia, G., Ryan, A. J. and Tomas, S. (2006). "Polymeric Vesicle Permeability: A Facile Chemical Assay." Langmuir **22**(11): 4910-4913.

Battaglia, G., Tomas, S. and Ryan, A. (2007). "Lamellarsomes: metastable polymeric multilamellar aggregates." Soft Matter **3**: 470-475.

Bechtel, B. (2010). OCT devices increasingly finding use outside retinal practice. Ocular Surger News U.S edition.

Ben-Haim, N., Broz, P., Marsch, S., Meier, W. and Hunziker, P. (2008). "Cell-Specific Integration of Artificial Organelles Based on Functionalized Polymer Vesicles." Nano Letters **8**(5): 1368-1373.

Bezerra, H. G., Costa, M. A., Guagliumi, G., Rollins, A. M. and Simon, D. I. (2009). "Intracoronary Optical Coherence Tomography: A Comprehensive Review: Clinical and Research Applications." JACC: Cardiovascular Interventions **2**(11): 1035-1046.

Bhargava, S., Chapple, C. R., Bullock, A. J., Layton, C. and MacNeil, S. (2004). "Tissue-engineered buccal mucosa for substitution urethroplasty." BJU Int **93**(6): 807-11.

Bhargava, S., Patterson, J. M., Inman, R. D., MacNeil, S. and Chapple, C. R. (2008). "Tissue-Engineered Buccal Mucosa Urethroplasty--Clinical Outcomes." European Urology **53**(6): 1263-1271.

Blackwood, K. A., McKean, R., Canton, I., Freeman, C. O., Franklin, K. L., Cole, D., Brook, I., Farthing, P., Rimmer, S., Haycock, J. W., Ryan, A. J. and MacNeil, S. (2008). "Development of biodegradable electrospun scaffolds for dermal replacement." Biomaterials **29**(21): 3091-3104.

Blot, W. J., McLaughlin, J. K., Winn, D. M., Austin, D. F., Greenberg, R. S., Preston-Martin, S., Bernstein, L., Schoenberg, J. B., Stemhagen, A. and Fraumeni, J. F., Jr. (1988). "Smoking and Drinking in Relation to Oral and Pharyngeal Cancer." Cancer Res **48**(11): 3282-3287.

Bullock, A. J., Barker, A. T., Coulton, L. and Macneil, S. (2007). "The effect of induced biphasic pulsed currents on re-epithelialization of a novel wound healing model." Bioelectromagnetics **28**(1): 31-41.

CancerResearchUK. (2005, 30th April 2005). "Oral cancer- survival statistics for England and Wales." Retrieved 22nd March, 2010, from http://info.cancerresearchuk.org/cancerstats/types/oral/survival/index.htm.

CancerResearchUK. (2009, 19th June 2009). "Cancer Incidence for common cancers- UK statistics." Retrieved 22nd March 2010, 2010, from http://info.cancerresearchuk.org/cancerstats/incidence/commoncancers/index.htm.

CancerResearchUK. (2009, 4th September 2009). "Oral Cancer- Risk factors." Retrieved 22nd March, 2010, from http://info.cancerresearchuk.org/cancerstats/types/oral/riskfactors/index.htm.

CancerResearchUK. (2009, 10 August 2009). "Oral Cancer- UK incidence statistics." Retrieved 22 March 2010, 2010, from http://info.cancerresearchuk.org/cancerstats/types/oral/incidence/index.htm.

Carlsson, J. and Yuhas, J. M. (1984). "Liquid-overlay culture of cellular spheroids." Recent Results Cancer Res **95**: 1-23.

Cerritelli, S., Velluto, D. and Hubbell, J. A. (2007). "PEG-SS-PPS: Reduction-Sensitive Disulfide Block Copolymer Vesicles for Intracellular Drug Delivery." Biomacromolecules **8**(6): 1966-1972.

Cevc, G. and Gebauer, D. (2003). "Hydration-driven transport of deformable lipid vesicles through fine pores and the skin barrier." Biophys J **84**(2 Pt 1): 1010-24.

Chai, W. L., Moharamzadeh, K., Brook, I. M., Emanuelsson, L., Palmquist, A. and van Noort, R. (2010). "Development of a novel model for the investigation of implant-soft tissue interface." J Periodontol **81**(8): 1187-95.

Chakrabarty, K. H., Dawson, R. A., Harris, P., Layton, C., Babu, M., Gould, L., Phillips, J., Leigh, I., Green, C., Freedlander, E. and Mac Neil, S. (1999). "Development of autologous human dermal-epidermal composites based on sterilized human allodermis for clinical use." Br J Dermatol **141**(5): 811-23.

Chen, R. W. S., Duker, J. S., Srinivasan, V. and Fujimoto, J. G. (2007). "Speed and Resolution Improve in Newest OCT." Review of Opthalmology: 84 - 88.

Chou, J. T. Y. (1957). "The Fixation of Adipose Fat by Potassium Dichromate." Quarterly Journal and Microscopical Science **98**(4): 431-433.

Choucair, A., Soo, P. L. and Eisenberg, A. (2005). "Active loading and tunable release of doxorubicin from block copolymer vesicles." Langmuir **21**(20): 9308-13.

Colley, H. E., Hearnden, V., Jones, A. V., Weinreb, P. H., MacNeil, S., Thornhill, M. H. and Murdoch, C. (2010). "Development of tissue engineered models of oral dysplasia and early invasive oral squamous cell carcinoma " in preparation.

Cooper, M. L., Andree, C., Hansbrough, J. F., Zapata-Sirvent, R. L. and Spielvogel, R. L. (1993). "Direct Comparison of a Cultured Composite Skin Substitute Containing Human Keratinocytes and Fibroblasts to an Epidermal Sheet Graft Containing Human Keratinocytes on Athymic Mice." J Investig Dermatol **101**(6): 811-819.

Corporation, M. (2008). "EpiOral Normal Human Buccal Tissue Models." from http://www.mattek.com/pages/products/epioral.

Costea, D. E., Dimba, A. O. E., Loro, L. L., Vintermyr, O. K. and Johannessen, A. C. (2005). "The phenotype of in vitro reconstituted normal human oral epithelium is essentially determined by culture medium." Journal of Oral Pathology & Medicine **34**(4): 247-252.

Costea, D. E., Kulasekara, K., Neppelberg, E., Johannessen, A. C. and Vintermyr, O. K. (2006). "Species-Specific Fibroblasts Required for Triggering Invasiveness of Partially Transformed Oral Keratinocytes." American Journal of Pathology **168**(6): 1889-1897.

Costea, D. E., Loro, L. L., Dimba, E. A. O., Vintermyr, O. K. and Johannessen, A. C. (2003). "Crucial Effects of Fibroblasts and Keratinocyte Growth Factor on Morphogenesis of Reconstituted Human Oral Epithelium." Journal of Investigative Dermatology **121**(6): 1479-1486.

Cottin, S., Ghani, K., de Campos-Lima, P. O. and Caruso, M. (2010). "Gemcitabine intercellular diffusion mediated by gap junctions: new implications for cancer therapy." Mol Cancer **9**(141): 141.

de la Fuente, M., Csaba, N., Garcia-Fuentes, M. and Alonso, M. J. (2008). "Nanoparticles as protein and gene carriers to mucosal surfaces." Nanomedicine **3**(6): 845-857.

de Ridder, L., Cornelissen, M. and de Ridder, D. (2000). "Autologous spheroid culture: a screening tool for human brain tumour invasion." Crit Rev Oncol Hematol **36**(2-3): 107-22.

Deshpande, P., Notara, M., Bullett, N., Daniels, J. T., Haddow, D. B. and MacNeil, S. (2009). "Development of a surface-modified contact lens for the transfer of cultured limbal epithelial cells to the cornea for ocular surface diseases." Tissue Eng Part A **15**(10): 2889-902.

Discher, B. M., Won, Y., Ege, D. S., Lee, J. C. M., Bates, F. S., Discher, D. E. and Hammer, D. A. (1999). "Polymersomes: Tough Vesicles Made from Diblock Copolymers." Science **284**: 1143-1146.

Discher, D. E. and Ahmed, F. (2006). "Polymersomes." Annu. Rev. Biomed.Eng. **8**: 323-341.

Discher, D. E. and Eisenberg, A. (2002). "Polymer vesicles." Science **297**(5583): 967-73.

Discher, D. E., Ortiz, V., Srinivas, G., Klein, M. L., Kim, Y., Christian, D., Cai, S., Photos, P. and Ahmed, F. (2007). "Emerging applications of polymersomes in delivery: From molecular dynamics to shrinkage of tumors." Progress in Polymer Science **32**(8-9): 838-857.

DTP. (2010). "Screening Services, NCI-60 DTP Human Tumor Cell Line Screen "   Retrieved 17th August 2010, from http://dtp.nci.nih.gov/branches/btb/ivclsp.html.

Du, J., Tang, Y., Lewis, A. L. and Armes, S. P. (2005). "pH-Sensitive Vesicles Based on a Biocompatible Zwitterionic Diblock Copolymer." J. Am. Chem. Soc. **127**(51): 17982-17983.

Dubessy, C., Merlin, J. M., Marchal, C. and Guillemin, F. (2000). "Spheroids in radiobiology and photodynamic therapy." Crit Rev Oncol Hematol **36**(2-3): 179-92.

Duncan, R. (2003). "The dawning era of polymer therapeutics." Nature Rev. Drug Discov. **2**: 347-360.

Duong, H. S., Le, A. D., Zhang, Q. and Messadi, D. V. (2005). "A novel 3-dimensional culture system as an in vitro model for studying oral cancer cell invasion." International Journal of Experimental Pathology **86**(6): 365-374.

Duvillard, C., Romanet, P., Cosmidis, A., Beaudouin, N. and Chauffert, B. (2004). "Phase 2 study of intratumoral cisplatin and epinephrine treatment for locally recurrent head and neck tumors." Ann Otol Rhinol Laryngol **113**(3 Pt 1): 229-33.

Elenbaas, B. and Weinberg, R. A. (2001). "Heterotypic Signaling between Epithelial Tumor Cells and Fibroblasts in Carcinoma Formation." Experimental Cell Research **264**(1): 169-184.

Epstein, H., Gutman, D., Cohen-Sela, E., Haber, E., Elmalak, O., Koroukhov, N., Danenberg, H. D. and Golomb, G. (2008). "Preparation of alendronate liposomes for enhanced stability and bioactivity: in vitro and in vivo characterization." Aaps J **10**(4): 505-15.

Essand, M., Gronvik, C., Hartman, T. and Carlsson, J. (1995). "Radioimmunotherapy of prostatic adenocarcinomas: effects of 131I-labelled E4 antibodies on cells at different depth in DU 145 spheroids." Int J Cancer **63**(3): 387-94.

EuropeanCommission. (2010). "Ban on animal testing - Cosmetics - Consumer Affairs."   Retrieved August 2010, 2010, from http://ec.europa.eu/consumers/sectors/cosmetics/animal-testing/index_en.htm.

Eves, P., Katerinaki, E., Simpson, C., Layton, C., Dawson, R., Evans, G. and Mac Neil, S. (2003). "Melanoma invasion in reconstructed human skin is influenced by skin cells--investigation of the role of proteolytic enzymes." Clin Exp Metastasis **20**(8): 685-700.

Eves, P., Layton, C., Hedley, S., Dawson, R. A., Wagner, M., Morandini, R., Ghanem, G. and Mac Neil, S. (2000). "Characterization of an in vitro model of human melanoma invasion based on reconstructed human skin." Br J Dermatol **142**(2): 210-22.

FDA. (2009, 28th December 2009). "Cellular and Gene Therapy Products." 2010, from http://www.fda.gov/BiologicsBloodVaccines/CellularGeneTherapyProducts/default.htm.

Feinberg, S. E., Aghaloo, T. L. and Cunningham, J. L. L. (2005). "Role of Tissue Engineering in Oral and Maxillofacial Reconstruction: Findings of the 2005 AAOMS Research Summit." Journal of Oral and Maxillofacial Surgery **63**(10): 1418-1425.

Friedrich, J., Ebner, R. and Kunz-Schughart, L. A. (2007). "Experimental anti-tumor therapy in 3-D: Spheroids - old hat or new challenge?" Int. J. Radiat. Biol. **83**(11-12): 849-871.

Friedrich, J., Seidel, C., Ebner, R. and Kunz-Schughart, L. A. (2009). "Spheroid-based drug screen: considerations and practical approach." Nat Protoc **4**(3): 309-24.

Fujimoto, J. G. (2003). "Optical coherence tomography for ultrahigh resolution in vivo imaging." Nat Biotechnol **21**(11): 1361-7.

Fuwa, N., Kodaira, T., Furutani, K., Tachibana, H., Nakamura, T. and Daimon, T. (2007). "Chemoradiation therapy using radiotherapy, systemic chemotherapy with 5-fluorouracil and nedaplatin, and intra-arterial infusion using carboplatin for locally advanced head and neck cancer - Phase II study." Oral Oncology **43**(10): 1014-1020.

Gaballah, K., Costea, D. E., Hills, A., Gollin, S. M., Harrison, P. and Partridge, M. (2008). "Tissue engineering of oral dysplasia." J Pathol **215**(3): 280-9.

Gabizon, A., Shmeeda, H. and Barenholz, Y. (2003). "Pharmacokinetics of pegylated liposomal Doxorubicin: review of animal and human studies." Clin Pharmacokinet **42**(5): 419-36.

Galey, W. M., Londsdale, H. K. and Nacht, S. (1976). "The in vitro permeability of skin and buccal mucosa to selected drugs and tritiated water." Journal of Investigative Dermatology **67**(6): 713-717.

Ganem-Quintanar, A., Falson-Rieg, F. and Buri, P. (1997). "Contribution of lipid components to the permeability barrier of oral mucosa." European Journal of Pharmaceutics and Biopharmaceutics **44**(2): 107-120.

Georgakoudi, I., Rice, W. L., Hronik-Tupaj, M. and Kaplan, D. L. (2008). "Optical Spectroscopy and Imaging for the Noninvasive Evaluation of Engineered Tissues." Tissue Engineering **14**(4): 1-20.

Ghoroghchian, P. P., Frail, P. R., Susumu, K., Blessington, D., Brannan, A. K., Bates, F. S., Chance, B., Hammer, D. A. and Therien, M. J. (2005). "Near-infrared-emissive polymersomes: Self-assembled soft matter for in vivo optical imaging." Proc Natl Acad Sci U S A **102**(8): 2922-2927.

Gottfried, E., Kunz-Schughart, L. A., Andreesen, R. and Kreutz, M. (2006). "Brave little world: spheroids as an in vitro model to study tumor-immune-cell interactions." Cell Cycle **5**(7): 691-5.

Green, S. K., Francia, G., Isidoro, C. and Kerbel, R. S. (2004). "Antiadhesive antibodies targeting E-cadherin sensitize multicellular tumor spheroids to chemotherapy in vitro." Mol Cancer Ther **3**(2): 149-59.

Hamakawa, H., Nakashiro, K., Sumida, T., Shintani, S., Myers, J. N., Takes, R. P., Rinaldo, A. and Ferlito, A. (2008). "Basic evidence of molecular targeted therapy for oral cancer and salivary gland cancer." Head Neck **30**(6): 800-9.

Hammer, D. A., Robbins, G. P., Haun, J. B., Lin, J. J., Qi, W., Smith, L. A., Ghoroghchian, P. P., Therien, M. J. and Bates, F. S. (2008). "Leuko-polymersomes." Faraday Discuss **139**: 129-41; discussion 213-28, 419-20.

Harries, M., Ellis, P. and Harper, P. (2005). "Nanoparticle albumin-bound paclitaxel for metastatic breast cancer." J Clin Oncol **23**(31): 7768-71.

Harrington, K. J., Nutting, C. M. and Pandha, H. S. (2005). "Gene therapy for head and neck cancer." Cancer Metastasis Rev **24**(1): 147-64.

Hauptmann, S., Zwadlo-Klarwasser, G., Jansen, M., Klosterhalfen, B. and Kirkpatrick, C. J. (1993). "Macrophages and multicellular tumor spheroids in co-culture: a three-dimensional model to study tumor-host interactions. Evidence for macrophage-mediated tumor cell proliferation and migration." Am J Pathol **143**(5): 1406-15.

Hearnden, V., Lomas, H., MacNeil, S., Thornhill, M., Murdoch, C., Lewis, A. L., Madsen, J., Blanazs, A., Armes, S. P. and Battaglia, G. (2009). "Diffusion studies of nanometer polymersomes across tissue engineered human oral mucosa." Pharmaceutical Research **26**(7): 1718-1728.

Hearnden, V., Sankar, V., Katrusha Hull, K., Juras, D. V., Greenberg, M., Kerr, A., Lockhart, P., Patton, L., Porter, S. and Thornhill, M. H. (in preparation). "New developments in topical and systemic oral mucosal drug delivery ".

Herrmann, R., Fayad, W., Schwarz, S., Berndtsson, M. and Linder, S. (2008). "Screening for compounds that induce apoptosis of cancer cells grown as multicellular spheroids." J Biomol Screen **13**(1): 1-8.

Hirschhaeuser, F., Menne, H., Dittfeld, C., West, J., Mueller-Klieser, W. and Kunz-Schughart, L. A. (2010). "Multicellular tumor spheroids: an underestimated tool is catching up again." J Biotechnol **148**(1): 3-15.

Hirschhaeuser, F., Walenta, S. and Mueller-Klieser, W. (2010). "Efficacy of catumaxomab in tumor spheroid killing is mediated by its trifunctional mode of action." Cancer Immunol Immunother **59**(11): 1675-84.

Hoogstraate, A. J., Cullander, C., Nagelkerke, J. F., Senel, S., Verhoef, J. C., Junginger, H. E. and Bodde, H. E. (1994). "Diffusion Rates and Transport Pathways of Florescien Isothiocynate (FITC)-Labelled Model Compounds Through Buccal Epithelium." Pharmaceutical Research **11**(1): 83-89.

Horning, J. L., Sahoo, S. K., Vijayaraghavalu, S., Dimitrijevic, S., Vasir, J. K., Jain, T. K., Panda, A. K. and Labhasetwar, V. (2008). "3-D tumor model for in vitro evaluation of anticancer drugs." Mol Pharm **5**(5): 849-62.

Hsieh, P. C., Jin, Y. T., Chang, C. W., Huang, C. C., Liao, S. C. and Yuan, K. (2010). "Elastin in oral connective tissue modulates the keratinization of overlying epithelium." J Clin Periodontol **37**(8): 705-11.

Hsiung, P.-L., Nambiar, P. R. and Fujimoto, J. G. (2005). "Effect of tissue preservation on imaging using ultrahigh resolution optical coherence tomography." Journal of Biomedical Optics **10**(6): 064033-9.

Huang, S. M., Bock, J. M. and Harari, P. M. (1999). "Epidermal growth factor receptor blockade with C225 modulates proliferation, apoptosis, and radiosensitivity in squamous cell carcinomas of the head and neck." Cancer Res **59**(8): 1935-40.

Huleihel, M., Salman, A., Erukhimovitch, V., Ramesh, J., Hammody, Z. and Mordechai, S. (2002). "Novel spectral method for the study of viral carcinogenesis in vitro." Journal of Biochemical and Biophysical Methods **50**(2-3): 111-121.

Hunziker, E., Spector, M., Libera, J., Gertzman, A., Woo, S. L. Y., Ratcliffe, A., Lysaght, M., Coury, A., Kaplan, D. and Vunjak-Novakovic, G. (2006). "Translation from Research to Applications." Tissue Engineering **12**(12): 3341-3364.

IARC, I. A. f. R. o. C. (2004). "CANCERMondial GLOBOCAN 2002."   Retrieved 22nd March 2010, 2010, from http://www-dep.iarc.fr/.

Inatomi, T., Nakamura, T., Koizumi, N., Sotozono, C. and Kinoshita, S. (2008). "Current progress and challenges in ocular surface reconstruction using cultivated epithelial sheet transplantation." Med J Malaysia **63 Suppl A**(42): 42.

Ivascu, A. and Kubbies, M. (2006). "Rapid generation of single-tumor spheroids for high-throughput cell function and toxicity analysis." J Biomol Screen **11**(8): 922-32.

Ivascu, A. and Kubbies, M. (2007). "Diversity of cell-mediated adhesions in breast cancer spheroids." Int J Oncol **31**(6): 1403-13.

Jeres, W., Upile, T., Conn, B., Hamdoon, Z., Betz, C. S., McKenzie, G., Radhi, H., Vourvachis, M., El Maaytah, M., Sandison, A., Jay, A. and Hopper, C. (2010). "In vitro examination of suspicious oral lesions using optical coherence tomography." British Journal of Oral and Maxillofacial Surgery **48**(1): 18-25.

Jiang, L., Ji, N., Zhou, Y., Li, J., Liu, X., Wang, Z., Chen, Q. and Zeng, X. (2009). "CAL 27 is an oral adenosquamous carcinoma cell line." Oral Oncol **45**(11): e204-7.

Keller, D. M. (2010). "Optical Approaches to Oral Cancer Screening and Diagnosis: An Expert Interview With Petra Wilder-Smith, DDS, PhD." Medscape Medical News, 2010, from http://www.medscape.com/viewarticle/720989.

Kelm, J. M., Timmins, N. E., Brown, C. J., Fussenegger, M. and Nielsen, L. K. (2003). "Method for generation of homogeneous multicellular tumor spheroids applicable to a wide variety of cell types." Biotechnol Bioeng **83**(2): 173-80.

Kendall, C., Isabelle, M., Bazant-Hegemark, F., Hutchings, J., Orr, L., Babrah, J., Baker, R. and Stone, N. (2009). "Vibrational spectroscopy: a clinical tool for cancer diagnostics." Analyst **134**(6): 1029-45.

Kinikoglu, B., Auxenfans, C., Pierrillas, P., Justin, V., Breton, P., Burillon, C., Hasirci, V. and Damour, O. (2009). "Reconstruction of a full-thickness collagen-based human oral mucosal equivalent." Biomaterials **30**(32): 6418-25.

Kinsukawa, J., Suefuji, Y., Ryu, F., Noguchi, R., Iwamoto, O. and Kameyama, T. (2000). "Dissemination of cancer cells into circulation occurs by incisional biopsy of oral squamous cell carcinoma." Journal or Oral Pathol Med **29**: 303- 307.

Klausner, M., Ayehunie, S., Breyfogle, B. A., Wertz, P. W., Bacca, L. and Kubilus, J. (2007). "Organotypic human oral tissue models for toxicological studies." Toxicology in Vitro **21**(5): 938-949.

Knuchel, R., Hofstadter, F., Jenkins, W. E. A. and Masters, J. R. W. (1989). "Sensitivities of Monolayers and Spheroids of the Human Bladder Cancer Cell Line MGH-U1 to the Drugs Used for Intravesical Chemotherapy." Cancer Res **49**(6): 1397-1401.

Konur, A., Kreutz, M., Knuchel, R., Krause, S. W. and Andreesen, R. (1998). "Cytokine repertoire during maturation of monocytes to macrophages within spheroids of malignant and non-malignant urothelial cell lines." Int J Cancer **78**(5): 648-53.

Kulkarni, U., Mahalingam, R., Pather, S. I., Li, X. and Jasti, B. (2009). "Porcine buccal mucosa as an in vitro model: Relative contribution of epithelium and connective tissue as permeability barriers." Pharmaceutics, Preformulation and Drug Delivery **98**(2): 471-483.

Kunz-Schughart, L. A. and Knuechel, M. K. R. (1998). "Multicellular spheroids: a three-dimensional in vitro culture system to study tumour biology." International Journal of Experimental Pathology **79**(1): 1-23.

Lasic, D. D. (1994). "Sterically Stabilized Vesicles." Angew. Chem. Int. Ed **33**(17): 1685-1698.

Lasic, D. D. (1997). "Recent developments in medical applications of liposomes: sterically stabilized liposomes in cancer therapy and gene delivery in vivo." J. Control. Release **48**: 203-222.

Lasic, D. D. and Papahadjopoulos, D. (1998). Medical Applications of Liposomes. Amsterdam, Elsevier.

Lauer, G. and Schimming, R. (2001). "Tissue-engineered mucosa graft for reconstruction of the intraoral lining after freeing of the tongue: A clinical and immunohistologic study." Journal of Oral and Maxillofacial Surgery **59**(2): 169-175.

Leung, K. (2004). Ferumoxtran. Molecular Imaging and Contrast Agent Database.

Levine, D. H., Ghoroghchian, P. P., Freudenberg, J., Zhang, G., Therien, M. J., Greene, M. I., Hammer, D. A. and Murali, R. (2008). "Polymersomes: a new multi-functional tool for cancer diagnosis and therapy." Methods **46**(1): 25-32.

Li, N., Sood, S., Wang, S., Fang, M., Wang, P., Sun, Z., Yang, C. S. and Chen, X. (2005). "Overexpression of 5-Lipoxygenase and Cyclooxygenase 2 in Hamster and Human Oral Cancer and Chemopreventive Effects of Zileuton and Celecoxib." Clinical Cancer Research **11**(5): 2089-2096.

Li, S., Byrne, B., Welsh, J. and Palmer, A. F. (2007). "Self-assembled poly(butadiene)-b-poly(ethylene oxide) polymersomes as paclitaxel carriers." Biotechnol Prog **23**(1): 278-85.

Ljungkvist, A. S., Bussink, J., Rijken, P. F., Raleigh, J. A., Denekamp, J. and Van Der Kogel, A. J. (2000). "Changes in tumor hypoxia measured with a double hypoxic marker technique." Int J Radiat Oncol Biol Phys **48**(5): 1529-38.

Lomas, H., Canton, I., MacNeil, S., Du, J., Armes, S. P. A., Ryan, A. J., Lewis, A. L. and Battaglia, G. (2007). "Biomimetic pH Sensitive Polymersomes for Efficient DNA Encapsulation and Delivery." Advanced Materials **19**(23): 4238-4243.

Lomas, H., Massignani, M., Abdullah, K. A., Canton, I., Lo Presti, C., MacNeil, S., Du, J., Blanazs, A., Madsen, J., Armes, S. P., Lewis, A. L. and Battaglia, G. (2008). "Non-cytotoxic polymer vesicles for rapid and efficient intracellular delivery." Faraday Discussions **139**: 143.

Lorch, J. H., Posner, M. R., Wirth, L. J. and Haddad, R. I. (2009). "Seeking alternative biological therapies: The future of targeted molecular treatment." Oral Oncology **45**(4-5): 447-453.

Mackenzie, I. C. and Fusenig, N. E. (1983). "Regeneration of organized epithelial structure." J Invest Dermatol **81**(1 Suppl): 189s-94s.

MacNeil, S. (2007). "Progress and opportunities for tissue-engineered skin." Nature **445**(7130): 874-80.

Madhav, N. V. S., Shakya, A. K., Shakya, P. and Singh, K. (2009). "Orotransmucosal drug delivery systems: A review." Journal of Controlled Release **140**(1): 2-11.

Madigan, N. N., McMahon, S., O'Brien, T., Yaszemski, M. J. and Windebank, A. J. (2009). "Current tissue engineering and novel therapeutic approaches to axonal regeneration following spinal cord injury using polymer scaffolds." Respiratory Physiology & Neurobiology **169**(2): 183-199.

Maeda, H., Bharate, G. Y. and Daruwalla, J. (2009). "Polymeric drugs for efficient tumor-targeted drug delivery based on EPR-effect." European Journal of Pharmaceutics and Biopharmaceutics **71**(3): 409-419.

Maeda, H., Wu, J., Sawa, T., Matsumura, Y. and Hori, K. (2000). "Tumor vascular permeability and the EPR effect in macromolecular therapeutics: a review." Journal of Controlled Release **65**(1-2): 271-284.

Maggi, L., Segale, L., Conti, S., Ochoa Machiste, E., Salini, A. and Conte, U. (2005). "Preparation and evaluation of release characteristics of 3TabGum, a novel chewing device." European Journal of Pharmaceutical Sciences **24**(5): 487-493.

Massignani, M., Blanazs, A., Madsen, J., Armes, S. P., Lewis, A. L. and Battaglia, G. (2008). "Engineering polymeric nanovectors for effective and rapid cellular delivery." in preparation.

Massignani, M., Canton, I., Patikarnmonthon, N., Warren, N., Armes, S. P., Lewis, A. and Battaglia, G. (2010). "Cellular delivery of antibodies: effective targeted subcellular imaging and new therapeutic tool." Nature Precedings (http://hdl.handle.net/10101/npre.2010.4427.1).

Massignani, M., Canton, I., Sun, T., Hearnden, V., Macneil, S., Blanazs, A., Armes, S. P., Lewis, A. and Battaglia, G. (2010). "Enhanced fluorescence imaging of live cells by effective cytosolic delivery of probes." PLoS One **5**(5): e10459.

Massignani, M., LoPresti, C., Blanazs, A., Madsen, J., Armes, S. P., Lewis, A. L. and Battaglia, G. (2009). "Controlling cellular uptake by surface chemistry, size, and surface topology at the nanoscale." Small **5**(21): 2424-32.

Matsumura, Y. (2008). Polymeric Micellar Delivery Systems in Oncology. **38:** 793-802.

Matsumura, Y. and Maeda, H. (1986). " A New Concept for Macromolecular Therapeutics in Cancer Chemotherapy: Mechanism of Tumoritropic Accumulation of Proteins and the Antitumor Agent Smancs." Cancer Res. **46**(12): 6387-6392.

Matyjaszewski, K. and Spanswick, J. (2005). "Controlled/living radical polymerization." Mater. Today **8**(3): 26-33.

Mazeron, R., Tao, Y., Lusinchi, A. and Bourhis, J. (2009). "Current concepts of management in radiotherapy for head and neck squamous-cell cancer." Oral Oncology **45**(4-5): 402-408.

McGregor, F., Muntoni, A., Fleming, J., Brown, J., Felix, D. H., MacDonald, D. G., Parkinson, E. K. and Harrison, P. R. (2002). "Molecular changes associated with oral dysplasia progression and acquisition of immortality: potential for its reversal by 5-azacytidine." Cancer Res **62**(16): 4757-66.

McGregor, F., Wagner, E., Felix, D., Soutar, D., Parkinson, K. and Harrison, P. R. (1997). "Inappropriate retinoic acid receptor-beta expression in oral dysplasias: correlation with acquisition of the immortal phenotype." Cancer Res **57**(18): 3886-9.

Meng, F., Engbers, G. H. M. and Feijen, J. (2005). "Biodegradable polymersomes as a basis for artificial cells: encapsulation, release and targeting." Journal of Controlled Release **101**(1-3): 187-198.

Meurens, M., Wallon, J., Tong, J., Noël, H. and Haot, J. (1996). "Breast cancer detection by Fourier transform infrared spectrometry." Vibrational Spectroscopy **10**(2): 341-346.

Moharamzadeh, K., Brook, I. M., Scutt, A. M., Thornhill, M. H. and Van Noort, R. (2008). "Mucotoxicity of dental composite resins on a tissue-engineered human oral mucosal model." J Dent **36**(5): 331-6.

Moharamzadeh, K., Brook, I. M., Van Noort, R., Scutt, A. M. and Thornhill, M. H. (2007). "Tissue-engineered oral mucosa: a review of the scientific literature." J Dent Res **86**(2): 115-24.

Moharamzadeh, K., Franklin, K. L., Brook, I. M. and van Noort, R. (2009). "Biologic assessment of antiseptic mouthwashes using a three-dimensional human oral mucosal model." J Periodontol **80**(5): 769-75.

Morgner, U., Drexler, W., Kartner, F. X., Li, X. D., Pitris, C., Ippen, E. P. and Fujimoto, J. G. (2000). "Spectroscopic optical coherence tomography." Optics Letters **25**(2): 111- 113.

Mosmann, T. (1983). "Rapid colorimetric assay for cellular growth and survival: Application to proliferation and cytotoxicity assays." Journal of Immunological Methods **65**(1-2): 55-63.

Movasaghi, Z., Rehman, S. and Rehman, I. u. (2008). "Fourier Transform Infrared (FTIR) Spectroscopy of Biological Tissues." Applied Spectroscopy Reviews **43**(2): 134 - 179.

Mueller, M. M. and Fusenig, N. E. (2004). "Friends or foes [mdash] bipolar effects of the tumour stroma in cancer." Nat Rev Cancer **4**(11): 839-849.

Murdoch, C., Hearnden, V., Colley, H., Massignani, M., Reeves, K. J., Canton, I., Madsen, J., Blanazs, A., Armes, S. P., Lewis, A. L., Mac Neil, S., Brown, N., Thornhill, M. and Battaglia, G. (2010). "Internalization and biodistribution of polymersomes into oral squamous cell carcinoma cells in vitro and in vivo." Nanomedicine **5**(10): 1025–1036.

Nanci, A. (2003). Ten Cate's Oral Histology-Development, Structure and Function. Missouri, USA, Mosby.

Nicholson, R. I., Gee, J. M. W. and Harper, M. E. (2001). "EGFR and cancer prognosis." European Journal of Cancer **37**(Supplement 4): 9-15.

Nyström, M., Thomas, G., Stone, M., Mackenzie, I., Hart, I. and Marshall, J. (2005). "Development of a quantitative method to analyse tumour cell invasion in organotypic culture." The Journal of Pathology **205**(4): 468-475.

Ohki, T., Yamato, M., Murakami, D., Takagi, R., Yang, J., Namiki, H., Okano, T. and Takasaki, K. (2006). "Treatment of oesophageal ulcerations using endoscopic transplantation of tissue-engineered autologous oral mucosal epithelial cell sheets in a canine model." Gut **55**(12): 1704-1710.

Oliver, R. J., Sloan, P. and Pemberton, M. N. (2004). "Oral biopsies: methods and applications." British Dental Journal **196**(6): 329-333.

Olsen, K. E. (1996). Holographic multi-stereogram constructed from computer images : Applied 3-D printer. Department of Physics. Bergen, University of Bergen.

Ophof, R., van Rheden, R. E., Von den, H. J., Schalkwijk, J. and Kuijpers-Jagtman, A. M. (2002). "Oral keratinocytes cultured on dermal matrices form a mucosa-like tissue." Biomaterials **23**(17): 3741-8.

Park, J. (2002). "Liposome-based drug delivery in breast cancer treatment." Breast Cancer Research **4**(3): 95 - 99.

Poh, C. F., Ng, S. P., Williams, P. M., Zhang, L., Laronde, D. M., Lane, P., MacAulay, C. and Rosin, M. P. (2007). "Direct fluorescence visualization of clinically occult high-risk oral premalignant disease using a simple hand-held device." Head and Neck **29**(1): 71-76.

Probes, M. (2001). "Vybrant™ Cell Metabolic Assay Kit (V-23110)." 2010, from http://probes.invitrogen.com/media/pis/mp23110.pdf.

Psyrri, A., Yu, Z., Weinberger, P. M., Sasaki, C., Haffty, B., Camp, R., Rimm, D. and Burtness, B. A. (2005). "Quantitative Determination of Nuclear and Cytoplasmic Epidermal Growth Factor Receptor Expression in Oropharyngeal Squamous Cell Cancer by Using Automated Quantitative Analysis." Clinical Cancer Research **11**(16): 5856-5862.

Ralston, D. R., Layton, C., Dalley, A. J., Boyce, S. G., Freedlander, E. and Mac Neil, S. (1999). "The requirement for basement membrane antigens in the production of human epidermal/dermal composites in vitro." Br J Dermatol **140**(4): 605-15.

Rameez, S., Alosta, H. and Palmer, A. F. (2008). "Biocompatible and Biodegradable Polymersome Encapsulated Hemoglobin: A Potential Oxygen Carrier." Bioconjugate Chem **19**(5): 1025-1032.

Rheinwald, J. G. and Green, H. (1975). "Serial cultivation of strains of human epidermal keratinocytes: the formation of keratinizing colonies from single cells." Cell **6**(3): 331-43.

Ridgeway, J. M., Armstrong, W. B., Guo, S., Mahmood, U., Su, J., Jackson, J. P., Shibuya, T., Crumley, R. L., Gu, M., Chen, Z. and Wong, B. J. F. (2006). "In Vivo Optical Coherence Tomography of the Human Oral Cavity and Oropharynx." Arch Otolaryngol Head and Neck Surgery **132**: 1074-1081.

Robbins, G. P., Saunders, R. L., Haun, J. B., Rawson, J., Therien, M. J. and Hammer, D. A. (2010). "Tunable leuko-polymersomes that adhere specifically to inflammatory markers." Langmuir **26**(17): 14089-96.

Rogers, S. N., Vedpathak, S. V. and Lowe, D. (2010). "Reasons for delayed presentation in oral and oropharyngeal cancer: the patients perspective." Br J Oral Maxillofac Surg **Epub ahead of print**.

Safra, T., Groshen, S., Jeffers, S., Tsao-Wei, D. D., Zhou, L., Muderspach, L., Roman, L., Morrow, C. P., Burnett, A. and Muggia, F. M. (2001). "Treatment of patients with ovarian carcinoma with pegylated liposomal doxorubicin: analysis of toxicities and predictors of outcome." Cancer **91**(1): 90-100.

Sakata, L. M., Deleon-Ortega, J., Sakata, V. and Girkin, C. A. (2009). "Optical coherence tomography of the retina and optic nerve - a review." Clin Experiment Ophthalmol **37**(1): 90-9.

Salamat-Miller, N., Chittchang, M. and Johnston, T. P. (2005). "The use of mucoadhesive polymers in buccal drug delivery." Advanced Drug Delivery Reviews **57**(11): 1666-1691.

Salmenpera, P., Kankuri, E., Bizik, J., Siren, V., Virtanen, I, Takahashi, S., Leiss, M., Fassler, R. and Vaheri, A. (2008). "Formation and activation of fibroblast spheroids depend on fibronectin-integrin interaction." Exp Cell Res **314**(19): 3444-52.

Sankar, V., Hearnden, V., Katrusha Hull, K., Juras, D. V., Greenberg, M., Kerr, A., Lockhart, P., Patton, L., Porter, S. and Thornhill, M. H. (in preparation). "Local Drug Delivery for Oral

Mucosal Diseases: Challenges and Opportunities." <u>Oral Diseases</u> **World Workshop on Oral Medicine V**.

Schenke-Layland, K., Riemann, I., Damour, O., Stock, U. A. and König, K. (2006). "Two-photon microscopes and in vivo multiphoton tomographs -- Powerful diagnostic tools for tissue engineering and drug delivery." <u>Advanced Drug Delivery Reviews</u> **58**(7): 878-896.

Schmalz, G. (2002). "Materials Science: Biological Aspects." <u>J Dent Res</u> **81**(10): 660-663.

Schmalz, G., Schuster, U., Koch, A. and Scheweikl, H. (2002). "Cytotoxicity of Low pH Dentin-Bonding Agents in a Dentin Barrier Test In Vitro." <u>Journal of Endodontics</u> **28**(3): 188-192.

Schwarz, R. A., Gao, W., Daye, D., Williams, M. D., Richards-Kortum, R. and Gillenwater, A. M. (2008). "Autofluorescence and diffuse reflectance spectroscopy of oral epithelial tissue using a depth-sensitive fiber-optic probe." <u>Applied optics</u> **47**(6): 825.

Scully, C. and Bagan, J. (2009). "Oral squamous cell carcinoma overview." <u>Oral Oncology</u> **45**(4-5): 301-308.

Scully, C. and Bagan, J. V. (2008). "Recent advances in Oral Oncology 2007: Imaging, treatment and treatment outcomes." <u>Oral Oncology</u> **44**(3): 211-215.

Selim, M., Bullock, A. J., Blackwood, K. A., Chapple, C. R. and Macneil, S. (2010). "Developing biodegradable scaffolds for tissue engineering of the urethra." <u>BJU Int</u> **Epub ahead of print**: 12.

Selvaratnam, L., Cruchley, A. T., Navsaria, H., Wertz, P. W., Hagi-Pavli, E. P., Leigh, I. M., Squier, C. A. and Williams, D. M. (2001). "Permeability barrier properties of oral keratinocyte cultures: a model of intact human oral mucosa." <u>Oral Dis</u> **7**(4): 252-8.

Shillitoe, E. (2009). "Gene therapy: the end of the rainbow?" <u>Head and Neck Oncology</u> **1**(1): 7.

Shimono, M. and Clementi, F. (1976). "Intercellular junctions of oral epithelium. I. Studies with freeze-fracture and tracing methods of normal rat keratinized oral epithelium." <u>J Ultrastruct Res</u> **56**(1): 121-36.

Shojaei, A. H. (1998). "Buccal Mucosa As A Route For Systemic Drug Delivery: A Review." <u>J Pharm Pharmaceut Sci</u> **1**(1): 15-30.

Skala, M. C., Riching, K. M., Gendron-Fitzpatrick, A., Eickhoff, J., Eliceiri, K. W., White, J. G. and Ramanujam, N. (2007). "In vivo multiphoton microscopy of NADH and FAD redox states, fluorescence lifetimes, and cellular morphology in precancerous epithelia." <u>Proc Natl Acad Sci U S A</u> **104**(49): 19494-9.

SkinEthic. (2008). "Ban on animal testing 2009: Are you ready?" from http://www.skinethic.com/news0001051c.asp.

SkinEthic. (2008). "Reconstructed Human Oral Epithelium." from http://www.skinethic.com/HOE.asp.

Slomianka, L. (2009). "Blue Histology, Oral Cavity and Oesophagus " Retrieved 12th Oct 2010, 2010, from http://www.lab.anhb.uwa.edu.au/mb140/corepages/oral/oral.htm.

Smart, T., Lomas, H., Massignani, M., Flores-Merino, M. V., Perez, L. R. and Battaglia, G. (2008). "Block copolymer nanostructures." <u>Nanotoday</u> **3**(3-4): 1-9.

Smith, L. E., Smallwood, R. and Mac Neil, S. (2010). "A Comparison of Imaging Methodologies for 3D Tissue Engineering." <u>Microscopy Research and Technique</u> **In press**.

Sood, S., Shiff, S. J., Yang, C. S. and Chen, X. (2005). "Selection of topically applied non-steroidal anti-inflammatory drugs for oral cancer chemoprevention." Oral Oncology **41**(6): 562-567.

Speight, P. M. (2007). "Update on Oral Epithelial Dysplasia and Progression to Cancer." Head and Neck Pathology **1**: 61-66.

Squier, C. A. and Hall, B. K. (1985). "The Permeability of Skin and Oral Mucosa to Water and Horseradish Peroxidase as Related to the Thickness of the Permeability Barrier." J Investig Dermatol **84**(3): 176-179.

Standish, B. A., Lee, K. K., Jin, X., Mariampillai, A., Munce, N. R., Wood, M. F., Wilson, B. C., Vitkin, I. A. and Yang, V. X. (2008). "Interstitial Doppler optical coherence tomography as a local tumor necrosis predictor in photodynamic therapy of prostatic carcinoma: an in vivo study." Cancer Res **68**(23): 9987-95.

Subarsky, P. and Hill, R. P. (2003). "The hypoxic tumour microenvironment and metastatic progression." Clin Exp Metastasis **20**(3): 237-50.

Sudhakar, Y., Kuotsu, K. and Bandyopadhyay, A. K. (2006). "Buccal bioadhesive drug delivery -- A promising option for orally less efficient drugs." Journal of Controlled Release **114**(1): 15-40.

Sun, T., Jackson, S., Haycock, J. W. and MacNeil, S. (2006). "Culture of skin cells in 3D rather than 2D improves their ability to survive exposure to cytotoxic agents." J Biotechnol **122**(3): 372-81.

Sun, T. P., Ching, C. T., Cheng, C. S., Huang, S. H., Chen, Y. J., Hsiao, C. S., Chang, C. H., Huang, S. Y., Shieh, H. L., Liu, W. H., Liu, C. M. and Chen, C. Y. (2010). "The use of bioimpedance in the detection/screening of tongue cancer." Cancer Epidemiol **34**(2): 207-11.

Sutherland, R. M., McCredie, J. A. and Inch, W. R. (1971). "Growth of multicell spheroids in tissue culture as a model of nodular carcinomas." J Natl Cancer Inst **46**(1): 113-20.

Thomas, S. M. and Grandis, J. R. (2009). "The current state of head and neck cancer gene therapy." Hum Gene Ther **20**(12): 1565-75.

Timmins, N. E., Dietmair, S. and Nielsen, L. K. (2004). "Hanging-drop multicellular spheroids as a model of tumour angiogenesis." Angiogenesis **7**(2): 97-103.

Tsai, M.-T., Lee, C.-K., Lee, H.-C., Chen, H.-M., Chiang, C.-P., Wang, Y.-M. and Yang, C.-C. (2009). "Differentiating oral lesions in different carcinogenesis stages with optical coherence tomography." Journal of Biomedical Optics **14**(4): 044028-7.

Upadhyay, K. K., Bhatt, A. N., Castro, E., Mishra, A. K., Chuttani, K., Dwarakanath, B. S., Schatz, C., Le Meins, J. F., Misra, A. and Lecommandoux, S. (2010). "In vitro and in vivo evaluation of docetaxel loaded biodegradable polymersomes." Macromol Biosci **10**(5): 503-12.

Upadhyay, K. K., Le Meins, J. F., Misra, A., Voisin, P., Bouchaud, V., Ibarboure, E., Schatz, C. and Lecommandoux, S. (2009). "Biomimetic doxorubicin loaded polymersomes from hyaluronan-block-poly(gamma-benzyl glutamate) copolymers." Biomacromolecules **10**(10): 2802-8.

VELscope. (2009). "Velscope The Oral Cancer Screening System." 2010, from http://www.velscope.com/velscope.php.

Vermorken, J., Mesia, R., Vega, V., Remenar, E., Hitt, R., Kawecki, A., Rottey, S., Amellal, N., Cupissol, D. and Licitra.L. (2007). Cetuximab extends survival of patients with recurrent or

metastatic SCCHN when added to first line platinum based therapy - Results of a randomized phase III (Extreme) study. American Society of Clinical Oncology.

Waite, C. L. and Roth, C. M. (2009). "PAMAM-RGD Conjugates Enhance siRNA Delivery Through a Multicellular Spheroid Model of Malignant Glioma." Bioconjugate Chemistry **20**(10): 1908-1916.

Wang, M. and Thanou, M. (2010). "Targeting nanoparticles to cancer." Pharmacological Research **62**(2): 90-99.

Wilder-Smith, P., Lee, K., Guo, S., Zhang, J., Osann, K., Chen, K. and Messadi, D. (2009). "In vivo diagnosis of oral dysplasia and malignancy using optical coherence tomography: Preliminary studies in 50 patients." Lasers in Surgery and Medicine **41**(5): 353-357.

Wu, J. G., Xu, Y. Z., Sun, C. W., Soloway, R. D., Xu, D. F., Wu, Q. G., Sun, K. H., Weng, S. F. and Xu, G. X. (2001). "Distinguishing malignant from normal oral tissues using FTIR fiber-optic techniques." Biopolymers **62**(4): 185-92.

Xi, S. and Grandis, J. R. (2003). "Gene Therapy for the Treatment of Oral Squamous Cell Carcinoma." Journal of Dental Research **82**(1): 11-16.

Yanjia, H. and Xinchun, J. (2007). "The role of epithelial-mesenchymal transition in oral squamous cell carcinoma and oral submucous fibrosis." Clinica Chimica Acta **383**(1-2): 51-56.

Yao, M., Epstein, J. B., Modi, B. J., Pytynia, K. B., Mundt, A. J. and Feldman, L. E. (2007). "Current surgical treatment of squamous cell carcinoma of the head and neck." Oral Oncology **43**(3): 213-223.

Zhang, H., Zhang, J. and Streisand, J. B. (2002). "Oral Mucosal Drug Delivery: Clinical Pharmacokinetics and Therapeutic Applications." Clinical Pharmacokinetics **41**(9): 661-680.

Zhou, W., Meng, F., Engbers, G. H. and Feijen, J. (2006). "Biodegradable polymersomes for targeted ultrasound imaging." J Control Release **116**(2): e62-4.

Zou, Y. and Guo, Z. (2003). "A review of electrical impedance techniques for breast cancer detection." Med Eng Phys **25**(2): 79-90.